STRUCTURAL ELUCIDATION AND DYNAMIC STUDIES OF MO TRIPEPTIDE DIASTEREOMERS (M = Tc-99m, Tc-99, Re): AN EXTENSION TO TARGETED RADIOPHARMACEUTICALS

by

MELCHOR V. CANTORIAS

A dissertation submitted to the Graduate Faculty in Chemistry in partial fulfillment of the requirements for the degree of Doctor of Philosophy, The City University of New York

2006

This manuscript has been read and accepted for the Graduate Faculty in Chemistry in satisfaction of the dissertation requirement for the degree of Doctor of Philosophy.

August 16, 2006 — Prof. Lynn C. Francesconi

Date — **Chair of Examining Committee**

August 16, 2006 — Prof. Gerald Koeppl

Date — **Executive Officer**

Prof. Klaus Grohmann

Prof. Randy Mootoo

Prof. Malgorzata Ciszkowska

Supervisory Committee

The City University of New York

Abstract

Structural Elucidation and Dynamic Studies of MO Tripeptide Diastereomers (M = Tc-99m, Tc-99, Re): an Extension to Targeted Radiopharmaceuticals

by

Melchor V. Cantorias

Adviser: Prof. Lynn C. Francesconi

Neotect^{TM} (^{99m}Tc depreotide), the first targeted radiopharmaceutical that entered clinical use as imaging agent for lung tumors, consisted of two species that were purportedly identified as syn and anti diastereomers based on NMR, mass spec, and IR data. Because their biological behaviors are significantly different, it was critical to obtain the absolute identity for each diastereomer. This dissertation has accomplished this goal using [M^{V}=O] tripeptide diastereomers. Moreover, since the identification of these diastereomers is general for all ^{99m}Tc tripeptide (comprised of L amino acids) complexes, this information will aid in the identification of the ^{99m}Tc and ^{188}Re radiopharmaceuticals when the $[M=O]^{+3}$ core in a tripeptide binding site is employed.

We isolated ^{99}Tc and Re diastereomers of several tripeptide ligands, including three (MKC, FKC, and YKC) that closely model ^{99m}Tc depreotide. Using X-ray crystallography, we show that, as expected, the TcO is bound to the ligand in a square pyramidal coordination environment. The crystallography demonstrated that the early

eluting peak (A) corresponds to the "anti" diastereomer where the Tc=O group is on the opposite side of the square plane formed by the ligand backbone relative to the pendant groups of the tripeptide ligand, and the later eluting peak (B) corresponds to the "syn" diastereomer, where the Tc=O group is on the same side of the plane as the residues of the tripeptide. Moreover, ^{1}H NMR and circular dichroism spectroscopy confirm that the $^{99/99m}$Tc tripeptide models have the same diastereomer profile as $^{99/99m}$Tc depreotide.

Observations made during the syntheses of ^{99}Tc and Re diastereomers provided hypotheses for the stability of diastereomers. Stability of diastereomers was addressed by quantitative kinetic studies of the interconversion of the ^{99m}Tc analogs. We postulate that hydrogen bonding of residues, for example the εNH_3 of lysine with the –yl oxygen of the Tc/Re=O or with a carbonyl of the tripeptide in syn complexes, may be a stabilizing force. Also, the potential hydrogen bonding of the Tc=O with the C-terminal amide appears to be a stabilizing factor in MO FGC anti (M=Tc,Re) according to experimental kinetic studies and preliminary DFT calculations.

Acknowledgments

First and foremost, I owe gazillion thanks to Professor Lynn C. Francesconi, my advisor. Her wonderful analysis and critique of my manuscript went leagues beyond reviewing and correcting my work, and provided invaluable input and guidance every step of the way. Her support was more than academic. One occasion that comes to mind occurred when I was slacking off. At that time she asked me the deceptively simple question, "Do you still want to finish your Ph.D.?" Although at the time I responded evasively, stating, "I'm not sure, I'll think about it," her concern for my success in that way gave me the kick I evidently needed, both personally and professionally, to renew my commitment to my career! These are among the things that define, for me, qualities of a great mentor, and for which I am grateful. Besides Professor Francesconi's being top notch, and in addition to academics and personal support, I also feel so privileged to have been given the opportunity to make an oral presentation for the Society of Nuclear Medicine in San Diego in June 2006, and to present a poster at the Pacifichem in Honolulu in December 2005. I feel honored and grateful that I was able to participate in those extra curricular activities.

I would of course also like to thank the many others who helped me and supported my preparation of this dissertation, including:

Dr. Robertha Howell, whose ideas and criticisms helped cultivate my interests and even formulate a direction for my research. Dr. Howell was always inspiring, and

always reminded me that there is a light at the end of the tunnel – thank you for being so wonderful!

Professor Klaus Grohmann, Professor Randy Mootoo, and Professor Malgorzata Ciszkowska, whose active interest in my work and insightful comments always suggested deeper significance and ramifications of my research.

Dr. Louis Todaro, Dr. Mike Blumenstein, and Dr. Cliff Soll, whose knowledge and expertise in their respective fields tremendously assisted me in solving crucial problems in the identification of the syn and anti diastereomers.

Professor Gerard Koeppl, whose professionalism in his administrative work as Chairman of the Chemistry Department and his commitment to graduate students provided the wonderful and well-organized program and environment in which I could achieve my goal.

Ms. Diane Adebowale, not only for being the indefatigable secretary of the department, but especially for our conversations, always warm and delightful, and somehow always putting me at ease!

The present and former members of the Francesconi Group: Dr. Benjamin Burton-Pye, Dr. Israel Mbomekalle, Lauren Wickstrom, Kimora Scotland, Donna McGregor, Laurence Bensaid, and Jing Jing, whose good camaraderie was more than enough to sustain me to go through years and years (and years and years and years) in the lab.

Amanda, Ernie, Rinna, Gary, Grace and Corrie, who helped me keep my sanity and provided constant encouragement, enjoyment, and friendship over brunches, lunches

and dinners in the East Village, walks and picnics in Central Park, rollerblading around Chelsea Piers, attending operas and concerts at Lincoln Center, and movies everywhere.

Joel and Milton, whose affordable housing on the Lower East Side gave me the opportunity to take a real bite out of the "big apple."

Fatoumata Camara, Sheuli Zakia, Dr. Jayshree Biswas, Dr. Neela Pooransingh, Amanda Pustam, Jordan Margolis, and Michal Masiak, whose hard work and patience in graduate school were always a great reminder and inspiration whenever I began to doubt my direction.

The Averill family, whose hospitable invitations to Thanksgiving and Christmas dinners provided me with a real family away from home.

Sean, whose interest, personal support, and friendship helped me appreciate some utterly simple things that make life so wonderful. And he also provided me with a place to write!

Although New York City has it all, I don't know how I would have survived without my periodic escapes with Gina, Cindy, Rob, and Doug (and John too!) – wonderful memories!

My younger sister, Judy, who, besides being so terrific and inspiring, and impressing me with her achievements, gives me so much by sharing with me her wonderful prose and poems.

My older siblings, Neneng and Toto, whose dedication to their careers and families provided great examples to pursue my goal.

Finally, I want to thank Tatay (my father) who has been a constant source of strength, without whom I simply could not have succeeded. Tay, thank you for showing

me that all things are possible until they are proved impossible. Thank you for your quiet strength and acceptance. Thank you for believing in me even during my own moments of doubt. Thank you for allowing me to be.

To all who believed in the importance of this field of research, and to those who have been confident in my ability to rise to the challenges it presents, thank you.

And of course, thanks to the interests in this research through SCORE grants of NIH and NSF.

To the memory of Nanay (my mother),
ERLINDA VERONQUE CANTORIAS

Not to forget how sweet your smile was.

Not to forget the way your hands felt against mine,
to comfort me at eight or at 30.

Not to forget your sweet scent that reminded me of
summer time and spring all at once.

Not to forget the long talks on the phone across the seas,

Not to forget how you said you loved me and
how I said I loved you for the last time.

– Nonoy

Table of Contents

List of Figures

List of Tables

List of Schemes

1. Introduction

1.1. Background and Significance

A diagnosis of cancer can be one of the most devastating life experiences. Cancer is a group of diseases characterized by uncontrolled growth and spread of abnormal cells. If the spread is not controlled, it can result in death. The disease is one of the leading causes of death in the U.S., only second to heart disease. A current study shows that 9.8 million Americans have a history of cancer, with an estimated 1.3 million new cases anticipated.[1] There is a constant appeal for new drugs and techniques in the fight and eventual elimination of the many types of known cancers. To date, this demand has yet to be realized, leaving a great and ongoing challenge for scientists and physicians to meet. To answer that challenge, there has been a strong emphasis on the development of radiopharmaceuticals and imaging techniques.[2-15]

Radiopharmaceuticals are drugs containing a radionuclide and when used for the purpose of diagnosis and therapy of various diseases, including cancer, they do not elicit physiological response from the patient. Technetium-99m, ^{99m}Tc, is the most widely used radionuclide for radiopharmaceutical imaging agents.[16-24] The growing demand for diagnostic tools has promoted the development of the newest class of imaging agents based on biologically active molecules (BAM), which serve as targeting vectors for radiopharmaceuticals.[25] These targeting vectors are linked to a ligand that will bind the radiometal tightly (**Figure 1-1)**. Tripeptides, with a cysteine in the third position at the

carboxylate terminus, are suitable ligands for linking to targeting vectors. Such tripeptides are generally, easily and conveniently linked to the targeting vector through solid-phase peptide synthesis; the thiolate sulfur, forming a five-membered ring, stabilizes the $Tc^{V}O$ core and the residues for the first two amino acids can be altered to optimize the bioligical handling by the radiopharmaceutical.

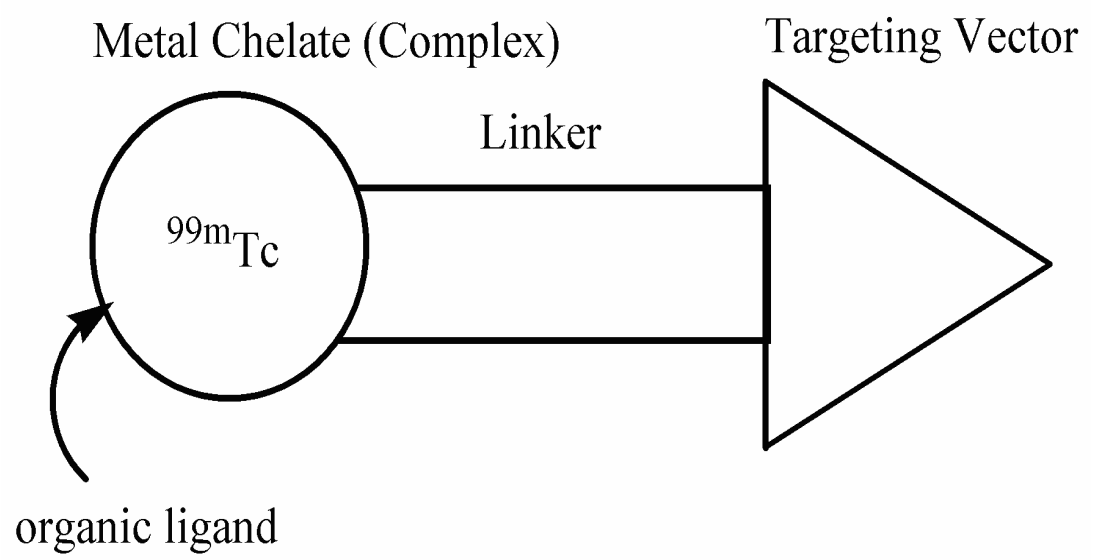

Figure 1-1. Generalized scheme for targeted ^{99m}Tc and other radiometal diagnostic agents.

A difficulty with tripeptide ligands is that upon complexation with TcO, two products, likely syn and anti diastereomers, are formed and these diastereomers have different elution profiles on Reverse Phase HPLC (RP-HPLC) and the diastereromers have not yet been assigned to the early or later eluting species. This is the case with a

recently approved radiopharmaceutical, NeoTect® (^{99m}Tc depreotide) that is used to evaluate lung nodules.[26-30] ^{1}H NMR and electrospray MS of the ^{99}Tc depreotide analogs of ^{99m}Tc depreotide show that they have the same sequence and binding site and are diastereomers.[31] Due to the fact that diastereomers can have significantly different biological behavior, as is the case with ^{99m}Tc depreotide, it is imperative that assignment of diastereomers be made for depreotide and in general, for all radiopharmaceuticals where an L-tripeptide sequence is used to bind to the ^{99m}Tc radiometal.

Using X-ray crystallography of ^{99}Tc and Re tripeptides we assigned the absolute configurations of the diastereomers. We then correlated the absolute configurations of the diastereomers to their HPLC profiles using proton NMR and circular dichroism. With assignment of absolute configurations of the diastereomers, we are now in position to understand the chemistry and energetics that impact the stability of the diastereomers.

Diagnostic techniques using radionuclides include Single Photon Emission Tomography (SPECT) and Positron Emission Tomography (PET). The PET scanner (**Figure 1-2**) is a state-of-the-art device consisting of multiple cameras in circular arrays. Two photons, that are 180 degrees apart, are detected by the cameras; hence, images with high resolution are created. PET is used for radiopharmaceuticals containing radionuclides that emit positrons such as ^{18}F and ^{11}C. Alternatively, the SPECT scanner (**Figure 1-3**) contains one camera, which rotates at different angles while detecting a single photon. It is specifically used for gamma-emitting radiopharmaceuticals such as ^{99m}Tc-based targeted radiopharmaceuticals. Although the PET technique provides superior quality images over the SPECT device, most medical professionals regularly opt to use SPECT as it is more cost-effective. For instance, ^{99m}Tc is readily available in

hospitals by convenient $^{99}Mo/^{99m}Tc$ generator[32-34] which reduces its price substantially. In contrast, positron-emitters are produced by cyclotrons which make PET less advantageous than SPECT. The cyclotrons are expensive instruments requiring specialized personnel and operators and generally, cannot be installed in an ordinary setting like a hospital. Unless production of positron emitting radionuclides becomes routine, SPECT remains the method of choice for biomedical imaging. Recent studies, however, concluded that 97% of the total United States population lives within 75 miles (easy driving distance) of a clinical PET facility.[35] Moreover, extensive research has been done on microfluidic devices to facilitate multistep synthesis and to improve yields of ^{18}F-FDG, a PET radiopharmaceutical.[36] Thus, in the coming years PET and SPECT will no longer be considered competitors but become complementary to each other.

Figure 1-2. Positron Emission Tomograpy (PET) device associated with positron-emitting radioisotopes such as F-18.

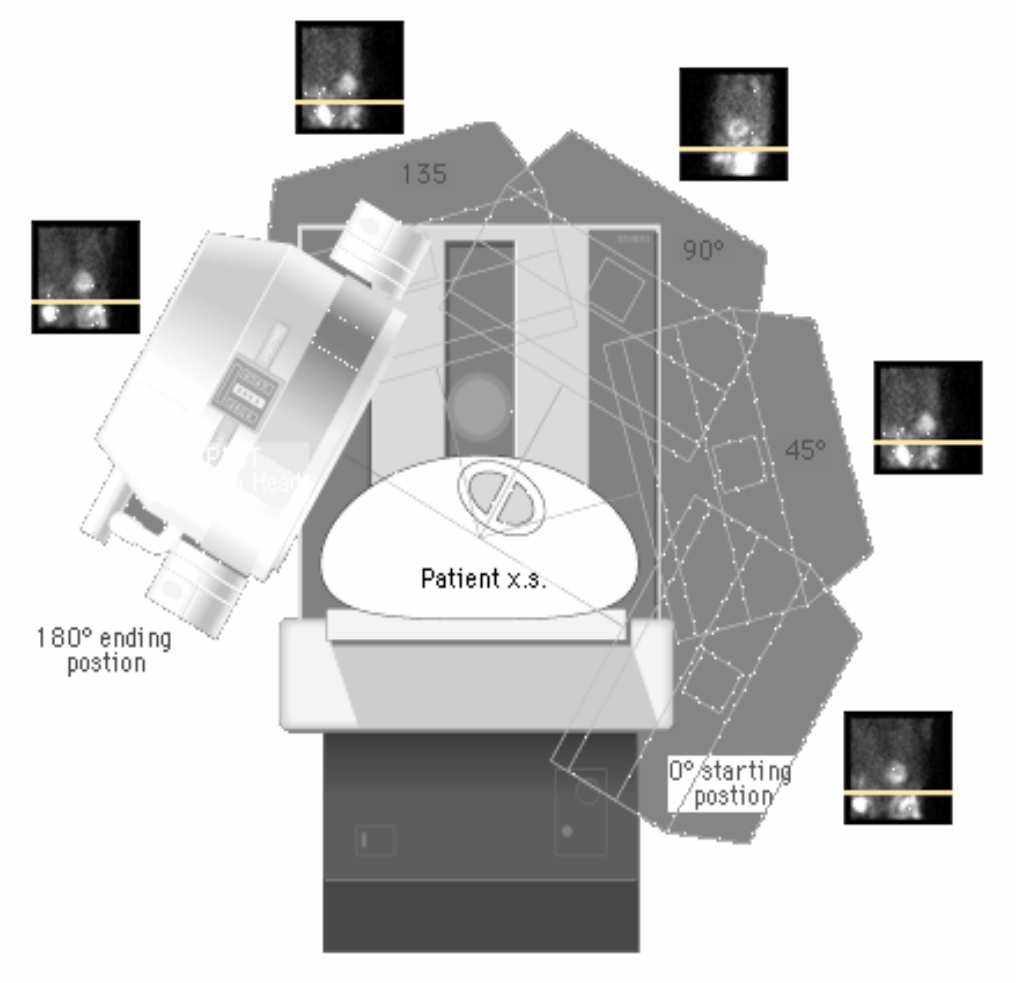

Figure 1-3. Single-Photon Emission Computed Tomograpy (SPECT) associated with gamma-emitting radioisotopes such as Tc-99m.

1.2. Chemistry of Technetium and its Congener Rhenium

Technetium and rhenium play a special role in nuclear medicine. There are several reviews that highlight the medical applications of Tc and Re.[18, 21, 37-47]

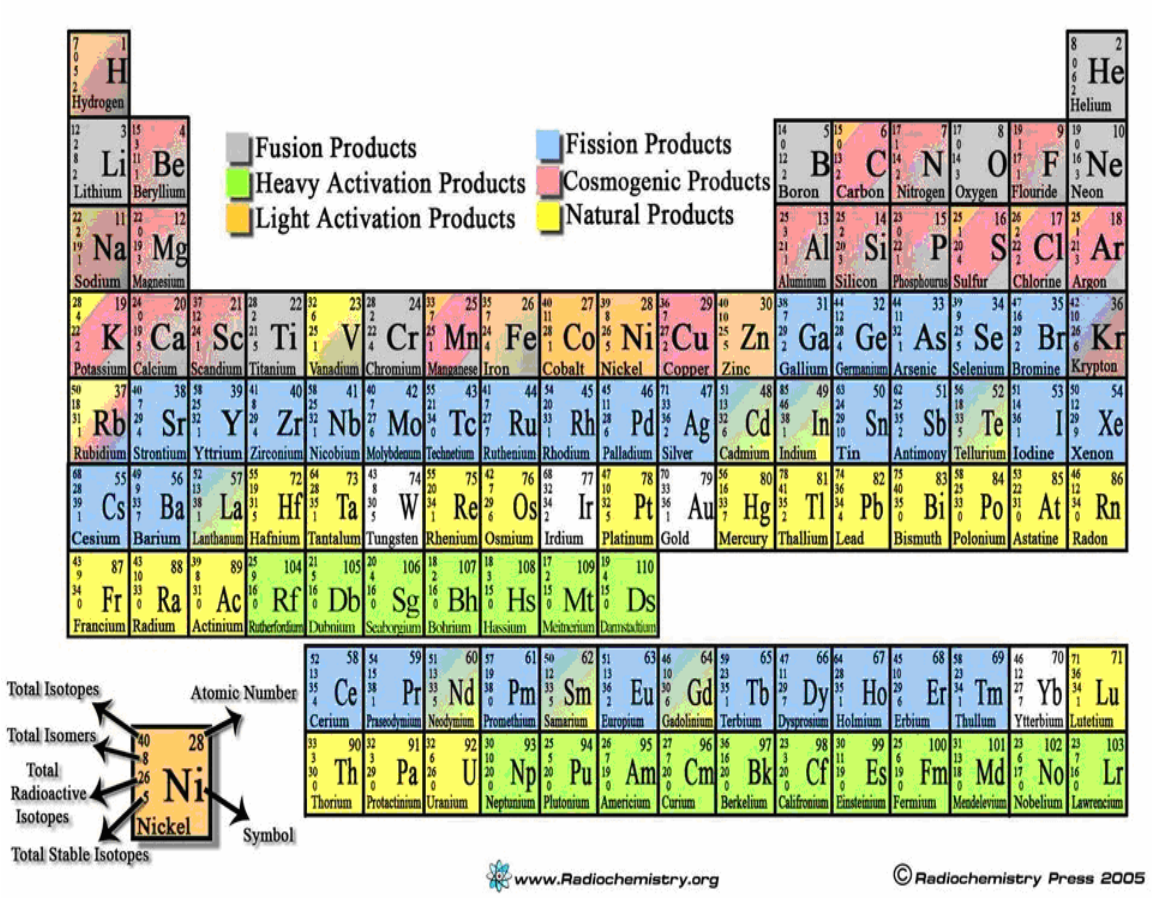

Figure 1-4. Nuclear Periodic Table

1.2.1. Technetium

Technetium (Tc) has an atomic number of 43 with atomic mass units ranging from 88 to 113, and lies in the second row of transition metal series. Its inclusion in the Periodic Table (**Figure 1-4**) was first predicted by Mendeleev in 1869 but the metal per se was discovered by Perrier and Segre in 1937.[48] To date, there are a total of fifty-five isotopes and twenty-one isomers that have been identified but the most commonly used isotope is technetium-99m or ^{99m}Tc, especially in nuclear medicine applications (more than 85% of the diagnostic scans done each year in hospitals) due to its excellent physical properties. For example, the 6-h half-life of ^{99m}Tc is ideally short, thus, the radiation dose is less burden to the patient. However, this is considered long enough to prepare, purify and inject the drug into the patient. The gamma-ray emission of 142 keV energy is the other most important advantage of ^{99m}Tc. This energy is suitable for studying deep-seated human organs using SPECT.

The first application of technetium as a radiopharmaceutical in the nuclear medicine clinic was at the University of Chicago where Paul Harper used $Na^{99m}TcO_4$ eluted from a ^{99}Mo/^{99m}Tc generator (**Figure 1-5**) to obtain images of the liver, brain, and thyroid.[49, 50] The first prototype of the ^{99}Mo/^{99m}Tc generator was developed by Walter Tucker and Margaret Greene at Brookhaven National Laboratory, New York. This generator takes advantage of the transient equilibrium between the parent radionuclide ^{99}Mo (66 h half-life) and the daughter radionuclide ^{99m}Tc (6 h half-life) as shown in **Scheme 1-1.**

Figure 1-5. The first $^{99}Mo/^{99m}Tc$ generator developed at Brookhaven National Laboratory, New York.

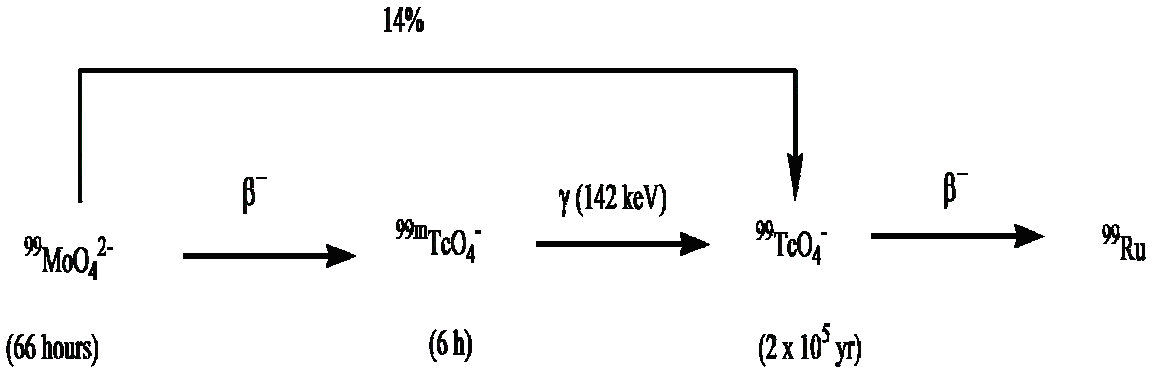

Scheme 1-1. Decay scheme of MoO_4^{-2} to $^{99m}TcCO_4$; the chemistry of the ^{99m}Tc generator.

The general prototype of $^{99}Mo/^{99m}Tc$ generator shown in **Figure 1-5** consists of a glass column evenly packed with alumina (Al_2O_3). ^{99}Mo is adsorbed as molybdenate (MoO_4^-) on the alumina. Saline elutes ^{99m}Tc in the form of sodium pertechnetate ($Na^{99m}TcO_4$) from the column, while ^{99}Mo remains unattached to it. Following elution, the ^{99m}Tc activity quickly reaccumulates reaching a maximum in about 23 hours. About 50% of this peak activity is reached within 8 hrs, so it is feasible to elute the generator every few hours if necessary.

Technetium possesses a diverse chemistry. Its complexes are known where the oxidation states is -1 to +7, having various coordination geometries with a variety of ligands filling the coordination requirements.[51] Some examples of Tc compounds with corresponding oxidation states and coordination geometries are shown in **Table 1-1**. For production of radiopharmaceuticals, $Na^{99m}TcO_4$ must be reduced from the +7 oxidation state to a lower oxidation state for complexation with chelating ligands. Reduction of TcO_4^- is most commonly accomplished by stannous chloride in the presence of chelating ligands which dictate the coordination complex that forms. Certain stable motifs, often

called “technetium cores” (**Figure 1-6**), form the basis of small coordination compounds and molecules that can be linked to biomolecules.[52]

Table 1-1. Oxidation States and Stereochemistry of Technetium

Oxidation State	Example	Coordination Geometry	Coordination Number	Magnetic Moment (μB)
+7 (d^0)	$[TcH_9]^{2-}$	trigonal prism	9	diamagnetic
	TcO_4^-	tetrahedron	4	diamagnetic
+6 (d^1)	TcO_4^{2-}	tetrahedron	4	1.60
+5 (d^2)	$[Tc(Diars)_2Cl_4]^+$	dodecahedron	8	0.9
+4 (d^3)	$[TcCl_6]^{2-}$	octahedron	6	4.05
+3 (d^4)	$[Tc(Diars)_2Cl_2]^+$	octahedron	6	diamagnetic
+2 (d^5)	$[TcCl_2(PhP(OEt)_2)_4]$	octahedron	6	diamagnetic
+1 (d^6)	$[Tc(CNC(CH_3)_3)_6]^+$	octahedron	6	diamagnetic
0 (d^7)	$[Tc_2(CO)_{10}]$	octahedron	6	diamagnetic
-1 (d^8)	$[Tc(CO)_5]^-$	trigonal bipyramid	5	diamagnetic

The concentration of $Na^{99m}TcO_4$ (plus $Na^{99}TcO_4$) eluted from the generator is normally very dilute, ranging from 0.1 μM to 0.1 nM. This and the short half-life means it is not possible to characterize ^{99m}Tc complexes using routine spectroscopic and analytical techniques. However, the long-lived ^{99}Tc isotopes ($t_{1/2}$ – ca. 200,000 yrs; β^-_{max}: 243 keV) can be used in place of ^{99m}Tc to determine the structure and chemistry and physicochemical properties of technetium radiopharmaceuticals as this isotope exists in

macroscopic quantities. Once the ^{99}Tc chemistry is clearly elucidated, this can be related back to the tracer radiopharmaceutical by reverse-phase HPLC concordance experiment.

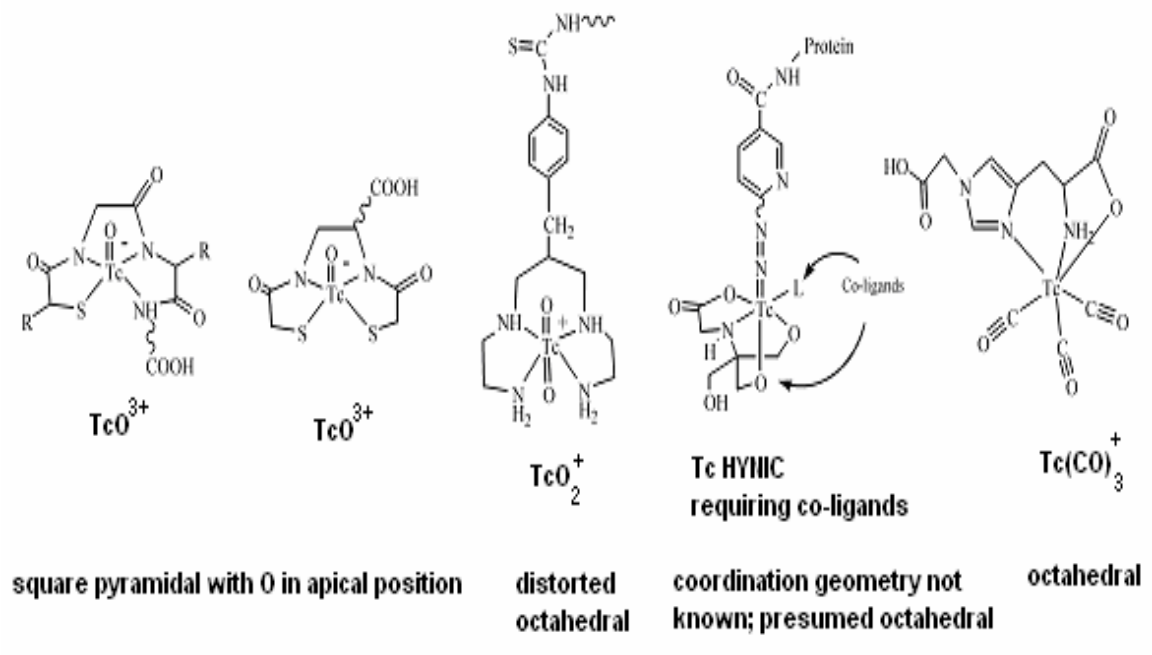

Figure 1-6. Different Technetium Cores: Tc=O, O=Tc=O, Tc=N=N, and Tc-$(CO)_3$.

1.2.2. Rhenium

In 1925, the Noddacks discovered rhenium (Re) as a naturally occurring mixture of two non-radioactive isotopes such as ^{185}Re (37.4%) and ^{187}Re (62.6%).[25] The element Re with the atomic number 75 belongs to Group VIIB on the Periodic Table (**Figure 1-4)**, located just below of Tc. The radioactive isotopes of interest in nuclear medicine are ^{186}Re (half-life = 90 hrs; β^- max = 1.07 MeV, 5 mm range) and ^{188}Re (half-life = 17 hrs; β^- max = 2.12 MeV, 11 mm range). ^{186}Re is generated by neutron radiation of ^{185}Re and ^{188}Re is available by radioactive decay from ^{188}W. Both ^{186}Re and ^{188}Re are obtained as perrhenate (ReO_4^-) and must be used in reduced kit formulations similar to ^{99m}Tc. Both ^{186}Re and ^{188}Re may be useful for radiotherapy. Additionally, ^{188}Re may offer a synergistic radiopharmaceutical kit that can function diagnostically and therapeutically at the same time, as it also emits gamma ray of 155 keV (15%).

Rhenium is often used as a "surrogate" for technetium. The overall structures of analogous Tc and Re complexes are expected to be similar because of the periodic relationship between the metals. Also, the individual bond parameters of both Tc and Re are expected to be similar because the two elements have nearly identical ionic radii due to the "lanthanide contraction". However, the differences between Tc and Re can be highly significant. ReO_4^- has a much higher reduction potential than TcO_4^- (-0.361 V and -0.548 V vs. SHE, respectively, pH = 13.5; ca. 0.17 M). It is observed that the Tc analog is always easier to reduce when different oxidation states of a wide array of Tc/Re analogs are studied. This observation is very helpful to explain why the ^{186}Re complex $[^{186}Re(III)\ (dmpe)_2]^+$ is retained in the heart as opposed to ^{99m}Tc analog that is reduced under physiological conditions to the $Tc^{II}(dmpe)_2$ neutral species and is washed out of the

heart.[53] However, Re complexes are more stable in higher oxidation states than the ^{99}Tc analogs. An example of the increased stability of Re compared to Tc can be seen in the bone imaging and potential therapeutic agents, based on HEDP (hydroxyethylidinediphosphonate). ^{186}Re-HEDP is more readily oxidized to ReO_4^- in vivo than is ^{99m}Tc-HEDP. The ^{186}Re HEDP that is not bound to the bone at the tumor site is washed off of the bone and excreted.[54, 55] Thus, the abnormal to normal bone uptake ratio increases with time. This is beneficial from the radiotherapeutic standpoint because it reduces radiation dose to normal tissue. In addition, rhenium has a slower ligand exchange rate than technetium;[56] rhenium may have an expanded coordination sphere compared to technetium; perrhennate forms complexes with citrate and oxalate more extensively than does pertechnetate.[57]

The nonradioactive rhenium, as a surrogate for technetium, is alternatively used for characterization of technetium-based radiopharmaceuticals. It is recommended to practice this with caution as the differences in chemistry between Tc and Re as outlined above may be relevant in the study of new, relatively unexplored ligand systems.

1.3. Radiopharmaceuticals

1.3.1. Definition

From the standpoint of nuclear medicine practitioners, radiopharmaceuticals are defined as radioactive drugs which do not cause physiological response or adverse reaction upon administration by the patient. There is a significant difference between radiopharmaceuticals and radiochemicals. Radiopharmaceuticals have undergone a very

lengthy and expensive regulatory process as well as extensive chemical and physical testing (pH, isotonicity, and chemical parameters) to insure that the final product is sterile, pyrogen-free, safe for human use, and is efficacious. This includes both animal and human studies prior to release of the product for sale. Radiochemicals used for chemical and biological research that does not involve humans, however, typically don't undergo this rigorous testing and neither their sterility nor pyrogenicity is guaranteed. Radiochemicals that are to be used for radiopharmaceutical products do need to be guaranteed to be sterile and pyrogen free.

Radiopharmaceuticals clinically designed for diagnostic imaging contains a radionuclide that emits gamma (γ) and positron (β^+). For therapy procedures, the radionuclides used are emitters of alpha (α) and beta (β^-) particles, and Auger/conversion electrons (e^-). Aside from Tc and Re, other examples of gamma and positron emitting radionuclides that are currently used or have potential use for medical applications are listed in **Table 1-2**. However, radiopharmaceuticals may also serve as tracers in research projects.

Table 1-2. Common Gamma and Positron Radionuclides Other Than ^{99m}Tc and ^{188}Re.

Radionuclide	Half-life	Production Methods	Maximum Particle Emmission	Gamma Emmission (keV)
^{67}Ga	3.26 days	Cyclotron	EC (100%)	91,93,185,296,388
^{68}Ga	67.63 min	^{68}Ge/^{68}Ga generator	1.899 MeV β^+ (90%) EC decay (10%)	1077 (3.3%) 511 (176%)
^{66}Ga	9.5 h	Cyclotron	4.153 MeV β^+ (57%) EC decay (43%)	2752 (23.5%) 1039 (38.4%) 834 (6.1%) 511 (117.3%)
^{62}Cu	9.74 min	^{62}Zn/^{62}Cu generator	2.96 MeV β^+ (97.8%) EC decay (2.2%)	511
^{64}Cu	12.7 h	Cyclotron	0.63 MeV β^+ (19%) EC decay (41%)	511
^{67}Cu	2.58 days	Accelerator	0.577 MeV β^-	184.6 (46.7%) 93.3 (16.6 %) 91.3 (7.3%)
^{111}In	2.83 days	cyclotron	EC decay	245 (94%) 171 (91%)
IT: isomeric transition; EC: electron capture				

1.3.2. Radiopharmaceutical Classifications

Radiopharmaceuticals are generally classified on the basis of how they are distributed in the body. Their biological distribution is a very important parameter to assess the normal physiological or pathological status of the patient. The drugs can be delivered to the site of disease in two ways. One approach is through blood flow or perfusion. Blood flow radiopharmaceuticals are the first generation of radiopharmaceuticals which were originally based on the metal coordination chemistry which includes the size, charge, lipophilicity or hydrophilicity, and other gross targeting/localizing characteristics imparted by the ligand to the overall complex.[58] Some examples of the FDA-approved blood flow radiopharmaceuticals are ^{99m}Tc-HMDP, ^{99m}Tc-HIDA, ^{99m}Tc-DTPA, and ^{99m}Tc-HMPAO (**Table 1-3**).

The second approach of drug delivery is via specific binding interactions of the drug itself with enzymes and cellular proteins, including receptors, monoclonal antibodies, and peptides. These new generation radiopharmaceuticals are called targeted radiopharmaceuticals as they are directly delivered to the target organ in a "magic bullet" fashion, a concept introduced by Paul Ehrlichs.[59] The early generation of targeted radiopharmaceuticals was introduced in the 1980s; these are ^{99m}Tc-ECD, ^{99m}Tc-MIBI, and ^{99m}Tc-MAG_3 (**Table 1-3**). The in vivo characteristics of these agents, such as blood clearance, protein binding, in vivo stability, and the physiologic mechanism necessary for localization, are dependent on the properties of the overall coordination complex, such as charge, size, lipophilicity. The structures and biological mechanism of uptake of these radiopharmaceuticals served as prototypes for the design of future organ imaging agents.

Tc apcitide and Tc depreotide (**Table 1-3**) are examples of recently FDA-approved targeted radiopharmaceuticals and are specifically classified under peptide-based radiopharmaceuticals. The next section discusses this topic in more details.

Table 1-3. FDA-Approved Tc- and Non-Tc-Based Radiopharmaceuticals

Chemical Name	Commercial Name	Manufacturer	Primary Function
1. ^{99m}Tc-d,l-HMPAO	Ceretec	Amersham International	Cerebral perfusion
2. ^{99m}Tc-MAG_3	TechneScan MAG_3	Mallinckrodt	Renal imaging agent
3. ^{99m}Tc-sestamibi	Cardiolite	DuPont-NEN	Myocardial perfusion imaging agent
4. ^{99m}Tc-HIDA	TechneScan HIDA	Mallinckrodt	Hepatobiliary imaging agent
	Choletec	Bristol-Myers Squibb	
	Hepatolite	DuPont-NEN	
5. ^{99m}Tc-HMDP	Osteoscan-HDP	Mallinckrodt	Skeletal imaging agent
6. ^{111}In-oxine	Indium In 111 Oxyquinoline Solution	Amersham International	Infection and inflammation imaging agents
7. ^{99m}Tc-L,L-ECD	Neurolite	DuPont-NEN	Brain imaging agent
8. ^{67}Ga-citrate	Neoscan	MediPhysics	Tumor and infection imaging agents
	Gallium Citrate Ga 67 Injection	Mallinckrodt	
	Gallium Citrate Ga 67, U.S.P.	DuPont-NEN	
9. ^{111}In-DTPA-octreotide	OctreoScan	MediPhysics	Tumor imaging agent
10. ^{99m}Tc apcitide	AcuTect	Schering AG	Deep Vein Thrombosis imaging agent
11. ^{99m}Tc depreotide	NeoTect	Schering AG	Lung tumor imaging agent

NB:

1. Blood-flow radiopharmaceuticals (3-6) and targeted-radiopharmaceuticals (1,2,7, 9-11)
2. HMPAO = hexamethylpropyleneamine oxime
3. Sestamibi = $[(2\text{-methoxy-2-methylpropyl})\text{isonitrile}]_6^+$
4. Oxine = $(\text{oxyquinoline})_3^+$
5. ECD = ethylenecysteine diester

6. DTPA = diethylenetriaminepentaacetic acid; Octreotide = D-phe-cyclo(cys-phe-D-trp-lys-thr-cys)-thr(ol)
7. Apcitide = *cyclo*-(D-Tyr-Apc-Gly-Asp-Cys)-Gly-Gly-Cys(Acm)-Gly-Cys(Acm)-Gly-Gly-Cys-NH_2
8. Depreotide = cyclic –Tyr-D-Trp-Lys-Val receptor binding sequence is restrained in a cycle and tethered to a β-diaminopropionate-lys-cys lys

1.4. Peptide-Based Radiopharmaceuticals

The ever expanding growth in the development of radiolabeled peptides for diagnostic and therapeutic applications in the last decade bodes well for the development of new and unique radiopharmaceuticals. The peptides' diverse variety of specific functions, intended by nature, provides them with a fundamental role in almost every field of medicine, with a primary function in nuclear medicine. Thus, with continued advancement in research, the present and future tools for diagnostic imaging and therapy of cancers and other diseases are peptide-based radiopharmaceuticals.[60-63]

1.4.1. Importance of Peptides

Peptides regulate many biological functions by acting as chemical messengers, neurotransmitters and highly active stimulators or inhibitors. Before the availability of peptides, antibodies and proteins were primarily considered as bioactive vehicles for targetry of radioactivity to tumor cells. However, the large size of antibodies and proteins (molecular weight > 600) take a relatively long time to localize and clear and can be matched to long-lived isotopes for imaging and therapy. Peptides, on the other hand, are small biologically active molecules that bind quickly to their specific receptors. The

general size of receptor-specific peptides consisting from 5 to 30 amino acids (molecular weight < 600) allows peptide-based radiopharmaceuticals to distribute uniformly in the body, penetrate readily in tissue, and clear efficiently from blood circulation. Other characteristics of small peptides, which make them sought-after in developing new technologies, include: (i) easy preparation, (ii) easy radiolabeling, (iii) diverse radiolabeling techniques, (iv) toleration of harsh conditions of chemical modifications or radiolabeling, (v) ability to attach bifunctional chelate (BFC) at the C- or N-terminus of the peptide, (vi) modifiable rate and route of excretion, (vii) better tumor-to-background ratio, (viii) low toxicity, (ix) low immunogenicity, and (x) a high affinity and specificity for receptors.[64, 65]

1.4.2. Peptide-Based Bifunctional Chelates

In general, bifunctional chelates (BFCs) are organic ligands with a linker, which have defined coordination sites available for ^{99m}Tc binding. Different types of BFCs that have been investigated for peptide-based radiopharmaceuticals include HYNIC-containing chelates (2-hydrazinonicotinamide), N_xS_{4-x} chelates, $Tc(CO)_3^+$-containing chelates, and water-soluble phosphine chelates. For the N_xS_{4-x} type, four systems can be made: N_4, NS_3, N_2S_2, and N_3S. Among the four systems, we observed that HYNIC and the N_3S motif were most commonly used as BFCs. For instance, MAG_3, from the renal imaging agent TechneScan™, is a peptide-based N_3S ligand. Upon coordination to the Tc(V) center, MAG_3 loses one proton on the thiolate sulfur and two protons on the two amide nitrogens to form an ionic complex. The resulting geometry of the complex is

square-pyramidal in which the oxo group is in the apical position. The carboxylate group is not coordinated to the metal and is necessary for efficient renal excretion of anion. A number of studies used MAG_3 and its derivatives as BFCs for ^{99m}Tc and ^{188}Re to examine the biochemistry of the biological targeting system.[42]

The first and thus far only, ^{99m}Tc targeted radiopharmaceuticals that are in clinical use are based on tripeptide ligand motifs linked to a cyclic peptide targeting vector. The first ^{99m}Tc radiopharmaceutical to be introduced to the clinic was ^{99m}Tc apcitide (AcuTect^{TM}) used for imaging deep vein thrombosis (DVT).[66] The second ^{99m}Tc labeled peptide with the N_3S BFC to enter clinical use is ^{99m}Tc depreotide (NeoTect^{TM}) , a lung tumor imaging agent.[31]

1.5. Stereoisomers of Radiopharmaceuticals

The N_xS_{4-x} and other bifunctional chelates may contain one or more chiral centers forming more than one stereoisomers upon complexation with ^{99m}Tc. The stereochemistry of the resultant diastereomers can greatly influence the biochemical function of radiopharmaceuticals. It is important to evaluate the individual products separately to ensure that they both possess good biological efficacy. The following discusses phenomena occurring in radiopharmaceutical diastereomers.

1.5.1. Examples of Diastereomers Impacting Biological Properties

Ceretec™. Also known as ^{99m}Tc-HMPAO[67, 68], Ceretec™ developed by Amersham International, is a brain imaging agent which utilizes the N_xS_{4-x} type ligand hexamethylpropyleneamineoxime (HMPAO). HMPAO, having two chiral centers and complexing with Tc-99m, loses three protons, thereby forming a neutral, square pyramidal Tc^V mono-oxo complexes: the D-L and meso analogues (**Figure 1-7**). Both of these analogues have been investigated. Research demonstrates that both the D-L and the meso-HMPAO analogues, both lipophilic and thus able to to cross the brain-barrier, convert to become more hydrophilic. This conversion occurs at different rates. The relatively slower conversion of the meso-HMPAO analogue allows it to diffuse out of the brain, whereas the more rapid conversion of the D-L analogue results in greater retention within the brain. In principle, the meso analogues derived from these mono-oxo complexes form two isomeric compounds differing in the orientation of the oxo group relative to the two methyl groups. In practice, only the complex with the Tc=O group syn to the methyls has been isolated.

Neurolite™. Also known as ^{99m}Tc-ECD.[69-71], Neurolite™ commercially available from Dupont, is a brain imaging agent based on a tetradentate N_2S_2 chelate. Like HMPAO, the ECD (ethylenecysteine diester) contains two chiral centers which lose three protons to form neutral, square pyramidal complexes (**Figure 1-7**) upon reaction with Tc^VO. The L-L forms of these complexes are trapped once across the blood-brain barrier due to enzymatic hydrolysis of one ester group by esterase enzyme, generating more hydrophilic complexes. The corresponding D-D complexes are inert to enzymatic hydrolysis and diffuse back across the blood-brain barrier. Such enzymatic conversion reactions also

occur in the blood during biodistribution, and, although these impair brain uptake, they facilitate clearance from the blood and non-target tissue via the kidneys.

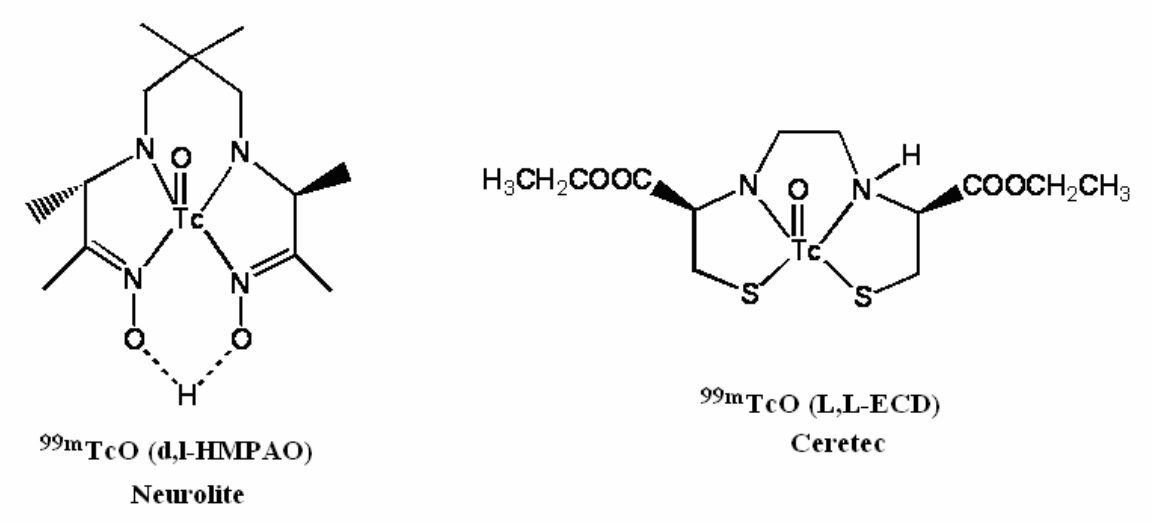

Figure 1-7. FDA-approved radiopharmaceuticals containing more than one isomer.

1.5.2. Anti and Syn Diastereomers by Peptides: Key Prior Knowledge for Understanding Interconversion

RP294 (Dimethylglycyl-seryl-cysteinylglycinamide). RP294, a peptide ligand with an N_3S donor set, was prepared to react with technetium and rhenium forming two diastereomers as syn and anti (**Figure 1-8**), which were characterized by ^{1}H NMR and ^{13}C NMR. Attempt to isolate these diastereomers via reverse-phase HPLC was not possible because of their rapid interconversion in aqueous solution at room temperature. A crystal selected from an aqueous solution of Re RP294 showed the syn diastereomer. When this solution was measured for ^{1}H NMR, the spectrum showed both the syn and

anti diastereomers. Similarly, the diastereomers formed from ^{99}Tc RP294 could not be separated and the distinction between syn and anti was solely based on their proton chemical shifts. With this uncontrolled interconversion, it was not possible to assign the diastereomers to their HPLC profile. However, this is the first evidence to show the diastereomer formation for Tc and Re tripeptide complexes.[72] RP294 was successfully conjugated to receptor binding peptides (tuftsin receptor antagonist: threonyl-L-lysyl-L-proplyl-L-prolyl-L-arginine) via the glycine linker.[73] Tc RP294 Receptor mediated uptake of the Tc complexes were observed and unbound radioactivity showed reasonably good clearance from the kidneys.

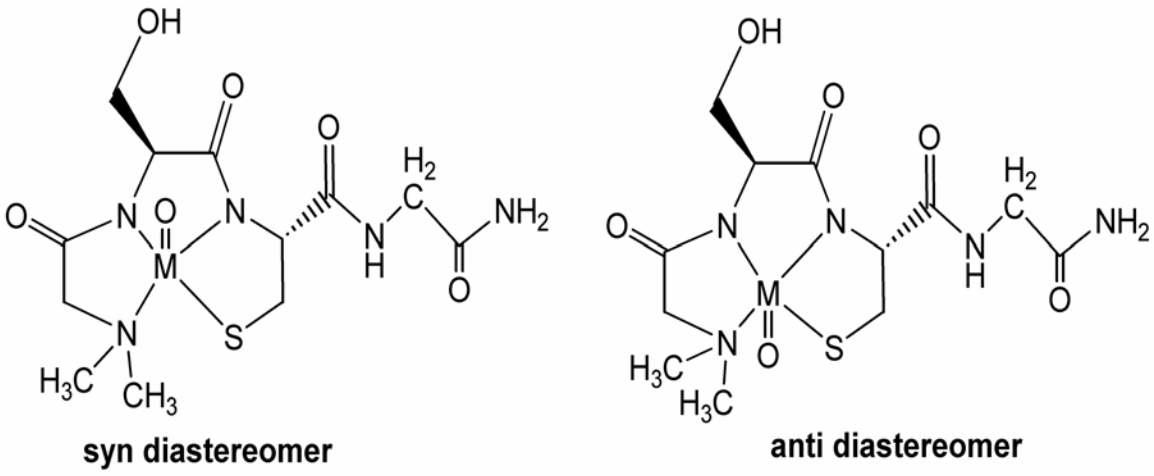

Figure 1-8. The syn and anti diastereomers of MO RP294 (M = ^{99}Tc, Re).

A 7 amino acid bombesin analog was attached to the ^{99} Tc RP294 conjugate via the glycine linker using solid phase synthetic methodology.[63] The bombesin analog targets the GRP receptor, found on tumors of the prostate and breast. A 5-aminovaleric acid spacer was attached to the glycine to form the linker portion; this was attached to the 7 amino acid binding site. On the macroscopic scale, the ^{99}Tc RP290 bombesin derivatives were the same as that for ^{99}Tc depreotide (see below), a yellow and a red compound could be isolated. However, upon standing the color of the fractions became identical over a period of 72 h at room temperature, a consequence of the diastereomer interconversion process that results in approximately equal concentrations of the two diastereomers. The syn and anti diastereomers were assigned based on NMR data.

P829 (Depreotide). P829 is a cyclic hexapeptide containing a somatostatin receptor (SSTR) binding sequence and a linear tetrapeptide. The radiopharmaceutical NeoTect™ (or ^{99m}Tc depreotide) (**Figure 1-9**) which is marketed by Schering AG for diagnosis of lung tumor, is based on this peptide.[31] The tetrapapetide portion with the sequence Dap-Lys-Cys-Lys (Dap = β-diaminopropionic acid) is a site for coordination with technetium. The chelation about the technetium is denoted "N_3S" because the coordinating atoms in the peptide include three nitrogens (two amide nitrogen atoms of Lys and Cys, and one amine nitrogen of Dap), and one sulfur (the thiol sulfur of Cys). Based on previous results for technetium(V) complexes of peptide-based ligands of the N_3S type, the [TcO] depreotide complex is expected to have a distorted square pyramidal structure, with the oxo group perpendicular to the plane of the peptide nitrogen and sulfur coordinating atoms.

Three chiral centers are incorporated into the coordination plane of [^{99}TcO] depreotide. Diastereomeric complexes of technetium (V) are known to form when ligands contain chiral centers on the portion of the chelate which constitutes the coordination plane. For such ligands, the technetium complex can form with the Tc=O group either *syn* or *anti* to the substituents.[72, 74-79] The two possible diastereomers are depicted in **Figure 1-10**. For discussion here, the two diastereomers will be referred to as *syn* or *anti* with regard to the position of the Dap and Lys^2 (the lysine which chelates to the technetium) side-chain relative to the Tc=O bond. Two main products are indeed formed when depreotide peptide is radiolabeled with ^{99m}Tc.

Generally, syn and anti diastereomers exhibit different HPLC profiles, as the specific diastereomer interacts with the HPLC column packing and mobile phases differently. In ^{99m}Tc depreotide, the early eluting peak, labeled "A" was found in ca. 10% yield and the later eluting peak "B" was 90% yield. Interestingly, peak A was pink in color while peak B was yellow. As the complexes were in solution, interconversion was not observed although the colors of the solutions became muted for a period of weeks, suggesting interconversion may have occurred. Their mass spectrometry, infrared spectroscopy and ^{1}H NMR spectroscopy confirm that they are diastereomers. However, the specific assignments of syn or anti could not be made on the basis of these techniques. In the case of ^{99m}Tc depreotide, the diastereomers represented by the early and late eluting peaks exhibited significantly different biological properties, although both have nanomolar affinities for the somatostatin receptor.

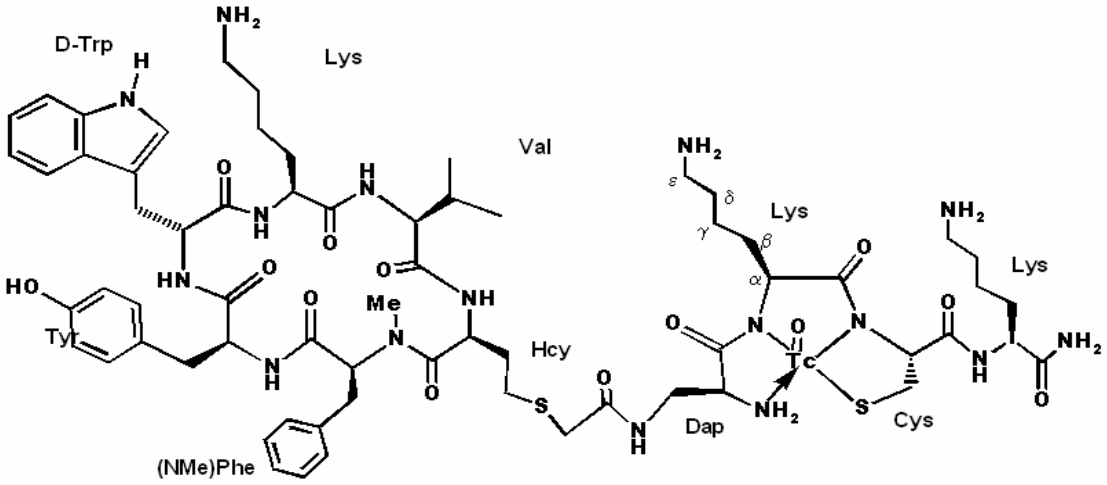

Figure 1-9. General structure of ^{99m}Tc depreotide (NeoTect^{TM})

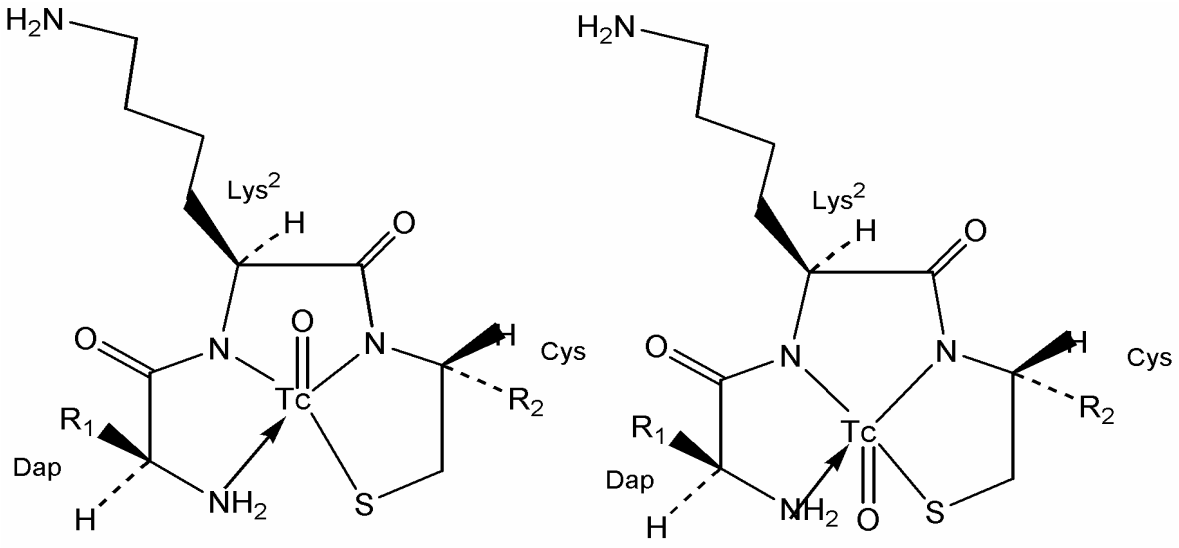

Syn **Anti**

Figure 1-10. Technetium binding regions of TcO depreotide depicting possible syn and anti isomers (syn and anti relative to the Lys side chain).

1.6. Studies of Metallotripeptide Diastereomers as Models for Targeted Radiopharmaceuticals

The general design for targeted radiopharmaceuticals strictly follows two strategies: (i) conjugate approach and (ii) integrated approach (**Figure 1-11)**. Whereas the conjugate design involves appendage of bifunctional chelate (BFC) to biologically active molecules for complexation of ^{99m}Tc, the integrated design involves direct use of biologically active molecules templated by ^{99m}Tc. Both designs are governed by the location of the receptor in the organ or body. For example, if the target receptor is located in the vascular or peripheral system, the receptor-specific radiopharmaceutical does not need to cross the blood-brain barrier (BBB) or cellular membrane. Hence, the size and charge of the radiopharmaceutical are not very critical in this case. If the drug must cross the BBB, however, it must be small, neutral, liphophilic, and stable in vivo. Additionally, the structure of the receptor and the nature of its interaction with the drug define another criterion in designing radiopharmaceuticals. Other concerns are the receptor density, affinity and non-specific binding of the drug.

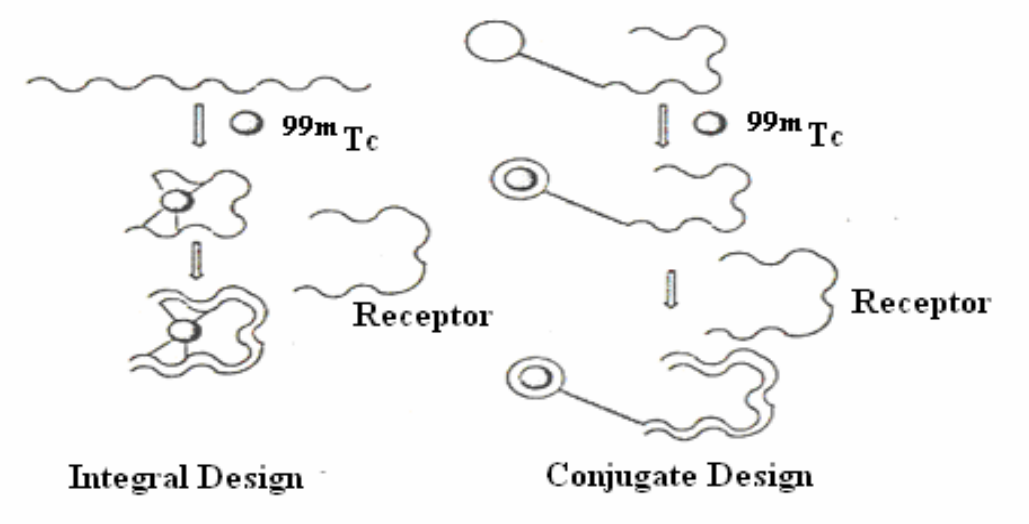

Figure 1-11. The integral and conjugate formats for targeted radiopharmaceuticals.

Incorporation of the radionuclide into the chelate portion of the targeted radiopharmaceutical is called "radiolabeling" or "labeling". Targeted radiopharmaceuticals should be labeled in such a way that their receptor binding properties and biological activity remain unchanged. There are three techniques to label peptides: (i) direct labeling, (ii) pre-labeling (or preformed chelate approach), and (iii) post-labeling (or post-conjugation or final-step-labeling method). These techniques developed for simple and efficient radiolabeling of peptides are based on methods used for radiolabeling of proteins and antibodies. However, the impact of radiolabeling on biological behavior is usually more profound on small peptides than on proteins and antibodies.

With the integrated approach, the direct labeling of peptides is applied. This involves the use of reducing agent to convert disulfide linkages into free thiolates, which

then bind to the ^{99m}Tc metal. A major disadvantage of this method is the lack of control over the coordination of the ^{99m}Tc metal and the stability of the resulting complex. With the conjugate approach, the peptides are labeled by the use of pre-labeling or post-labeling methods. The difference between the two methods lies in the order in which ^{99m}Tc complex is formed. In the post-labeling technique, complexation occurs after the BFC has been attached onto the targeting molecule. With the pre-labeling technique, the ^{99m}Tc complexed by BFC is initially prepared and purified before being attached to the targeting molecule. In both techniques, the BFC must coordinate to ^{99m}Tc to form a complex that is kinetically stable in vivo, and the BFC must have an active moiety (also known as linker) that can react with a functional group on the targeting molecule without altering the radiopharmaceutical's biological properties. Pre-labeling is not suitable for radiopharmaceutical use because there can be many synthetic manipulations after the addition of the radionuclide. "Post labeling" requires only addition of the radionuclide to prepare the radiopharmaceutical, and is suitable for radiopharmaceutical kit formation.

In order to understand the stability and biodistribution of targeted radiopharmaceuticals, it is important to isolate and identify the structures of individual diastereomers. Crystallography has demonstrated its significance as an instrument for elucidating the structures of the small coordination complexes. NMR and other techniques can then be used to expand the structural understanding to other analogs. As it is difficult to crystallize intermediate size peptides, such as depreotide and its metal complexes, the model tripeptides of ^{99}Tc and Re provide a crystallographic standard upon which we can assign the diastereomers of ^{99m}Tc depreotide and a model to begin to understand the chemical biology of the ^{99m}Tc depreotide species.

In this work, we have isolated and characterized the *syn* and *anti* diastereomers of [^{99}Tc/ReO] tripeptides that mimic the binding site of ^{99m}Tc depreotide. We have chosen tripeptide ligands that model the binding site of ^{99m}Tc depreotide, and do not undergo interconversion appreciably so that the diastereomers can be isolated, crystallized and characterized. For consistency with depreotide, the syn and anti designations refer to the positions of the first and second amino acid residues with respect to the Tc=O bond.

Crystallography of the model metallotripeptides, isolated in this study, allow assignment of the specific diastereomers. ^{1}H NMR and Circular Dichroism Spectroscopy of the ^{99}Tc model tripeptide complexes match those of ^{99}Tc depreotide, allowing unambiguous structural elucidation of the $^{99m/99}$Tc depreotide diastereomers and diastereomers formed from tripeptides containing L amino acids.[80] To understand the features of the amino acid residue that stabilize one diastereomer over another in a radiopharmaceutical kit, we have investigated the kinetics and thermodynamic parameters of the diastereomeric interconversion. Finally, this study investigates the influence of the residue on the pK_a of the ^{99}Tc and Re tripeptide diastereomers using proton NMR techniques for pK_a measurements.

1.7. References

1. *Cancer Facts and Figures*. 2005, American Cancer Society.
2. Femia, F. J., *Coordination chemistry of rhenium: design of radiopharmaceuticals for diagnostics and therapeutics in nuclear medicine*. Ph.D. Dissertation, Syracuse University **2001**.
3. Fitzsimmons, J. M., *The synthesis and characterization of metal complexes for imaging and therapy*. Ph.D. Dissertation, University of Columbia **2005**.
4. Rusckowski, M., Qu, T., Gupta, S., Ley, A., Hnatowich, D. J., *Journal of Nuclear Medicine*, **2001**. *42*(12): 1870
5. Blower, P., *Dalton Trans.*, **2006**: 1705.
6. Alberto, R., Pak, J. K., Staveren, D. v., Mundwiler, S. Benny, P., *Peptide Science*, **2004**. *76*(4): 324.
7. Heeg, M. J., Jurisson, S. S., *Acc. Chem. Res.*, **1999**. *32*(12): 1053.
8. Rusckowski, M., Qu, T., Gupta, S., Ley, A., Hnatowich, D. J., *J Nucl Med*, **2001**. *42*(12): 1870.
9. Schibli, R., Schubiger, A., *European Journal of Nuclear Medicine and Molecular Imaging*, **2002**. *29*(11): 1529.
10. Stalteri, M. A., Bansal, S., Hider, R. Mather, S. J., *Bioconjugate Chem.*, **1999**. *10*(1): 130.
11. Thakur, M. L., Kolan, H., Li, J., Wiaderkiewicz, R., Palella, V. R., Duggaraju, R.Schally, A. V., *Nuclear Medicine and Biology*, **1997**. *24*: 105.
12. Lazarova, N., *Technetium and rhenium radiopharmaceutical agents in nuclear medicine: design and synthesis*. Ph.D. Dissertation, Syracuse University **2005**.

13. Riddoch, R. W., *Solid-phase synthesis of radiotracers*. Ph.D. Dissertation, McMaster University **2004**.

14. Safi, B., Mertens, J., Proft, F. D., Alberto, R., Geerlings, P., *J. Phys. Chem. A*, **2005**. *109*: 1944.

15. Volkert, W. A., Hoffman, T. J., *Chem. Rev.*, **1999**. *99*: 2269.

16. Frost, S., *J. Nucl. Med.*, **1998**. *39*(3): 20N.

17. Volkert, W. A., Jurisson, S., *Top. Curr. Chem.*, **1996**. *176*: 123.

18. Deutsch, E., Libson, K., Jurisson, S., Lindoy, L. F., *Prog. Inorg. Chem.* , **1983**. *30*: 75.

19. Melnik, M., Van Lier, J. E., *Coord. Chem. Rev.*, **1987**. *77*: 275.

20. Mazzi, U., *Polyhedron*, **1989**. *8*: 1633.

21. Jurisson, S., Berning, D., Jia, W., Ma, D., *Chem. Rev.*, **1993**. *93*: 1137.

22. Tisato, F., Refosco, F., Bandoli, G., *Coord. Chem. Rev.*, **1994**. *135*: 325.

23. Johannsen, B., Spies, H., *Top. Curr. Chem.*, **1996**. *176*: 79.

24. Frost, S., *J. Nucl. Med.*, **1998**. *39*(2): 27N.

25. Dilworth, J. R., Parrott, S. J., *Chem. Soc. Rev.*, **1998**. *27*: 43.

26. Grewal, R. K., Dadparvar, S., Yu, J. Q., Babaria, C. J., Cavanaugh, T., Sherman, M., Jacobstein, J., *Cancer J.*, **2002**. *8*(5): 400.

27. Morehead, R. S., Shih, W. J., *Clin. Nucl. Med.*, **2001**. *26*(11): 910.

28. Danielsson, R., Baath, M., Svensson, L., Forlov, U., Kolbeck, K. G., *Eur. J. Nucl. Med. Mol. Imaging*, **2005**. *32*(8): 925.

29. Martins, T., Lino, J. S., Ramos, S., Oliveira, L., *Cancer Biother. Radiopharm.*, **2004**. *19*(2): 253.

30. Cholewinski, W., Kowalczyk, J. R., Stefaniak, B., Stefaniak, J., Poniatowicz-Frasunek, E., Tarkowska, A., *Eur. J. Nucl. Med. Mol. Imaging*, **2004**. *31*(6): 820.

31. Cyr, J. E., Pearson, D. A., Nelson, C. A., Lyon, B. A., Zheng, Y., Bartis, J., He, J., Cantorias, M. V., Francesconi, L. C., *manuscript in preparation*.

32. *Ultra-TechneKow DTE (Technetium Tc 99m Generator), Mallinckrodt Medical, Inc., St. Louis, MO 63134*, **1996**.

33. *Technetium Tc 99m Generator, Medi-Physics, Inc., Amersham Healthcare, Arlington Heights, Illinois 60005*, **1997**.

34. Vinberg, N., Kristensen, K., *European Journal of Nuclear Medicine and Molecular Imaging*, **1980**. *5*(5): 435.

35. Patterson II, J. C., Mosley, M. L., *Mol. Imaging Biol.*, **2005**. *0*: 1.

36. Lee, C.-C., Sui, G., Elizarov, A., Shu, C. J., Shin, Y.-S., Dooley, A. N., Huang, J., Daridon, A., Wyatt, P., Stout, D., Kolb, H. C., Witte, O. N., Satyamurthy, N., Heath, J. R., Phelps, M. E., Quake, S. R., Tseng, H.-R., *Science*, **2005**. *310*: 1793.

37. Bandoli, G., Domella, A., Porchia, M., Refoso, F., Tisato, F., *Coord. Chem. Rev.*, **2001**. *214*: 43.

38. Deutsch, E., Libson, K., Vanderheyden, J., Ketring, A. R., Maxon, H. R., *Nucl. Med. Biol.*, **1986**. *13*: 465.

39. *Clinical SPECT Imaging*, ed. E.L. Kramer and J.J. Sanger. 1995, New York: Raven Press.

40. Clarke, M., Podbielski, L., *Coord. Chem. Rev.* , **1987**. *78*: 253.

41. Hom, R. K., Katzenellenbogen, J. A., *Nucl. Med. & Biol.*, **1997**. *24*: 485.

42. Dilworth, J. R. Parrott, S. J., *Radiopharmaceutically relevant chemistry of technetium and rhenium*, in *Current directions in radiopharmaceutical research and development*, 1996, Kluwer Academic Publishers. p. 29.

43. Tisato, F., Porchia, M., Bolzati, C., Refosco, F., Vittadini, A., *Coord. Chem. Rev.*, **2006**.

44. Banerjee, S., Raghavan, M., Pillai, A. Ramamoorthy, N., *Semin. Nucl. Med*, **2001**. *31*(4): 260.

45. Banerjee, S. R., Maresca, K. P., Francesconi, L., Valliant, J., Babich, J. W., Zubieta, J., *Nucl. Med. Biol.*, **2005**. *32*: 1.

46. Alberto, R., Schibli, R., Waibel, R., Abram, U. Schubiger, A. P., *Coord. Chem. Rev.*, **1999**. *190-192*: 901.

47. Bandoli, G., Tisato, F., Dolmella, A. Agostini, S., *Coord. Chem. Rev.*, **2006**. *250*: 561.

48. Perrier, C., Segré, E., *Nature* **1937**. *140*: 193.

49. Harper, P. V., Beck, R., Charleston, D. Lathrop, K. A., *Nucleonics*, **1964**. *22*(1): 50.

50. Harper, P. V., Lathrop, K. A., Richards, P. J., *Nucl. Med.*, **1964**. *16*: 533.

51. Liu, S., Edwards, D. S., *Chem. Rev.* , **1999**. *99*: 2235.

52. Francesconi, L. C., Cantorias, M. V., Howell, R. C., *Metal-based imaging agents*, in *Encyclopedia of Inorganic Chemistry*, Wiley & Sons, in press.

53. Darab, J. G., Smith, P. A., *Chem. Mater.*, **1996**. *8*: 1004.

54. Roodt, A., Libson, K., *J. Nucl. Med.*, **1989**. *30*: 732.

55. Volkert, W. A., Deutsch, E. A., *Adv. Metals Med.*, **1994**. *1*: 115.

56. Johnson, D. L., Fritzberg, A. R., Hawkins, B. L., Kasina, S., Eshima, D., *Inorg. Chem.*, **1984**. *23*: 4204.

57. Vajo, J. J., Aikens, D. A., Ashley, D., Poeltl, D. E., Bailey, R. A., Clark, H. M., Bunce, S. C., *Inorg. Chem.*, **1981**. *20*: 3328.

58. Mahmood, A., Jones, A. G., *Technetium radiopharmaceuticals*, in *Handbook of Radiopharmaceuticals*, 2003, Wiley & Sons.

59. Ehrlich, P., *The collected papers of Paul Ehrlich*, ed. F. Himmelweite, M. Marquard, and H. Dale. Vol. 1. 1956, Elmsford, New York: Pergamon

60. Weiner, R. E., Thakur, M. L., *BioDrugs*, **2005**. *19*(3): 145.

61. Hunter, D. H., Luyt, L. G., *J. Labelled Cpd. Radiopharm.*, **2000**. *43*: 403.

62. Giblin, M. F., Jurisson, S. S., Quinn, T. P., *Bioconjugate Chem.*, **1997**. *8*: 347.

63. Valliant, J. F., Riddoch, R. W., Hughes, D. W., Roe, D. G., Fauconnier, T. K., Thornback, J. R., *Inorganica Chimica Acta*, **2001**. *325*(1-2): 155.

64. Langer, M., Beck-Sickinger, A. G., *Curr. Med. Chem.-Anti-Cancer Agents*, **2001**. *1*: 71.

65. Okarvi, S. M., *Med. Res. Rev.*, **2004**. *24*(3): 357.

66. Francesconi, L. C., Zheng, Y., Bartis, J., Blumenstein, M., Costello, C., DeRosch, M. A., *Inorg. Chem.*, **2004**. *43*(9): 2867.

67. Leonard, J. P., Nowotnik, D. P., Neirinckx, R. D., *J Nucl Med*, **1986**. *27*(12): 1819.

68. Neirinckx, R. D., Canning, L. R., Piper, I. M., Nowotnik, D. P., Pickett, R. D., Holmes, R. A., Volkert, W. A., Forster, A. M., Weisner, P. S.Marriott, J. A., *J Nucl Med*, **1987**. *28*(2): 191.

69. Efange, S. M. N., Kung, H. F., Billings, J., Guo, Y. Z. Blau, M., *J. Nucl. Med.*, **1987**. *28*: 1012.

70. Kung, H. F., *Semin. Nucl. Med*, **1990**. *20*: 150.

71. Kung, H. F., Guo, Y. Z., Yu, C. C., Billings, J., Subraman, V.Calabrese, J. C., *J. Nucl. Med.*, **1989**. *32*: 433.

72. Wong, E., Fauconnier, T., Bennett, S., Valliant, J., Nguyen, T., Lau, F., Lu, L. F. L., Pollak, A., Bell, R. A., Thornback, J. R., *Inorganic Chemistry*, **1997**. *36*(25): 5799.

73. Wong, E., Bennett, S., Lawrence, B., Fauconnier, T., Lu, L. F. L., Bell, R. A., Thornback, J. R.Eshima, D., *Inorg. Chem.*, **2001**. *40*: 5695.

74. Baidoo, K. E., Lever, S. Z., *Bioconjugate Chem.*, **1990**. *1*: 132.

75. Bormans, G., *J. Lab. Comp. Radiopharm.*, **1993**. *33*: 1065.

76. Cyr, J. E., Nowotnik, D. P., Pan, Y., Gougoutas, J. Z., Malley, M. F., Di Marco, J., Nunn, A. D.Linder, K. E., *Inorg. Chem.*, **2001**. *40*(14): 3555.

77. Epps, L. A., *Appl. Radiat. Isot.*, **1987**. *38*: 661.

78. Luyt, L. G., Jenkins, H. A., Hunter, D. H., *Bioconjugate Chem.*, **1999**. *10*: 470.

79. Rao, T. N., *J. Am. Chem. Soc.*, **1990**. *112*: 5798.

80. Cantorias, M. V., Howell, R., Todaro, L., Cyr, J., Rogers, R. D., Francesconi, L. C., *manuscript in preparation.*

2. Synthesis and Purification of Peptides

2.1. Introduction

Peptides are made up of naturally occurring amino acids (α-amino carboxylic acids) linked by amide (peptide) bonds. They are essentially found in mammals in the form of hormonal messengers, steroids, tyrosine derivatives, the catecholamines, and iodinated tyrosines. Peptides that are synthesized in the brain are called neuropeptides as opposed to regulatory peptides which occur in the gut, lymphatic tissue, and endocrine system. Basically, peptides are designed by nature to bind to their specific receptors to perform as messengers or to inhibit or stimulate important life functions. These diverse roles played by peptides have resulted in an increased demand for synthetic short peptide sequences and their analogs to model biological systems.[1, 2]

Peptide synthesis is generally straightforward and short peptides can be synthesized in the lab. There are two standard techniques one can choose. The least popular classical technique known as the solution-phase peptide synthesis is considered complicated, time-consuming and skill intensive due to extensive purification procedures.[3] Alternatively, solid-phase peptide synthesis (SPPS) is the current method of choice for preparing biologically active peptides suitable for drug discovery process. The SPPS has been developed considerably since its introduction by Merrifield in the 1960s.[4] The enormous support for the SPPS format lies on the fact that its methodology is more versatile than the solution phase technique. The ease of manipulation which is innate to the solid phase route, allows the use of excess starting materials aimed at

driving the reactions to completion. In addition, it is often easy to isolate the products due to the ease of filtering off the solid support from the reaction mixture. Other benefits when compared to the solution phase methods are the ease of automation and the pseudo dilution effect[5] which can be synthetically useful in crosslinking or cyclisation reactions.

For our own specific needs, the main approach for the solid-phase synthesis is via continuous-flow process. A continuous-flow technique vis-à-vis a batch technique is usually more desirable as it allows for more homogeneous reaction medium, and eliminates the tedious procedure of manual as well as mechanical shaking required by the batch mode.[6] As a result we have devised a methodology that employs such a technique through the use of standard laboratory equipment[7] such as Pharmacia peristaltic pump, PTFE and Nalgene tubings, and glass columns of varied sizes to suit the amount of peptides required. Our improvised apparatus (**Figure A-1, Appendix Section**) was designed to approach conditions that might be present in a commercial solid phase synthesizer. Standard scintillation vials are used as replaceable reservoirs. Washing of the resin after each stage is accomplished by placing the column on an adapted filter flask. This too constitutes a preferable washing routine to the more familiar batch process. Due to the automated nature of the synthesis, it is possible to leave the device unmonitored for long periods of time which makes this tool ideal for low-budget research.

2.2. Rational for the Design of Tripeptides

Tripeptides synthesized for this study are used as ligands for Tc or Re and contain an N_3S motif. The rationalization of the peptide design is based on cysteine at the carboxylate terminus (**Figure 2-1**). This allows the formation of a 5-membered chelate ring (**Figure 2-2**) when bound to the metal that is considered more stable than a six membered ring that would form if cysteine were at the amine terminus. At least one thiolate donor is necessary to stabilize Tc(V)=O complexes.[8, 9] Upon complexation of Tc(V)=O to tripeptides, the amide protons are lost forming neutral Tc=O complexes with strong amide N-Tc bonds.[10, 11]

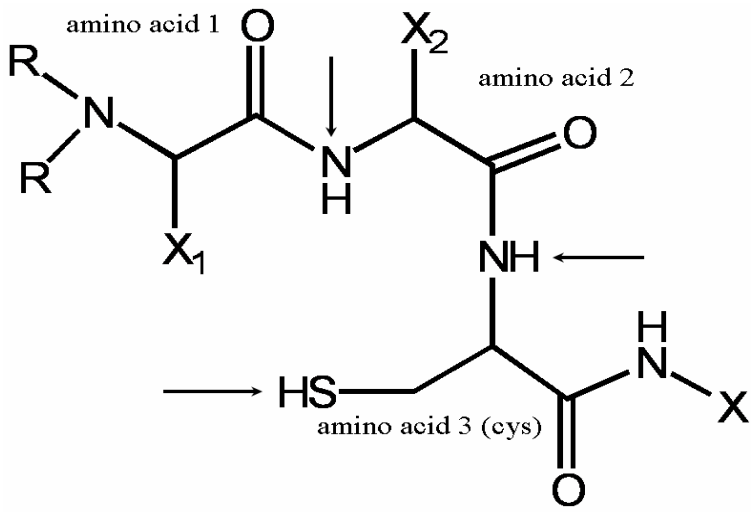

Figure 2-1. Generalized tripeptide with N_3S motif (xxx-xxx-cys where xxx = variable amino acids on position 1 and 2). Deprotonation occurs where the arrows pointed when complexed with radiometal such as Tc or Re.

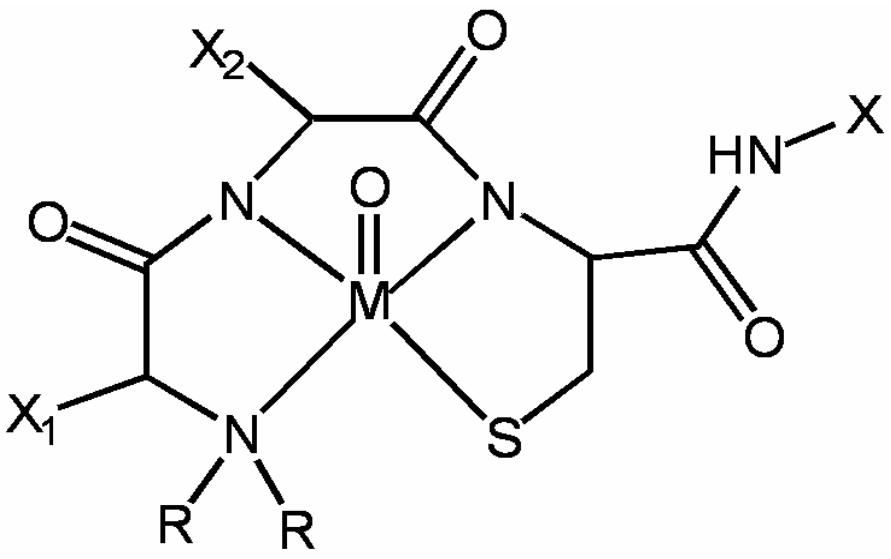

Figure 2-2. Three 5-membered rings making up the structure of [M^{V}=O] tripeptide complexes. The cysteine ring is common to all the models; hence, it can have a signature pattern unique only for anti diastereomers, as well as for syn diastereomers.

In an attempt to isolate diastereomers that are water soluble and would not interconvert rapidly, we hypothesized that we could minimize interconversion by judicious choice of amino acid in the first and second positions of the tripeptide. We also hypothesized that the polarity, stereochemistry and H-bonding capability with Tc=O group may influence the interconversion between diastereomers. Therefore, we prepared tripeptides with amino acids in positions 1 and 2 that varied in size, bulk, polarity and H-bonding opportunity (**Figure 2-1**). For example, we can use phenylalanine or tyrosine as a bulky group. Moreover, the amino group of lysine residue and carboxylic group of aspartic acid residue may display hydrogen-bonding interactions. The following abbreviations are used to represent the L-amino acids for our studies, as recommended by the IUPAC-IUB Biochemical Nomenclature Commission:[12]

Amino Acid	1-Letter Code	3-Letter Code
Aspartic acid	D	Asp
Cysteine	C	Cys
Glycine	G	Gly
Lysine	K	Lys
Methionine	M	Met
Phenylalanine	F	Phe
Serine	S	Ser
Tyrosine	T	Tyr

2.3. Experimental

2.3.1. Materials

Fmoc-protected L-amino acids and Rink amide MBHA resin were purchased from NovaBiochem. N-hydroxybenzotriazole (HBTU) was purchased from ChemTech. 2-(1H-benzotriazole-1-yl)1,1,3-tetramethyluronium (HOBt), N,N-diisopropylethylamine (DIPEA), piperidine, phenol, thioanisole, triisopropylsilane (TIS), and 1,2-ethanedithiol (EDT) were purchased from Sigma-Aldrich. HPLC-grade acetonitrile, trifluoroacetic acid (TFA) and N,N-dimethylformamide (DMF) were purchased from Fisher Scientific. Nanopure water was obtained from a Millipore filtration system equipped with a 0.22 μm filter. All chemicals were used as received without further purification. The ε-benzoyl lysine-glycine-cysteine and P2450 peptides were synthesized at Diatide, Londonderry, New Hampshire.

2.3.2. Instrumentation and Analytical Methods

A RAININ Dynamax HPLC system equipped with a Dynamax UV-1 UV-visible detector and two Dynamax model SD-200 pumps using 25-mL pump heads was employed. All HPLC experiments were monitored at a λ = 220 nm. For both analytical and preparative work, the mobile phase consisted of (A) 0.1 % TFA in H_2O and (B) acetonitrile. For analytical HPLC, the following parameters were used: (1) Column - Waters DeltaPak 5µ C_{18} 100 Å, 3.9 x 150 mm; (2) Mobile Phase Gradient - 0% - 55% B over 30 min; (3) Flow Rate - 1.0 mL/min; (4) Software - Dynamax HPLC Method Manager. For preparative work, the method consisted of Waters DeltaPak 5µ C_{18} 300 Å, 19.0 x 300 mm column and Dynamax HPLC Method Manager. In here, the mobile phase gradient was 0 % - 55 % B over 30 min at a flow rate of 24 mL/min. Mass spectral data were acquired on an Agilent Technologies 1100 Series LC/MSD model G1946D using electrospray ionization in the positive-ion mode.

2.3.3. General Procedure for Preparation of Tripeptide Ligands

The following method is the synthesis of Phe-Gly-Cys (FGC), and this was the general protocol (**Scheme 2-1**) that was used for the other tripeptide ligands. Rink amide MBHA resin (260 mg, 0.203 mmol) was placed in a glass column and a continuous stream of DMF passed through the column for 15 min. The resulting swollen resin was Fmoc-deprotected by passing 40% piperidine solution in DMF through the column for 15 min. All traces of piperidine were removed by washing the resin exhaustively with DMF and methanol on an improvised washing station (**Figure A1, Appendix Section**). The

Kaiser test, also known as ninhydrin test,[13] was performed before and after each amino acid coupling reaction to ensure successful Fmoc removal (**positive result:** dark blue beads and dark blue solution) and complete coupling (**negative result:** white beads and tinge blue solution), respectively. In-situ activation of the first amino acid was carried out by dissolving equimolar amounts (0.608 mmol) of the Fmoc-Cys(Trt)-OH (356 mg), HOBt (82.2 mg), HBTU (231 mg), and DIPEA (106 μL) in DMF (2.0 mL). The activated Fmoc-Cys(Trt)-OH solution was then cycled through the resin-packed column for 4 h. The resin was washed again exhaustively with DMF and methanol. The Fmoc protecting group was removed again before loading the next amino acid. Fmoc-Gly-OH (181 mg, 0.608 mmol) was activated next and passed over the resin for 4 h. Again, the Fmoc group was removed and the final amino acid, Fmoc-Phe-OH (236 mg, 0.608 mmol), was activated and cycled for 4 h. The resin was then further treated with 40% piperidine to remove the terminal Fmoc. The dried resin was transferred into a scintillation vial. The peptide was cleaved simultaneously with the removal of the acid-labile protecting groups using two cocktails: **Cocktail 1**: 0.75 g phenol, 0.25 mL EDT, 0.5 mL water, 0.5 mL thioanisole, and 10 mL TFA; **Cocktail 2:** 9.4 mL TFA, 0.1 mL TIS, 0.25 mL thioanisole, and 0.25 mL water. Cocktail 1 was added to the vial containing the resin and stirred for 3 h. Cocktail 1-resin mixture was quantitatively transferred into 200-mL beaker and ca. 150 mL cold diethyl ether was added into it to precipitate out the tripeptide. The resulting white precipitate and colored-yellow resin were filtered out through a glass frit. The filtrate was discarded and the residue was suspended in Cocktail 2 with stirring for 3 h, followed by peptide reprecipitation in cold ether. Finally, the peptide-resin mixture was filtered out through the glass frit. The

peptide was then separated from the resin by adding a minimum amount of water into the frit. The filtrate containing the dissolved peptide was collected and lyophilized to yield the white powder.

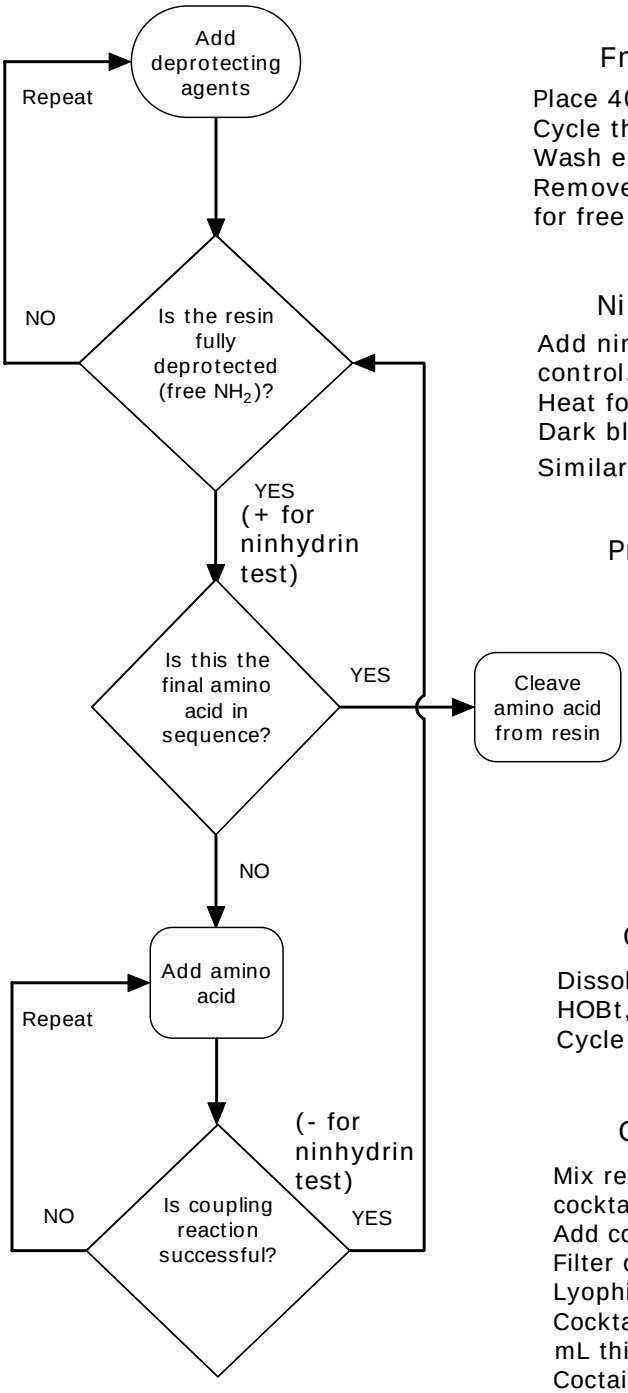

Fmoc Deprotection Procedure

Place 40% piperidine/DMF in vial.
Cycle this solution through system for 15 min.
Wash exhaustively.
Remove small quantity of resin beads and test for free NH_2.

Ninhydrin Test for free NH_2 moiety

Add ninhydrin reagents to resin beads and control.
Heat for 5 min.
Dark blue beads (+)...NH_2 with no Fmoc
Similar color to control (-)... NH2 with Fmoc

Protocol for Washing Resin

Remove vial from apparatus and place on filter flask.
Wash exhaustively with DMF.
Wash exhaustively with methanol.
Wash exhaustively with DMF.
Sample for Ninhydrin test is removed after the wash with methanol.
For cleavage step, the resin is washed again with methanol, air dried, then washed with ether and air dried.

Coupling of Amino Acid

Dissolve equimolar amounts of amino acid, HOBt,HBTU, and DIPEA in DMF.
Cycle mixed solution thru resin for 4 h.

Cleavage of Peptide from Resin

Mix resin with desired peptide in 1st and 2nd cocktails simultaneously for 3 h.
Add cold ether to precipitate peptide.
Filter off resin and collect filtrate.
Lyophilize filtrate to obtain solid peptide.
Cocktail 1: 0.75 g phenol, 0.5 mL water, 0.5 mL thioanisole, 10 mL TFA.
Coctail 2: 9.4 mL TFA, 0.1 mL TIS, 0.25 mL thioanisole, 0.25 mL water.

Scheme 2-1. Summarized Protocol for the Solid-Phase Peptide Synthesis

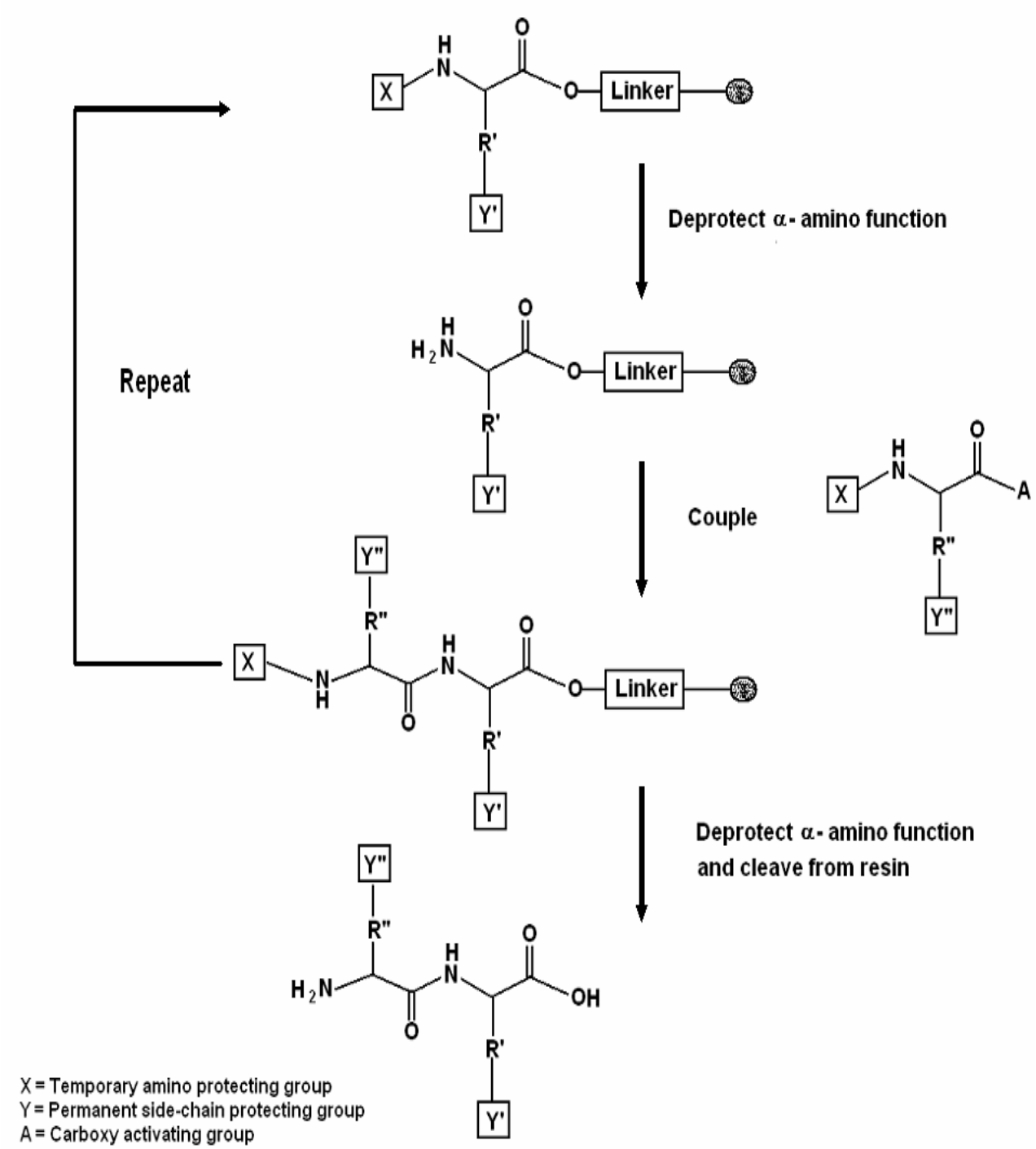

Scheme 2-2. Generalized Approach to Solid-Phase Peptide Synthesis[6]

2.3.4. Purification of Peptides

1 mg of crude peptide was dissolved in 1 mL of nanopure water. A 5-μL aliquot of the peptide solution was then injected onto the reverse-phase HPLC analytical column. If the peptide were less than 95% pure, a preparative HPLC procedure was required.

The conditions of the preparative HPLC are given in the Experimental section, **2.3.2**. Generally about 8 mg of the crude peptide were injected onto the column. Fractions from the HPLC purifications were collected separately in a 50-mL centrifuge tube. The fractions of the same elution time were combined and lyophilized overnight, producing a white powder from each component. Finally, a 1-mg lyophilized product dissolved in 1 ml of nanopure water was prepared and subjected to HPLC and mass spectral analyses.

2.4. Results and Discussion

The SPPS methodology was tailored from various sources, including Chan and White's Fmoc Solid Phase Synthesis.[6, 14, 15] Our protocol adopts a base labile protecting group to the N-α-amino acid, which is called 9-fluorenylmethoxycarbonyl or commonly known as Fmoc. The use of N-α-Fmoc protected amino acids allows preparation of peptides containing acid labile residues or acid sensitive peptide bonds, or in which acid catalyzed side reactions may occur. Generally, all peptides used for our studies were prepared based on the strategy described in **Scheme 2-2**. However, for the tripeptide models, the C-terminus was capped as an amide but the N-terminus was acetylated-free.

The use of the Rink amide MBHA resin (100-200 mesh)[16] should allow this format. The initial Fmoc amino acid was first bound to the Rink amide resin (loading capacity: 0.40-0.80 mmol/g) via an acid labile linker containing norleucine spacer. The second Fmoc amino acid was then coupled without preactivation (*in situ*). After the desired peptide sequence was obtained, the tripeptide-Rink amide support and the base stable side-chain blocking groups were acid cleaved by 83% and 94% TFA sequentially. In addition, three-fold excess of amino acids and coupling reagents were used with respect to the amount of the resin initially calculated. In some isolated cases, five-fold excess of amino acids was necessary to effect successful coupling reaction. To eliminate or at least minimize side-reaction products, a second cocktail containing TIS was carried out to optimize final cleavage reaction. However, transferring precipitated products from the first cocktail to the second must be thoroughly efficient as this may result in the reduction of peptide yields.

The HPLC analysis of the crude FGC revealed about four side-products and a very hydrophilic major product eluted at 5.05 min (**Figure 2-3.1**). The crude sample was then purified using preparative reverse-phase HPLC approach, in which the peptide was monitored at 220-nm wavelength and collected at a 3.35-min retention time. The retention time difference between the analytical and preparative techniques was attributable to the difference in length between the analytical and preparative columns. According to **Figure 2-3.2**, the chromatogram showed a clean HPLC profile (about 98% pure) suggesting a successful purification of the crude peptide. Mass spectral analysis of this sample produced a spectrum (**Figure 2-2.3**) showing an isotopic pattern for FGC, where the highest spectral line corresponds to the formulation [M+H = 325] of the

protonated form of the peptide. By and large, the overall yield of all tripeptides after HPLC purifications was from 75% - 85%. The peptides prepared in this study are: (1) tripeptides containing all L-amino acids - FGC, FKC, FDC, MKC, YKC, YSC, YDC, and YGC (Note: ε-benzoylKGC and P2450 were also included in this study but prepared by Diatide, Inc.); and (2) tripeptides containing at least one D-amino acid – FKc and FkC. The small letter case represents the D-amino acid.

2.5. Conclusion

The improvisation of a semi-automated, solid-phase peptide synthesizer has proven beneficial to our research interest. Our goal to produce peptides in significant quantities had been a major issue until the development of a synthesizer that generates a high yield. This proved to be indispensable as the end result was cost effective and time saving, and has provided flexibility in manipulations for the design of tripeptides.

The existing protocol for the solid-phase peptide synthesis available in the literature was modified to increase efficiency in peptide production. The important added feature to the newly designed protocol was the use of two cleavage cocktail reagents in sequence. This often resulted in high percent purity of the peptides, thus, preparative HPLC purification step was normally skipped from the protocol.

Indeed, we have succeeded in the production of a variety of tripeptide ligands that are sterically bulky, hydrophilic and possess hydrogen bonding capabilities, which are the requirements necessary for clean isolation of Re and Tc tripeptide diastereomers.

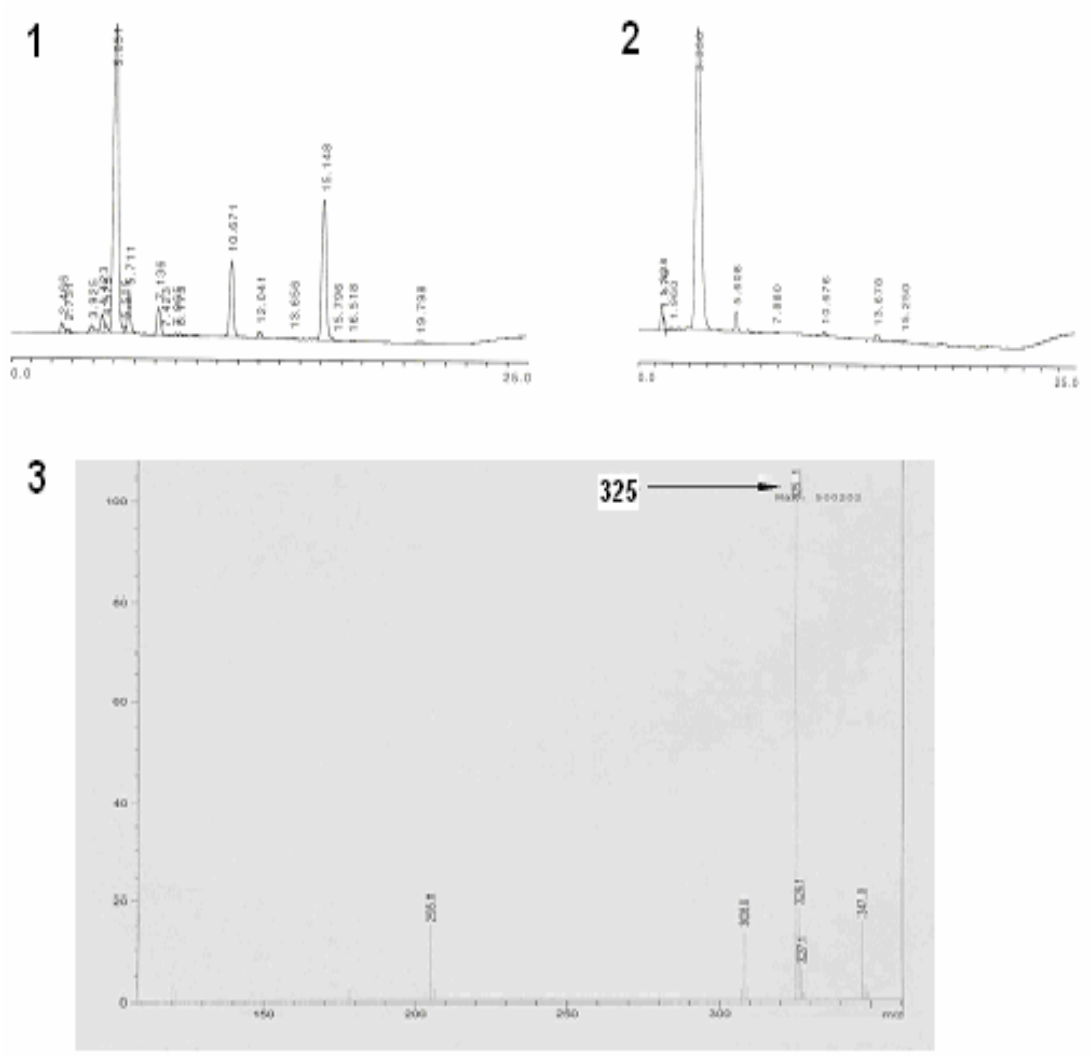

Figure 2-3. Analysis and purification of FGC involves (1) analytical RP-HPLC, (2) preparative RP-HPLC, and (3) Mass Spectrometry.

2.6. References

1. Langer, M., Beck-Sickinger, A. G., *Curr. Med. Chem.-Anti-Cancer Agents*, **2001**. *1*: 71.
2. Costopoulos, B., Benaki, D., Pelecanou, M., Mikros, E., Stassinopoulou, C. I., Varvarigou, A. D.,Archimandritis, S. C., *Inorg. Chem.*, **2004**. *43*: 5598.
3. Okarvi, S. M., *Med. Res. Rev.*, **2004**. *24*(3): 357.
4. Merrifield, R. B., *J. Am. Chem. Soc. 85*: 2149.
5. Jayalekshmy, P., Mazur, S., *J. Am. Chem. Soc.*, **1976**. *98*: 6710.
6. Chan, C., White, P. D., *Fmoc solid phase peptide synthesis*. 2000, New York: Oxfor University Press, Inc.
7. Floyd, C. D., Lewis, C. N., Whittaker, M., *Chem. Brit.*, **1996**. *32*: 31.
8. Bormans, G., Peeters, O. M., Vanbilloen, H., Blaton, N., Verbruggen, A., *Inorg. Chem.*, **1996**. *33*: 6240.
9. Francesconi, L. C., Zheng, Y., Bartis, J., Blumenstein, M., Costello, C., DeRosch, M. A., *Inorg. Chem.*, **2004**. *43*(9): 2867.
10. Bandoli, G., Domella, A., Porchia, M., Refoso, F., Tisato, F., *Coord. Chem. Rev.*, **2001**. *214*: 43.
11. Dilworth, J. R., Parrott, S. J., *Radiopharmaceutically relevant chemistry of technetium and rhenium*, in *Current directions in radiopharmaceutical research and development*, 1996, Kluwer Academic Publishers. p. 29.
12. *IUPAC-IUB Commission of Biochemical Nomenclature in J. Biol. Chem.*, **1972**. *247*: 977.

13. Kaiser, E., Colescott, R., Bossinger, C. D., Cook, P. I., *Anal. Biochem.*, **1970**. *34*(595).

14. Brown, A. R., Herinkens, P. H. H., Ottenheijin, H. C. J., Rees, D. C., *New Tools in Synthesis*, **1998**. *5*: 817.

15. Field, G. B., Noble, R. L., *Int. J. Peptide Protein Res.*, **1990**. *35*: 161.

16. *Novabiochem Catalog 2006/2007*: EMD Biosciences.

3. Synthesis and Characterization of ^{99}TcO Tripeptide Diastereomers

3.1. Introduction

Despite the research activity on targeted Tc radiopharmaceuticals, only two targeted ^{99m}Tc agents based on peptide targeting vectors have been developed and commercialized. We have contributed to the development of both AcuTect™ [1], used for imaging deep vein thrombosis, and NeoTect™ [2], employed for evaluation of lung tumor masses. In both cases, the targeting vector is tethered to a tripeptide chelate containing an N_3S motif that binds the ^{99m}Tc radiometal.

As mentioned in Chapter 1, complexation of ^{99m}Tc=O to chiral peptides almost always results in the formation of diastereomers. This is common to all ^{99m}Tc and ^{188}Re peptide complexes. It is well known that diastereomers can have different biological behavior. Therefore, it is necessary to identify the absolute configuration of the diastereomers for further drug development for diagnosis (^{99m}Tc) or radiotherapy (^{188}Re). Knowledge of the structure of ^{99m}Tc or ^{188}Re peptides, such as depreotide, can also give information on the interaction with the specific receptors. Also, issues of stability can begin to be addressed with some structural knowledge.

In case of NeoTect™ (^{99m}Tc depreotide), two diastereomers are formed in the radiopharmaceutical kit, having distinctly different biological behavior. Isolation of the ^{99}Tc depreotide diastereomers identified the binding site for the Tc and clearly showed that the species were diastereomers. Crystal structures are the only method to identify

absolute configurations of diastereomers. Once the crystal structures of standards are known, then unknowns can be compared by spectroscopic techniques. The problem is that it is difficult to crystallize medium size peptides, such as ^{99m}Tc depreotide, due to the multiple configurations that the molecules can assume in the crystallizing solution. Therefore, to identify the absolute configuration of ^{99m}Tc depreotide diastereomers, as well as for the general ^{99m}Tc tripeptide (L amino acid) case, we have prepared a number of model tripeptide ^{99}Tc complexes. These model tripeptides mimic the binding site in depreotide; in these tripeptides we varied the amino acids (L configuration) always maintaining cysteine at the carboxylate terminus to anchor and stabilize the complex. We have isolated and crystallized the ^{99}Tc diastereomers. Their color profile, reverse-phase HPLC profile and NMR and Circular Dichroism spectroscopy match exactly with depreotide diastereomers. Thus, now the specific structures of the diastereomers of Tc complexes of N_3S tripeptides can be understood. Moreover, we report here two structural types based on deprotonation process as revealed by X-ray crystallography.

3.2. Experimental

3.2.1. Materials

Fmoc-protected L-amino acids and Rink amide MBHA resin were purchased from NovaBiochem. N-hydroxybenzotriazole (HBTU) was purchased from ChemTech. 2-(1H-benzotriazole-1-yl)1,1,3-tetramethyluronium (HOBt), N,N-diisopropylethylamine (DIPEA), piperidine, phenol, thioanisole, triisopropylsilane (TIS), and 1,2-ethanedithiol

(EDT) were purchased from Sigma-Aldrich. HPLC-grade acetonitrile, trifluoroacetic acid (TFA) and N,N-dimethylformamide (DMF) were purchased from Fisher Scientific. Nanopure water was obtained from a Millipore filtration system equipped with a 0.22 μm filter. All chemicals were used as received without further purification. The ε-benzoyl lysine-glycine-cysteine and P2540 peptide were synthesized at Diatide, Londonderry, New Hampshire.

^{99}Tc is a low-energy (0.292 MeV) β^- emitter with a half-life of 2.12 x 10^5 years. This isotope should be handled in a fume hood using appropriate radioactive protocols. $NH_4{}^{99}TcO_4$ was obtained from Oak Ridge National Laboratory, Oak Ridge, TN. 30% H_2O_2 was added to an aqueous solution of $NH_4{}^{99}TcO_4$ to oxidize any $^{99}TcO_2$ present. The ammonium pertechnetate solution was standardized prior to use as previously described.[3] The reagent $[TcOCl_4]N(C_4H_9)_4$ was prepared following a published procedure.[4] ^{99m}Tc-pertechnetate (^{99}Mo/^{99m}Tc generator) was obtained from Cardinal Health (Bronx, NY).

3.2.2. Instrumentation and Analytical Methods

A RAININ Dynamax HPLC system equipped with a Dynamax UV-1 UV-visible detector and two Dynamax Model SD-200 pumps using 25-mL pump heads was employed. All HPLC experiments were monitored at a λ = 220 nm. A home-built detector composed of Tennelec Minibin components such as power supply, high voltage supply, and amplifier, was interfaced to the HPLC system to monitor gamma (γ) ray of ^{99m}Tc. For both analytical and preparative work, two mobile phase systems were used.

Mobile phase system 1 (MBS-1) consisted of (A) 0.1 % TFA in H_2O and (B) 100% acetonitrile. Mobile phase system 2 (MBS-2) consisted of A) 0.1 % TFA in H_2O and (B) 0.1 % TFA in 90:10 acetonitrile:water. For analytical HPLC, three methods were used: **Method 1** – Column: Waters DeltaPak 5µ C_{18} 100 Å, 3.9 x 150 mm; MBS-1 Gradient: 0% - 55% B over 30 min; Flow Rate: 1.0 mL/min; Software: Dynamax HPLC Method Manager**;** **Method 2** – Column: Waters XTerra 5µ C_{18} 100 Å, 3.9 x 150 mm; MBS-1 Gradient: 0 % - 55 % B over 15 min; Flow Rate: 1.0 mL/min; Software: ProStar WorkStation; **Method 3** – Column: Waters DeltaPak 5µ C_{18} 100 Å, 3.9 x 150 mm; MBS-2: 4% - 8% B over 15 min, then 8% - 30% B over 2 min; Flow Rate: 1.0 mL/min; Software: Star Chromatography Workstation Version 6.

For preparative work, **Method 4** consisted of Waters DeltaPak 5µ C_{18} 300 Å, 19.0 x 300 mm column and the software used was Dynamax HPLC Method Manager; the mobile phase gradient (MBS-1) was 0 % - 55 % B over 30 min at a flow rate of 24 mL/min. Finally, **Method 5** was carried out with the following parameters: Column: Waters DeltaPak 5µ C_{18} 300 Å, 19.0 x 300 mm; MBS-2 Gradient: 4% - 8% B over 30 min, then 8% - 30% B over 4 min; Flow Rate: 24.0 mL/min; Software: Star Chromatography Workstation Version 6.

The ^{99}Tc compounds were analyzed at the University of Illinois Mass Spectrometry Center. Infrared spectra were recorded from KBr disks on a Perkin Elmer 1600 FT-IR spectrometer in the range 600 - 3000 nm and were referenced to polystyrene film. Proton NMR spectra including TOCSY (total correlation spectroscopy), NOESY (nuclear Overhauser effect spectroscopy), as well as COSY (correlation spectroscopy) were recorded on a Varian Inova 500-MHz NMR spectrometer at T = 296 K. The

chemical shift was referenced to H_2O as an internal reference. Circular Dichroism spectra of methanolic solutions of the ^{99}Tc tripeptides were collected on a JASCO-J710 spectropolarimeter where the optical system was fed by a pre-purified nitrogen compressed gas at a flow rate of 5 L/min.

3.2.3. Synthesis of $^{99}Tc^{V}O$ [Phe-Gly-Cys] (TcO FGC) and Other ^{99}Tc Tripeptides Complexes

20.5 mg (0.041 mmol) of $N(C_4H_9)_4[^{99}TcOCl_4]$ was dissolved in 2 mL methanol. 14.6 mg (0.045 mmol) of FGC and 6.2 mg (0.075 mmol) of sodium acetate were combined. The methanolic $^{99}TcOCl_4^-$ solution was then added to the peptide-acetate solid mixture. This resulted in a dark purple solution which was analyzed on the HPLC using Method 1, *vide supra*, resulting in two major peaks. Isolation and purification was subsequently accomplished using semi-preparative HPLC following Method 4, *vide supra*. Two distinct colors were observed during fraction collection and after lyophilization. The first eluting compound was pink in color and the late eluting compound was yellow. The powders that resulted from lyophilization were also pink for the early eluting compound A and yellow for the later eluting compound B. Pentane-vapor-diffusion technique was also used here to grow crystals for x-ray analysis. The same method was used for the synthesis of other ^{99}Tc tripeptide complexes.

3.2.4. General Crystallization Procedure for ^{99}Tc Tripeptide Complexes for X-Ray Crystal Structure Experiments

3 mg of sample was dissolved in a 2-mL vial with a minimum amount of ethylacetate or methylene chloride. A few drops of ethanol were added to completely dissolve the sample. The small vial was placed without a cover into a 20-mL vial containing about 5 mL pentane. The larger vial was then capped and allowed to stand at 10 ^{o}C. Crystals were formed within days.

3.2.5. Synthesis and Crystallization of $^{99}Tc^{V}O$ Benzoyl [ε-Lys-Gly-Cys] ($^{99}Tc^{V}O$ Benzoyl KGC)

This synthesis and crystallization was performed by L. C. Francesconi and is included here because this complex aids in elucidating the crystallographic patterns seen by the diastereomers. The peptide, 9.8 mg, 0.024 mmol, was dissolved in 0.5 mL methanol. To this stirring solution 0.71 mL of a 0.034 mM $Na[^{99}TcO(ethyleneglycol)_2]$ in methanol stock solution was added. The solution immediately turned yellow brown and was capped and stirred for 5 hours. Two fractions were collected by preparative HPLC (32-34 min and 39-42 min). As for the aqueous preparation, the first eluting peak was pink and the late eluting peak was yellow. The fractions were lyophilized to form powders. Also, as for the aqueous ^{99}Tc preparations, the powders resulting from the lyophilization were pink for the early eluting compound A and yellow for the later eluting compound B. Crystallization of compound B was achieved by evaporation of a methanol-acetonitrile solution.

3.2.6. Synthesis of $^{99}Tc^{V}O$ P2540: The Actual Metal Chelate Moiety of TcO Depreotide

In a microcentrifuge tube, 16.5 mg P2540 peptide was dissolved instantly in 200 μL nanopure water. In another microcentrifuge tube, 10.36 mg $NH_4{}^{99}TcOCl_4$ was dissolved in 200 μL methanol following the addition of 5 drops of ethylene glycol (eg) forming a clear, blue solution. This ^{99}Tc eg solution was then added to the water-based peptide drop-by-drop with a pasteur pipette. The final solution turned yellow-orange instantly. After several minutes upon standing, it changed to dark-brown. The crude solution was checked immediately on an analytical HPLC using **Method 3**. This gave two major products, the early eluting Product A and the late eluting Product B.

200 μL of the crude solution prepared above was injected onto the preparative column using **Method 5**. The total run time for this method was 40 min. As expected, two major peaks that were considered diastereomers appeared at 20 and 27 min. Likewise, we call the early eluting compound Product A and the late eluting compound, Product B. Two minor peaks at 34 and 35 min were apparently observed. Interestingly, the void volume at 3 min showed a peak that may contain unreacted TcO. Two fractions of Product A (pink) and three fractions of Product B (yellow) were collected and lyophilized immediately. The colors of the solid products were also pink and yellow for Products A and B, respectively. Fractions for minor peaks and void volume were also collected and lyophilized but only Product A and Product B were characterized.

3.2.7. Radiolabeling of Tripeptides with ^{99m}TcO

To a 1.5-mL microcentrifuge tube, 25 μL of the tripeptide solution (0.6 mg/mL in saline) and 10 μL of sodium tartrate (50 mg/mL in ammonium buffer which contains 0.5 M NH_4CO3, 0.25 M NH_4OAc, and 0.18 M NH_4OH) were added and mixed. In a lead shielded fumehood, the tripeptide-tartrate solution was radiolabeled by adding 100 μL of sodium pertechnetate containing 500-600 μCi, and followed by 5 μL $SnCl_2 \cdot 2H_2O$ (1 mg/mL in 0.01 M HCl). The solution (pH 8) was vortexed briefly, heated for 30 min in a boiling water bath, and cooled down for 2 min. HPLC analyses, monitoring the γ ray, were generally performed with a ca. 35-μCi sample.

3.2.8. Procedure for Analysis of ^{99}TcO Tripeptide Complexes

3.2.7.1. NMR Spectroscopy

For samples taken in acidic aqueous solvents, about 3 mg of ^{99}Tc diastereomer was dissolved in 600 μL of 0.01 M HCl. 60 μL of D_2O (from 700-μL ampoule package, Cambridge Isotope Lab) was then added to the acidified solution. The sample solution was transferred into a 5-mm NMR tube. One-dimensional H-NMR spectra were collected at 64 scans. 2D NMR (COSY, TOCSY, and NOESY) were collected at 128 scans for each spectrum.

For samples taken in organic solvents, about 3 mg of ^{99}Tc diastereomer was dissolved in 650 μL of DMSO-d6 (from 700-μL ampoule package, Cambridge Isotope Lab). The sample solution was transferred into a 5-mm NMR tube. One-dimensional

^{1}H-NMR spectra were collected at 64 scans. 2D NMR (COSY, TOCSY, and NOESY) were collected at 128 scans for each spectrum.

3.2.7.2. Circular Dichroism Studies

1 mg of ^{99}Tc tripeptide complex was dissolved in 1 mL methanol. 250 μL of the aliquot was placed in a 250-μL CD cell. The sample was scanned from 170 - 600 nm with +/- 50 degree sensitivity. The CD spectra were collected with baseline and background corrections using pure methanol.

3.2.7.3. HPLC Co-elution Studies

5 μL of the prepared ^{99}Tc tripeptide crude mixture was withdrawn into a 25-μL Hamilton syringe. To the same syringe, a volume containing ca. 35-μCi dose of the analogous ^{99m}Tc tripeptide solution was added. The total volume was injected into the HPLC system. The co-elution, monitored by UV for the ^{99}Tc species and radiometric (γ) detection for the tracer ^{99m}Tc species, demonstrates that, under the HPLC conditions, the two species are chemically identical.

3.3. Results and Discussion

3.3.1. Synthesis and Isolation of ^{99}TcO Tripeptides

On the basis of our hypothesis and others' previous work, we designed tripeptide ligands of N_3S motif whose first and second amino acid residues are sterically bulky and provide hydrogen bonding capabilities while maintaining water solubility of the resulting complexes to closely mimic ^{99}Tc depreotide. Thus, the minimal interconversion was expected and indeed, observed. Moreover, we found that interconversion of diastereomers was accelerated in base and minimized in organic solvents and under acidic conditions, *vide infra*. Therefore we could isolate pure diastereomers by using acidic mobile phases and organic conditions for the preparation and crystallization of the diastereomers. Employment of either organic or acidic aqueous solvent, crystallization of the diastereomers can be possibly realized.

The reaction of $Tc^{V}O$ with tripeptides in methanol was conducted at room temperature. The addition of sodium acetate facilitated deprotonation. In the absence of acetate, the reactions still proceeded as expected because the metal ions have a closed shell d^2 electronic configuration and easily accept π electron density from the deprotonated amide and thiol groups.

The synthesis of most of the ^{99}TcO tripeptide complexes, except for the FKC complex, produced two major products in 1:1 ratio. For the FKC complex, the ratio of the two species was 1:9. According to an HPLC chromatogram (**Figure 3-1**), we generally assigned the early eluting compound as Product A and the late eluting compound as Product B. These products were isolated on a preparative reverse-phase HPLC using **Method 4**, and lyophilized to form powders. Diastereomers A and B of the Tc tripeptides were strikingly different. Either in solution or lyophilized state, Product A

was pink in color while Product B was yellow (**Figure 3-2**). This color profile for the two species of Tc complexes has been noted previously. For example, ^{99}Tc RP290-bombesin derivatives formed yellow and red fractions that each turned to a brown color over 3 days at room temperature, indicating that the diastereomers were undergoing interconversion.

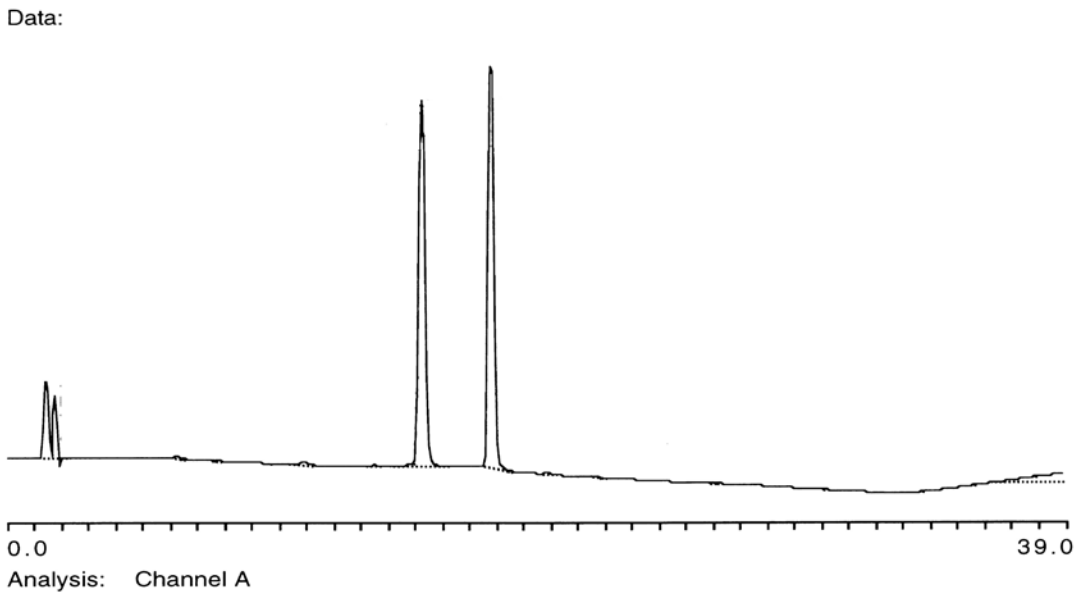

Figure 3-1. Reverse-Phase HPLC analysis of ^{99}Tc FGC using Method 1, Section 3.2.2. The retention times of the early eluting compound A and the late eluting compound B are 15.2 and 17.6 min, respectively.

The reaction of Na [TcO(ethyleneglycol)$_2$] with the peptide ε-lys-gly-cys in methanol yielded two complexes that were isolated by prep HPLC; the complexes were

not water soluble, but soluble in acetonitrile and slightly soluble in methanol. Crystallization of the yellow peak B was from slow evaporation of an acetonitrile solution. Attempted crystallization of compound A (pink) did not yield X-ray quality crystals.

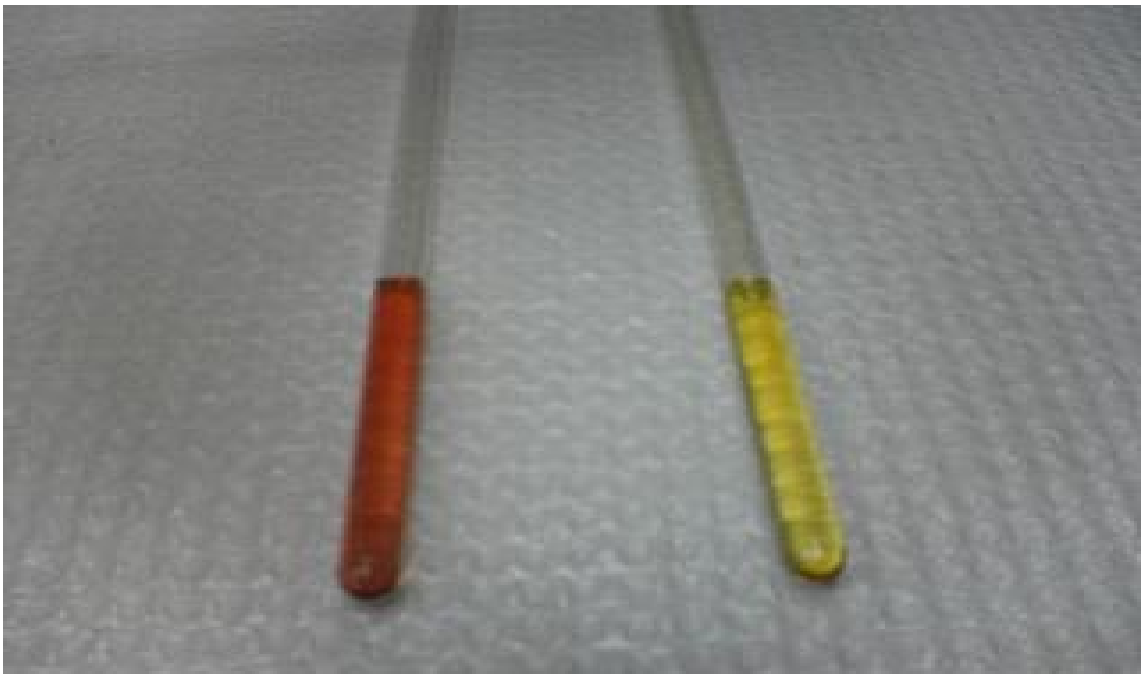

Figure 3-2. ^{99}TcO FKC Product A (left) and ^{99}TcO FKC Product B (right) dissolved in DMSO-d6 for NMR analysis. Product A identified later as anti is pink in both liquid and solid states. Solid and liquid Product B identified as syn are both yellow.

Infrared spectroscopy data were consistent with the formulations for the diastereomers. The ^{99}Tc=O tripeptides showed a $\nu_{Tc=O}$ stretch at 940 cm^{-1} which is

consistent with other Tc(V)=O square pyramidal, nitrogen-sulfur neutral complexes. HPLC retention time and IR data are given in **Table A1** (**Appendix Section**).

3.3.2. Synthesis of Tracer ^{99m}TcO Complexes

The tracer ^{99m}TcO complexes were synthesized by reduction of $^{99m}TcO_4^-$ with stannous ion. Analytical HPLC generally showed that two peaks corresponding to the 2 diastereomers form. **Figure 3-3** shows the HPLC concordance experiment of $^{99m/99}$TcO FKC where the tracer ^{99m}Tc peptide complexes co-elute with the ^{99}Tc peptide complexes, thus verifying that the structure and chemistry of the tracer is the same as the macroscopic compound under these conditions. The kit was prepared at room temperature. Upon heating the kit at 100 ^{o}C for 15 minutes, only the second peak (B) was present. This experiment suggests that the species B that we identified as the "syn" diastereomer, *vide infra*, is more stable than the "anti" diastereomer.

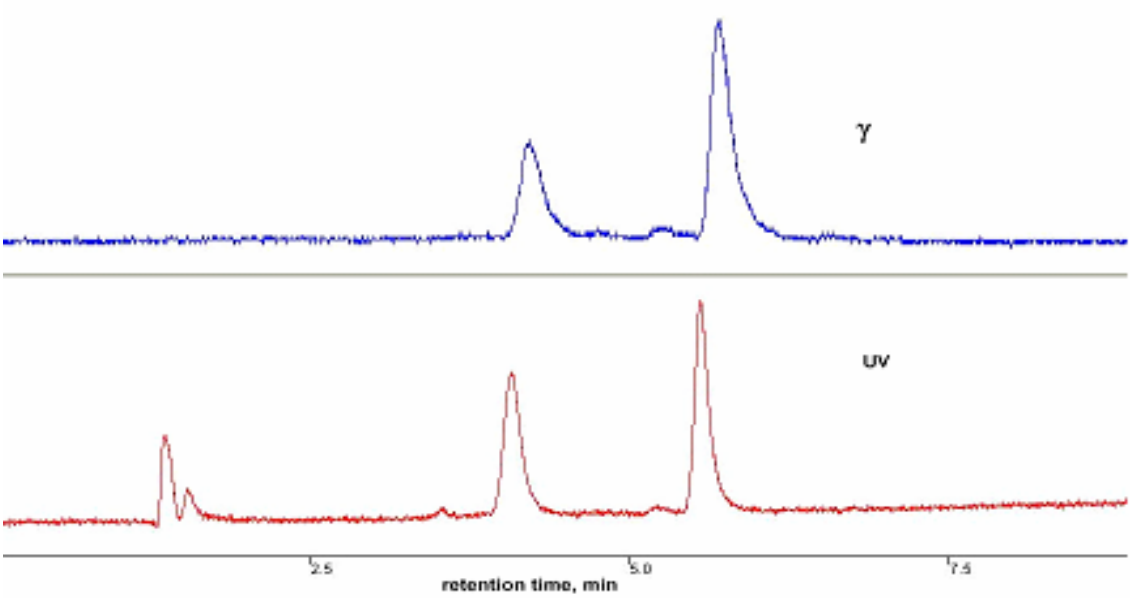

Figure 3-3. HPLC coelution studies of $^{99/99m}$TcO FKC. Top trace: gamma detection of ^{99m}TcO FKC; bottom trace: UV detection of ^{99}TcO FKC. The co-elution indicates that the complexes on the tracer scale possess the same structure and chemistry as the characterized complexes on the macroscopic scale.

3.3.3. X-ray Crystallography of ^{99}TcO Compounds

X-ray crystal structure of the "anti" diastereomer (A) for ^{99}TcO FGC, and of the "syn" diastereomer (B) for ^{99}TcO ε-benzoyl KGC were performed. The X-ray crystal structures of the A and B compounds correspond to the early and late eluting peaks on the HPLC chromatogram, respectively. The X-ray crystal structures show that the early eluting complex is the "anti" diastereomer and the later eluting complex corresponds to the "syn" diastereomer. The samples did not undergo interconversion during the crystallization process as verified by analytical HPLC taken on samples during crystallization as well as on the crystalline sample.

The crystal and structure refinement data for the ^{99}Tc TcO FGC anti and TcO ε-benzoyl KGC syn are given in **Table 3-1** and for ^{99}TcO YKC syn, crystallized from aqueous solution, are provided in **Table A2** (**Appendix Section**). Selected bond lengths and angles for Tc diastereomers are listed in **Table 3-2;** and deviations of the amine and amide nitrogen atoms and the thiolate sulfur from the square plane constructed from these atoms are listed in **Table 3-3.** Ball and Stick diagrams for the crystal structures of Tc diastereomers are given in **Figure 3-4**, and ORTEP diagrams for the three species are presented in **Figure A2** (**Appendix Section**).

Table 3-1. Crystal and structure refinement data for ^{99}TcO tripeptide diastereomers.

	TcO FGC anti	**TcO (εK)GC syn**
empirical formula	C14 H19 N4 O5 S Tc	C18 H26 N5 O6 S Tc
Fw	453.39	538.5
Cryst syst	orthorhombic	Orthorhombic
space group	P2(1) 2(1) 2(1)	P2(1)2(1)2(1)
Temp, K	100(2)	173(2)
wavelength, Å	0.71073	0.71073
a, Å	6.6340(13)	8.8731(1)
b, Å	14.613(3)	11.4664(2)
c, Å	18.220(4)	21.2205(3)
α, deg	90	90
β, deg	90	90
γ, deg	90	90
V, Å^3	1766.3(6)	2159.03(5)
Z	4	4
Calcd density, g/cm^3	1.705	1.657
abs coeff, mm^{-1}	0.966	0.809
F (000)	920	1104
θ range, deg	3.00–27.47	1.92–27.80
limiting indices	-8 ≤ h ≤ 8 -18 ≤ k ≤ 18 -23 ≤ l ≤ 23	-8 ≤ h ≤ 11 -14 ≤ k ≤ 14 -27 ≤ l ≤ 20
reflns collected/unique	3869 / 3869 [R(int)=0.0000]	13189 / 5043 [R(int)=0.0502]
refinement meth	full-matrix least-squares on F^2	full-matrix least-squares on F^2
data / restraints / parameters	3869 / 0 / 226	5038 / 0 / 281
GOF on F^2	1.097	1.193
final R indices [I>2σ(I)]	R1= 0.0372 wR2=0.0858	R1=0.0507 wR2= 0.0950
R indices (all data)	R1=0.0454 wR2= 0.0911	R1=0.0493 wR2= 0.0829
largest diff.peak and hole (eÅ^{-3})	0.664 and –0.809	0.686 and –0.559

Table 3-2. Selected Bond Lengths (Å) and Bond Angles (deg) for ^{99}Tc Tripeptide Diastereomers. (1 = ^{99}TcO FGC anti; 2 = ^{99}TcO (εK)GC syn; 3-5 = ^{99}TcO YKC syn).

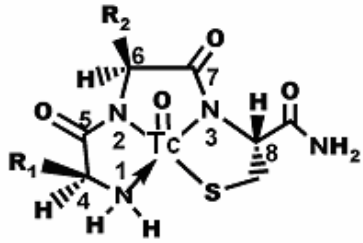

syn (εKGC)

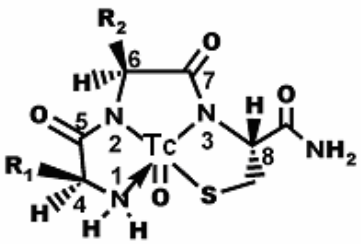

anti (FGC)

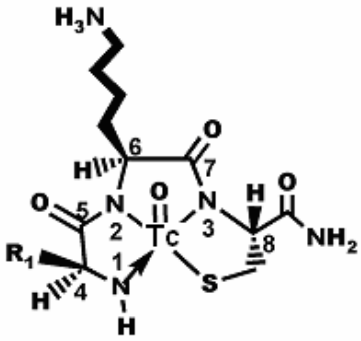

syn (YKC)

Bond Length, Å	**1**	**2**	**3**	**4**	**5**
M-O	1.678(5)	1.664(3)	1.678(3)	1.687(3)	1.655(3)
M-S	2.2828(17)	2.2814(14)	2.2975(13)	2.2747(13)	2.3005(13)
M-N1	2.103(5)	2.111(4)	1.910(4)	1.922(4)	1.911(4)
M-N2	1.980(5)	1.980(4)	1.998(4)	1.993(4)	1.994(4)
M-N3	1.965(5)	1.987(4)	2.027(3)	2.015(4)	2.037(4)
N1-C4	1.479(13)	1.511(6)	1.456(6)	1.442(6)	1.447(7)
Bond Angle, deg					
N1-M-N2	77.5(4)	76.93(16)	78.79(16)	78.42(16)	78.67(17)
N1-M-S	92.8(2)	88.53(12)	89.76(12)	89.76(12)	89.78(13)
N2-M-N3	79.3(2)	78.15(16)	77.42(15)	77.78(14)	77.16(15)
N3-M-S	82.46(15)	82.69(12)	82.05(11)	81.85(12)	81.55(11)
O-M-N1	107.8(4)	114.76(16)	110.92(16)	112.76(19)	112.8(2)
O-M-N2	112.4(2)	113.39(18)	113.16(16)	110.20(16)	110.88(15)
O-M-N3	110.4(2)	113.63(17)	113.44(15)	115.48(17)	114.98(17)
O-M-S	111.07(16)	108.64(13)	110.23(13)	109.85(12)	110.37(12)
C5-N2-C6	121.2(6)	120.5(4)	121.5(4)	123.6(4)	124.1(4)
C7-N3-C8	115.1(5)	115.9(4)	117.0(4)	117.7(4)	117.1(4)
C5-N2-M	121.8(5)	121.0(3)	120.8(3)	120.2(3)	118.8(3)
C6-N2-M	117.0(4)	118.4(3)	116.8(4)	115.3(3)	115.9(3)
C7-N3-M	118.6(4)	119.6(3)	118.7(3)	118.2(3)	118.1(3)
C8-N3-M	124.6(4)	123.1(3)	123.5(3)	123.9(3)	124.3(3)
C4-N1-M	111.7(5)	111.0(3)	118.5(3)	119.7(3)	119.5(3)
C5-C4-N1	109.6(6)	107.7(4)	108.2(4)	108.3(4)	107.0(4)

Table 3-3. Deviations of the N_3S from the square plane for ^{99}Tc diastereomers.

	TcO FGC anti	Tc(εK)GC syn	TcO YKC syn 1
S	0.0861	0.0321	-0.0187
N1 (amine)	-0.0955	-0.0356	0.0214
N2 (amide)	0.1159	0.0431	-0.0249
N3 (amide)	-0.1065	-0.0396	0.0222

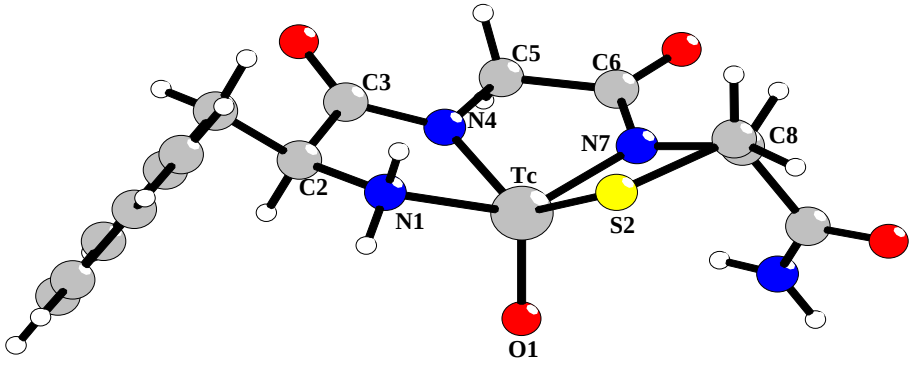

^{99}TcO FGC anti

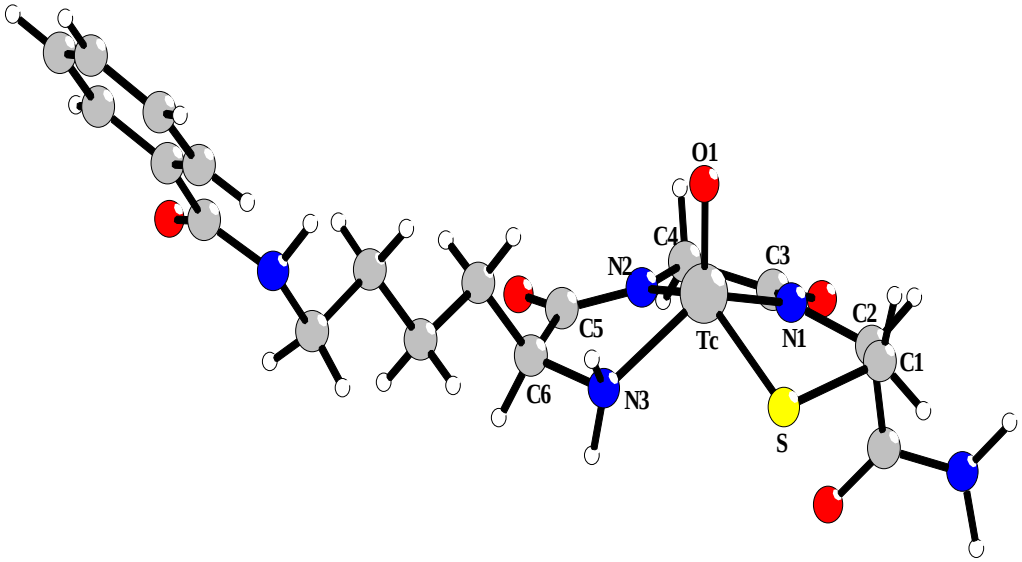

^{99}TcO (εK)GC syn

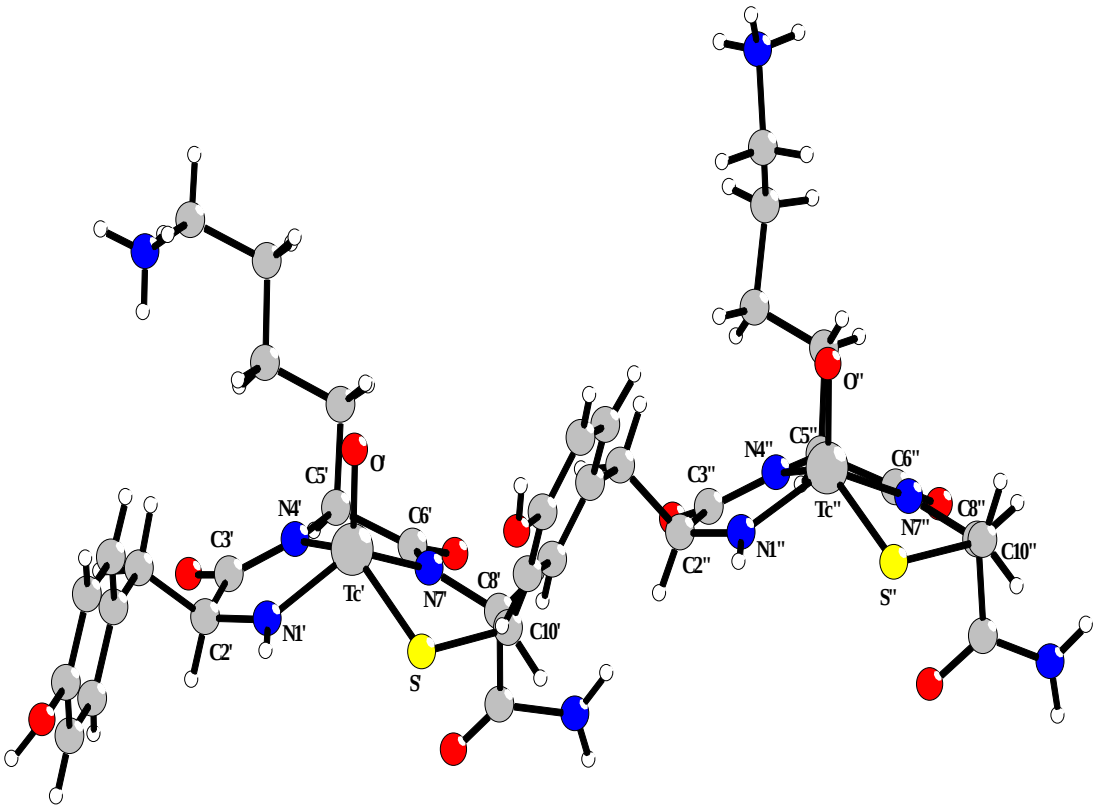

^{99}TcO YKC (2 of the 3 independent molecules, prepared under highly basic aqueous conditions)

Figure 3-4. Ball and Stick diagrams for the crystal structures of selected TcO tripeptide diastereomers.

Interestingly, the X-ray crystallography revealed two structural types that are related by a deprotonation process. The TcO FGC and TcO ε-benzoyl KGC complexes, crystallized from organic solution, exhibit one type of structure where the N_1 of the first amino acid (phenylalanine for FGC and ε-benzoyl lysine for KGC) is an amine nitrogen. In contrast, the TcO YKC, crystallized from highly basic aqueous solution, shows a different solid-state structure wherein the N_1 of the tyrosine is deprotonated and exhibits

multiple bonding with the ^{99}Tc. Studies strongly suggest that in acidic and organic solution the N_1 of the TcO YKC is in the amine form. The same phenomenon was observed for the ReO analog. Detailed discussions on technetium X-ray crystallography in comparison with the rhenium X-ray crystallography are found in the next chapter.

3.3.4. Details of the NMR Spectroscopy of ^{99}Tc Compounds and Comparison to ^{99}Tc depreotide

Proton NMR spectra of the ^{99}Tc complexes, taken in acidic solution, taken together with the crystal structures are diagnostic of the specific ^{99}Tc diastereomer. All of the protons for the ^{99}Tc model peptides have been assigned and are presented in **Table A3** (**Appendix Section**). We do not often observe the amine protons, even in H_2O, as these tend to exchange rapidly. We attribute this to exchange of the amine protons in aqueous solution. Such exchange leading to the absence of the amine protons is a common occurrence which is known to be dependent on factors such as pH and concentration. We do observe, however, the amide protons that cap the carboxylate terminus, but not the amide protons of the amino acids 2 and the cysteine. This is consistent with the loss of these protons on metal complexation.

Upon reaction with ^{99}Tc, two diastereomers are formed and the protons of the three chelate rings formed by the tripeptide are shifted from the free peptide. The chemical shifts and coupling constants are in agreement with previous studies that report ^{99}Tc tripeptides, although in those cases, the diastereomers have not been unambiguously assigned.[5-7] The first and second amino acids do not give much information about the

diastereomer identification. However, the alpha protons of the third (cysteine) amino acids for the anti diastereomers are shifted to higher frequency compared to the uncomplexed peptide. Moreover, the alpha and beta protons of the cysteine show distinct patterns for the syn and anti diastereomers of ^{99}Tc tripeptide complexes that are consistent with ^{99}Tc depreotide.

The chemical shifts for the alpha (α) and beta (β) cysteine protons for Tc peptide diastereomers tabulated in **Table 3-4**, reveal a signature that is similar to Tc depreotide diastereomers. The α-proton resonances are significantly downfield shifted for anti diastereomers compared to syn diastereomers. Also, the β-proton resonances for anti diastereomers are split into a doublet or a doublet of doublets, while the syn diastereomers exhibit a single β-proton resonance. The chemical shifts and the splitting are consistent with previous studies of TcO tripeptides and with the study of ^{99}Tc depreotide.

Table 3-4. Comparison of proton NMR data for the α and β protons of cysteine for ^{99}TcO tripeptides and ^{99}TcO depreotide.

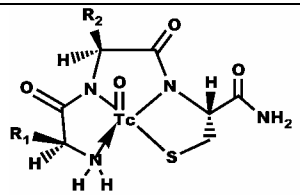

Syn Diastereomer

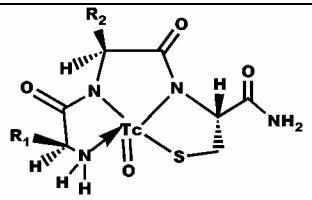

Anti Diastereomer

	^{99}Tc Peptide	R_1	R_2	$\delta_{Cys\ \alpha\text{-}H}$ (ppm)	$\delta_{Cys\ \beta\text{-}H}$ (ppm)	J_{Cys} (Hz)
ANTI (Product A)	^{99}Tc FGC	$-CH_2C_6H_5$	-H	5.58 (dd)	3.53, 3.71	$J_{H\alpha\text{-}H\beta1} = 7.8$, $J_{H\alpha\text{-}H\beta2} = 3.7$, $J_{H\beta1\text{-}H\beta2} = 12.3$
	^{99}Tc FKC	$-CH_2C_6H_5$	$-(CH_2)_4NH_2$	5.71 (dd)	3.57, 3.83	$J_{H\alpha\text{-}H\beta1} = 7.6$, $J_{H\alpha\text{-}H\beta2} = 2.2$, $J_{H\beta1\text{-}H\beta2} = 12.5$
	^{99}Tc MKC	$-CH_2CH_2SCH_3$	$-(CH_2)_4NH_2$	5.68 (dd)	3.56, 3.82	$J_{H\alpha\text{-}H\beta1} = 7.8$, $J_{H\alpha\text{-}H\beta2} = 2.0$, $J_{H\beta1\text{-}H\beta2} = 12.7$
	^{99}Tc YKC	$-CH_2C_6H_4OH$	$-(CH_2)_4NH_2$	--	--	--
	^{99}Tc YSC	$-CH_2C_6H_4OH$	$-CH_2OH$	5.75 (dd)	3.56, 3.79	$J_{H\alpha\text{-}H\beta1} = 7.8$, $J_{H\alpha\text{-}H\beta2} = 2.4$, $J_{H\beta1\text{-}H\beta2} = 12.5$
	^{99}Tc YDC	$-CH_2C_6H_4OH$	$-CH_2COOH$	5.62 (dd)	3.57, 3.79	$J_{H\alpha\text{-}H\beta1} = 7.8$, $J_{H\alpha\text{-}H\beta2} = 3.4$, $J_{H\beta1\text{-}H\beta2} = 12.5$
	^{99}Tc YGC	$-CH_2C_6H_4OH$	-H	5.57 (dd)	3.48, 3.72	$J_{H\alpha\text{-}H\beta1} = 7.6$, $J_{H\alpha\text{-}H\beta2} = 3.7$, $J_{H\beta1\text{-}H\beta2} = 12.7$
	^{99}Tc P829	See Figure 1-9	See Figure 1-9	5.58 (dd)	3.36, 3.62	
SYN (Product B)	^{99}Tc FGC	$-CH_2C_6H_5$	-H	--	--	--
	^{99}Tc FKC	$-CH_2C_6H_5$	$-(CH_2)_4NH_2$	5.23 (d)	3.80	$J_{H\alpha\text{-}H\beta1} = 6.4$
	^{99}Tc MKC	$-CH_2CH_2SCH_3$	$-(CH_2)_4NH_2$	5.26 (dd)	3.87	$J_{H\alpha\text{-}H\beta1} = 5.4$, $J_{H\alpha\text{-}H\beta2} = 3.4$
	^{99}Tc YKC	$-CH_2C_6H_4OH$	$-(CH_2)_4NH_2$	5.25 (d)	3.83	$J_{H\alpha\text{-}H\beta1} = 6.6$
	^{99}Tc YSC	$-CH_2C_6H_4OH$	$-CH_2OH$	5.26 (dd)	3.84	$J_{H\alpha\text{-}H\beta1} = 6.6$, $J_{H\alpha\text{-}H\beta2} = 2.2$, $J_{H\beta1\text{-}H\beta2} = 12.7$
	^{99}Tc YDC	$-CH_2C_6H_4OH$	$-CH_2COOH$	5.25 (dd)	3.85	$J_{H\alpha\text{-}H\beta1} = 5.9$, $J_{H\alpha\text{-}H\beta2} = 3.9$
	^{99}Tc YGC	$-CH_2C_6H_4OH$	-H	--	--	--
	^{99}Tc P829	See Figure 1-9	See Figure 1-9	5.20 (d)	3.80	

3.3.5. Circular Dichroism Spectroscopy of ^{99}TcO Compounds

Circular dichroism spectra were recorded in methanol at 25^{o}C for the anti and syn diastereomers of the ^{99}TcO tripeptides. The CD spectra for selected examples of the anti and syn diastereomers of ^{99}TcO tripeptides, TcO εKGC, and ^{99}TcO depreotide (^{99}Tc P829), taken in methanol at 25^{o}C are shown in **Figure 3-5**. The ellipticities at different wavelengths are tabulated in **Table A4** (**Appendix Section**). CD bands observed between 180-250 nm are attributed to transitions of the peptide backbone.[7] Examination of absorption and CD spectroscopy of Tc thiolates from the literature suggests that the transitions found at ca. 400 nm are likely due to a thiolate to Tc(V) charge transfer (CT) transition.[8, 9] The band at ca. 470 nm (syn diastereomers) and ca. 500 nm (anti diastereomers) are assigned to ligand field transitions, similar to spectral data of characterized TcO^{3+} complexes with thiolate ligands and square pyramidal coordination, as found in the literature.[8, 10, 11] The bands at ca. 350 nm may be higher energy ligand field bands or CT transitions.[8] The lowest energy ligand field band is centered at 500 nm for the anti diastereomers and centered at 460 nm for the syn diastereomers. It is these transitions that give the Technetium-99 complexes their distinctive colors: the anti diastereomers are all pink and the syn diastereomers are all yellow (**Figure 3-2**).

The TcO FGC–anti (A), TcO εbenzoyl KGC–syn (B) and TcO YKC–syn (B) complexes have been examined by X-ray crystallography. The CD spectra of these compounds along with other diastereomers are displayed in **Figure 3-5**. It is clearly seen that in the region from 300-600 nm that encompasses the LMCT and ligand field transitions, the CD patterns differ between the families of compounds A and B.

Compounds A all show bands with a positive Cotton Effect between 300-400 nm and a broad asymmetrical band with a negative Cotton effect between 400-600 nm. All of the compounds B show a broad asymmetrical band at 350 nm with a shoulder at around 400 nm, with a negative Cotton effect and a broad weak band with a positive Cotton effect, centered at 460 nm. Thus, since compound A has been identified for TcO FGC to be the anti diastereomer via X-ray crystallography, the other ^{99}TcO tripeptides that elute first on Reverse-phase HPLC and exhibit the same absorbance in the CD spectra, also are the anti diastereomer. Similarly, the syn diastereomer has been identified for all ^{99}TcO tripeptides as the later eluting complexes.

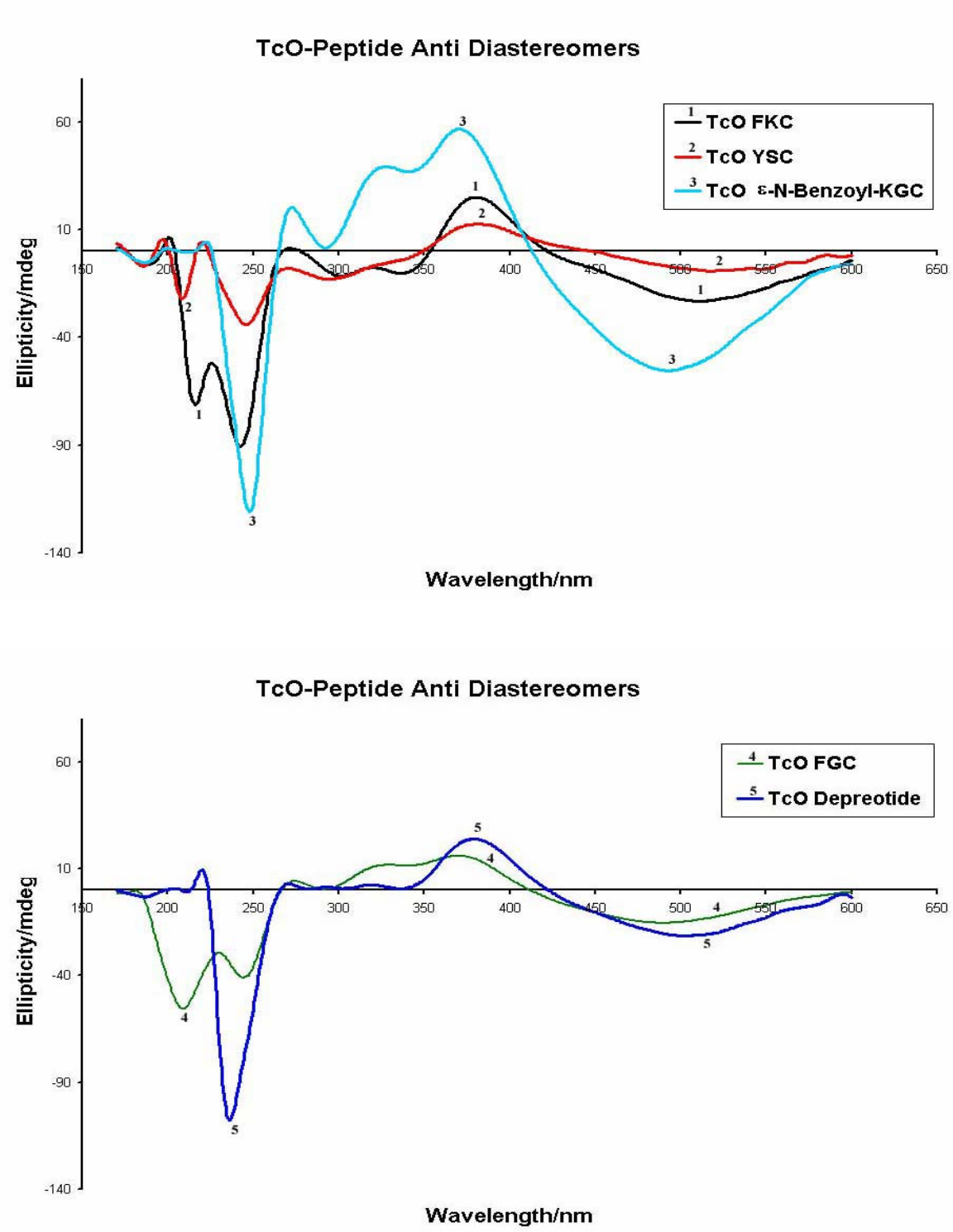

Figure 3-5. Circular dichroism spectra for ^{99}TcO tripeptide anti diastereomers in comparison with ^{99}TcO depreotide diastereomer, taken in methanol.

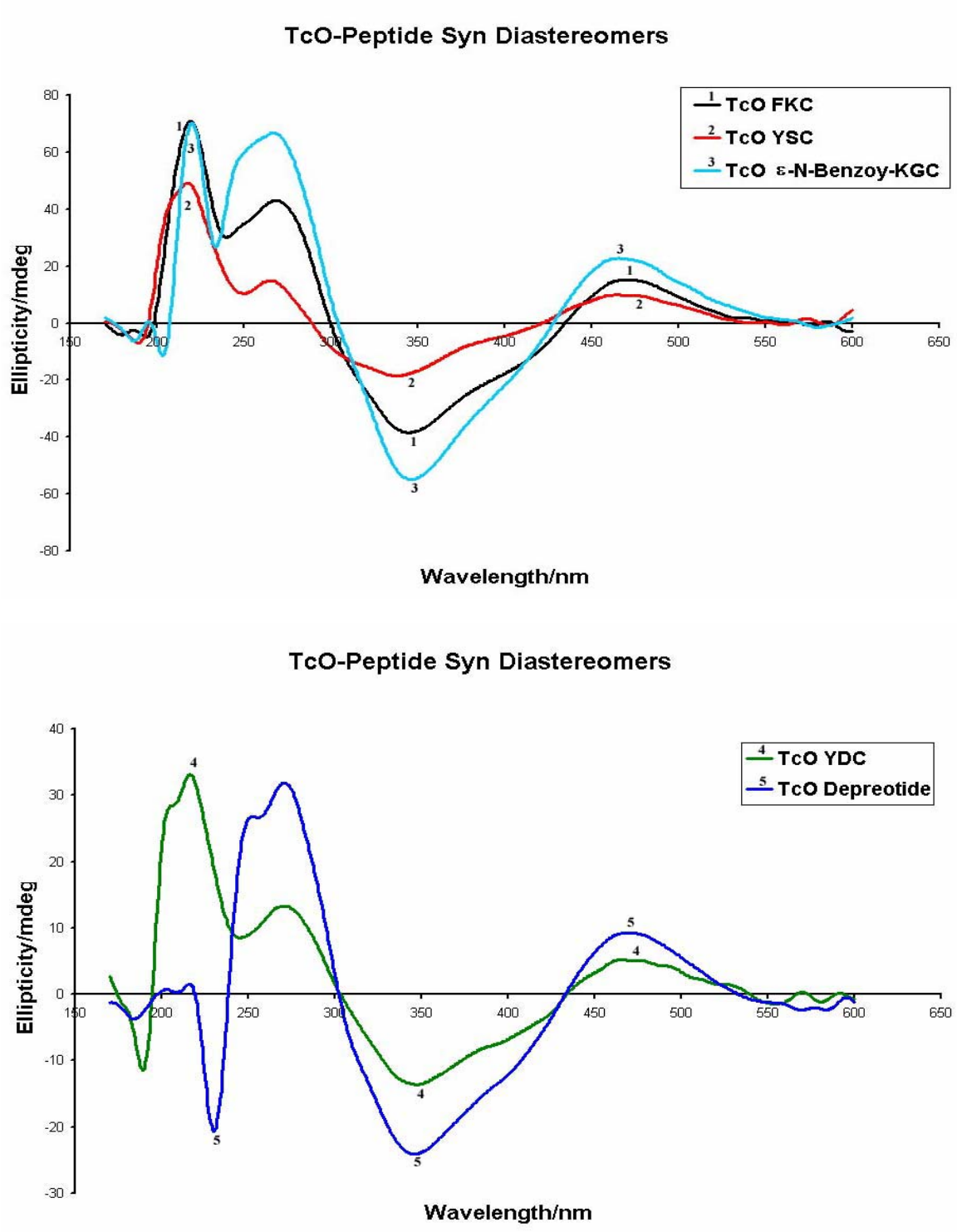

Figure 3-6. Circular dichroism spectra for ^{99}TcO tripeptide syn diastereomers in comparison with ^{99}TcO depreotide diastereomer, taken in methanol.

3.3.6. Synthesis and Characterization of ^{99}TcO P2540: The Chelating Site of TcO Depreotide

P2540 (**Figure 3-6**) is a linear hexapeptide containing the same N_3S chelating site as the depreotide with the following amino acid sequence: AcNH-tyr-gly-dap-lys-cys-lys-$CONH_2$. **Figure 3-7** shows a schematic representation of the peptide complexed with Tc. This peptide bears a close similarity to depreotide and we undertook the synthesis and characterization as a means to obtain a much closer comparison with Tc depreotide. When the aqueous solution of P2540 was reacted with methanolic solution of TcO eg, two species were formed on the analytical RP-HPLC showing the early and late eluting major peaks at 8.1 and 12.4 min, respectively (**Figure 3-8**). After prep HPLC purification and lyophilization, solid Product A is pink in color and solid Product B is pink. A black powder was produced for the void volume and a trace of yellow color can be observed for the more liphophilic, minor products. Only Products A and B were characterized by NMR (**Figure 3-9, Table 3-5**), IR (**Figure 3-10**), CD (**Figure 3-11, Figure 3-12**), and mass spec (**Table A5, Appendix Section**). The mass spec data for the two diastereomers are consistent with $[M+H]^+$ formulations at m/z = 837. Similarly, the IR data for the diastereomers showing a $\nu_{Tc=O}$ stretch at 978 cm^{-1} are consistent with other Tc(V)=O square pyramidal, nitrogen-sulfur neutral complexes. Crystallization attempts of these two diastereomers in organic and highly basic aqueous solutions were unsuccessful.

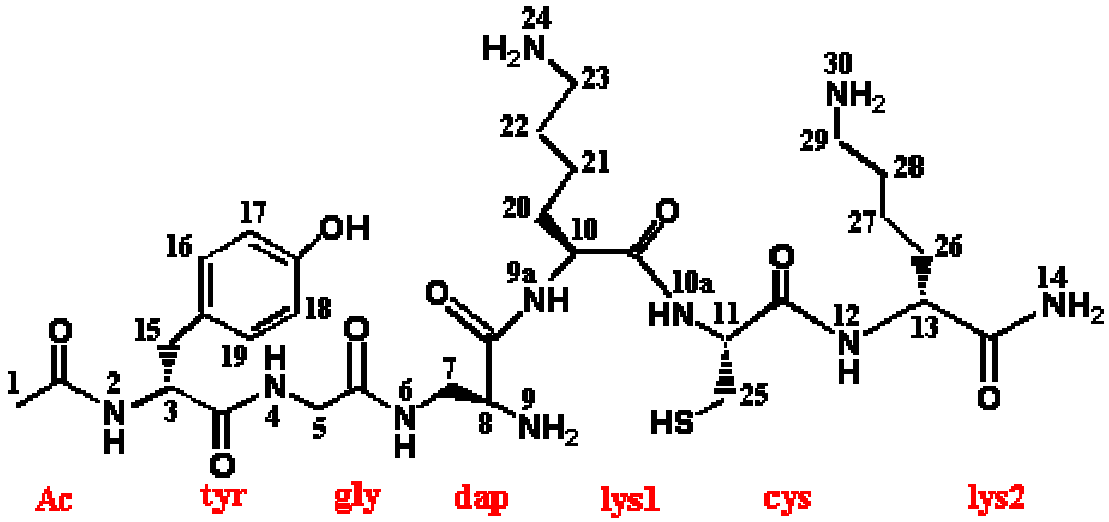

Figure 3-7. The structure of the free peptide P2540 showing proton numbering for chemical shift assignment.

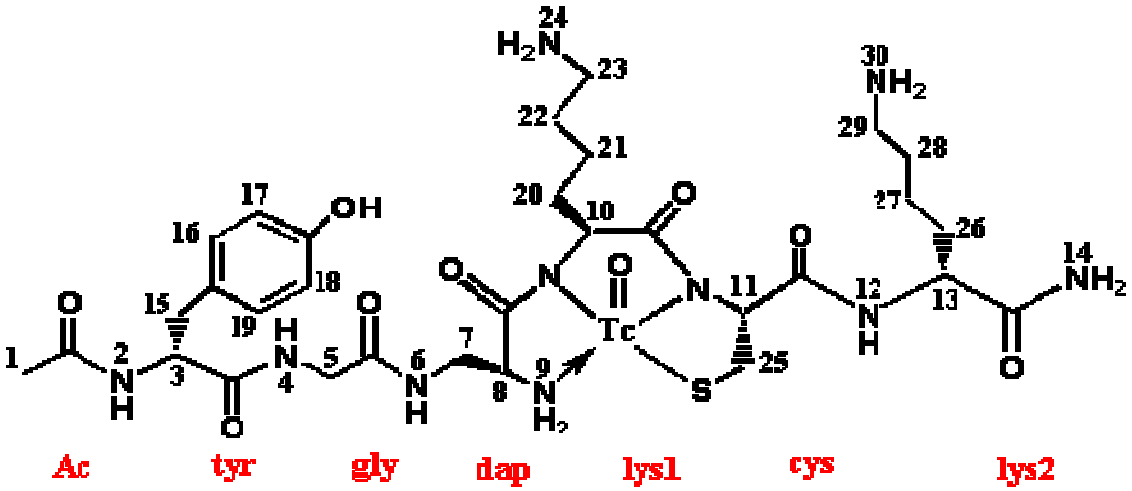

Figure 3-8. TcO P2540 showing deprotonation of the N_3S binding site region.

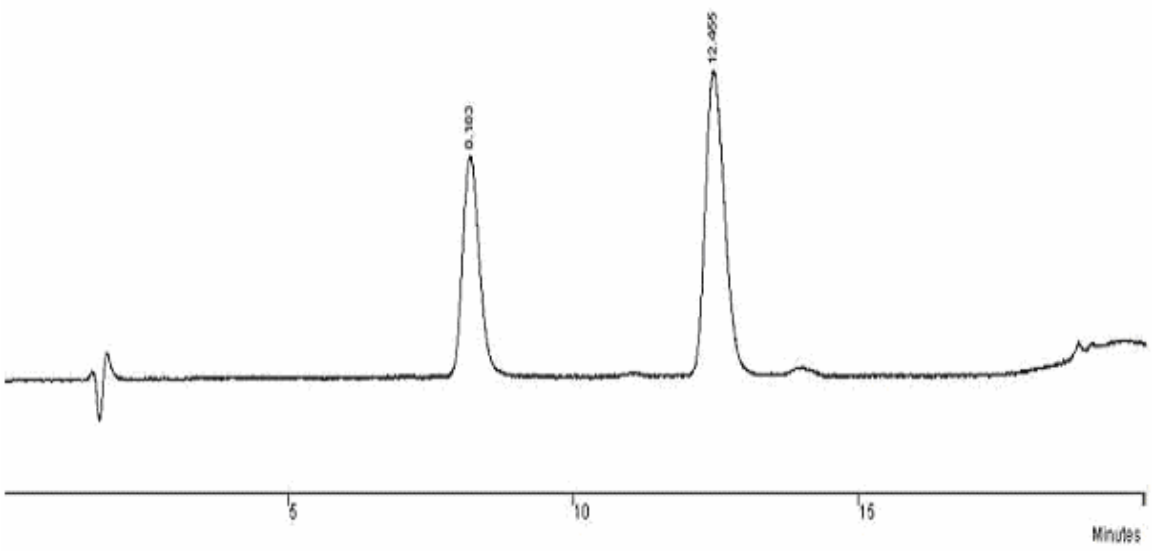

Figure 3-9. HPLC analysis of the crude solution of ^{99}TcO P2540 using the following reverse phase HPLC parameters: Column: Waters DeltaPak 5µ C_{18} 100 Å, 3.9 x 150 mm; MBS-2: 4% - 8% B over 15 min, then 8% - 30% B over 2 min; Flow Rate: 1.0 mL/min; Software: Star Chromatography Workstation Version 6.

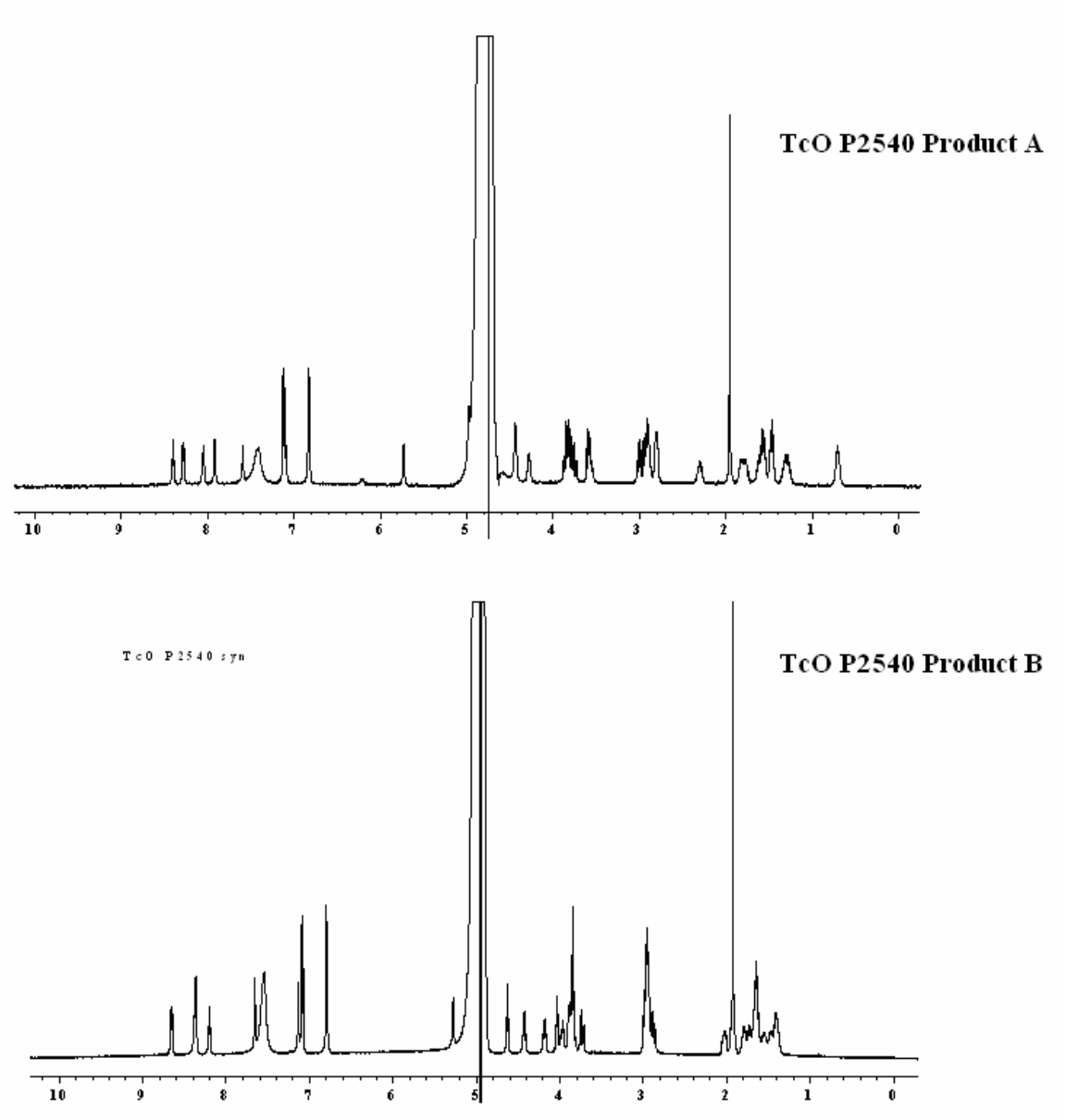

Figure 3-10. ^{1}H NMR spectra for ^{99}TcO P2540 diastereomers taken in 0.01M HCl in H_2O.

Table 3-5. Proton chemical shift assignment for the free peptide P2540 and the diastereomers of the complexed peptide.

Proton	^{99}TcO P2540 Product A	^{99}TcO P2540 Product B	P2540 Peptide	Δ^1_A, Δ_B
1 CH_3 Ac	1.99	1.92	1.92	
2 NH tyr	8.30	8.22	8.23	
3 α tyr	4.42	4.39	4.41	
4 NH gly	8.43	8.26	8.37	
5 α gly	3.74, 3.85	3.71, 3.82	3.72, 3.86	
6 NH dap	8.05	8.15	8.02	
7 β dap	3.57, 3.83	3.86, 3.90	3.60, 3.72	
8 α dap	4.45	4.00	4.11	+ 0.34, - 0.11
9 NH_2 dap	6.20	-	-	
9a NH lys1	-	-	8.77	
10 α lys1	4.98	4.60	4.32	+ 0.66, + 0.28
10a NH cys	-	-	8.56	
11 α cys	5.73	5.29	4.43	+ 1.30, + 0.86
12 NH lys2	7.94	8.49	8.51	
13 α lys2	4.27	4.14	4.16	
14 NH_2 terminus	7.10, 7.59	7.00, 7.54	7.06, 7.60	
15 β tyr	2.94, 3.00	2.84, 2.93	2.85, 2.96	
16, 19 Ar	7.12	7.09	7.13	
17, 18 Ar	6.84	6.76	6.81	
20 β lys1	1.85, 2.33	1.90, 1.97	1.74	
21 γ lys1	0.70	1.43	1.36	- 0.66, + 0.07
22 δ lys1	1.46	1.63	1.62	
23 ε lys1	2.92	2.96	2.95	
24 ε-NH_2 lys1	7.42	7.52	7.48	
25 β cys	3.60, 3.80	3.80	2.86	
26 β lys2	1.64, 1.78	1.76	1.70	
27 γ lys2	1.35	1.43	1.36	
28 δ lys2	1.57	1.63	1.62	
29 ε lys2	2.95	2.96	2.95	
30 ε-NH_2 lys2	7.45	7.52	7.48	

[1] Δ = difference between ^{99}Tc complex and P2540 peptide chemical shifts on the binding site.

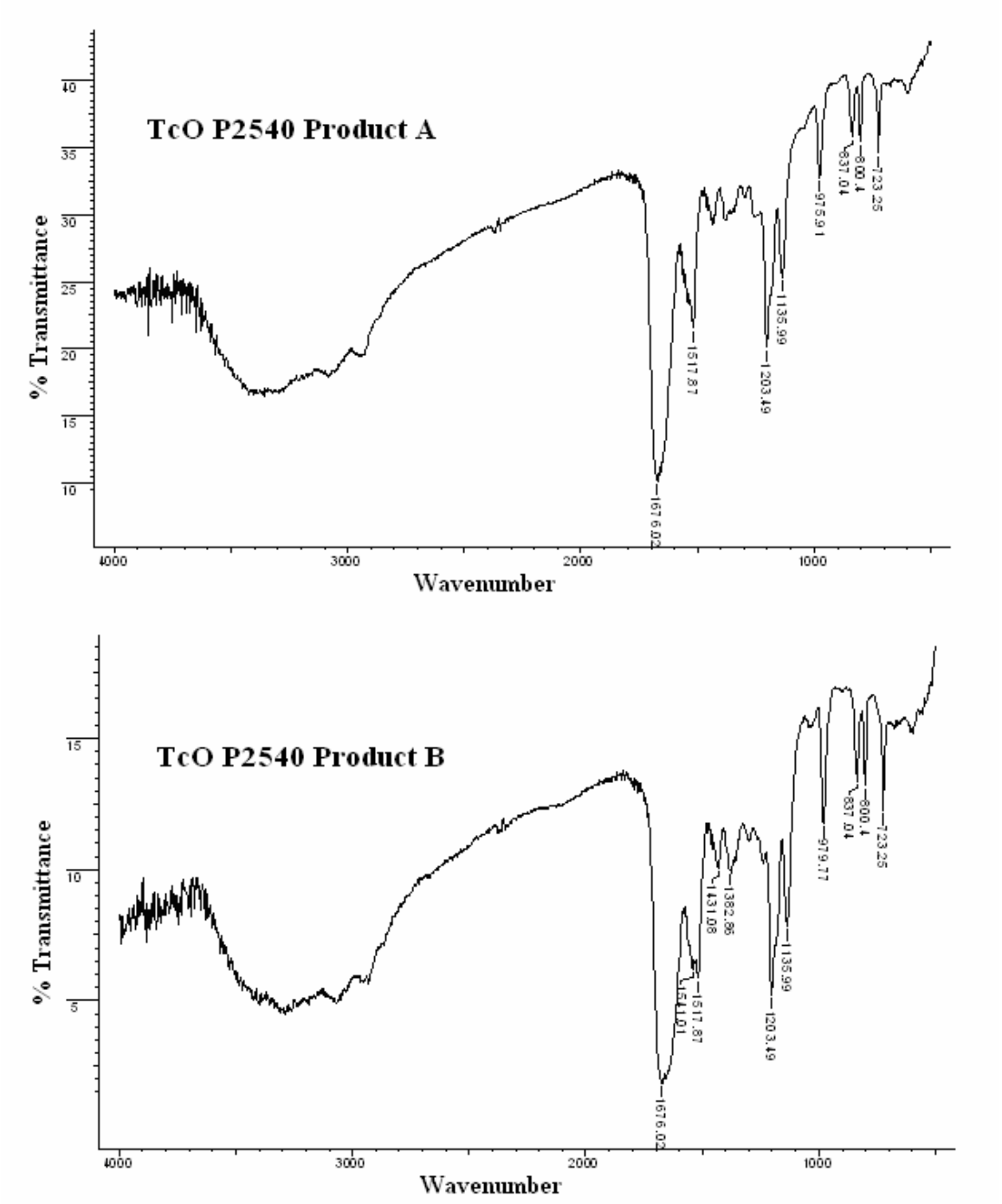

Figure 3-11. IR spectra for ^{99}TcO P2540 diastereomers showing Tc=O stretch at 976 cm^{-1} (Product A) and 980 cm^{-1} (Product B).

Using 1-D proton NMR data as well as the TOCSY data, the chemical shifts assigned for the free peptide P2540 were compared to the two diastereomers (Products A and B) of the complexed peptide. **Table 3-5** showed some interesting results that were also observed for the depreotide and the syn and anti diastereomers of the complexed depreotide. Amino acid protons that are not part of the binding site region showed unperturbed chemical shifts of the TcO P2540 Product A and Product B with respect to the free peptide. No chemical shifts were observed for the amide protons of lys1 (proton no. 9a) and cys (proton no. 10a) but the chemical shift for the amine proton on dap (proton no. 9) was present. This is consistent with the loss of two amide protons but not of the amine proton in an N_3S bifunctional chelation of TcO, as expected and as found for the tripeptides.

The alpha proton (proton no. 11) resonance on cys of TcO P2540 Product A shifts significantly more downfield compared to TcO P2540 Product B. Also, Product A shows two beta proton resonances (cysteine, proton no. 25) and Product B, only one proton beta resonance (cysteine, proton no. 25). These two chemical shift signatures are basis for the identification of syn and anti diastereomers of the TcO tripeptide models. Therefore, as we found for the tripeptides, TcO P2540 Product A can be assigned as anti and Product B, as syn.

There are two exceptions noted in **Table 3-5** in which the peptide protons adjacent to the technetium center exhibit NMR signal shifts upfield upon complexation of the ligand with technetium. The dap H_α (proton no. 8) resonance of ^{99}TcO P2540 Product B and the lys1 H_γ (proton no. 21) resonance of ^{99}TcO P2540 Product A shift upfield by 0.11 and 0.66 ppm, respectively. We do not know the physical phenomenon

responsible for these upfield chemical shifts; however, the shifts are consistent within the diastereomers of the tripeptides, of TcO P254O, and of TcO depreotide.[2]

The CD spectra of TcO P2540 diastereomers are also consistent with the TcO tripeptide models and TcO depreotide (**Figure 3-11**), further suggesting that the Product A is anti and Product B is syn. When compared to the free peptide (**Figure 3-12**), the ellipticity of Product B at about 200 nm is positive which is similar to the free peptide. In contrast, Product A has a negative ellipticity at this region, which means that the peptide backbone has to change its conformation to form the anti diastereomer when complexed with Tc.

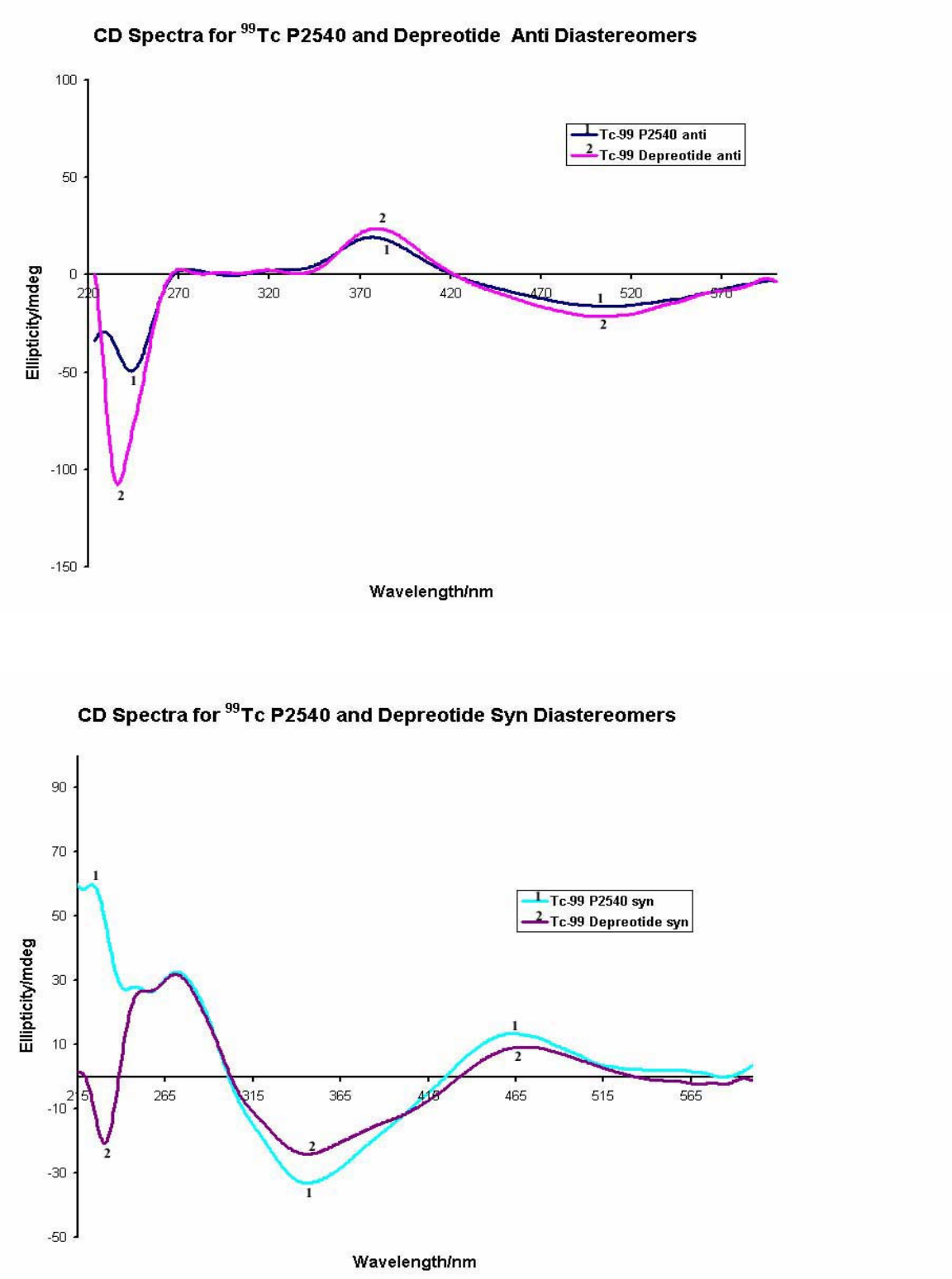

Figure 3-12. CD profiling of syn and anti diastereomers taken in methanol. Only the Vis region can be used for comparison between TcO P2540 and TcO depreotide.

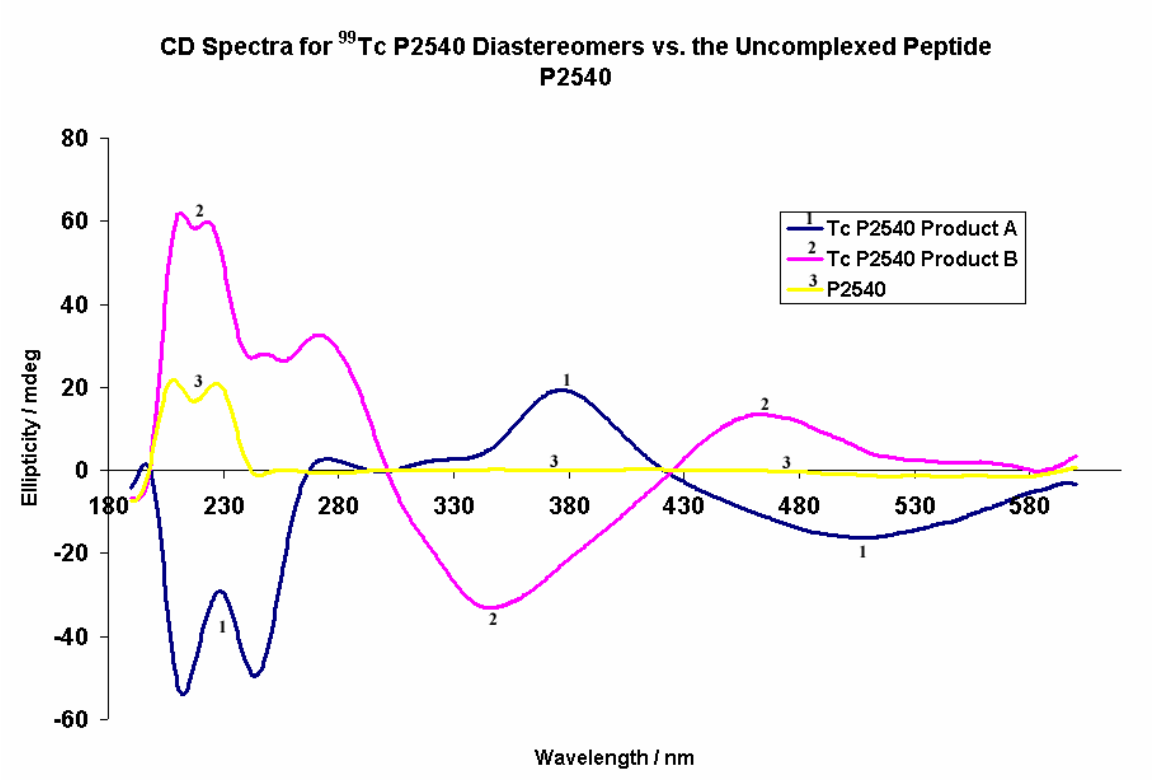

Figure 3-13. TcO P2540 Product A and Product B are a diastereomeric pair as shown by their CD profiles. The conformation of the peptide backbone is retained in Product B but not in Product A.

3.4. Conclusion

The assignment of the specific diastereomers of ^{99m}TcO depreotide and for any ^{99m}TcO radiopharmaceutical is an important issue in radiopharmaceutical development. Crystallization, the only method to identify the diastereomers, is generally untenable for intermediate size peptides due to multiple conformations. Tripeptides that model the depreotide Tc binding site were synthesized and the ^{99}Tc and Re complexes were prepared (see next chapter for details of Re diastereomers). We hypothesized that

interconversion could be minimized by choosing amino acids whose residues were sterically bulky or possessed Hydrogen bonding capabilities. We also found that basic conditions enhanced interconversion and that organic solvents minimized interconversion of the diastereomers.

The ^{99}TcO and ReO tripeptide complexes could be crystallized and related to TcO depreotide by proton NMR and Circular dichroism experiments. This is also true with TcO P2540, a hexapeptide containing an exact semblance of the binding site region of Tc depreotide. We continue to investigate the stability conferred on specific diastereomers due to the amino acid residues in proximity to the Tc center by theoretical and experimental means.

3.5. References

1. Francesconi, L. C., Zheng, Y., Bartis, J., Blumenstein, M., Costello, C., DeRosch, M. A., *Inorg. Chem.*, **2004**. *43*(9): 2867.
2. Cyr, J. E., Pearson, D. A., Nelson, C. A., Lyon, B. A., Zheng, Y., Bartis, J., He, J., Cantorias, M. V., Francesconi, L. C., *manuscript in preparation*.
3. Boyd, G. E., *Journal of Chemical Education*, **1959**. *36*: 3.
4. Davison, A., Trop, H. S., Depamphilis, B. V., Jones, A. G., *Inorganic Syntheses*, **1982**. *21*: 160.
5. Wong, E., Fauconnier, T., Bennett, S., Valliant, J., Nguyen, T., Lau, F., Lu, L. F. L., Pollak, A., Bell, R. A., Thornback, J. R., *Inorganic Chemistry*, **1997**. *36*(25): 5799.
6. Liu, S., Edwards, D. S., *Chem. Rev.*, **1999**. *99*: 2235.
7. Cheng, Y., Yan, Y.-B. Liu, J., *Inorg. Biochem.*, **2005**. *99*: 952.
8. Jones, W. B., *et al. Inorg. Chem.*, **1994**. *33*: 5571.
9. Depamphilis, B. V., Jones, A. G., Davison, A., *Inorg. Chem.*, **1983**. *22*: 2292.
10. Bryson, N., *et al. Inorg. Chem.*, **1988**. *27*: 2154.
11. Franklin, K., Howard-Lock, H., Lock, C., *Inorg. Chem.*, **1982**. *21*: 1941.

4. Synthesis and Characterization of ReO Tripeptide Diastereomers

4.1. Introduction

The incorporation of Re chemistry in the study of Tc compounds is standard protocol in radiopharmaceutical development. The natural non-radioactive mixture of isotopes of Re is often considered a "surrogate" for Tc; studies with analogous Re compounds can lend insights into understanding the chemistry of the radioactive Tc complexes. In this study, ReO tripeptide models, along with TcO tripeptide models, were used to identify the diastereomers of TcO depreotide. We were not surprised that we encountered subtle differences between ReO and TcO tripeptide complexes. For example, the colors of the anti and syn diastereomers are strikingly different in TcO tripeptides but not in ReO tripeptides . Moreover, the NMR and CD spectral features of Tc and Re are not exactly similar. These differences are telling us that we cannot solely rely on the information derived from Re chemistry alone to describe ^{99m}Tc chemistry. Therefore, in nuclear medicine applications, the extension from ^{99m}Tc to ^{188}Re is not always straight forward.

Just as the availability of the ^{99}Mo/^{99m} Tc generator drove the research to develop ^{99m}Tc radiopharmaceuticals, the recent availability of the ^{188}W/^{188}Re generator is driving research to develop ^{188}Re radiotherapeutic agents. The ^{188}W/^{188}Re generator works on the same principle as the Tc generator, providing high specific activity ^{188}Re, in the form of $^{188}ReO_4^-$.[1-4] ^{188}Re has excellent properties for radiotherapy; ^{188}Re (half-life of 16 hours)

emits a high-energy beta (E_{max}=2.11 MeV) with a range of 3 mm that is useful for cell killing and also generates a gamma ray of 155 keV (15%) that is useful for tracking the radiotherapeutic Re agent. It is envisioned that kit formulations can be prepared for ^{188}Re radiotherapeutic agents, similar to the ^{99m}Tc radiopharmaceutical kits. The potential pairing of ^{99m}Tc and ^{188}Re for dosimetry and for targeted radiotherapy, respectively, is an attractive concept.

In this dissertation, we report the syntheses and characterization of syn and anti diastereomers of ReO tripeptide complexes, including selected X-ray crystal structures. As described in the previous chapter (**Chapter 3**) for the ^{99}Tc YKC syn diastereomer, we noted amine-amide equilibrium for the Re FKC syn diastereomer. We examined this deprotonation phenomenon here using potentiometric titrations as well as NMR titrations, techniques to determine the pK_a for selected compounds. We can offer a hypothesis as to the deprotonation of the FKC syn species.

4.2. Experimental

4.2.1. Materials

Fmoc-protected L-amino acids and Rink amide MBHA resin were purchased from NovaBiochem. N-hydroxybenzotriazole (HBTU) was purchased from ChemTech. 2-(1H-benzotriazole-1-yl)1,1,3-tetramethyluronium (HOBt), N,N-diisopropylethylamine (DIPEA), piperidine, phenol, thioanisole, triisopropylsilane (TIS), and 1,2-ethanedithiol (EDT) were purchased from Sigma-Aldrich. HPLC-grade acetonitrile, trifluoroacetic

acid (TFA) and N,N-dimethylformamide (DMF) were purchased from Fisher Scientific. Nanopure water was obtained from a Millipore filtration system equipped with a 0.22 μm filter. All chemicals were used as received without further purification. $N(C_4H_9)_4[ReOBr_4(OP(C_4H_9)_3]$ was prepared according to a published procedure.[5]

4.2.2. Instrumentation and Analytical Methods

A RAININ Dynamax HPLC system equipped with a Dynamax UV-1 UV-visible detector and two Dynamax model SD-200 pumps using 25-mL pump heads were employed. All HPLC experiments were monitored at a λ = 220 nm. For both analytical and preparative work, the mobile phase consisted of (A) 0.1 % TFA in H_2O and (B) acetonitrile. For analytical HPLC, Method 1 parameters are described as follows: (1) Column - Waters DeltaPak 5μ C_{18} 100 Å, 3.9 x 150 mm; (2) Mobile Phase Gradient - 0% to 55% B over 30 min at a flow rate of 1.0 mL/min; (3) Software - Dynamax HPLC Method Manager. For preparative work, Method 2 consisted of Waters DeltaPak 5μ C_{18} 300 Å, 19.0 x 300 mm column and the software used was Dynamax HPLC Method Manager. The mobile phase A for this method was ramped from 0 % to 55 % B over 30 min at a flow rate of 24 mL/min.

Mass spectral data were acquired for Re compounds on an Agilent Technologies 1100 Series LC/MS Model G1946D using electrospray ionization in the positive-ion mode. Infrared spectra were recorded from KBr disks on a Perkin Elmer 1600 FT-IR spectrometer in the range 600 - 3000 nm and were referenced to polystyrene film. Proton

NMR spectra including TOCSY (total correlation spectroscopy), NOESY (nuclear Overhauser effect spectroscopy), as well as COSY (correlation spectroscopy) were recorded on a Varian Inova 500 MHz NMR spectrometer at T = 296 K. The chemical shift was referenced to H_2O as an internal reference. Circular Dichroism spectra of aqueous solutions of the Re tripeptides were collected on a JASCO-J710 spectropolarimeter where the optical system was fed by pre-purified nitrogen compressed gas at a flow rate of 5 L/min.

4.2.3. Synthesis of $Re^{V}O$ [Phe-Gly-Cys] (ReO FGC) and Other ReO Tripeptide Complexes

The tripeptide, phe-gly-cys (14.6 mg, 0.045 mmol), $N(C_4H_9)_4$ $[ReOBr_4(OP(C_4H_9)_3)]$ (40.3 mg, 0.041 mmol), and sodium acetate (6.15 mg, 0.075 mmol) were dissolved in 2 mL methanol. The resulting mixture became a dark brown solution instantly and was stirred for 2 min. The crude solution was analyzed on an HPLC system using **Method 1**, showing two major peaks which represent the two diastereomers. The diastereomeric products were then isolated and purified using semi-preparative HPLC, **Method 2**. The collected HPLC fractions were lyophilized, yielding a fluffy powder for each product. The early and late eluting compounds were peach in color. The same method was used for the synthesis of other ReO tripeptide complexes.

4.2.4. General Crystallization Procedure for ReO Tripeptide Complexes for X-Ray Crystal Structure Experiments

3 mg of sample was dissolved in a 2-mL vial with a minimum amount of ethylacetate or methylene chloride. A few drops of ethanol were added to completely dissolve the sample. The small vial was placed without a cover into a 20-mL vial containing about 5 mL pentane. The larger vial was then capped and allowed to stand at 10 ^{o}C. Crystals were formed within days.

4.2.5. Crystallization of $Re^{V}O$ [Phe-Lys-Cys] (ReO FKC)

Crystals for the diastereomers of $Re^{V}O$ [phe-lys-cys] were grown by two methods. In the first method, the compound was dissolved in 1:1 ethanol/methylene chloride and allowed to slowly evaporate. The second method involved slow evaporation of an aqueous solution of the compound after addition of 100 μL of 1% NaOH in D_2O. Specifically, ca. 5 mg of the syn compound was dissolved in about 125 μL of water. The color and pH of the resulting solution was dark brown and 3.8, respectively. 100 μL of 1 % sodium hydroxide (in D_2O) was immediately added to the solution. The color of the solution turned yellow-brown and the final pH was 13.3. The vial containing this sample was left overnight under the fume hood without cover. Yellow-brown crystals were formed within an hour.

4.2.6. Procedure for Analysis of ReO Tripeptide Complexes

4.2.6.1. NMR Spectroscopy

For samples taken in acidic aqueous solvents, about 3 mg of Re diastereomer was dissolved in 600 μL of 0.01 M HCl. 60 μL of D_2O (from 700-μL ampoule package, Cambridge Isotope Lab) was then added to the acidified solution. The sample solution was transferred into a 5-mm NMR tube. One-dimensional H-NMR spectra were collected at 64 scans. 2D NMR (COSY, TOCSY, and NOESY) were collected at 128 scans for each spectrum.

For samples taken in organic solvents, about 3 mg of Re diastereomer was dissolved in 650 μL of DMSO-d6 (from 700-μL ampoule package, Cambridge Isotope Lab). The sample solution was transferred into a 5-mm NMR tube. One-dimensional H-NMR spectra were collected at 64 scans. 2D NMR (COSY, TOCSY, and NOESY) were collected at 128 scans for each spectrum.

4.2.6.2. Circular Dichroism Studies

1 mg of Re tripeptide complex was dissolved in 1 mL methanol. 250 μL of the aliquot was placed in a 250-μL CD cell. The sample was scanned from 170 to 600 nm with +/- 50 degree sensitivity. The CD spectra were collected with baseline and background corrections using pure methanol.

4.2.7. Speciation Studies of ReO FKC and ReO FGC Diastereomers Through pKa Measurements

4.2.7.1. Procedure for Simultaneous Potentiometric and NMR Titrations

Standard solutions of NaOD and DCl were used. 1.5 – 5.0 mg of ReO FKC syn or ReO FGC anti was dissolved in 700 μL of a freshly prepared 0.01 M DCl in D_2O. The sample was transferred into a 5-mm NMR tube, and the pH of the solution was measured immediately and recorded. Then, the proton NMR was measured at this pH, at 15 ^oC with a total number of scans of 8. The number of scans was adjusted later as the sample concentration became diluted upon titration. After the first NMR measurement, the sample was titrated with NaOD (volume between 2 and 20 μL; concentration between 0.03 and 0.10 N). The pH and the volume of NaOD added were recorded only when the pH of the solution changed from 0.4 to 1 unit interval, and then the NMR of the sample was measured on the Varian Inova 500-MHz NMR instrument at T = 288 K. We continued the titration and NMR measurements until pH 13.29. Likewise, ReO FGC anti, and FKC and FGC ligands were also titrated using the above procedure (**Figure 5A, Appendix Section**). The pK_a of the ligands can provide information on how the amino acid residue affects the pK_a of the diastereomers. HPLC was measured upon completion of the experiment to verify the integrity of the compound. In one case, ReO FKC syn (starting pH 2, due to addition of excess acid) was titrated with NaOH to pH 12 and then back titrated with HCl. Upon completion of the back titration, the HPLC showed the ReO FKC syn contaminated with some of the anti complex. This experiment suggests the stability range of these metallotripeptides is from pH 2 to pH 12.

4.2.7.2. Determination of pK_a

The pK_a's of the diastereomers and the tripeptide ligands were obtained by constructing potentiometric titration curves for the individual samples. For example, in **Figure 4-1**, the number of milliequivalents of NaOD was plotted against pH of the ReO FKC syn solution. Using the "eye-ball technique", the pK_a's of the sample can be estimated by locating the regions of the curve with minimum slope. In this case, we observed two pKa's which were estimated as 5.2 and 12.0. The pK_a's can be accurately determined using the techniques described as follows.

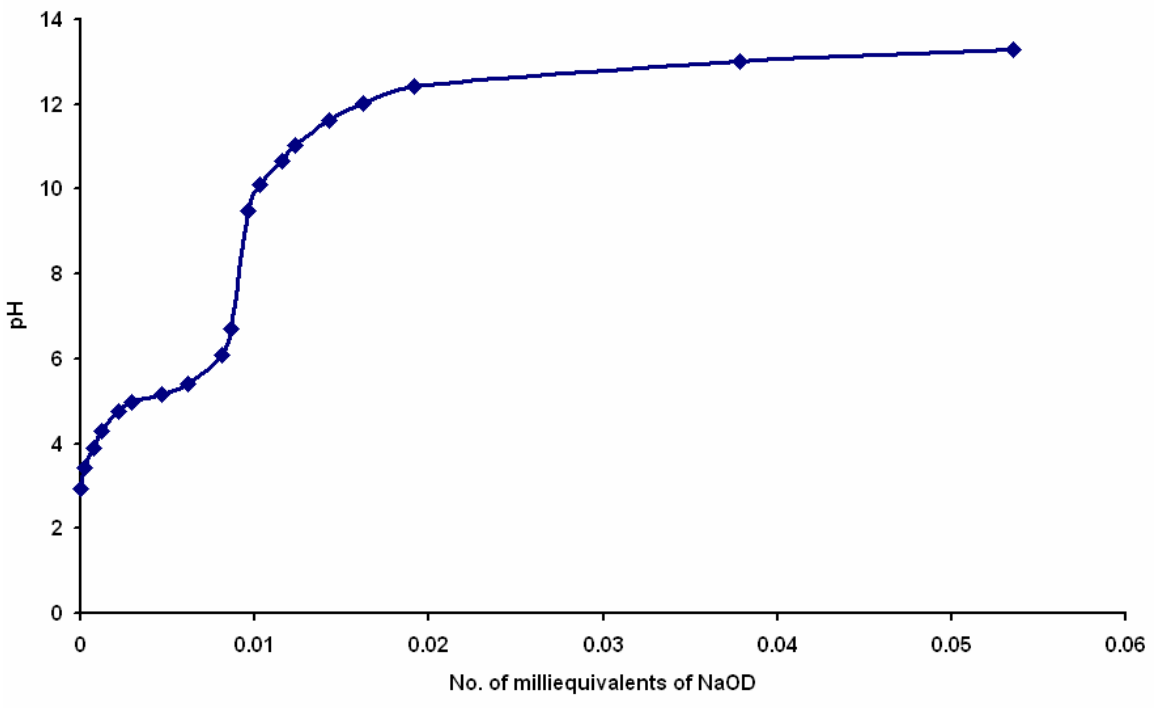

Figure 4-1. Potentiometric titration curve for ReO FKC syn (0.012M in D_2O).

To determine pKa values and assign the protons being titrated at each step, the NMR titration technique is very useful for compounds containing more than one dissociable proton. For example, we followed a NMR titration procedure described elsewhere[6] to determine the pK_a values for ReO FKC syn where the phenylalanine amine proton is dissociable as is an ε lysine proton . The NMR titration curve was constructed by plotting pH vs. 100 $[(\delta_{obs} - \delta_{HL}) / (\delta_L - \delta_{HL})]$, where:

δ_{obs} = chemical shift (i.e., of beta proton on phenylalanine region) at any pH

δ_{HL} = chemical shift at the lowest pH

δ_L = chemical shift at the highest pH.

A summary of the calculations for the titration of ReO FKC syn with NaOD is shown in **Table 4-1** and a plot for this calculated titration is shown in **Figure 4-2** This plot was then fitted to Hill sigmoidal curve via SigmaPlot, which is symmetrical about the inflection point. The pK_a was thus calculated according to Hill equation: $y = ax^b / (c^b + x^b)$. By letting y = 50 (half of the equivalence point), and substituting the following values generated by the SigmaPlot: a = 97.5, b = 10.5, and c = 5.6, into the Hill equation, then x = 5.63.

Therefore, the calculated pK_a is 5.63 which is assigned to the pK_a for the amine NH_2 terminus of the ReO FKC syn diastereomer. This method was used to calculate the pK_a for the NH_3^+ on the lysine side-chain of the ReO FKC syn diastereomer in which the chemical shifts of the ε-proton for the lysine residue were monitored. This pK_a is equal to 11.48 (**Figure A5, Appendix Section**). . The titration and calculations for ReO FGC anti are shown in the **Appendix Section**.

Table 4-1. Chemical shifts (middle column) of beta proton on phenylalanine region of ReO FKC syn at various pH during titration. The first and third columns represent the x- and y-axes for construction of NMR titration curve according to Popov.[6]

pH	δ, ppm (beta proton of phe)	100 [($\delta_{obs} - \delta_{HL}$) / ($\delta_{L} - \delta_{HL}$)]
2.93	3.373	0.0
3.43	3.352	9.3
3.90	3.348	11.1
4.29	3.358	6.7
4.76	3.330	19.1
4.98	3.318	24.4
5.17	3.317	24.9
5.42	3.299	32.9
6.09	3.210	72.4
6.72	3.174	88.4
9.50	3.166	92.0
10.11	3.148	100.0
10.67	3.151	98.7
11.03	3.167	91.6
11.62	3.165	92.4
12.03	3.145	101.3
12.41	3.154	97.3
13.01	3.148	100.0
13.29	3.148	100.0

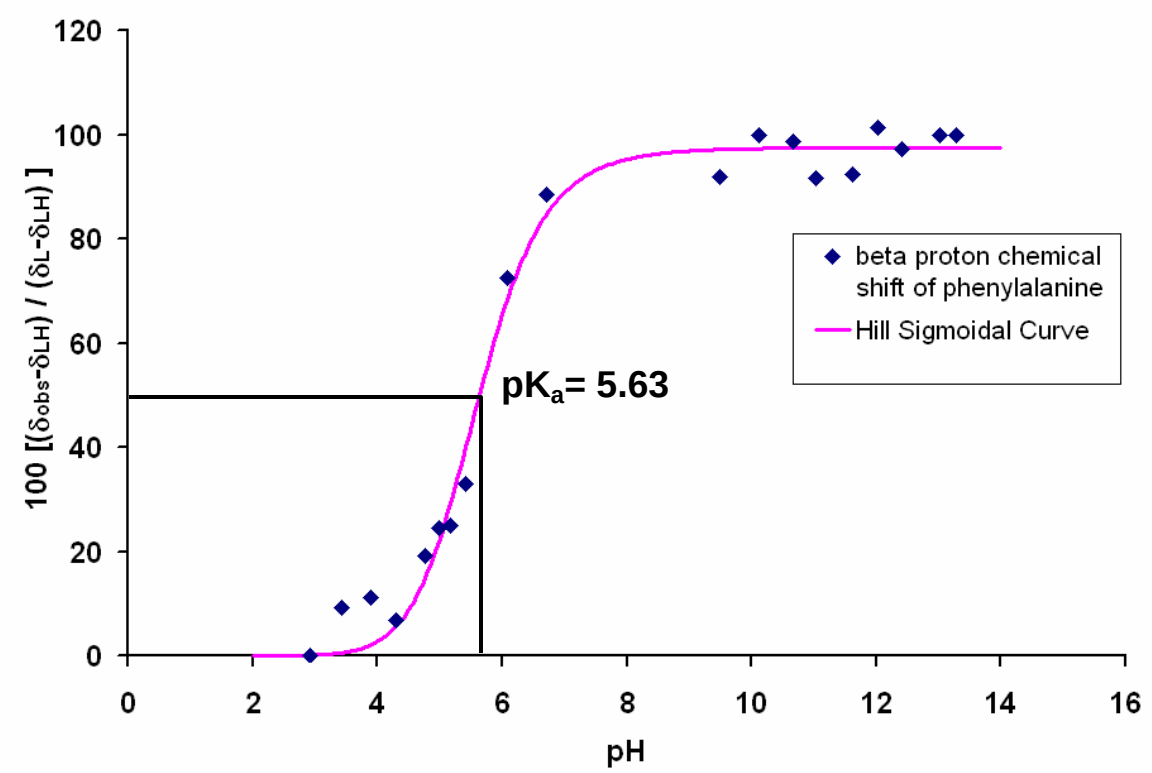

Figure 4-2. NMR titration curve for 0.012M ReO FKC syn with pK_a = 5.63 (solid line), plotted by SigmaPlot via Hill sigmoidal curve fit. Triangles refer to experimental NMR-titration points.

4.3. Results and Discussion

4.3.1. Synthesis and Isolation of ReO Tripeptides

Following the design of Tc tripeptide complexes, the Re analogs were synthesized in an organic solvent to minimize interconversion of diastereomers. Moreover, the isolation of the Re diastereomers was accomplished using acidic mobile phase solvents on the preparative Reverse-Phase HPLC; this also eliminated interconversion of

diastereomers. When the Re precursor, the tripeptide ligand, and sodium acetate were dissolved simultaneously in methanol at room temperature, the dissolution of the compounds was fast producing a dark-brown solution. As observed in Tc analogs, this rapid reaction were also expected because the d^2 electronic configuration of Re is similar to Tc, whereby the d^2 shell is accessible for π electron donation by the deprotonated amide and thiol groups from the tripeptide ligand.

In the synthesis of ReO tripeptide complexes, as expected, two major products were formed. A 1:1 ratio was observed for the ReO FGC and 1:9 ratio for the FKC complex, a similar pattern observed for Tc analogs. In general, both diastereomers A and B of the Re tripeptides had similar peach colors after lyophilization to powders. This is one characteristic of Re analogs that is distinct from Tc complexes. Tc syn and anti diastereomers have distinctively different colors; the syn is yellow in color and the anti is pink.

For the preparation of ReO FGC A and B, we observed that the solid sample of B, once lyophilized contained a very small contaminant of A. Moreover, when the sample of B was dissolved in basic water, interconversion to an equilibrium mixture of A and B (60/40, based on UV) was observed. The conversion of B to A for ^{99}TcO FGC, however, was faster than for Re, consistent with periodic trends, and we were not able to isolate enough of ^{99}TcO FGC Product B for physical characterization. In general, Tc compounds are more labile compared to Re. The relative lability of Tc and relative inertness of Re is another distinction between Tc and Re that can often be problematic when using Re analogs to understand Tc radiopharmaceuticals.

Infrared spectroscopy data for Re=O tripeptides showed a $\nu_{Re=O}$ stretch at 986 cm^{-1} which is consistent with other Re^{V}=O square pyramidal N_3S complexes. HPLC retention time and IR data are given in **Table A1** (**Appendix Section**).

4.3.2. X-ray Crystallography of Re Compounds in Comparison with Tc Compounds

X-ray crystal structures of ReO FGC syn and anti and ReO FKC syn complexes were performed. In all cases, the X-ray crystal structures show that the early eluting peak (A) corresponds to the "anti" diastereomer and the later eluting peak (B) corresponds to the "syn" diastereomer. The crystal and structure refinement data for Re tripeptide diastereomers (ReO FGC syn and anti; ReO FKC syn) are given in **Table 4-2**. Selected bond lengths and angles are listed together with Tc analogs in **Table 4-3.** Deviations of the amine and amide nitrogen atoms and the thiolate sulfur from the square plane constructed from these atoms are also listed in **Table 4-4** juxtaposed with Tc complexes. The crystal structure refinement data and bond lengths and angles for ReO FKC syn, crystallized from aqueous solution, are provided in the **Appendix Section** (**Tables A2** and **A3)**, respectively. Ball and Stick diagrams for the crystal structures of ReO FGC syn and anti, and ReO FGC syn are given in **Figure 3-3**, and ORTEP diagrams for the three diastereomers are presented in **Figure A2** (**Appendix Section**)**.**

As observed for the Tc analogs, the ReO FGC syn and anti diastereomers that were crystallized from organic solutions have one type of structure where the N_1 (**see Figure on Table 4-3**) of the first amino acid (phenylalanine) is an amine nitrogen. On the contrary, the ReO FKC, also crystallized from organic solution as well as from highly

basic aqueous solution, shows a different solid-state structure wherein the N_1 of the phenylalanine is deprotonated and exhibits multiple bonding with the Re.

A comparison of the first structural type including structures of the MO [phe-gly-cys] (MO FGC) (M=^{99}Tc, Re) complexes, the TcO [ε-benzoyl lys-gly-cys] (TcO ε-benzoyl KGC) syn complex and the structure of the previously published ReO RP294, ReO [dimethylglycine serine cysteine] crystal structure, show typical metal-N_{amine}, metal-N_{amide} and metal-S_{thiol} bond lengths and angles.[7-10] There are subtle differences in bond lengths and angles, possibly due to amino acids and the specific syn or anti diastereomer. The ReO FGC syn and anti complexes, the TcO FGC anti complex, and the TcO ε-benzoyl KGC syn complex show typical bond lengths for the M-N_{amine} (M-N_1, **Table 4-3**) that range from 2.111 – 2.165 Å, consistent with N_{amine}-M bond lengths from the literature, including the ReO RP290 syn complex.[11] The angles about the N_{amine} atoms are close to 109.5 deg, the tetrahedral angle, consistent with a sp^3 hybridized nitrogen atom and a "single" bond to the metal atom. Interestingly, the M-N_{amine} bond length for RP290 (2.165 (6)) is significantly larger than the M-N_{amine} bond length found in the other tripeptide complexes (2.103 (5) – 2.129 (3)); this may be due to steric factors associated with the dimethylamine compared to the amine of the tripeptide complexes. This longer bond length may also attest to the subtle changes in bond lengths and angles imposed by simple amino acid changes.

Table 4-2. Crystal and structure refinement data for ReO tripeptide diastereomers.

	ReO FGC anti	ReO FGC syn	ReO FKC syn
empirical formula	C14 H19 N4 O5 Re S	C14 H17 N4 O4 Re S	C20 H32 N5 O5 Re S
fw	541.59	523.58	640.77
cryst syst	orthorhombic	monoclinic	orthorhombic
space group	P2(1) 2(1) 2(1)	P2(1)	P2(1) 2(1) 2
temp, K	100(2)	100(2)	100(2)
wavelength, Å	0.71073	0.71073	0.71073
a, Å	6.6340(13)	10.520(2)	17.500(4)
b, Å	14.722(3)	6.8020(14)	10.578(2)
c, Å	18.159(4)	11.335(2)	13.384(3)
α, deg	90	90	90
β, deg	90	97.84(3)	90
γ, deg	90	90	90
V, Å^3	1773.5(6)	803.5(3)	2477.6(9)
Z	4	2	4
calcd density, g/cm^3	2.028	2.164	1.718
abs coeff, mm^{-1}	7.002	7.719	5.028
F (000)	1048	504	1272
θ range, deg	2.99–27.44	3.50–27.47	3.02–27.48
limiting indices	-8 ≤ h ≤ 8 -19 ≤ k ≤ 18 -23 ≤ l ≤ 23	-12 ≤ h ≤ 13 -8 ≤ k ≤ 8 -10 ≤ l ≤ 14	-22 ≤ h ≤ 22 -11 ≤ k ≤ 13 -17 ≤ l ≤ 14
reflns collected/unique	13890 / 4040 [R(int)=0.1134]	6177 / 3333 [R(int)=0.0440]	27202 / 5634 [R(int)=0.0564]
refinement meth	full-matrix least-squares on F^2	full-matrix least-squares on F^2	full-matrix least-squares on F^2
data / restraints / parameters	4040 / 6 / 226	3333 / 1 / 219	5634 / 0 / 319
GOF on F^2	1.037	0.997	1.054
final R indices [I>2σ(I)]	R1=0.0495 wR2= 0.1105	R1=0.0253 wR2= 0.0599	R1=0.0272 wR2= 0.0492
R indices (all data)	R1=0.0542 wR2= 0.1134	R1=0.0271 wR2= 0.0611	R1=0.0345 wR2= 0.0512
largest diff.peak and hole (eÅ^{-3})	3.458 and –1.978	1.124 and –1.094	0.596 and –0.587

Table 4-3. Selected Bond Lengths (Å) and Bond Angles (deg) for MO Tripeptide Diastereomers (M = ^{99}Tc, Re). (1 = ^{99}TcO FGC anti; 2 = ReO FGC anti; 3 = ReO FGC syn; 4 = ^{99}TcO (εK)GC syn; 5 = ReO FKC syn).

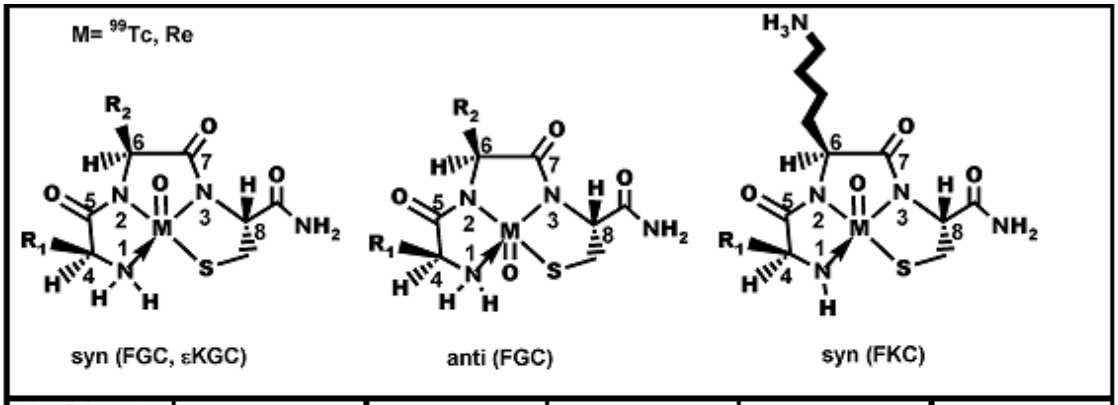

Bond Length, Å	1	2	3	4	5
M-O	1.678(5)	1.682(7)	1.659(2)	1.664(3)	1.690(3)
M-S	2.2828(17)	2.256(2)	2.2588(10)	2.2814(14)	2.2975(12)
M-N1	2.103(5)	2.116(7)	2.129(3)	2.111(4)	1.931(9)
M-N2	1.980(5)	1.992(7)	1.968(3)	1.980(4)	2.005(4)
M-N3	1.965(5)	1.987(7)	1.985(3)	1.987(4)	2.004(3)
N1-C4	1.479(13)	1.483(10)	1.480(5)	1.511(6)	1.464(6)
Bond Angle, deg					
N1-M-N2	77.5(4)	77.6(3)	77.75(12)	76.93(16)	77.98(16)
N1-M-S	92.8(2)	89.5(2)	88.68(8)	88.53(12)	91.08(12)
N2-M-N3	79.3(2)	79.0(3)	78.96(12)	78.15(16)	77.13(15)
N3-M-S	82.46(15)	82.6(2)	82.75(8)	82.69(12)	81.93(11)
O-M-N1	107.8(4)	107.4(3)	107.90(13)	114.76(16)	112.07(15)
O-M-N2	112.4(2)	117.0(3)	116.49(12)	113.39(18)	111.39(15)
O-M-N3	110.4(2)	110.3(3)	110.72(12)	113.63(17)	115.48(14)

Table 4-4. Deviations of the N_3S from the square plane for ^{99}Tc and Re diastereomers.

	TcO FGC anti	ReO FGC anti	ReO FGC syn	Tc(εK)GC syn	ReO FKC syn	TcO YKC syn 1
S	0.0861	0.0980	-0.0486	0.0321	-0.0239	-0.0187
N1 (amine)	-0.0955	-0.1083	0.0536	-0.0356	0.0269	0.0214
N2 (amide)	0.1159	0.1311	-0.0669	0.0431	-0.0320	-0.0249
N3 (amide)	-0.1065	-0.1208	0.0619	-0.0396	0.0289	0.0222

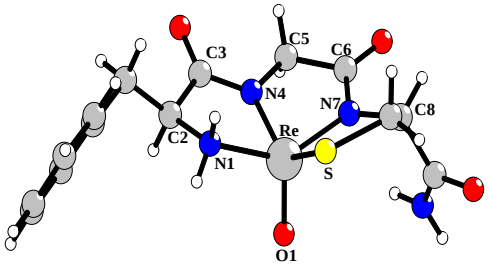

ReO FGC anti

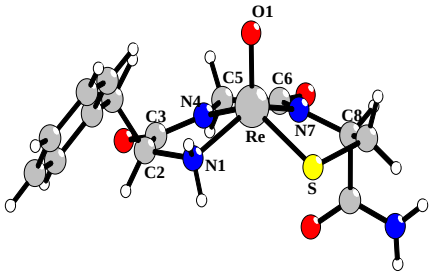

ReO FGC syn

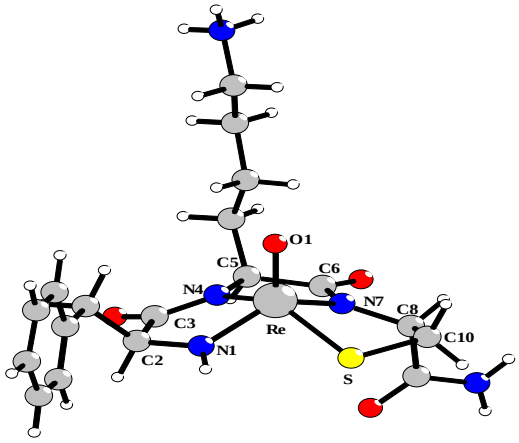

ReO FKC syn

Figure 4-3. Ball and Stick diagrams of ReO tripeptide crystal structures

The M-N_{amide} (M-N_2 and M-N_3, **Table 4-3**) bond lengths in the ReO FGC syn and anti complexes and Tc(εK)GC syn and TcO FGC anti are significantly less than the M-N_{amine} bond lengths, as expected, ranging from 1.954 to 1.992 Å with the ReO FGC- syn and ReO RP240-syn showing the shortest M-N_{amide} bond lengths. These short bond lengths, along with angles about the N_{amide} atoms of 117 – 122 deg, suggest sp^2 hybridized nitrogen atoms and substantial multiple bonding to the metal ion, consistent with the loss of the amide proton as evidenced from NMR and Mass Spectral data. The M-S_{thiol} bond length ranges from 2.256 to 2.2828 Å, that are in the range of M-S_{thiol} bond lengths reported in the literature. [8, 9, 12-17] These X-ray crystallography results demonstrated clearly that the pendant groups (phenylalanine, ε-benzoy-lysine) are in the anti position for the early eluting (on reverse phase HPLC) product A and in the syn position for the later eluting product B.

The second crystalline type, found for crystal structures of the ^{99}Tc and Re FKC compounds, show different solid-state structures from those described above due to deprotonation of the primary amine. Three structures were solved on three crystals that were obtained using two crystallization methods, one from organic solution, similar to the FGC series, above, and one from a basic aqueous solution. In these three structures, it is very clear that the M-N_1 bond is too short (1.931(9)Å) to be considered a metal-amine bond; this bond length implies a stronger M-N bond and suggests that the N_1 forms a cyclic amide bearing one proton. The loss of a proton is further substantiated in the C_4-N_1-M bond angles about N_1 that approach 120°, suggesting a sp^2 hybridized cyclic amide nitrogen. It appears that, under both crystallization conditions, the ReO FKC syn and the ^{99}TcO YKC syn adopt a structure wherein the amine is deprotonated; this deprotonation

renders the chelate ring slightly more planar than the FGC series. The deviations from a square plane formed by S, N1, N2 and N3 are slight for the FKC complexes compared to the FGC series (**Table 4-4**). The bond angles around the amide N_2 and N_3 atoms (**Table 4-3**) are similar in the FKC and XGC series, all close to 120°, as expected for sp^2 hybridized amide nitrogen atoms. Importantly, we observed again that the phenylalanine and lysine residues are in the syn conformation, for these species that arise from the later eluting product, B.

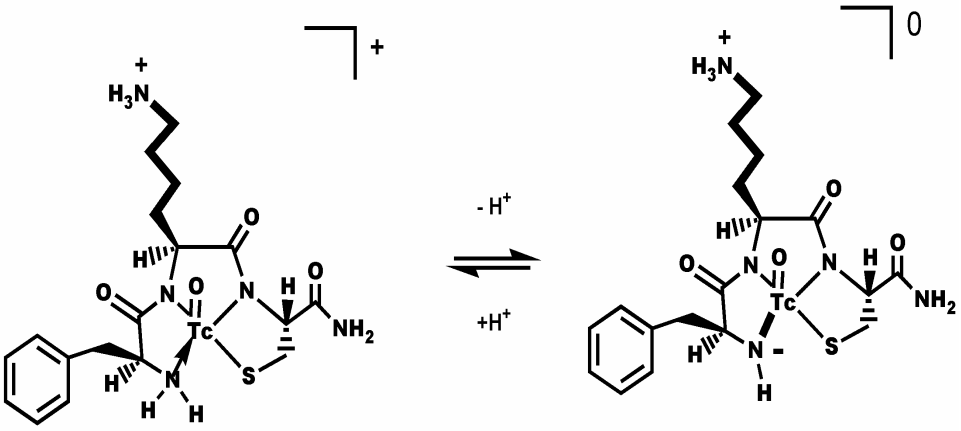

Scheme 4-1. Postulated equilibrium between the TcO FKC-N_{amine} and the deprotonated TcO FKC- N_{amide}.

The chemistry of these systems can be understood by analysis of the crystallography data of all species along with their proton NMR data. Under acidic aqueous conditions (pH 3-4), all complexes of Re tripeptides uniformly show very sharp proton NMR data, suggesting one species is present and that no species exchange or

interconversion is occurring. All of the protons can be assigned except for the amine protons that are not observed (**Table A4, Appendix Section**). We attribute this to exchange of the amine protons in aqueous solution, which is similar to what we observed for the ^{99}Tc tripeptides as discussed in **Chapter 3** and is common in aqueous solution. The proton NMR data for ^{99}TcO and ReO FKC and FGC complexes in organic solution, DMSO, clearly show that both of the phenylalanine amine protons are present, as well as the C-terminal amide protons and also the 3 protons for the ε-NH_3^+ of the lysine residue in FKC analogs (**Table A4 and Figure A3, Appendix Section**). The observation of the amine protons for the ^{99}TcO and ReO FKC complexes in DMSO strongly suggest that the amine is present in diluted organic solution. Our data are consistent with data from another study in which the two amine protons of a similar ^{99}TcO Lys-Tyr-Cys tripeptide complex, taken in DMSO, were also observed[18].

We observe this deprotonation only with the complexes where lysine is in the second position, not for the Phe-Gly-Cys or ε-Lys-Gly-Cys complexes. The complexes are prepared and crystallized in a similar fashion. We postulate that this deprotonation occurs in the organic crystallization solutions as the concentration of the species increases upon evaporation. The driving force for the deprotonation in the organic solution may be the formation of a zwitterionic neutral species; in this case with an ε-NH_3^+ of the lysine residue and the formal NH^- (amide) of the first amino acid (phenylalanine, tyrosine) bound to the M^VO. The deprotonation also apparently occurs in basic solution (pK_a determination discussed below, *vide infra*) and we have isolated crystals from an aqueous basic solution (pH>12) (**Table A2**, **Figure A2**). The complex is very stable: in addition

to the isolation of crystals at pH>12 we find that the complex remains intact in pH titrations from pH 1.7 to >12.

Potentiometric titration data (including NMR titrations) performed on ReO FKC syn, show a pKa of 5.63 this pK_a represents the equilibrium involving deprotonation of the amine, **Scheme 4-1**, according to NMR titrations monitoring chemical shifts of the β-H of the phenylalanine. The pK_a for the NH_2 of ReO FGC anti was 6.8. Based on these data as well as the observation of sharp proton NMR data for MO FKC (M=^{99}Tc, Re) (aqueous, pH 3-4), we are certain that, under the acidic pH of preparation and ^{1}H NMR analysis, vide supra, the amine species is present. The amine species is also clearly present in dilute organic solution according to NMR data, **Table A4** and **Figure A3**. Moreover, the Circular Dichroism data, taken in methanol, for all ^{99}Tc peptides and for the Re peptides are quite similar, attesting to the similarity of the complexes. Under highly basic conditions, the deprotonated cyclic "amide" is likely present, according to our crystal structure data. The pK_a determinations for MO FKC anti (M=Tc,Re) and TcO FKC syn, as well as other tripeptides, will be important in understanding the details of the structure and chemistry of the depreotide species under physiological conditions.

Mass spectral data are consistent with the proposed structures of all the MO tripeptide complexes, but cannot distinguish between an N1 amine (M^+) or N1 amide ($[M + H]^+$) formulation. For both the Tc and Re tripeptide diastereomers, presented in **Table A6** (**Appendix Section**) both a molecular ion $[M+H]^+$ and smaller peaks attributed to the sodium adducts $[M+Na]^+$ were detected. Mass spectral data are also consistent with the amine formulations for all of the tripeptides. The Re analogs exhibit the characteristic Re isotopic pattern; **Appendix Section**, **Figure A4** shows the calculated and observed mass

spectral data for the ReO FKC analogs. While the mass spectral data are consistent with the crystal structures for the FGC and the ε-KGC species, the mass spectral data for the ReO FKC, syn and anti complexes, can fit for both the amine species and the deprotonated amide species, seen in the crystal structure. For ReO FKC, both positive and negative electrospray data were collected. The $[M+H]^+$ peaks, the $[M-H]^-$ data and the isotope patterns fit very well for a molecular ions of $ReC_{18}H_{26}N_5O_4S$; this fits for both an amine for the phenylalanine with an unprotonated NH_2 for the lysine or a deprotonated nitrogen for phenylalanine and an NH_3^+ for the lysine residue.

TcO[ε-KGC] shows clearly the expected monoisotopic mass, 521.056, for both diastereomers. Interestingly, the *syn* diastereomer appears to be a tightly-associated dimer with $[M_2+Na]^+$ at m/z 1065. This persists as the base peak even upon tenfold dilution. The ions associated with the monomer are present at lower abundance. Low abundance peaks corresponding to the trimer are also present in a series beginning at m/z 1563 $[3(521)+ 23]^+$.

The HPLC profiles have been very consistent from compound to compound. It is presumed that if a protonation-deprotonation equilibrium (**Scheme 4-1**) were occurring under HPLC conditions, resulting in even a minor change in the chelate ring structure, the retentions times of the complexes would be quite different. Such a phenomenon has been observed previously, where deprotonation of a ^{99}Tc N_2S_2 compound occurred, resulting in a flattening out of the chelate ring and a longer retention time.[8] We also have observed reaction chemistry occurring on the macroscopic ^{99}Tc and Re levels with the tripeptide, YDC resulting in the formation of new peaks in the HPLC. These data

will be discussed in the next Chapter. Also, under the acidic HPLC conditions, it is likely that the amine would be protonated.

In summary, we postulate that the crystal structure of the ReO FKC and TcO YKC reflects a deprotonation that occurs in the crystallizing solution, as the concentration is increased. Also this deprotonation occurs under highly basic conditions. However, under acidic aqueous and dilute organic conditions, such as we use for synthesis, isolation and NMR and CD experiments, it is likely that the ReO FKC and TcO YKC compounds have similar structures as the other tripeptides, namely an amine nitrogen in the first amino acid. We are presently determining the pKa of the deprotonation in aqueous solution for the metallotripeptides.

4.3.3. Speciation Studies of ReO FKC Through pK_a Measurements

Figures 4-2 and 4-4 show the NMR titration curves for ReO FKC syn. In this experiment, we monitored the chemical shifts of beta proton on the phenylalanine region, and epsilon proton on the lysine region. Following the Popov procedure[6], the pK_a's for the NH_2 (phenylalanine) terminus and the epsilon-NH_3^+ (lysine) are calculated as 5.63 and 11.66, respectively. The pK_a for the NH_2 terminus of the FKC ligand, is 7.27, much higher compared to that of ReO FKC syn metal complex (**Figure 4-5, Figure A5**). Also, the pK_a for the epsilon-NH_3^+ is slightly lower in the FKC ligand (11.48) than in ReO FKC syn (11.66). Thus, we postulate that the epsilon-NH_3^+ may interact with C=O on phenylalanine or Re=O core. Such an interaction may weaken the Re-O bonds and the Re-N2 and Re-N3 bonds, thus favoring deprotonation of the phenylalanine NH_2 terminus

to form a strong Re-N1 bond to stabilize the syn complex (**Figure 4-6**). According to Marzilli et al., the low pKa indicates that $[Re^{V}=O]^{3+}$ is highly electron-deficient such that the deprotonated amine becomes a stronger donor to the metal center than the amine itself.[19]

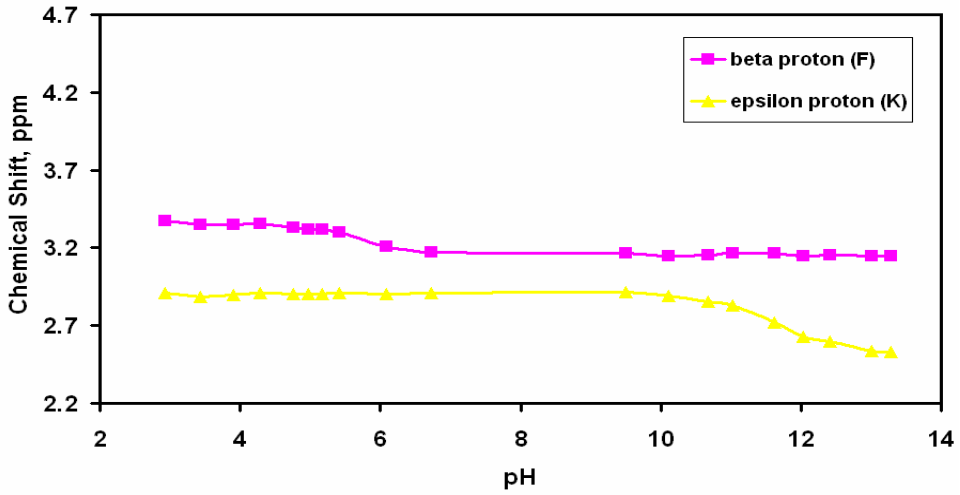

Figure 4-4. NMR titration curves for ReO FKC syn (B)

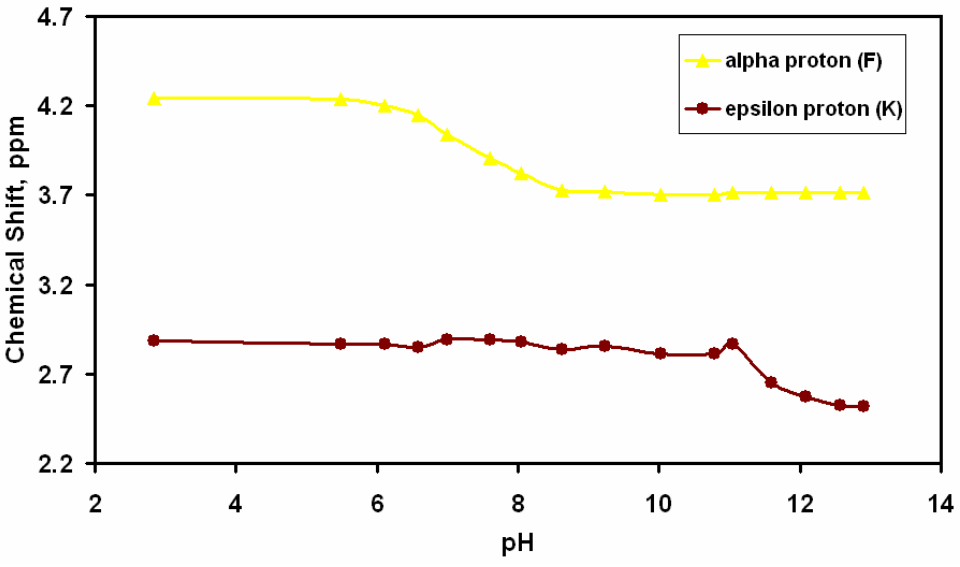

Figure 4-5. NMR titration curves for FKC tripeptide ligand.

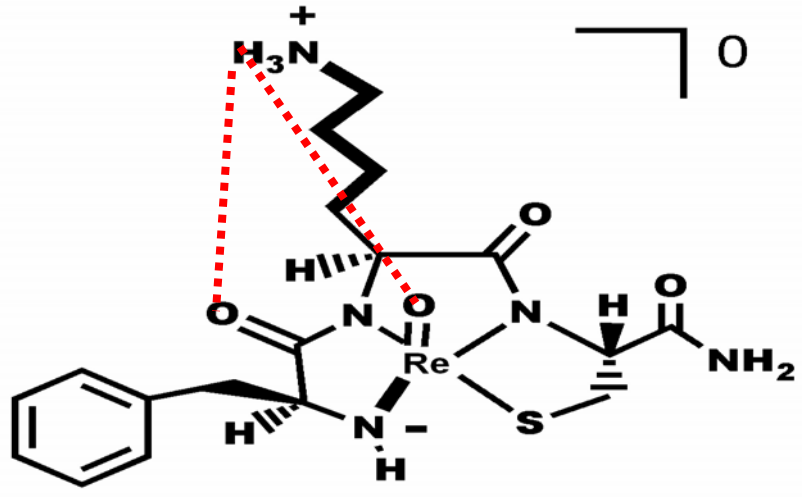

Figure 4-6. ReO FKC structure showing intramolecular interaction: the NH_3^+ moiety of the lysine residue may interact with the C=O of the phenylalanine region or the Re=O core leading to deprotonation of the the NH_2 terminus as shown by the X-ray crystallography data.

To test our deprotonation hypothesis, we also examined the pK_a's of FGC and ReO FGC anti (**Figure A5, Appendix Section**). The pK_a (NH_2 terminus) of the unbound ligand is 7.43, and for the ReO FGC anti is 6.75. The Re metal increases the acidity of the phenylalanine NH_2 group, as expected, however the absence of the lysine residue renders the phenylalanine NH_2 terminus of the ReO FGC anti less acidic than for the ReO FKC syn species. It makes sense that the phenylalanine NH_2 of ReO FGC anti is less acidic than the phenylalanine NH_2 of ReOFKC syn because there is no hydrogen bonding interaction to weaken the bonds of the Re-N and S donor atoms and encourage deprotonation of the phenylalanine amine to form a strong, short Re-N bond. The pKa measurement is consistent with the solid-state crystal structure of ReO FGC syn and anti

diastereomers, whereby the N_{amine}-Re bond is longer than the N_{amide}-Re and the angle about the N_{amine} is sp^3 hybridized.

During the titration of ReO FKC syn, we observed that precipitates formed from pH 5 until pH 11. The formation of precipitate is a function of the concentration. We attributed this observation to formation of neutrally charged species. Marzilli et al. observed low solubility when a neutral species formed.[19] Thus, to complete the equilibrium process in **Scheme 4-1**, we postulate the speciation equilibrium of ReO FKC syn shown in **Scheme 4-2**. At pH below the pK_a of the phenylalanine amine, 5.6, the syn diastereomer of ReO FKC is fully protonated and the species in solution is positively charged. The NH_2 terminus of ReO FKC syn becomes deprotonated at pH 5.6-11.7 to form a neutral zwitterionic species and precipitation occurs. At pH above the pKa of the ε-NH_3^+ , 11.7, the diastereomer is further deprotonated at the ε-NH_3^+ moiety to form a negatively charged species that redissolves in aqueous solution.

We also attempted to measure the pK_a of the ReO FKC anti. When the sample solution was titrated starting at pH 2, a gradual pH change was observed until about pH 4. The NMR spectra measured in the pH range of 2 to 4 were identical. However, when the pH of the solution abruptly changed from pH 4 to pH 12 upon addition of an excess NaOD solution, the NMR spectrum revealed the syn analog. When we tried to back titrate the sample with DCl, we didn't recover the original spectrum of the anti diastereomer. It is difficult to obtain the pKa of the anti ReO FKC due to conversion to the syn compound at high pH values.

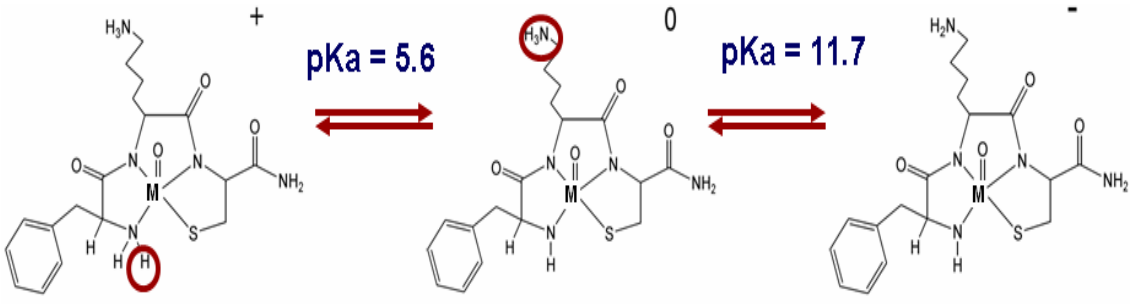

Scheme 4-2. Speciation of MO FKC in solution.

4.3.4. Details of the NMR Spectroscopy of Re Compounds

Proton NMR spectra of the Re complexes, taken in acidic solution, taken together with the crystal structures are diagnostic of the specific Re diastereomer. All of the protons for the Re model peptides have been assigned and are presented in **Table A4** (**Appendix Section**). In comparison with Tc diastereomers, we also did not observe the amine protons in water for Re analogs. Similarly, the amide protons of the amino acid 2 and the cysteine-thiol proton were not observed either, indicating loss of protons when the tripeptide ligand complexed with Re.

A diagnostic pattern observed for Tc diastereomers can also be extended to their Re analogs. For example, the alpha protons of the third (cysteine) amino acids are shifted to higher frequency for the Re anti diastereomers and to lower frequency for the syn analogs, compared to the uncomplexed peptide. The α-proton resonances (cysteine) are significantly downfield shifted for anti diastereomers compared to syn diastereomers. However, there is one feature that distinguishes the Re diastereomers from the Tc

diastereomers. In Tc tripeptide system, the syn diastereomer exhibits one β-proton resonance on cysteine while the anti diastereomer exhibits two β-proton resonances. In the Re tripeptide system, on the other hand, two β-proton resonances on cysteine are observed for both diastereomers.

4.3.5. Circular Dichroism Spectroscopy of Re Compounds

Circular dichroism spectra were recorded in methanol at 25^{o}C for the anti and syn diastereomers of the Re tripeptides. The CD spectra of the anti and syn diastereomers of ReO FGC are shown in **Figure 4-8** and tabulated in **Table A5** (**Appendix Section**). The UV region gives information on the peptide backbone. Both diastereomers exhibit small negative Cotton effects in the far UV region (ca. 190 nm) indicating an absorption band due to $\pi \rightarrow \pi^*$ transitions from the peptide backbone. The positive and negative Cotton effects seen at around 230 nm, for the syn and anti diastereomers, respectively, is an indicator of the peptide backbone absorption where $n \rightarrow \pi^*$ transitions, due to the carbonyl, can occur. A positive shoulder for the syn compound is observed at around 240 nm.

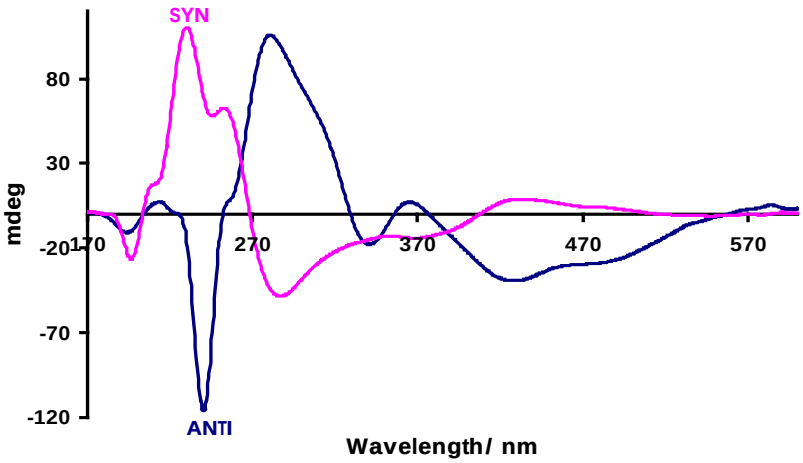

Figure 4-7. Circular dichroism spectra of syn and anti Re FGC diastereomers dissolved in methanol.

A strong positive Cotton effect and the negative Cotton effect found at around 300 nm, for the ReO FGC-anti and syn diastereomers, respectively are assigned to oxygen to rhenium charge-transfer transition as they were previously assigned for rhenium-Schiff base complexes.[20] The weak bands at lower energy, in the visible region, at ca. 400 nm and 480 nm, likely result from ligand to metal charge transfer (LMCT) transitions. The pronounced Cotton effects observed for the LMCT transitions demonstrate asymmetric induction from the enantiopure organic ligand to the metal center. Moreover, since both diastereomers were fully characterized by X-ray diffraction experiments, the CD profiles of other diastereomers can be compared to the ReO FGC spectra. Thus the absolute configurations for Re tripeptide diastereomers can be assigned.

The region below 300 nm reveals absorptions due primarily to the peptide backbone[21] and is not diagnostic for the syn and anti diastereomers. As expected, this region becomes complicated for peptides larger than tripeptides that have many residues giving rise to transitions in the near UV region. Transitions that involve the metal ion, such as LMCT and ligand field transitions, occur in the region above 300 nm and these transitions are, of course, the most revealing and important for assignment of diastereomers. The LMCT energy transition which largely contributes to this region, dictates the structure and color of diastereomers. In the case of rhenium analogs, all of the complexes that we isolated were brown-red in color, consistent with the visible bands for both diastereomers having the same maxima in their absorbance.

4.4. Conclusion

We have successfully assigned the anti and syn diastereomers of ReO tripeptides containing all L-amino acids to their HPLC profile, based on the same techniques used for the identification of TcO analogs. To date, six crystal structures, including TcO complexes, were obtained. More importantly, a complete pair of syn and anti crystal structures for ReO FGC is an important piece of evidence to support our structural assignment for the diastereomers. The X-ray work shows clearly that the early eluting (more hydrophilic) MO tripeptide (M=Tc,Re) corresponds to the anti diasteromer and the later eluting peak (less hydrophilic) corresponds to the syn diastereomer.

Also, in all crystal structures of ReO FKC syn and To YKC, we find that the amine of the first amino acid is deprotonated. This deprotonation is consistent with pK_a determination of the ReO FKC syn molecule where the pK_a is 5.6 much lower than the pK_a of the amine of ReO FGC (pK_a: 6.8). The crystal structures and the pK_a measurements together provide a picture that the lysine may interact with another portion of the molecule, such as the Re=O, rendering the phenylalanine amine acidic and easily prone to deprotonation to form a strong Re-N_{amide} bond.

4.5 References

1. Ehrhardt, G., *et al. J. Nucl. Med.*, **1987**. *28*: 656.
2. Knapp, F. F., *et al. Anticancer Research*, **1997**. *17*: 1783.
3. Guhlke, S., *et al. J. Labelled Compounds and Radiopharm.*, **1997**. *39*: 294.
4. Ehrhardt, G., *et al. Radioactivity Radiochem.*, **1992**. *3*: 38.
5. Rose, D. J., Maresca, K. P., Kettler, P. B., Chang, Y. D., Soghomomian, V., Chen, Q., Abrams, M. J., Larsen, S. K., Zubieta, J., *Inorg. Chem.*, **1996**. *35*(12): 3548.
6. Popov, K., Ronkkomaki, H. Lajunen, L. H. J., *Pure Appl. Chem.*, **2006**. *78*: 663.
7. Canney, D. J., *et al. J. Med. Chem.*, **1993**. *36*: 1032.
8. Francesconi, L. C., *et al. J. Med. Chem.*, **1994**. *37*: 3282.
9. Francesconi, L. C., Graczyk, G., Wehrli, S., Shaikh, S. N., McClinton, D., Liu, S., Zubieta, J.Kung, H. F., *Inorg. Chem.*, **1993**. *32*(14): 3114.
10. Jurisson, S. S., Schlemper, E. O., Troutner, D. E., Canning, L. R., Nowotnik, D. P., Neirinckx, R. D., *Inorg. Chem.*, **1986**. *25*: 543.
11. Wong, E., Fauconnier, T., Bennett, S., Valliant, J., Nguyen, T., Lau, F., Lu, L. F. L., Pollak, A., Bell, R. A., Thornback, J. R., *Inorganic Chemistry*, **1997**. *36*(25): 5799.
12. Liu, S., Edwards, D. S., *Chem. Rev.* , **1999**. *99*: 2235.
13. Grummon, G., Rajagopalan, R., Palenik, G., Koziol, A., Nosco, D., *Inorganic Chemistry*, **1995**. *34*: 1764.
14. Kung, H. F., Guo, Y. Z., Yu, C. C., Billings, J., Subraman, V., Calabrese, J. C., *J. Nucl. Med.*, **1989**. *32*: 433.

15. Mahmood, A., Baidoo, K. E., Lever, S. Z., *Technetium and Rhenium in Chemistry and Nuclear Medicine 3*, 1989, Cortina International Raven Press. p. 119.

16. Melnik, M., Van Lier, J. E., *Coord. Chem. Rev.*, **1987**. *77*: 275.

17. Ohmomo, Y., Franceconi, L. C., Kung, M., Kung, H., *J.Med.Chem.*, **1992**. *35*: 157.

18. Takayama, T., Suzuki, K., Sekine, T., Kudo, H., *Radiochimica Acta*, **2000**. *88*(3-4): 247.

19. Hansen, L., Lipowska, M., Melendez, E., Xu, X., Hirota, S., Taylor, A. T., Marzilli, L. G., *Inorg. Chem.*, **1999**. *38*: 5351.

20. Bereau, V. M., Khan, S. I., Abu-Omar, M. M., *Inorg. Chem.*, **2001**. *40*: 6767.

21. Cheng, Y., Yan, Y.-B., Liu, J., *Inorg. Biochem.*, **2005**. *99*: 952.

5. Understanding Stability of $^{99m/99}$TcO and ReO Tripeptide Diastereomers

5.1. Introduction

Identification of the absolute configurations of the syn and anti diastereomers and correlating these structures to their HPLC profiles, accomplished in this project, Chapters 3 and 4, provide us with the opportunity to understand the features of the tripeptides and the metal tripeptide complexes that result in stabilization of certain diastereomers. Such a fundamental understanding of the forces that stabilize specific diastereomers should be very useful in designing ^{99m}Tc and ^{188}Re radiopharmaceuticals wherein the most stable diastereomer can be selected.

We and others have observed that diastereomers, represented by peaks on the HPLC, interconvert to form an equilibrium mixture. [1-3] The more stable diastereomer, of course, would show the most intensity monitoring the gamma ray of ^{99m}Tc or the UV of ^{99}Tc or Re. At the outset of our studies, we hypothesized that large amino acid residues and possibly, residues containing moieties that can hydrogen bond with Tc=O bond are two factors that are responsible for interconversion of diastereomers. To test this hypothesis and, specifically to synthesize pure diastereomers, we chose tripeptides with some bulk in the first position to mimic depreotide, but still maintain water solubility on the macroscopic level as the ^{99}Tc and Re complexes. Also amino acids were chosen that possessed the potential to hydrogen bond with the M=O bond (M = $^{99/99m}$Tc, Re); specifically we chose lysine with H-bonding potential as the second amino acid. Our

studies, using ^{99}Tc and Re, show that the diastereomer interconversion indeed appears to be related to the bulk of the side chain and suggests that hydrogen bonding opportunities of the residues with the M=O unit, may stabilize the syn diastereomer. We report here observations, followed up by kinetic and thermodynamic data that bear on understanding the stability of the diastereomers through the interconversion process. We are investigating this further through a combination of theoretical studies and experimental studies.

5.2. Experimental

5.2.1. Materials

Fmoc-protected L-amino acids and Rink amide MBHA resin were purchased from NovaBiochem. N-hydroxybenzotriazole (HBTU) was purchased from ChemTech. 2-(1H-benzotriazole-1-yl)-1,1,3-tetramethyluronium (HOBt), N,N-diisopropylethylamine (DIPEA), piperidine, phenol, thioanisole, triisopropylsilane (TIS), and 1,2-ethanedithiol (EDT) were purchased from Sigma-Aldrich. HPLC-grade acetonitrile, trifluoroacetic acid (TFA) and N,N-dimethylformamide (DMF) were purchased from Fisher Scientific. Nanopure water was obtained from a Millipore filtration system equipped with a 0.22 μm filter. All chemicals were used as received without further purification.

^{99}Tc is a low-energy (0.292 MeV) β^- emitter with a half-life of 2.12 x 10^5 years. This isotope should be handled in a fume hood using appropriate radioactive protocols.

$NH_4{}^{99}TcO_4$ was obtained from Oak Ridge National Laboratory, Oak Ridge, TN. 30% H_2O_2 was added to an aqueous solution of $NH_4{}^{99}TcO_4$ to oxidize any $^{99}TcO_2$ present. The ammonium pertechnetate solution was standardized prior to use as previously described.[4] The reagent $[TcOCl_4]N(C_4H_9)_4$ was prepared following a published procedure.[5] $N(C_4H_9)_4$ $[ReOBr_4(OP(C_4H_9)_3]$ was prepared according to a published procedure.[6] ^{99m}Tc-pertechnetate (^{99}Mo/^{99m}Tc generator) was obtained from Cardinal Health (Bronx, NY).

5.2.2. Instrumentation and Analytical Methods

RAININ Dynamax HPLC system equipped with a Dynamax UV-1 UV-visible detector and two Dynamax model SD-200 pumps using 25-mL pump heads was employed. The software used was Varian Star LC Workstation Ver. 6 and all HPLC experiments were monitored at a λ = 220 nm. A home-built detector composed of ORTEC components such as power supply, high voltage supply, and amplifier, was interfaced to the HPLC system to monitor gamma (γ) ray of ^{99m}Tc. For both analytical and preparative work, the mobile phase consisted of (A) 0.1 % TFA in H_2O and (B) 0.1 % TFA in ACN/H_2O (90/10). Three methods were used in these studies: (1) Analytical Method 1 – Column: Waters DeltaPak 5μ C_{18} 100 Å, 3.9 x 150 mm; Mobile Phase Gradient: 4 % - 35 % B over 10 min; Flow Rate: 1.0 mL/min; (2) Analytical Method 2 – Column: Waters DeltaPak 5μ C_{18} 100 Å, 3.9 x 150 mm; Mobile Phase Gradient: 10 % - 40 % B over 10 min; Flow Rate: 1.2 mL/min; and (3) Preparative Method – Column:

Waters DeltaPak 5μ C_{18} 300 Å, 19.0 x 300 mm; Mobile Phase Gradient: 4 % - 35 % B over 20 min; Flow Rate: 24.0 mL/min.

Mass spectral data were acquired on an Agilent Technologies 1100 Series LC/MS model G1946D using electrospray ionization in the positive and/or negative-ion mode. Infrared spectra were recorded from KBr disks on a Perkin Elmer 1600 FT-IR spectrometer in the range 600 - 3000 nm and were referenced to polystyrene film.

5.2.2.1. Preparation of Phosphate Buffers

Two buffer systems were used to prepare 100 mL of 0.5 M sodium phosphate solution with pH ranging from 5 to 10.

For pH < 10, the buffer system consisted of $NaH_2PO_4 \cdot H_2O$ and $Na_2HPO_4 \cdot 7H_2O$. For pH = 10, the buffer system consisted of $Na_2HPO_4 \cdot 7H_2O$ and $Na_3PO_4 \cdot 12H_2O$. **Table 5-1** shows the actual proportion (in moles) of each component to prepare 0.5 M phosphate buffers at pH 5, 8, 9, and 10. The solid components were dissolved initially in about 80 mL of nanopure water. To facilitate dissolution of highly saturated component, warming the solution was required. When all the components were totally dissolved, the solution was diluted to 100 mL with nanopure water. Finally, the resulting pH of the buffer solutions was adjusted with a few drops of 2.5 M sodium hydroxide to reach the desired pH. All buffers were stored at 37 ^{o}C prior to use.

Table 5-1. Amount (in moles) of hydrated sodium salts needed to prepare 100 mL of 0.5 M phosphate buffers at different pH values.

pH	Amount of Component 1, mol x 10^{-4}	Amount of Component 2, mol x 10^{-4}
5	5.998 (Na_2HPO_4•$7H_2O$)	494.0 (NaH_2PO_4•H_2O)
8	466.0 (Na_2HPO_4•$7H_2O$)	34.00 (NaH_2PO_4•H_2O)
9	497.0 (Na_2HPO_4•$7H_2O$)	3.399 (NaH_2PO_4•H_2O)
10	2.099 (Na_3PO_4•$12H_2O$)	498.0(Na_2HPO_4•$7H_2O$)

5.2.3. Procedure for Synthesis of Phe-Gly-Cys (FGC) and Phe-Lys-Cys (FKC)

The protocol described in 2.2.3. was used to prepare FGC and FKC ligands.

5.2.4. Procedure for Synthesis of ^{99}Tc/ReO FGC and ^{99}Tc/ReO FKC Diastereomers

The protocol described in 3.2.3 was used to prepare technetium-99 complexes of FGC and FKC. The protocol described in 4.2.3 was used to prepare the rhenium complexes of FGC and FKC.

5.2.5. Procedure for Monitoring Interconversion of Macroscopic ReO FGC Diastereomers using HPLC-UV Detection

Monitoring qualitative compound concentration and chemistry using UV detection interfaced with HPLC techniques is well-established..[2, 3, 7-9] However, to use UV detection accurately to understand qualitatively and especially, quantitatively, the stability of diastereomers and interconversion to the more stable diastereomer it is necessary that the extinction coefficients of the two diastereomers are known. In the case of ReO FGC complex, to a first approximation, the syn and anti diastereomers possess the same extinction coefficients because the tripeptide ligands making up the syn and anti diastereomers are the same and the detection is monitored at 220 nm where the absorption is due only to the peptide backbone of the FGC ligand. The Re=O and the charge transfer transitions will not contribute to the total absorption band because these functional groups absorb in the visible region.[10] To a first approximation, the area under the absorbance peak accurately reflects the concentration of the species.

However, for the macroscopic work (^{99}Tc and Re), reported in a subsequent section, we did not process the area under the absorbance curves at 220-nm with the peakfit program and therefore, we are not producing data on rates and equilibrium constants. Our data accurately reflect the time to equilibrium and we can designate the more stable species and estimate the equilibrium ratios.

Stability in Water: The solutions used for this study were prepared by dissolving 1.0 mg of both syn or anti diastereomers of ReO FGC in 1.0 mL of nanopure water at pH 6. 10 μL each of the prepared solution was injected onto the HPLC using **Analytical Method 1**. Injections were made as a function of time to monitor progress of the interconversion of diastereomers at this pH.

Stability in Methanol/Water: To monitor the diastereomer stability at pH 5, 2.0 mg of the complex was dissolved in 1.0 mL of methanol and 1.0 mL of sodium acetate buffer (0.5 M, pH 5) was immediately added into it. Diastereomer stability at pH 9 was monitored similarly: 1.0 mL of ammonium chloride (0.5 M, pH 9) was added into the methanolic solution of the complex. The interconversion was monitored by HPLC using **Analytical Method 1**.

5.2.6. Procedure for Monitoring Interconversion of tracer ^{99m}TcO Diastereomers Using HPLC-Gamma Detection

5.2.6.1. Radiolabeling of FGC and FKC with ^{99m}TcO

The radiolabeling procedure used by Liu et al.[11] was modified and adapted for these experiments. To a microcentrifuge tube, 25 μL of the tripeptide solution (0.6-1 mg/mL in saline) and 10 μL of sodium tartrate solution (50 mg/mL in ammonium buffer containing 0.5 M ammonium bicarbonate, 0.25 M ammonium acetate, and 0.18 M ammonium hydroxide) were added and mixed. In a lead-shielded fumehood, the tripeptide-tartrate solution was radiolabeled by adding 100 μL of sodium pertechnetate containing 2 – 4 mCi, and followed by 5 μL stannous chloride dihydrate (1 mg/mL in 0.01 M hydrochloric acid). The solution was vortexed briefly and was used immediately for the interconversion experiments described below. The diastereomers were not separated. The pH of the final ^{99m}Tc tripeptide solution was 8.98. This ^{99m}Tc peptide

solution was buffered, as described in the following section and was used for subsequent equilibrium studies.

5.2.6.2. Interconversion Experiments Monitored by Reverse-Phase HPLC

All phosphate buffers were stored at 37 ^{o}C. For each experiment, 100 μL of a buffer solution was added to the radiolabeled tripeptide solution. The pH of the ^{99m}Tc tripeptide solution was the same as the pH of the buffer. The microcentrifuge tube containing the buffered reaction solution with a total volume of 240 μL was then inserted in a heating block maintained at 37 ^{o}C. 10 μL of the radiolabeled solution was removed as a function of time and injected onto the HPLC analytical column. For a very fast interconversion reaction, for example at pH above 10, it was necessary to quench the reaction by taking out 20-μL aliquot from the heated reaction solution and chilling it in an ice-bath. The aliquots did not require further warming when ready for the HPLC analysis. The progress of the interconversion of ^{99m}Tc diastereomers was monitored, by gamma detection, using **Analytical Method 1 or 2**. At the end of the interconversion experiment, the pH of the buffered sample solution was checked and no significant change of the pH was observed.

5.2.6.3. Peak Fitting Procedure for Chromatograms

For a HPLC-gamma detection technique, the integrated area under the curve (in volts) of a chromatogram is directly proportional to the concentration of a substance

being determined. To compare the concentrations of the ^{99m}Tc species, the chromatograms were subjected to peak fit analyses using the software package PeakFit ver. 4.12. This software also tested for the presence of other small peaks. In the initial step in the peak fitting procedure, an appropriate method to find hidden peaks is chosen. One typical example is the deconvolution method which is a mathematical procedure often used to remove the smearing or broadening of peaks arising because of the imperfections in an instrument's measuring system. After the deconvolution step, the components peaks were resolved via non-linear fitting procedure using the EMG (exponentially-modified Gaussian) convolution model. Detailed discussions on different convolution models and mastery of the software can be found in the user's manual.[12]

Figure 5-1 illustrates an example of peak fitting of the data set derived from an HPLC chromatogram of ^{99m}TcO FGC. As displayed in the figure, the top trace shows the two peaks due to the diastereomers and the bottom trace shows the fit (goodness of fit of 0.9913). The fitting procedure verifies that there are no hidden peaks under the two peaks of the diastereomers. Also, the integrated areas under the curve for the first peak (A or anti) and the second peak (B or syn) on this particular chromatogram were reported as 0.003136 and 0.001361 volts, respectively (see **Table 5-2** at t = 1500 s).

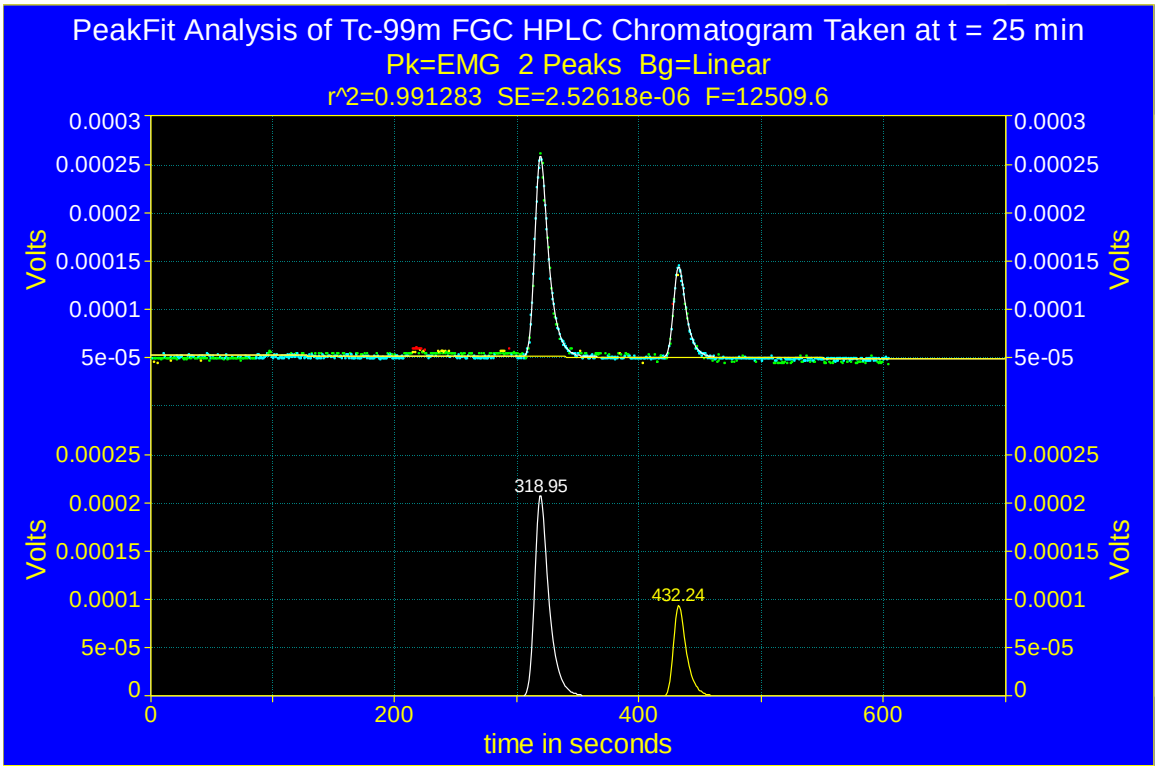

Figure 5-1. Example of data set from a chromatogram (top trace) fitted to an EMG model (bottom trace) using PeakFit ver. 4.12 software.

5.2.6.4. Data Analysis

5.2.6.5. Basis for Construction of First-Order Linear Plot

The interconversion of isomers is a first order process[13] and has been examined previously[14, 15]; the interconversion of syn and anti diastereomers has also been considered as a first order process.[7]

In general, the first-order reaction close to equilibrium is best described by

$$A \underset{k_{-1}}{\overset{k_1}{\rightleftharpoons}} B \qquad (1)$$

where A and B are two diastereomers.

Accordingly, the concentration of A is reduced by the forward reaction (rate constant is represented by k_1) but it is increased by the reverse reaction (rate constant is represented by k_{-1}). The net rate of change is therefore:

$$-\frac{d[A]}{dt} = k_1[A] - k_{-1}[B] \qquad (2)$$

If the initial concentration of **A** is $\mathbf{[A]_o}$, and no **B** is present initially, then at all times $\mathbf{[A] + [B] = [A]_o}$. Therefore, equation **(2)** becomes

$$-\frac{d[A]}{dt} = k_1[A] + k_{-1}([A]_o - [A]) = (k_1 + k_{-1})[A] - k_{-1}[A]_o \qquad (3)$$

The solution of this first-order differential equation[13] is

$$[A] = ([A]_o - [A]_{eq}) \exp\{-(k_1 + k_{-1})\}t + [A]_{eq} \qquad (4)$$

where $\mathbf{[A]_{eq}}$ is the concentration of A at equilibrium. By bringing $\mathbf{[A]_{eq}}$ and $\mathbf{([A]_o - [A]_{eq})}$ to the left side and then taking natural logarithms, we can rewrite equation **(4)** as:

$$\ln \frac{([A] - [A]_{eq})}{([A]_o - [A]_{eq})} = -(k_1 + k_{-1})t \qquad (5)$$

Further rearrangement of equation **(5)** leads to a positive slope equal to $\mathbf{k_1 + k_{-1}}$ when time **t** is plotted against $\mathbf{\ln\{([A]_{eq} - [A]_o) / ([A]_{eq} - [A])\}}$, generating a linear graph that

intercepts through the origin. Since the equilibrium constant $\mathbf{K_{eq}}$ can be derived from the ratio of $\mathbf{[A]_{eq}}$ to $\mathbf{[B]_{eq}}$ at the endpoint of the experiment, thus, the rate constants $\mathbf{k_1}$ and $\mathbf{k_{-1}}$ can be uniquely determined from the plot.

5.2.6.6. Sample calculations to obtain equilibrium contstant (K_{eq}) and rate constants (k_1 and k_{-1})

The equilibrium reaction for the interconversion for the ^{99m}TcO FGC complexes, is described in equation **(6)**, below. The notation Syn (B) denotes the "syn" diastereomer (represented by the later eluting peak B) and Anti (A) denotes the "anti" diastereomer (represented by the early eluting peak A). Our earlier work, see Chapters 3 and 4, identified the diastereomers.

$$\text{Syn (B)} \underset{k_{-1}}{\overset{k_1}{\rightleftharpoons}} \text{Anti (A)} \qquad (6)$$

In equation **(6)** k_1 is the rate constant for the forward reaction and k_{-1}, the rate constant for the reverse reaction. **Figure 5-2** shows an experiment wherein the conversion of the syn ^{99m}Tc FGC to the anti complex at pH 10.5 and 37 ^{o}C, is monitored. It can be seen from **Figure 5-2** that the later eluting peak (B, syn) decreases while the first peak (A, anti) increases. The equilibrium is reached over a time period of less than two hours. **Table 5-2** shows the integrated areas of the peaks A and B at different time intervals. The fourth column of the table represents the fractions of the syn (B) which are then used for evaluating the term $\mathbf{\ln ([B]_{eq}-[B]_o)/([B]_{eq}-[B])}$ found in the last column, in which:

$[B]_o$ = fraction of syn at t = 0,

[B] = fraction of syn at any time t, and

$[B]_{eq}$ = fraction of syn at equilibrium.

The natural log values are plotted with times (in sec). If the reaction is first order, a linear graph, with a slope equal to $\mathbf{k_1 + k_{-1}}$, is expected (**Figure 5-3**). In order for k_1 and k_{-1} to be determined, we first calculate the K_{eq} by dividing the area of the anti (A) with that of the syn (B) at the time of equilibrium (the last entry in the second and third columns, respectively). Thus k_1 and k_{-1} can now be algebraically manipulated using the following equations: $K_{eq} = k_1 / k_{-1}$ and slope = $k_1 + k_{-1}$.

Calculations:

$K_{eq} = [A]_{eq} / [B]_{eq} = 0.002976 / 0.000834 =$ **3.57**

$K_{eq} = k_1 / k_{-1} \rightarrow k_1 = K_{eq} \times k_{-1} = 3.57\ k_{-1}$ **(7)**

From the linear graph: slope = $0.0011 = k_1 + k_{-1}$ **(8)**

Expressing k_{-1} in terms of $k_1 \rightarrow k_{-1} = 0.0011 - k_1$ **(9)**

Substituting equation **(7)** into equation **(9)**: $k_{-1} = 0.0011 - 3.57k_{-1}$

Solving for k_{-1}, thus, $k_{-1} =$ **2.41×10^{-4}**

Substituting into equation **(7)**: $k_1 = 3.57\ (2.41 \times 10^{-4}) =$ **8.59×10^{-4}.**

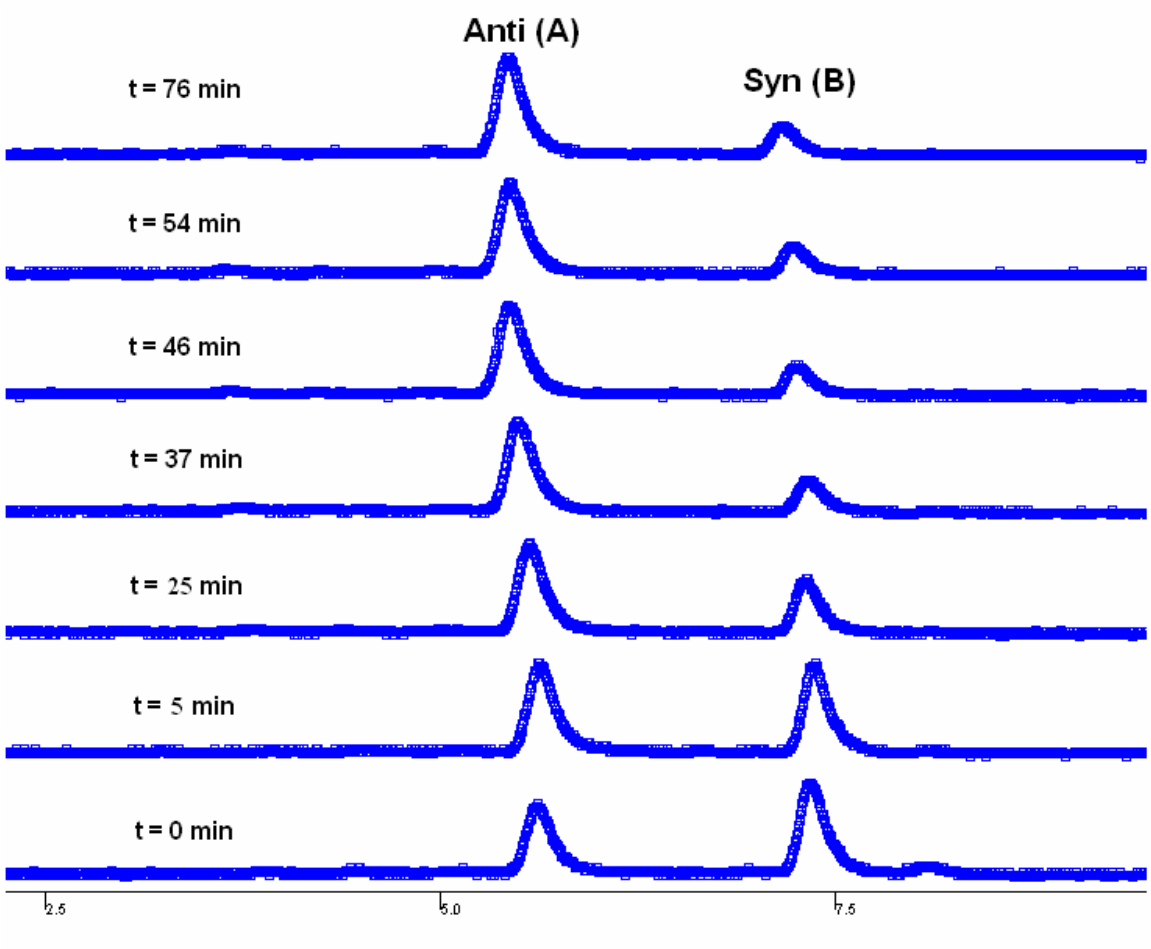

Figure 5-2. HPLC analyses of ^{99m}TcO FGC at different time intervals showing interconversion of syn (B) to anti (A) under the following conditions: pH 10.5, 37 ^{o}C. The equilibrium is t = 76 min.

Table 5-2. The interconversion ^{99m}TcO FGC, pH 10.5, 37 ^{o}C. Recorded areas for peaks A (column 2) and B (column 3) using PeakFit analysis and the evaluation of the natural log term (last column).

time, s	A, volts	B, volts	B/(A+B)	$[B]_{eq} - B_o$	$[B]_{eq} - [B]$	$\frac{[B]_{eq}-[B]_o}{[B]_{eq}-[B]}$	$\ln\left(\frac{[B]_{eq}-[B]_o}{([B]_{eq}-[B])}\right)$
0	0.001903	0.002532	0.570954	-0.3521	-0.3521	1	0
300	0.002486	0.002363	0.487355	-0.3521	-0.2685	1.31136057	0.271065204
1500	0.003136	0.001361	0.302635	-0.3521	-0.08378	4.20277647	1.435745371
2220	0.003023	0.00104	0.25587	-0.3521	-0.03701	9.51313475	2.252673449
2760	0.003016	0.00095	0.239454	-0.3521	-0.0206	17.0955644	2.838819037
3240	0.002992	0.000886	0.228521	-0.3521	-0.00966	36.4388851	3.595636476
4560	0.002976	0.000834	0.218858	-0.3521	0	N/A	N/A

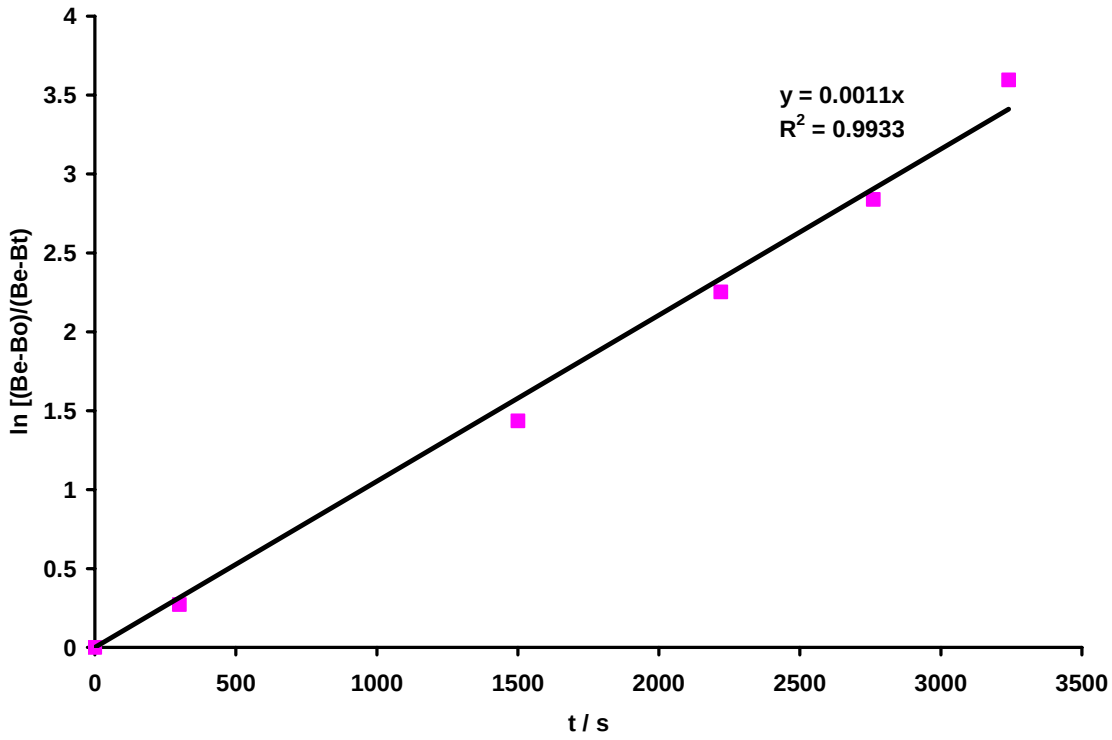

Figure 5-3. Linear plot for the first-order rate of reaction for ^{99m}TcO FGC syn to anti interconversion, pH 10.5, 37 ^{o}C.

Using the same procedure as for FGC, we also determined the rate constants and equilibrium constants of ^{99m}TcO FKC. Since the interconversion for this case is from anti

to syn, the natural log parameter is expressed in terms of A (anti) as shown by equation **(5)**.

5.3. Results and Discussion

5.3.1. Interconversion of Macroscopic ReO and ^{99}TcO Diastereomers – Preliminary Results

The syntheses of the macroscopic ^{99}Tc and Re tripeptide complexes were monitored by analytical HPLC. Observations made during the synthesis of the macroscopic ^{99}Tc and Re FGC suggested that species B (subsequently identified as the syn diastereomer) was formed rapidly and converted to species A (the anti diastereomer). The equilibrium A:B ratio of 90:10 was attained in less than 30 minutes for TcO FGC and in about four hours for ReO FGC.

Upon isolation of the pure A (anti) and B (syn) diastereomers of ReO FGC, we were then able to monitor the interconversion more rigorously. When dissolved in water at pH 6, ReO FGC anti was relatively stable and no interconversion from anti to syn occurred within many days. However, as shown in **Figure 5-4**, we did see interconversion of ReO FGC syn (B) to anti (A) when the isolated syn complex was dissolved in water at pH 6. Thus, we can conclude that the anti diastereomer of ReO FGC is more stable than the syn diastereomer and under low pH aqueous condition, the interconversion of diastereomers can be minimized.

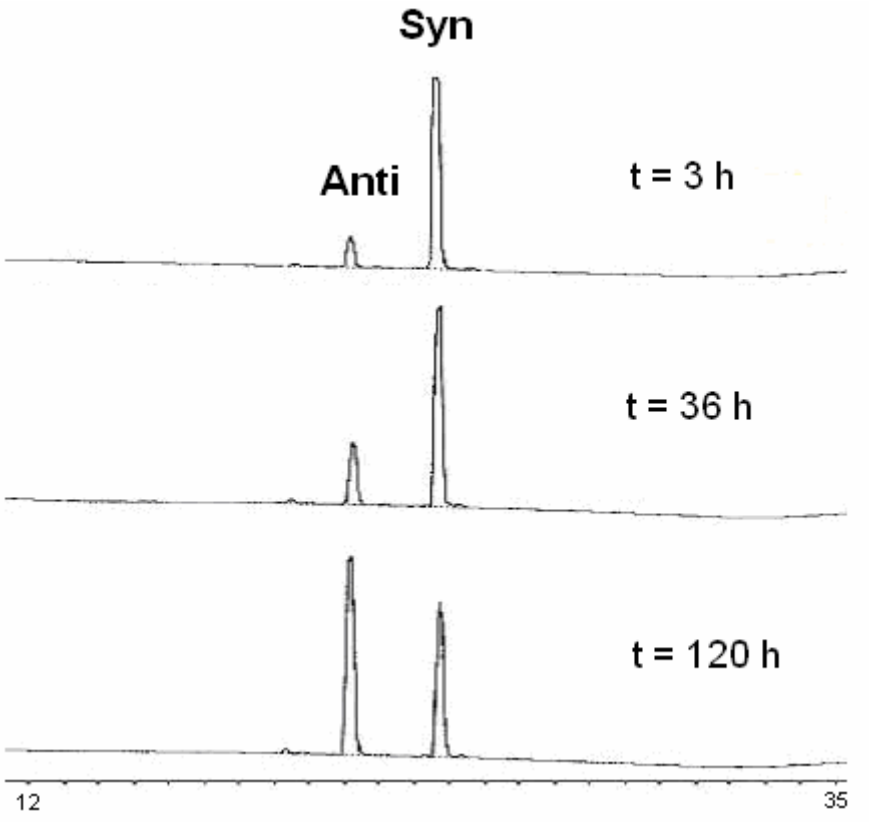

Figure 5-4. HPLC analyses of the pure ReO FGC syn diastereomer dissolved in water at pH 6. The interconversion of syn (B) to anti (A) was monitored over time.

When the purified solid of ReO FGC anti was dissolved in methanol and buffered with 0.5 M NH_4Cl at pH 9, we observed anti to syn interconversion according to **Figure 5-5 (left)**. This result suggests that the interconversion of diastereomers can be facilitated by introduction of base. Moreover, as expected, the base-catalyzed interconversion of diasteromers was observed in the reverse reaction , shown in **Figure 5-5 (right)** when the pure ReO FGC syn was dissolved in methanol following the addition of 0.5 M NH_4Cl at pH 9. These experiments were not carried out quantitatively, however, we observe in

Figure 5-5 (right) that the syn converted to the anti forming an equilibrium mixture with the anti**:**syn ratio of about 90**:**10 in about two hours, whereas in **Figure 5-5 (left)** the syn to anti interconversion may have not reached the equilibrium mixture in more than 3 hours. It is likely and expected that the rates of interconversion (syn to anti and anti to syn) are different. However, under the same conditions the equilibrium can be reached from both syn and anti position and basic conditions appear to increase the rate of the interconversion. This experiment is consistent with our synthetic efforts described in Chapters 3 and 4, and attests to the stability of the anti diastereomer over the syn diastereomer for ReO FGC complex.

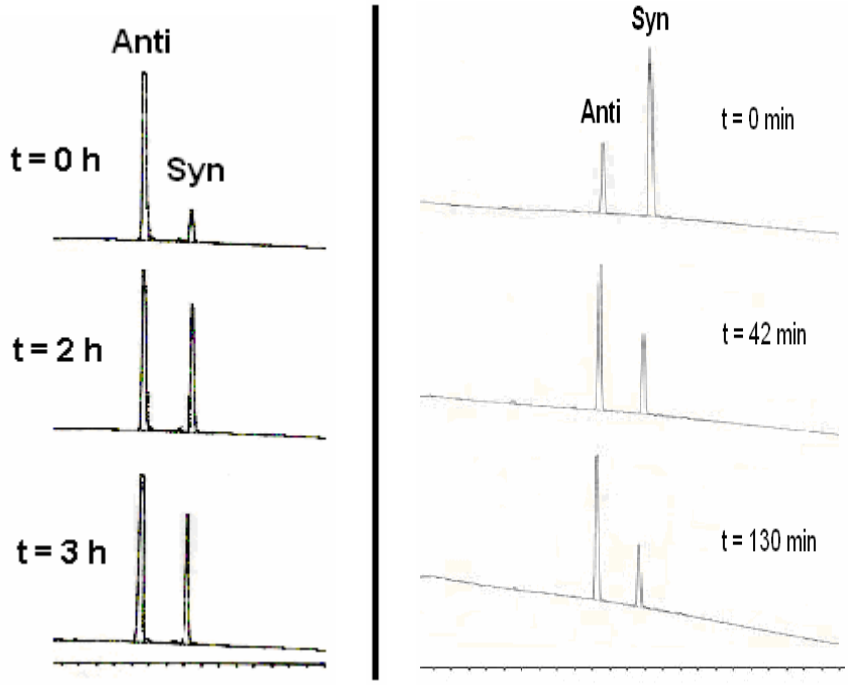

Figure 5-5. HPLC analyses of ReO FGC diastereomers dissolved in methanol and buffered with 0.5 M NH_4Cl at pH 9. The interconversion from anti to syn (left) and the interconversion from syn to anti (right) were monitored over time.

Using Analytical Method 1 in **Section 4.2.1 of Chapter 4,** the HPLC analysis of the dark brown crude solution for the synthesis of ReO FKC reproducibly produced also two major peaks shown in **Figure 5-6** with ratios ca. 10**:**90 anti**:**syn. This result suggests that, in contrast to ReO FGC, the B (syn) diastereomer of ReO FKC is more stable than the A (anti) diastereomer. We suggest that the favored syn configuration may be due to the spatial orientation of the lysine residue allowing the ε-NH_2 to hydrogen bond with Re=O as described by the molecular model on **Figure 5-6**.

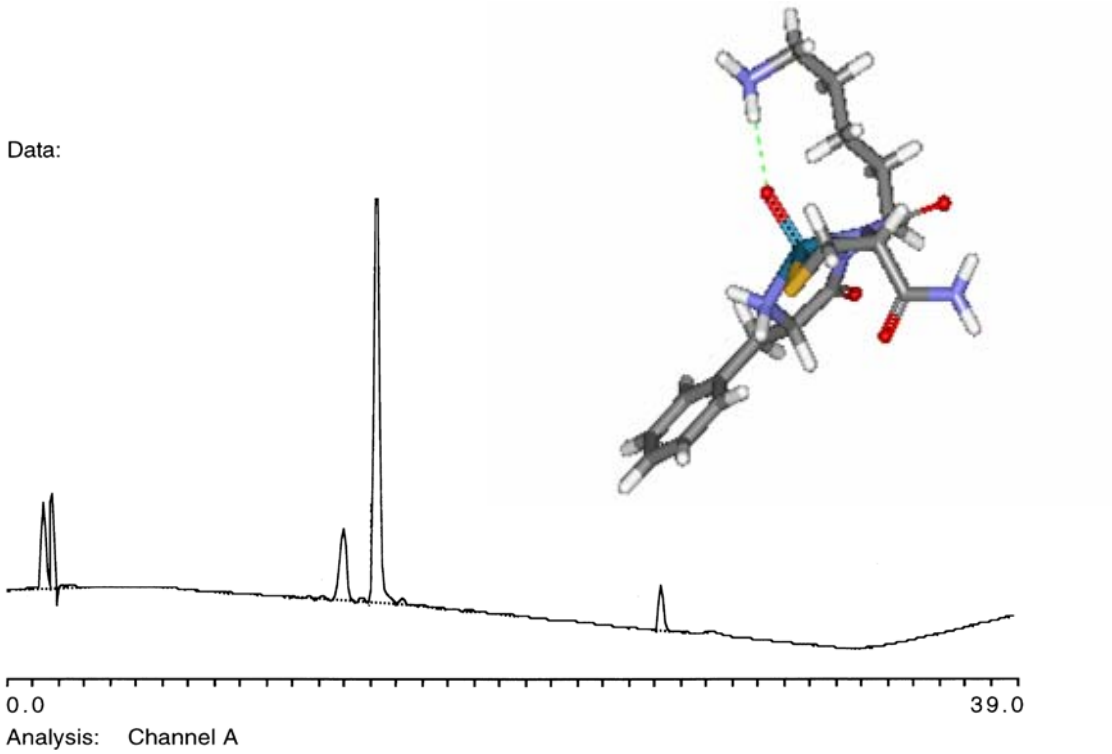

Figure 5-6. HPLC analysis of the reaction solution for the formation of ReO FKC where anti to syn ratio is 10:90. The third peak at retention time of about 25 min is an impurity from the FKC peptide. (Inset: molecular model of the more stable diastereomer (syn) showing H-bonding interaction between the lysine residue and Re=O group).

Another interesting behavior we observed is when aspartic acid (D) was placed in the second position of the tripeptide (FDC). The initial HPLC chromatogram taken immediately after the tripeptide and the ReO reagent were mixed together in methanol is shown in **Figure 5-7**. At time t = 0, two peaks assigned as A and B were observed at retention times of 15 and 16 min, respectively. At t = 48 h, additional two peaks assigned as C and D formed at retention times of 19 and 21 min, respectively. The HPLC fractions of C and D were collected and lyophilized forming brownish purple powder. A circular dichroism profile (**Figure 5-8**) was taken for these two species, confirming that

the products C and D are diastereomeric species. Products A and B were also collected and lyophilized but did not produce a substantial amount for characterization as they converted easily to C and D**.**

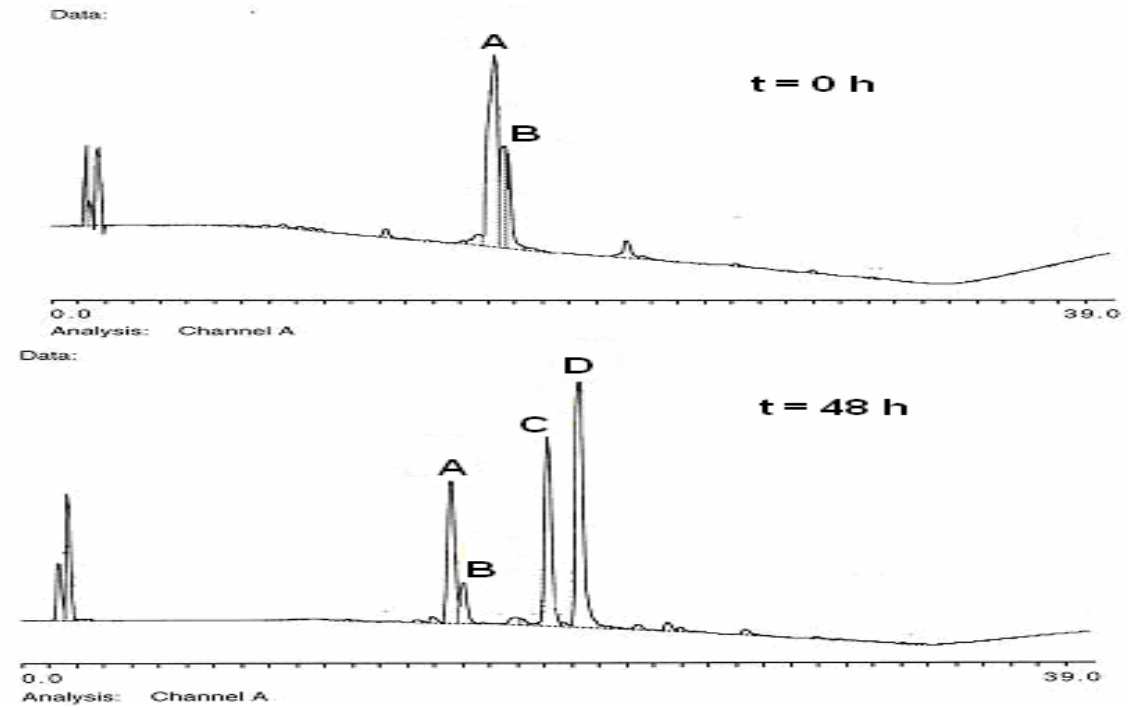

Figure 5-7. HPLC analysis of ReO FDC showing only two species, A and B, that may be diastereomers; after 48-hour equilibration, two more species, C and D, appeared. It is likely that C and D are diastereomers as well (see Figure 5-8).

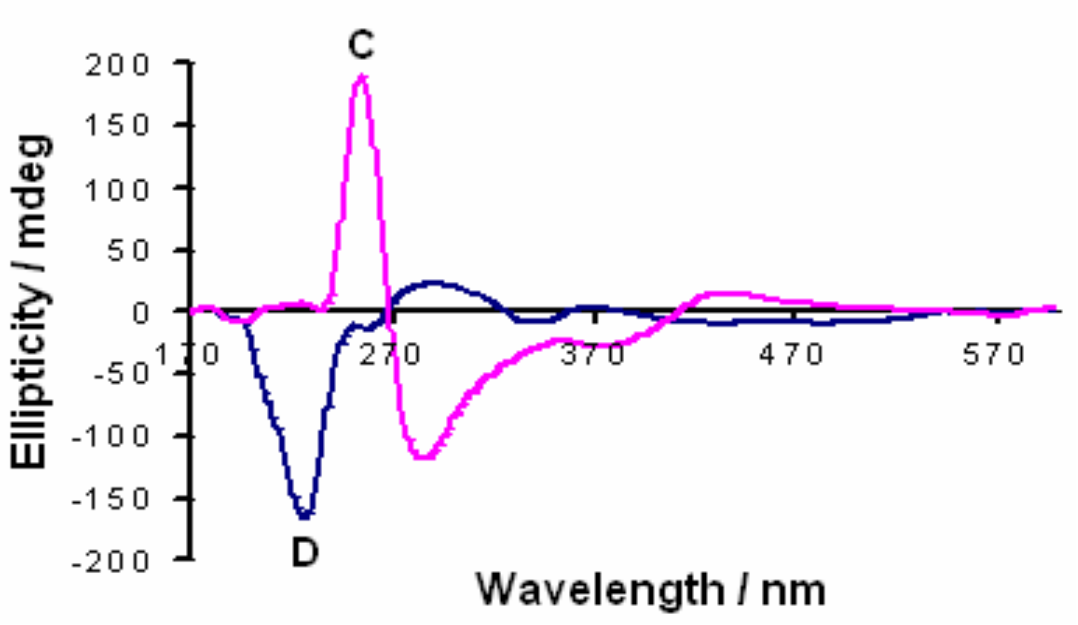

Figure 5-8. Circular dichroism spectra of ReO FDC-C (blue) and ReO FDC-D (purple) dissolved in methanol.

In a study of Tc/Re RP 294, $(Me)_2$Gly-Ser-Cys(Acm)-Gly-NH_2 (**Figure 5-9**), Wong postulated that water was involved in a mechanism whereby a water molecule binds to the sixth position of the metal trans to the –yl oxo ligand and a series of proton transfers (to the dimethylamine nitrogen and to the original –yl oxygen atom) results in the interconverted species.[3] In our work, we find that base accelerates the conversion reactions of ^{99}Tc,Re tripeptides. We also observed deprotonation of the amine nitrogen atom, a process that is consistent with the Wong hypothesis of proton transfers. Hydrogen bonding may also play a role in stabilization of diastereomers. For example, lysine in the second position appears to stabilize the "syn" diastereomer possibly by H bonding of the ε- NH_2 to the Tc=O, perhaps prohibiting the conversion process, because for Tc/Re FKC no interconversion is observed. Inspection of the packing diagrams of

ReO FKC (**Figure 5-10**), suggest that hydrogen bonding occurs between the ε- NH_3^+ and a Re=O of an adjacent molecule.

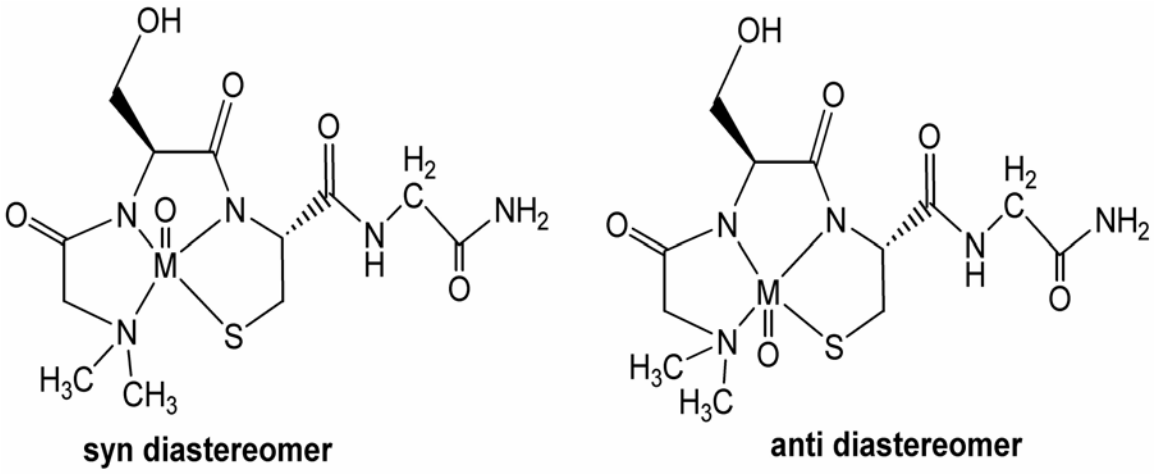

Figure 5-9. The syn and anti diastereomers of MO RP294 (M = Tc/Re)

Table 5-3 shows the observed times to equilibria for selected M=O tripeptide diastereomers from preparative Reverse-Phase HPLC work. The concentrations at equilibrium are estimated based on the area of the peaks. The starting concentrations are difficult to obtain and we estimate these as 50:50 based on our experience with macroscopic synthesis of ^{99}Tc and Re tripeptides. The rates of conversion appear to be influenced by the OH and NH functional groups, as well as by the length of the side-chain residue in the second position of the tripeptide ligand. Interconversion occurs more rapidly for Tc than for Re, in accordance with periodic trends.

From crystal structure data, there appears to be a possible interaction of the O bound to the ^{99}Tc or Re with the amide N (cysteine) for the MO FGC (M=^{99}Tc, Re). The DFT calculations, performed by M. Benard and M.-M. Rohmer on ReO FGC are consistent with a slightly higher stability of the anti diastereomer than the syn diastereomer.[16] These data are consistent with the studies reported above, wherein the equilibrium favors the anti diastereomer; thus the anti diastereomer exhibits a higher stability than the syn.

In contrast, the ^{99}Tc and Re FKC show a different behavior. First of all, crystal structure of the ReO FKC syn shows a possible interaction of the ε-NH_3^+ of the lysine with a Re=O of an adjacent molecule (in an adjacent unit cell as shown in **Figure 5-10**). These data suggest that hydrogen bonding may be possible in the syn diastereomer. Preliminary DFT studies (assuming an amine for N1 that is present in solution according to NMR data under acidic conditions and in organic solution, Chapters 3 and 4) show that, considering solvent, the syn diastereomer is slightly more stable than the anti. These data are consistent with the observations reported here that the syn diastereomers for the ^{99}Tc FKC and Re FKC are more stable than the anti.

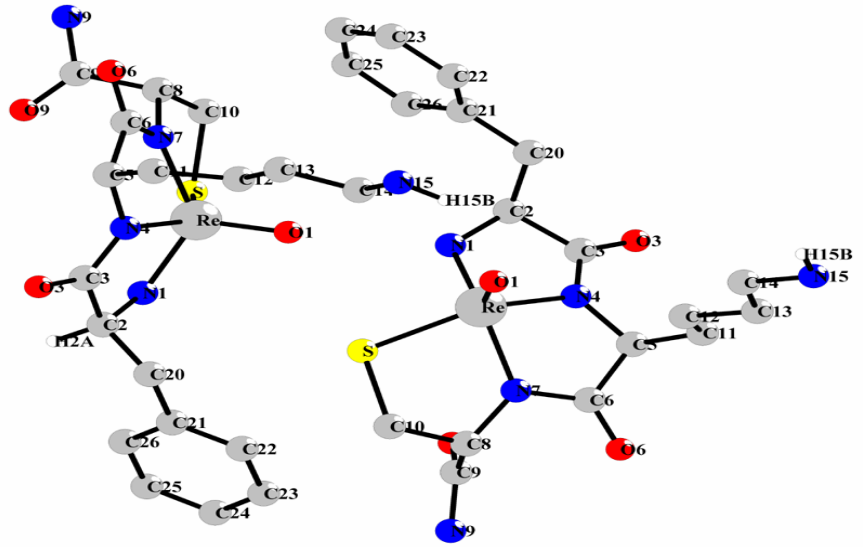

Figure 5-10. Crystal packing diagram of ReO FKC showing one pair of molecules; hydrogen atoms are omitted for simplicity except for H15B. The atomic distance between H15B (ε-NH_3^+) of the lysine residue from one molecule and O1 of the Re=O center from the neighboring molecule is 2.58 Å. This distance is within the range of strong intermolecular hydrogen-bonding interaction.

We postulate that in the absence of the lysine residue, the major factor in determining stability is the interaction of the –yl oxygen (Tc=O or Re=O) with the NH_2 (amide) of the cysteine, thus accounting for the stability of the MO FGC-anti species (M=Tc,Re). When the lysine is present in the molecule, the potential interaction of the ε-NH_3^+ with either the C=O of the tripeptide or the –yl oxygen bound to the Re may provide the dominant factor in determining stability of the syn diastereomer.

We focus on the FGC and FKC tripeptides in our subsequent studies with ^{99m}Tc to probe quantitatively the stabilities and the factors that influence stabilities of diastereomers.

Table 5-3. Conversion of MO (Phe-Xxx-Cys) [M = ^{99}Tc, Re] in methanolic solution to an equilibrium mixture.

	^{99}Tc		**Re**	
Xxx	**Time to equilibrium**	**Equilibrium A:B ratio**	**Time to equilibrium**	**Equilibrium A:B ratio**
Gly	20 min	90:10	4.1 hr	90:10
Ser	5 hr	30:70	14 hr	30:70
Lys	2 min	10:90	2 min	10:90

5.3.2. Interconversion of the Tracer ^{99m}TcO Peptide Diastereomers

Analytical Methods 1 and 2, **Section 5.2.2,** were employed to monitor the interconversion of the tracer compounds. Diastereomers did not interconvert at low pH. Even when buffered at pH 5.03, ^{99m}Tc FKC showed no significant change when monitored over 4 hours, **Figure 5-11**. Interconversion to equilibrium mixtures did occur at pH greater than 6 or 7 and thus, we monitored the interconversion at pH 8, 9, and 10, at 37 ^{o}C. In addition, the interconversion was so rapid at pH 10 that we collected aliquot samples from the heated radiolabeled solutions at time intervals of 0, 5, 10, 15 min, and so on, and placed them in an ice bath to quench the reaction. The cold aliquots, without warming up, were injected onto the HPLC for analyses. In this way we could collect early time points.

Although the kinetics at the tracer level can be very different from the macroscopic level, both showed similar interconversion process. For instance, mixtures containing primarily the syn (peak B) converts to mixtures containing primarily the anti

(peak A) for the ^{99m}TcO FGC complex (**Figures 5-2, 5-12, and 5-13**), whereas for the ^{99m}TcO FKC complex (**Figures 5-14, 5-15 and 5-16**), solutions containing primarily the anti convert to solutions containing primarily the syn. Also, we found that the equilibrium point is reached much faster in ^{99m}TcO FKC than in ^{99m}TcO FGC. All these observations are also true for the macroscopic analogs. However, considering the reaction conditions to be quite different for the macroscopic and tracer, the equilibria may be achieved differently. **Figure 5-17** describes the time dependence of the syn and anti diastereomer concentrations for ^{99m}TcO FKC and ^{99m}TcO FGC at pH 10.5, 37 ^{o}C. For pH 5.03, 8.02, and 9.01 at 37 C, the time dependence of the anti and syn diastereomer concentrations is shown in **Figure A6** (**Appendix Section**).

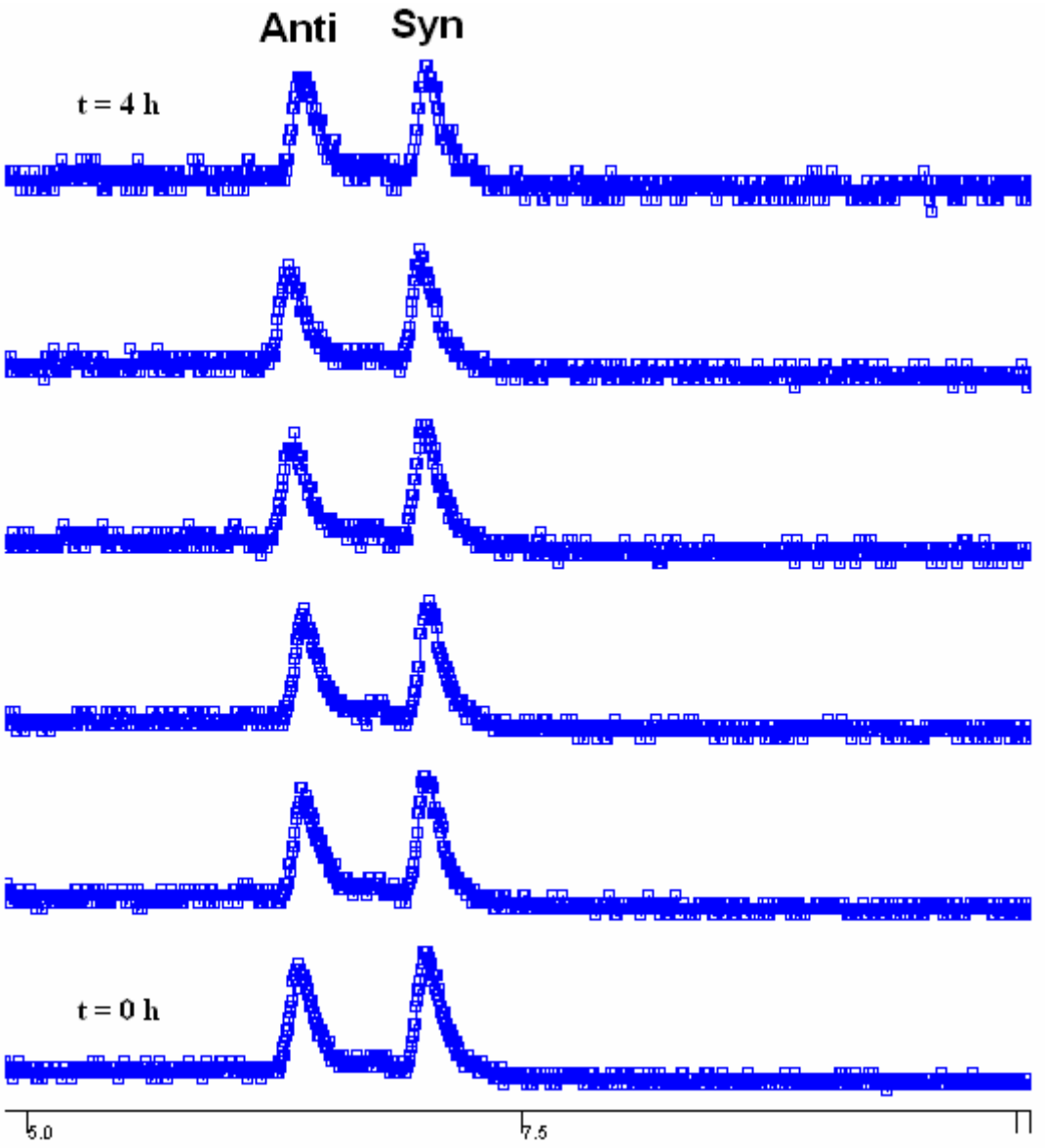

Figure 5-11. HPLC chromatograms of ^{99m}TcO FKC showing no interconversion of diastereomers at pH 5.03 (37 ^{o}C).

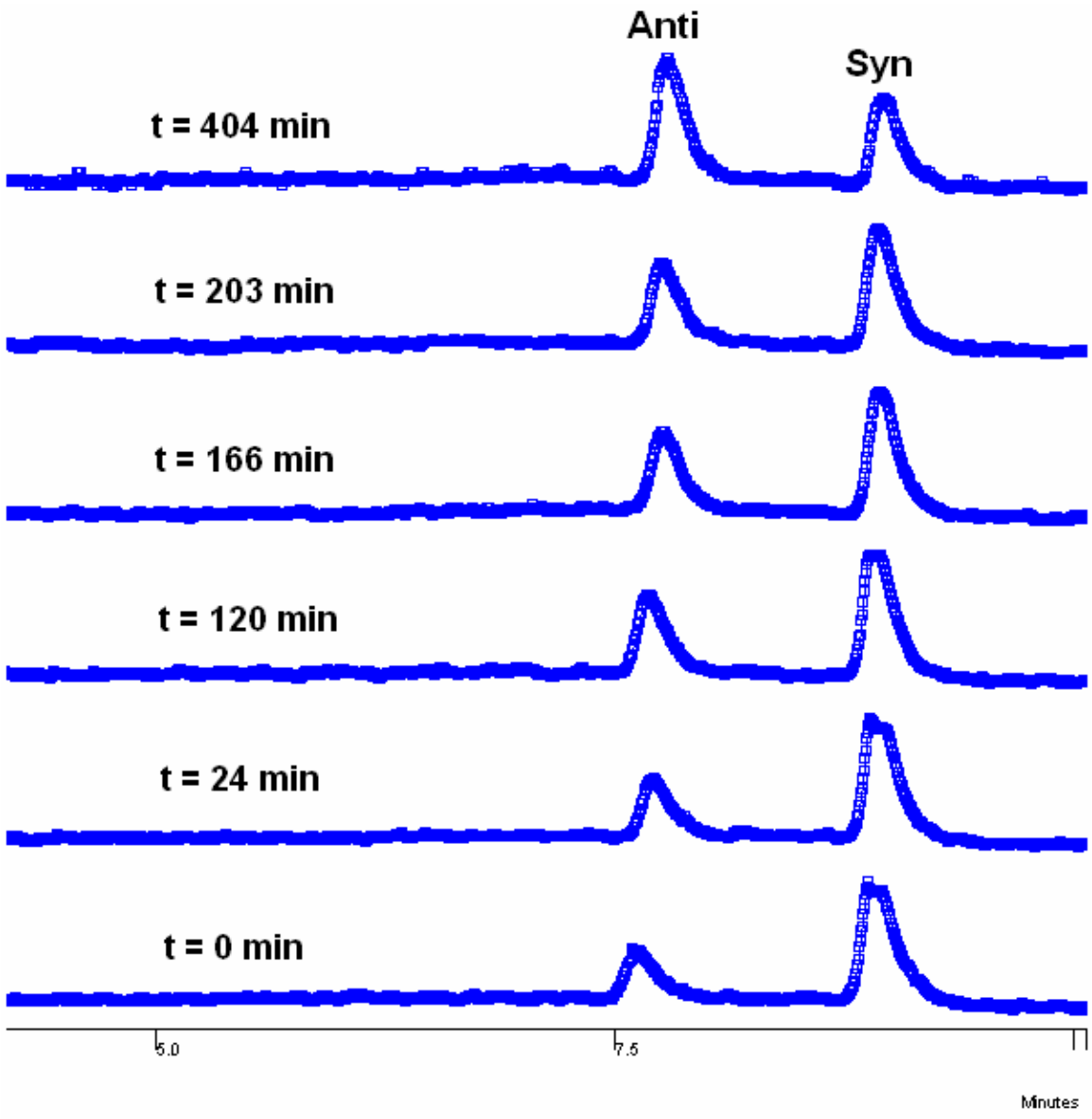

Figure 5-12. HPLC analyses of ^{99m}TcO FGC at pH 8.02 (37 ^{o}C).

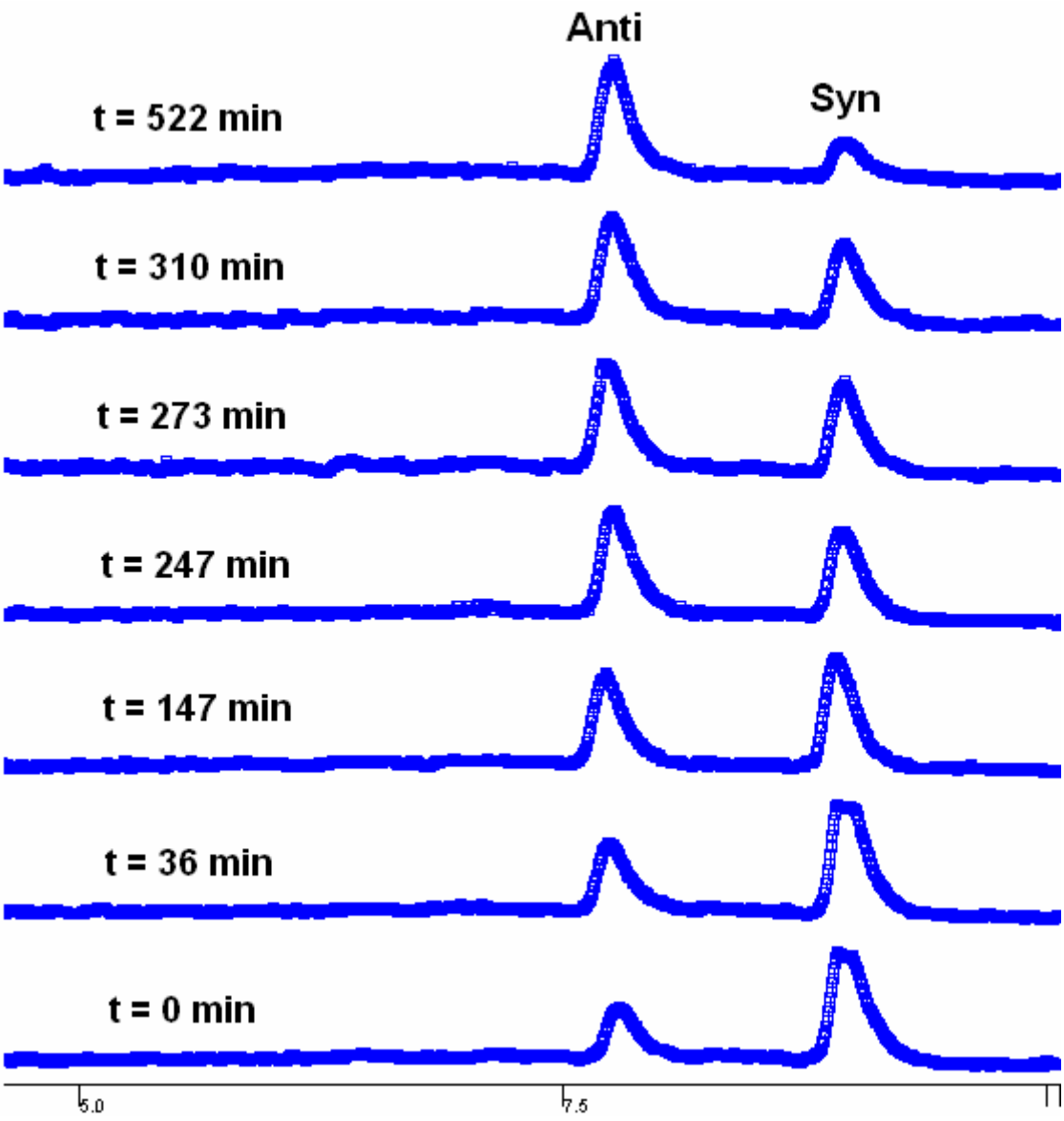

Figure 5-13. HPLC analyses of ^{99m}TcO FGC at pH 9.01 (37 ^{o}C).

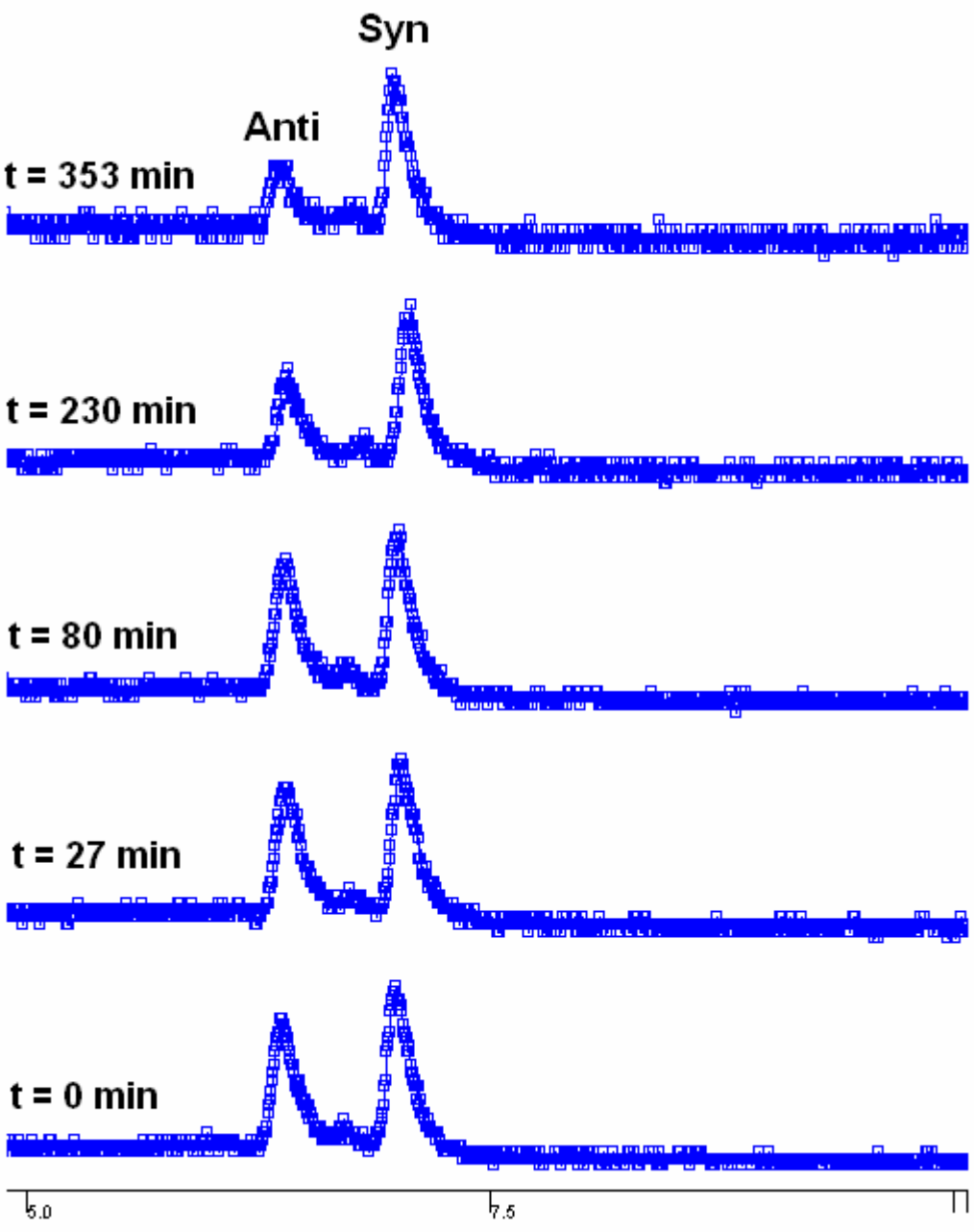

Figure 5-14. HPLC analyses of ^{99m}TcO FKC at pH 8.02 (37 ^{o}C)

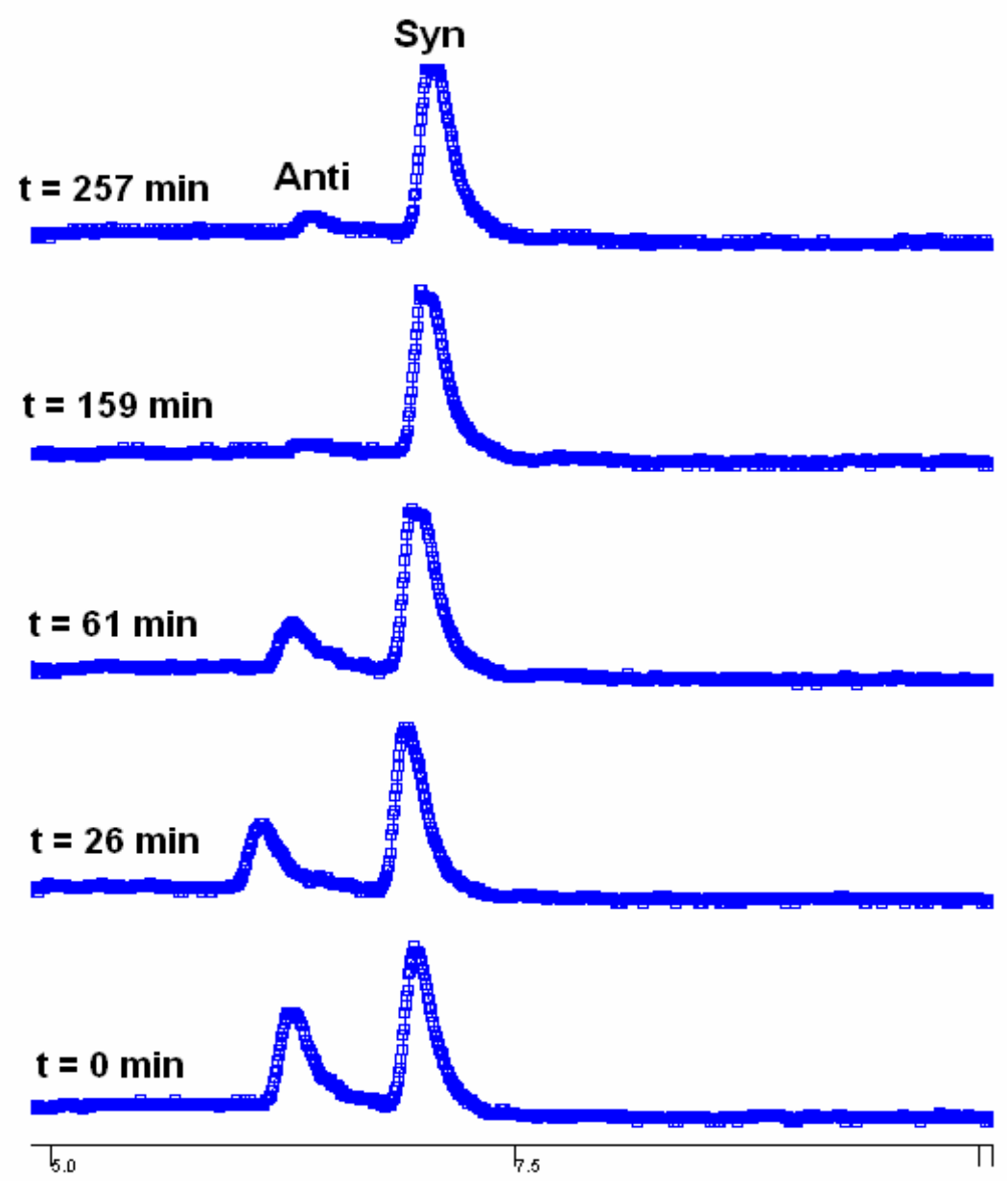

Figure 5-15. HPLC analyses of ^{99m}TcO FKC at pH 9.01 (37 ^{o}C).

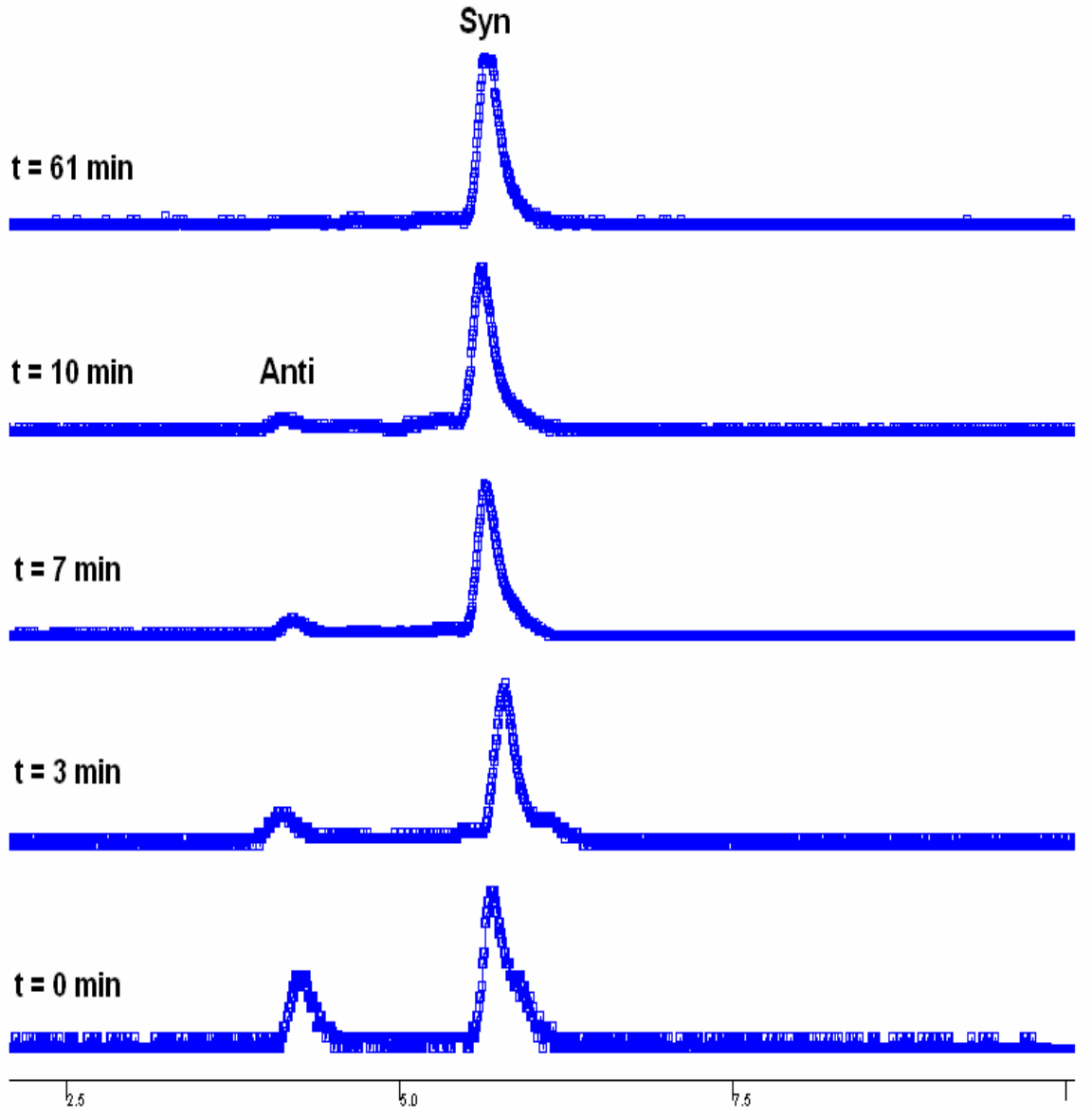

Figure 5-16. HPLC analyses of ^{99m}TcO FKC at pH 10.5 (37 ^{o}C).

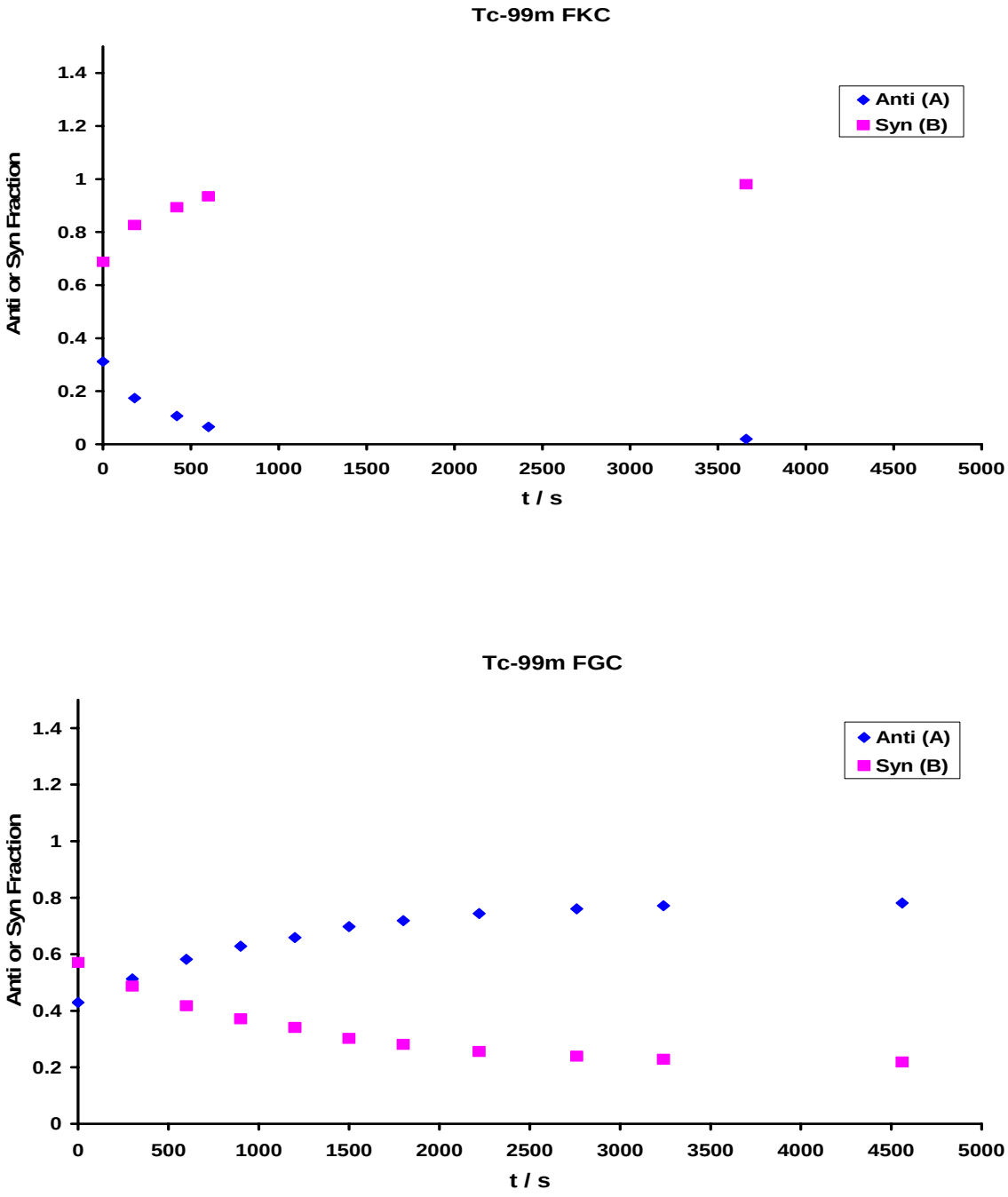

Figure 5-17. Time dependence of ^{99m}Tc FGC and FKC syn and anti diastereomer conversion. Top: ^{99m}Tc FKC anti to syn interconversion according to equation (1) [Buffer: 0.5 M Na_2HPO4 / Na_3PO4 at pH 10.5, 37 ^{o}C]; Bottom: ^{99m}Tc FGC syn to anti interconversion according to equation (6) [Buffer: 0.5 M Na_2HPO4 / Na_3PO4 at pH 10.5, 37 ^{o}C].

Figure 5-18 illustrates the first-order linear plots (eq 1-9) for the rate of interconversion of diastereomers at pH 8.02, 9.01, and 10.5. The graphs suggest that interconversion is catalyzed by base because the slope is steeper at higher reaction pH. The corresponding rate constants (k_1, k_{-1}) and equilibrium constants (K_{eq}) are listed in **Table 5-4**. In this study, we have shown that k_{-1} is lower than k_1 in both FGC and FKC systems at any pH conditions. Additionally, for both systems, ^{99m}TcO FGC and ^{99m}TcO, the k_1 and k_{-1} increase as the pH of the reaction increases, consistent with a base catalyzed reaction. These results imply that the anti is the more stable configuration in TcO FGC complex. DFT calculations support this observation, finding that the anti diastereomer is stabilized by 3 kcal over the syn diastereomer when solvent is included in the calculation.[17, 18]

For the TcO FKC complex on the other hand, the syn is more stable than the anti. For example, the observed K_{eq} for this interconversion at pH 10.5 and 37 ^{o}C is 40. However, the DFT calculations, considering the structure shown in **Figure 4-6 (see Chapter 4)** wherein the N of phenylamine is an amine (found in acidic solution and organic solution) are inconsistent with our kinetics experiments. These calculations show that the anti diastereomer is the more stable form in the gas phase. When solvent is considered, the syn conformation is slightly preferred. The inconsistency of the DFT calculations and the kinetics experiments may be due to the ease of deprotonation of the phenylalanine amine to form a metal-amide bond in the syn species, as observed in crystallographic experiments (**Chapters 3 and 4**) and in pKa determinations (**Chapter 4**).

The kinetics experiments, coupled with the physical data shown in Chapters 3 and 4, including X-ray crystal structures and pK_a data of Re FGC and Re FKC, point to the

possibility that the conversions of diastereomers and their stabilities are driven by the deprotonation of the phenylalanine amine. Evidence suggesting that deprotonation of the amine may be the source of the stabilities of the metallotripeptides are twofold. First, the pK_a's of ReO FKC and ReO FGC are 5.6 and 6.8, respectively, indicating that under acidic conditions the protonated amine is present and there is limited or no interconversion under acidic conditions. Even at pH 6, interconversion is slow. Second, basic conditions drastically accelerate the interconversion process. It is very likely that, for ^{99m}Tc FGC, under the basic conditions of the kinetics experiments, the amine deprotonation, resulting in a strong N_{amide}-Tc bond and concomitantly weaker bonds of Tc to the second and third N_{amide} of the peptide, to the $S_{thiolate}$ and to the –yl oxygen, sets up a favorable situation for H bonding with the C-terminal amide. This propensity for hydrogen bonding of the Tc=O with the cysteine amide drives the equilibrium to the more stable anti diastereomer.

On the other hand, in the case of the ^{99m}Tc FKC, the amine deprotonation, that occurs at lower pH, results in the same strong N_{amide}-Tc bond and concomitantly weaker bonds of Tc to the other donor atoms, including the –yl oxygen. This weak Tc=O may be receptive to hydrogen bonding with the ε-amine in the syn diastereomer.

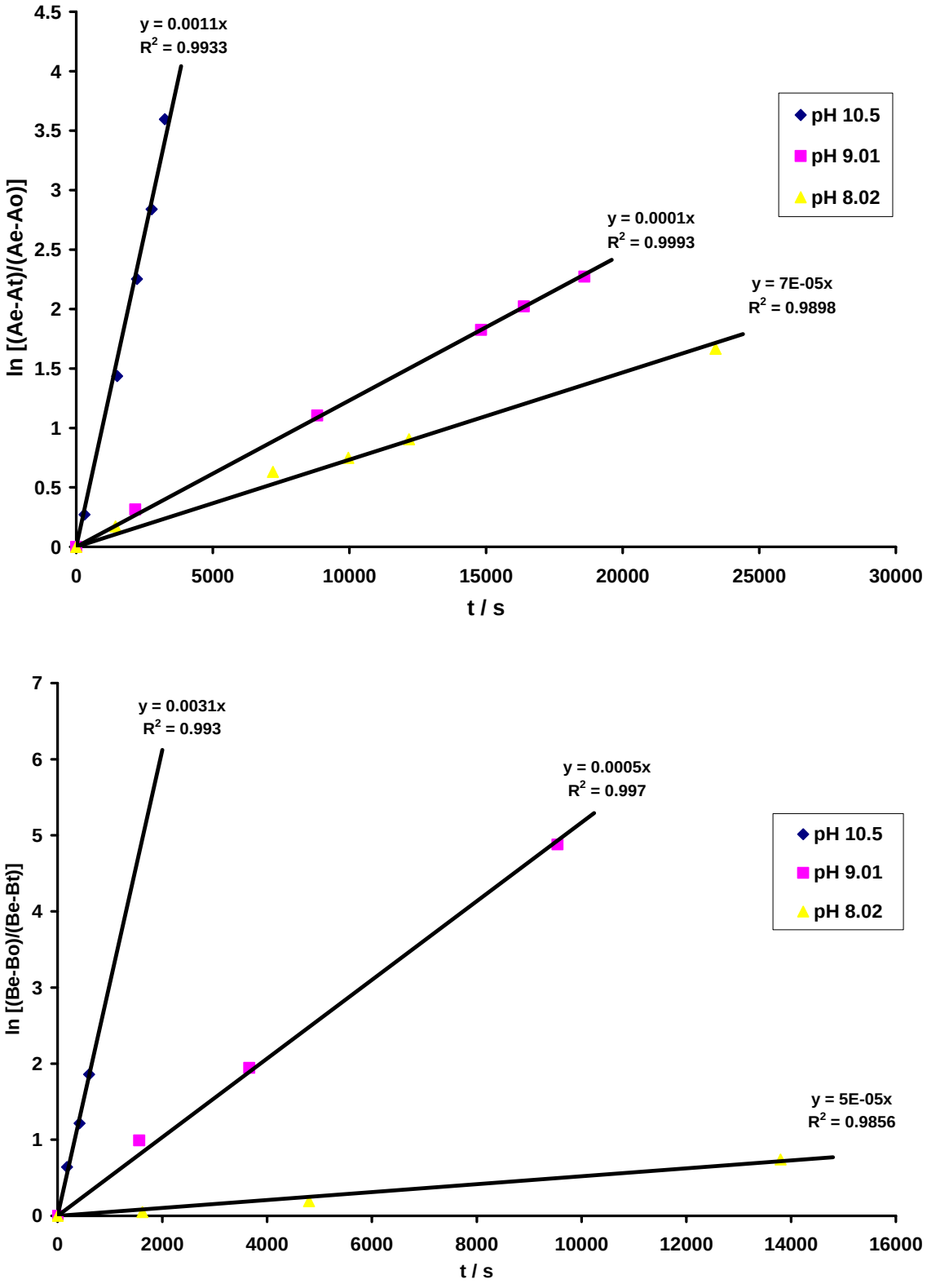

Figure 5-18. Linear plots for the first-order reaction for the interconversion of the diastereomers of ^{99m}Tc FGC (top) and ^{99m}Tc FKC (bottom) at 37 ^{o}C.

Table 5-4. Equilibrium and rate constants for ^{99m}TcO FGC and ^{99m}TcO FKC obtained at different pH values and 37 ^{o}C. The equilibria involved are shown below:

^{99m}TcO FGC : Syn (B) $\underset{k_{-1}}{\overset{k_1}{\rightleftharpoons}}$ Anti (A)

^{99m}TcO FKC : Anti (A) $\underset{k_{-1}}{\overset{k_1}{\rightleftharpoons}}$ Syn (B)

pH	K_{eq} $\frac{[anti]}{[syn]}$ $\frac{[syn]}{[anti]}$		$k_1 \times 10^5$, s^{-1}		$k_{-1} \times 10^5$, s^{-1}	
	FGC	FKC	FGC	FKC	FGC	FKC
8.02	1.44	2.03	4.13	3.35	2.87	1.65
9.01	1.79	5.68	6.41	42.5	3.59	7.48
10.5	3.59	39.8	78.3	481	21.8	12.1

5.4. Conclusion

We have suggested in the experiments in this chapter that hydrogen bonding may play an important role in the stabilization of diastereomers. The kinetic and thermodynamic data generated in this study along with the crystallography in previous chapters supports this idea. The ratio of K_{eq} for ^{99m}Tc FGC and the isomer distribution of ^{99}Tc and Re FGC that is consistent with the K_{eq}, suggest that the anti diastereomer is more stable than the syn. This is likely due to a hydrogen bonding interaction between the –yl oxygen and a proton on the C-terminal amide group.

On the other hand, the diastereomer distribution is for ^{99m}TcO FKC, with lysine in the second position. In this case, the syn diastereomer is favored and the K_{eq} is an order of magnitude larger than that for FGC (40 vs 4, at pH 10.5, 37 ^{o}C respectively). We postulate that this reversal of diastereomer distribution and the higher K_{eq} is due to a possible H-bonding capability of the εN-H with the ^{99m}Tc, ^{99}Tc and Re=O or with a carbonyl residue on the peptide. Theoretical calculations based on the Density Functional Theory (DFT) simulations also corroborate these values.

Future studies will be to measure the rate constants as a function of pH and temperature so that activation parameters can be obtained. Also, the FSC ligand may be a future tripeptide to consider as it appears to exhibit an intermediate diastereomer selectivity behavior between the FGC and FKC in the macroscopic ^{99}Tc and Re analogs. The syn/anti ratio of 70/30 for both the ^{99}Tc and Re analogs suggests that hydroxymethyl of the serine in the second position selects for the syn diastereomer but to a lesser extent than the εN-H of the lysine in FKC. According to the ReO RP294 syn structure[3], the OH of the serine points in towards the Re=O but the distances may be too long for H-bonding. In this case, the possible H-bonding contribution of the C-terminal amide may be a dominant force in the stability of the diastereomers and thus, their equilibrium ratios.

5.5. References

1. Takayama, T., Suzuki, K., Sekine, T. Kudo, H., *Radiochimica Acta*, **2000**. *88*(3-4): 247.
2. Valliant, J. F., Riddoch, R. W., Hughes, D. W., Roe, D. G., Fauconnier, T. K., Thornback, J. R., *Inorganica Chimica Acta*, **2001**. *325*(1-2): 155.
3. Wong, E., Fauconnier, T., Bennett, S., Valliant, J., Nguyen, T., Lau, F., Lu, L. F. L., Pollak, A., Bell, R. A.Thornback, J. R., *Inorganic Chemistry*, **1997**. *36*(25): 5799.
4. Boyd, G. E., *Journal of Chemical Education*, **1959**. *36*: 3.
5. Davison, A., Trop, H. S., Depamphilis, B. V., Jones, A. G., *Inorganic Syntheses*, **1982**. *21*: 160.
6. Rose, D. J., Maresca, K. P., Kettler, P. B., Chang, Y. D., Soghomomian, V., Chen, Q., Abrams, M. J., Larsen, S. K., Zubieta, J., *Inorg. Chem.*, **1996**. *35*(12): 3548.
7. Bormans, G., Peeters, O. M., Vanbilloen, H., Blaton, N., Verbruggen, A., *Inorg. Chem.*, **1996**. *33*: 6240.
8. Jurisson, S., Halihan, M. M., Lydon, J. D., Barnes, C. L., Nowotnik, D. P., Nunn, A. D., *Inorg. Chem.*, **1998**. *37*: 1922.
9. Francesconi, L. C., Graczyk, G., Wehrli, S., Shaikh, S. N., McClinton, D., Liu, S., Zubieta, J., Kung, H. F., *Inorg. Chem.*, **1993**. *32*(14): 3114.
10. Bereau, V. M., Khan, S. I., Abu-Omar, M. M., *Inorg. Chem.*, **2001**. *40*: 6767.
11. Liu, C.-b., Liu, G.-z., Liu, N., Zhang, Y. u.-m., He, J., Rusckowski, M., Hnatowich, D. J., *Nuclear Medicine and Biology*, **2003**. *30*(2): 207.

12. *PeakFit™ v.4.12 Users Guide*. 2003, SeaSolve Software Inc.: Framingham, MA.

13. McQuarrie, D. A., Simon, J. D., *Physical Chemistry: A Molecular Approach*. 1997, Sausalito, California: University Science Books.

14. Ismael, A. A., Sauriol, F. Butler, I. S., *Inorg. Chem.*, **1989**. *28*: 1007

15. Jurisson, S. S., Hirth, W., Linder, K. E., Rocco, R. J. D., Narra, R. K., Nowotnik, D. P., Nunn, A. D., *Nuclear Medicine and Biology*, **1991**. *18*(7): 735.

16. Benard, M., Rohmer, M.-M., Cantorias, M. V., Francesconi, L. C., *manuscript in preparation*.

17. Marie-Madeleine, Marc, Cantorias, M. V., Francesconi, L. C., *manuscript in preparation*.

6. Synthesis and Characterization of ReO and TcO Tripeptide Diastereomers Containing D-Amino Acid

6.1. Introduction

All amino acids except for glycine have two forms of stereoisomers, namely, L- and D-amino acids (**Figure 6-1**). L-amino acids are naturally produced and considered the most important building blocks of proteins, whereas D-amino acids are synthetically made. The stereoisomerism of amino acids is due to the chirality of the alpha carbon. A chiral carbon has four substituents none of which are equivalent, in contrast to an achiral carbon with at least two substituents that are equivalent. Achiral carbons become 'prochiral' when one of these two equivalent substituents is affected by a subsequent enzymatic reaction, resulting in a product containing a chiral center. The same is true of a substrate which has an sp^2 carbon which becomes sp^3 in the product.[1]

Following the Fischer-Rosanoff convention, the L- and D-amino acids may be depicted as follows:

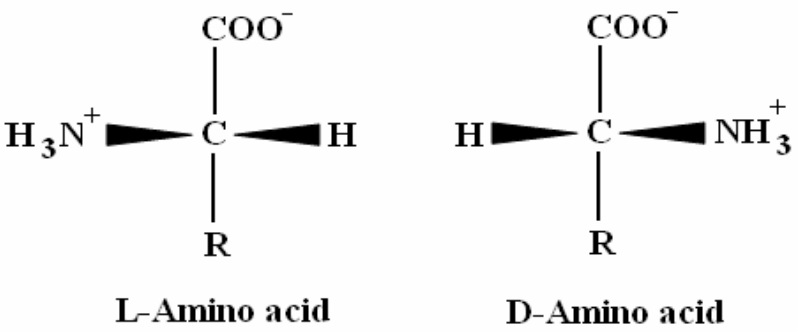

Figure 6-1. The L- and D-stereoisomers of amino acids. The L-enantiomer is the source of chirality in biological molecules.

The L/D nomenclature was originally based on optical rotation, as opposed to the other nomenclature (R/S) which was defined on the basis of a chiral center. Both nomenclatures refer to the right-handed (D or R) and left-handed (L or S) chiral centers.[2] In order to identify the configuration of amino acids as either L or D, one must first determine the R and S configurations using the Cahn-Ingold Prelog priority sequence rules.[3] In amino acids, the sequence of priority to four ligands attached to the alpha-carbon is $COO^- > NH_3^+ > R > H$, as depicted in **Figure 6-1**. Starting with the ligand of highest priority and continuing in a clockwise direction to the ligand of lowest priority, the configuration is designated "R" (LATIN: rectus, right); if counterclockwise, the configuration is designated "S" (LATIN: sinister, left). Since S is conventionally assigned as L, and R as D, then the left and right structures above are designated L- and D-amino acids, respectively.

Although the chemical and physical properties of L- and D-amino acids are almost identical, it was believed that the formation of polypeptides and proteins evolved only by selection of L-amino acids[4], which were assumed to be present in higher animals. D-amino acids were thought otherwise to be utilized as building blocks for antibiotics present in the cell walls of microorganisms or bacteria. A result of chance[5] is a simple way to explain this preference of evolution toward L-amino acids, but this can also be attributed to stabilization of polypeptides by neutral current interactions that led to decreased energies. As the resulting homochirality dictates the spatial architecture of biological polymers, it therefore plays a major role in enzymatic specificity and structural interactions, which are known to be essential for life.

Recent advances in analytical methodology[6-18] revealed that there are more unknown metabolisms of D-amino acids that are found in higher organisms than previously thought.[1] Free D-amino acids were reported to be found in mammalian tissues. The presence of D-Ser[19], D-Ala and D-Asp in the human brain[20] was also reported. Several articles[21, 22] indicate D-amino acids are essential to both animal and human survival.

Commercial applications of D-amino acids are well-known in food, agriculture, and pharmaceutical industries. For example, D-amino acids are utilized as intermediates for the preparation of β-lactam antibiotics such as semi-synthetic cephalosporins and penicillins[23]; D-Ala is produced as synthetic sweetener such as alitame.[24] Other well-established applications are through synthesis of biologically active substances that incorporate D-amino acids instead of their L- counterparts. This might lead to metabolically stable and long acting products.[25]

In our present work, we incorporate D-amino acids in our tripeptide ligand system for two reasons. First, the D-configuration may confer extra stability to the resulting chelate because, in general, peptides comprised of D-amino acids may be resistant to enzymatic degradation. Second, structural and chemical analyses of the Tc and Re complexes may allow further understanding of the parameters that influence stability of complexes. We report here the radiolabeling experiments on the phe-lys-cys series: FKC, FKc, and FkC, where small case letter denotes D-amino acid. We also describe here the synthesis and characterization of the ReO analogs containing D-amino acids.

6.2. Experimental

6.2.1. Materials

Fmoc-protected L-amino acids and Rink amide MBHA resin were purchased from NovaBiochem. N-hydroxybenzotriazole (HBTU) was purchased from ChemTech. 2-(1H-benzotriazole-1-yl)1,1,3-tetramethyluronium (HOBt), N,N-diisopropylethylamine (DIPEA), piperidine, phenol, thioanisole, triisopropylsilane (TIS), and 1,2-ethanedithiol (EDT) were purchased from Sigma-Aldrich. HPLC-grade acetonitrile, trifluoroacetic acid (TFA) and N,N-dimethylformamide (DMF) were purchased from Fisher Scientific. Nanopure water was obtained from a Millipore filtration system equipped with a 0.22 μm filter. All chemicals were used as received without further purification.

^{99}Tc is a low-energy (0.292 MeV) β^- emitter with a half-life of 2.12 x 10^5 years. This isotope should be handled in a fume hood using appropriate radioactive protocols. $NH_4{}^{99}TcO_4$ was obtained from Oak Ridge National Laboratory, Oak Ridge, TN. 30% H_2O_2 was added to an aqueous solution of $NH_4{}^{99}TcO_4$ to oxidize any $^{99}TcO_2$ present. The ammonium pertechnetate solution was standardized prior to use as previously described.[26] The reagent $[TcOCl_4]N(C_4H_9)_4$ was prepared following a published procedure.[27] $N(C_4H_9)_4$ $[ReOBr_4(OP(C_4H_9)_3]$ was prepared according to a published procedure.[28] ^{99m}Tc-pertechnetate (^{99}Mo/^{99m}Tc generator) was obtained from Cardinal Health (Bronx, NY).

6.2.2. Instrumentation and Analytical Methods

RAININ Dynamax HPLC system equipped with a Dynamax UV-1 UV-visible detector and two Dynamax model SD-200 pumps using 25-mL pump heads was employed. The software used was Varian Star LC Workstation Ver. 6 and all HPLC experiments were monitored at a λ = 220 nm. A home-built detector composed of Tennelec Minibin components such as power supply, high voltage supply, and amplifier, was interfaced to the HPLC system to monitor gamma (γ) ray of ^{99m}Tc. For both analytical and preparative work, the mobile phase consisted of (A) 0.1 % TFA in H_2O and (B) 0.1 % TFA in ACN/H_2O (90/10). Three methods were used in these studies: (1) Analytical Method 1 – Column: Waters DeltaPak 5μ C_{18} 100 Å, 3.9 x 150 mm; Mobile Phase Gradient: 4 % - 35 % B over 10 min; Flow Rate: 1.0 mL/min; (2) Analytical Method 2 – Column: Waters DeltaPak 5μ C_{18} 100 Å, 3.9 x 150 mm; Mobile Phase Gradient: 15 % - 28 % B over 15 min; Flow Rate: 1.0 mL/min; and (3) Preparative Method – Column: Waters DeltaPak 5μ C_{18} 300 Å, 19.0 x 300 mm; Mobile Phase Gradient: 4 % - 35 % B over 20 min; Flow Rate: 24.0 mL/min.

Mass spectral data were acquired on an Agilent Technologies 1100 Series LC/MSD Model G1946D using electrospray ionization in the positive and/or negative-ion mode. Infrared spectra were recorded from KBr disks on a Perkin Elmer 1600 FT-IR spectrometer in the range 600 - 3000 nm and were referenced to polystyrene film.

6.2.3. General Procedure for Synthesis of Tripeptide Ligands

The method used to prepare the tripeptide ligands with L amino acids, such as FKC, described in **Section 2.2.2**, was used to prepare FkC, and FKc.

6.2.4. Procedure for Synthesis of ReO FKc

The same method that was described in **Section 4.2.3** to prepare ReO FKC was also used to prepare ReO FKc. The diastereomers of ReO FKc were isolated, purified, and characterized by mass spec, IR, ^{1}H NMR and CD spectroscopy.

6.2.5. Procedure for Synthesis of ^{99}TcO FKC, ^{99}TcO FkC, and ^{99}TcO FKc

The same method that was described in **Section 3.2.3** was also used to prepare ^{99}TcO FKC, ^{99}TcO FkC, and ^{99}TcO FKc. The resulting crude reaction solutions were used without further purification as standards for the ^{99m}Tc complexes. The diastereomers were not isolated.

6.2.6. Radiolabeling of Tripeptides with ^{99m}Tc and Co-elution Experiment

To a microcentrifuge tube, 25 μL of the tripeptide solution (0.6 mg/mL in saline) and 10 μL of sodium tartrate (50 mg/mL in ammonium buffer which contains 0.5M NH_4CO_3, 0.25M NH_4OAc, and 0.18M NH_4OH) were added and mixed. In a lead shielded fumehood, the tripeptide-tartrate solution was radiolabeled by adding 100 μL of

sodium pertechnetate containing about 500 μCi, and then followed by addition of 5 μL $SnCl_2 \cdot 2H_2O$ (1 mg/mL in 0.01 M HCl). After the solution was vortexed briefly, the microcentrifuge tube was inserted in a heating block maintained at 100 ^oC. After 15 minutes, the solution was cooled down to about 5 min. The co-elution experiments with ^{99}Tc complexes were conducted following the procedure described in **Section 3.2.7.3**.

6.2.7. Naming the diastereomers of the ReO Phe-Lys-Cys Series

We denote the complexes first by their tripeptide composition, eg. ReO FKC, ReO FkC, ReO FKc. The upper case denotes the L amino acid and lower case denotes the D amino acid. We then denote the "syn" and "anti" diastereomers based on the disposition of the Re=O group and the **lysine** group of the second amino acid. For example, those ReO complexes bearing a lysine in the second position of the tripeptide ligand, in which the side-chain residue of the lysine is oriented opposite to the M=O bond (M=^{99}Tc, ^{99m}Tc, Re) will be denoted as the "anti" diastereomer. Those complexes where the lysine residue lies on the same side of the square plane as the oxo ligand, are denoted syn.

Using WebLab ViewerPro, we constructed the following molecular models for the anti and syn diastereomers of ReO FKC, ReO FkC and ReO FKc (**Figure 6-2**). They are named according to the strategy given above.

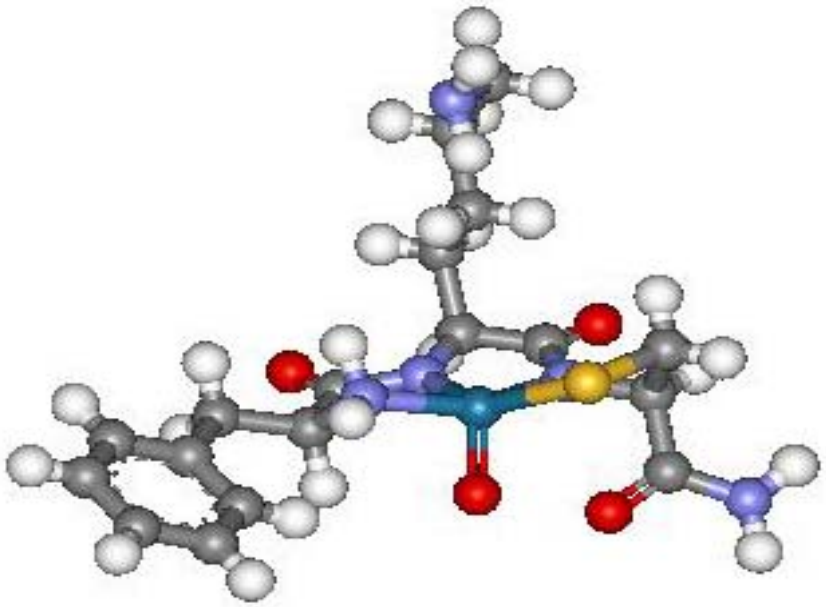

ReO FKC anti

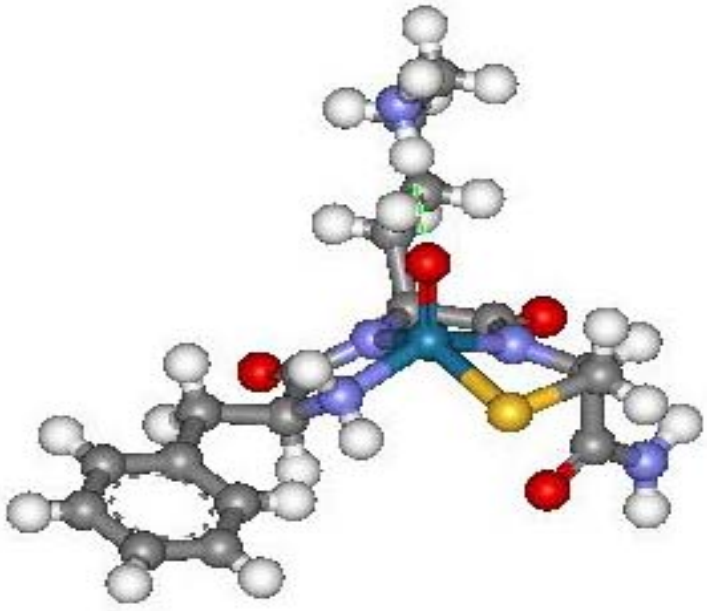

ReO FKC syn

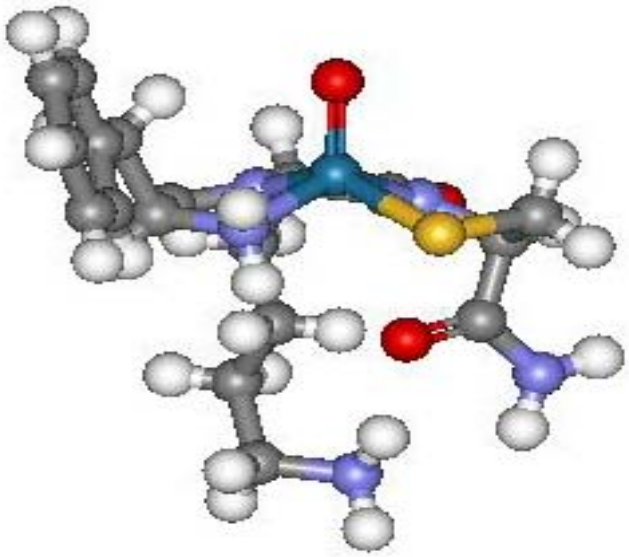

ReO FkC anti

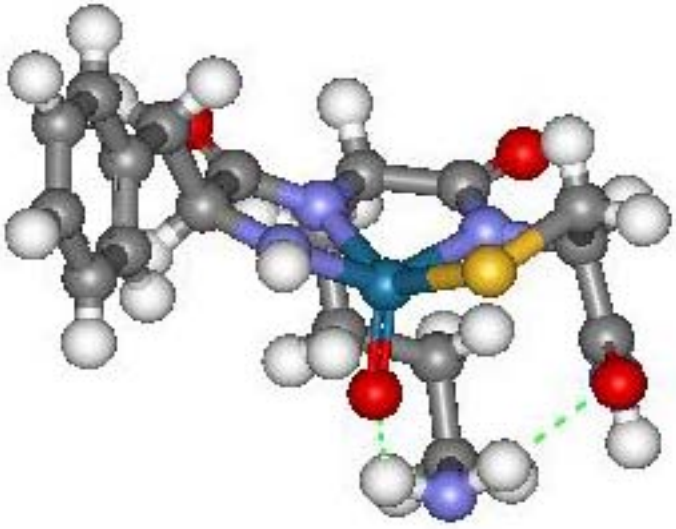

ReO FkC syn

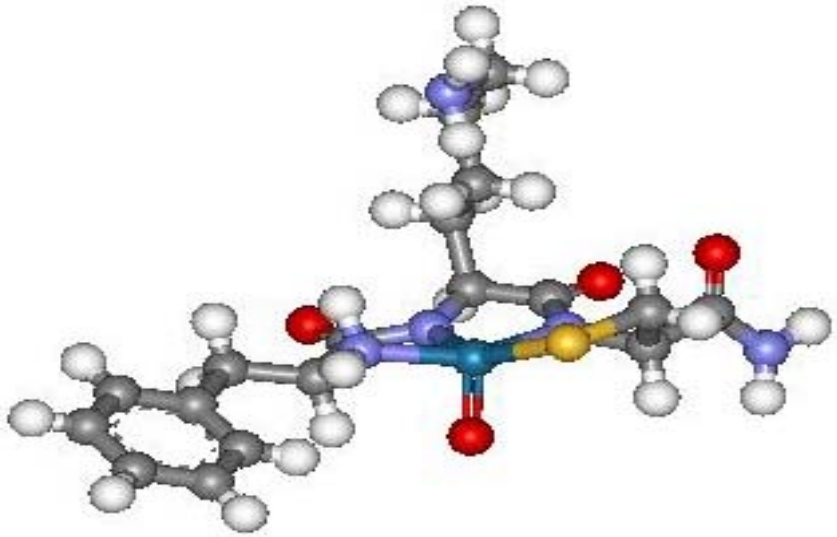

ReO FKc anti

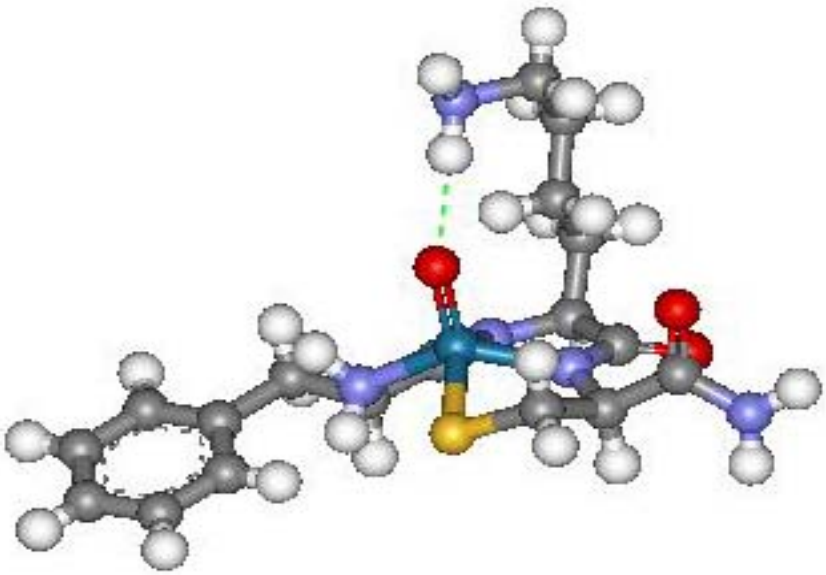

ReO FKc syn

Figure 6-2. Molecular models for L- and D-analogs of ReO Phe-Ly-Cys series. Note that all syn configurations show possible hydrogen-bonding interaction between Re=O and ε-NH_2 of the lysine residue; additional hydrogen bonding interaction of ε-NH_2 with the terminal amide N of cysteine can possibly occur in ReO FkC syn configuration.

6.3. Results and Discussion

6.3.1. Synthesis and Characterization of ReO FKc

The analysis of the ReO FKc crude solution was performed using Analytical Method 1. The isolation of ReO FKc diastereomers was done using the Preparative Method. This purification method is similar to **Section 4.2.2**. In each case, two products A and B were formed with retention times of 5.1 and 6.2, respectively, based on the HPLC conditions of the Analytical Method 1. When A was separated from B, collected, lyophilized, and dissolved in water for HPLC analysis, we found that solution A gave a clean chromatogram showing only the early eluting peak (**Figure 6-3**). Mass spectral analysis of this solution showed a formulation consistent with the expected molecular weight of 595 for ReO FKc (**Figure 6-4)**. The IR spectrum (**Figure 6-5**) of the same compound displayed a Re=O stretch of 986 nm, a value within the range expected for Re(V)=O square pyramidal N_3S complexes.

On the other hand, when the peak corresponding to compound B was collected upon prep HPLC, lyophilized to a solid powder and dissolved in water, we observed that some of B converted to A over the few days of the process of fraction collection and lyophilization, as indicated by the analytical HPLC chromatogram shown in **Figure 6-6**. Thus, these results suggest that ReO FKc-B is less stable than ReO FKc-A.

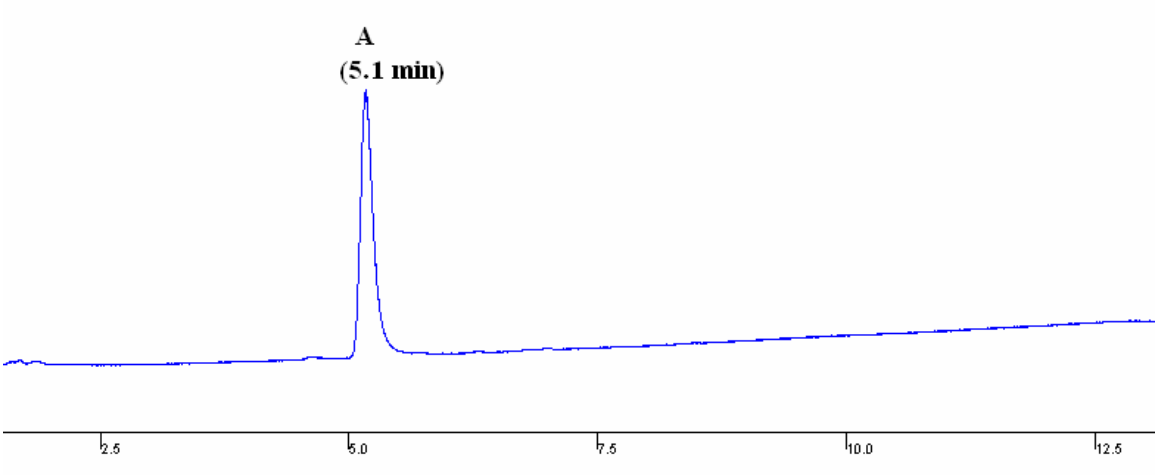

Figure 6-3. HPLC chromatogram of the isolated ReO FKc-A using Analytical Method 1.

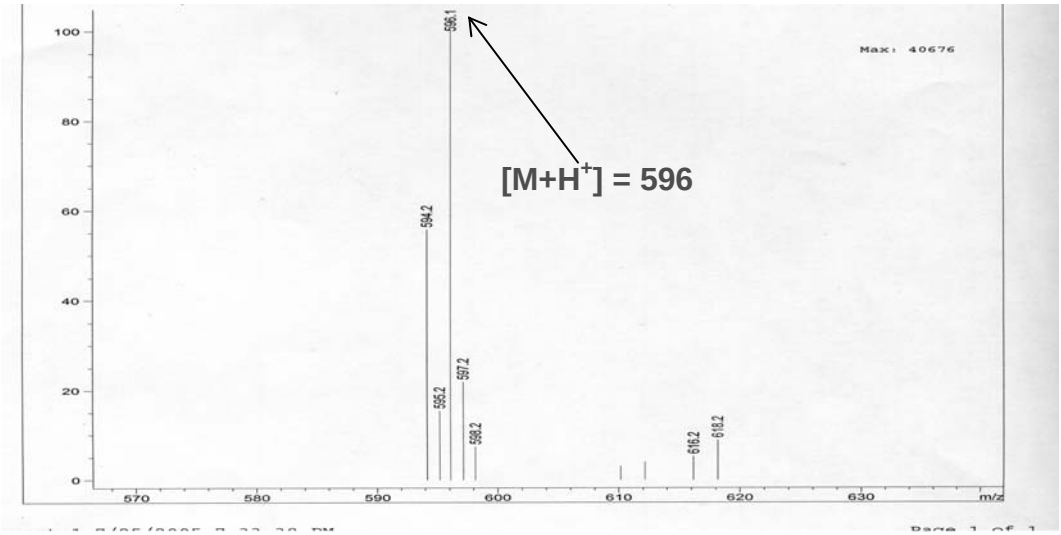

Figure 6-4. Mass spectrum of ReO FKc-A showing mass formulations consistent with expected molecular weight.

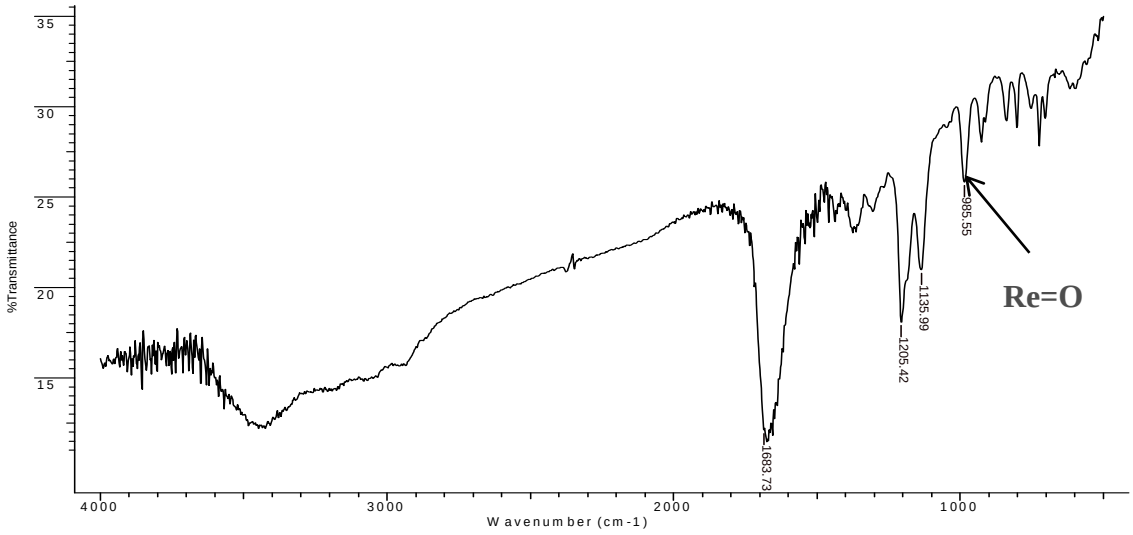

Figure 6-5. IR spectrum of ReO FKc-A.

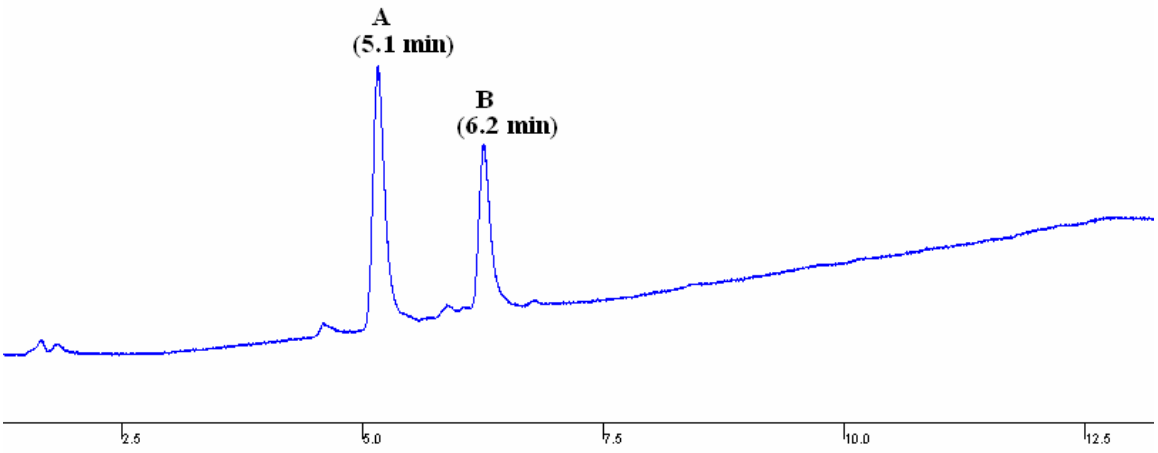

Figure 6-6. HPLC chromatogram of the isolated ReO FKc-B using Analytical Method 1. Over the time to collect and lyophilize the sample, species B converted to A.

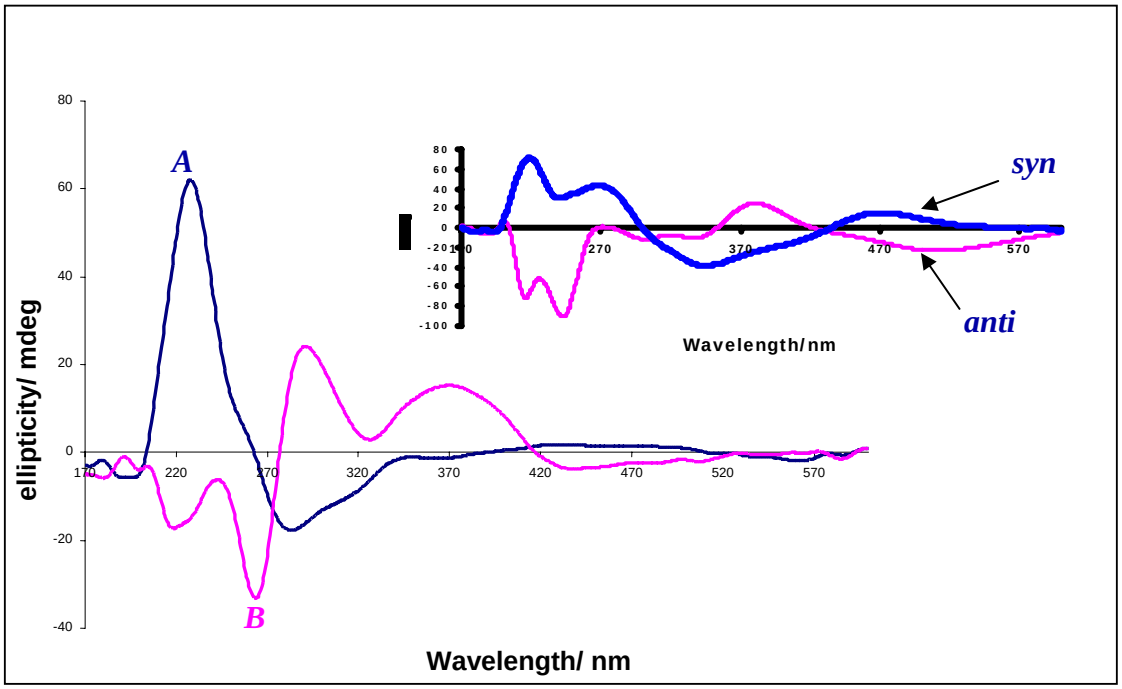

Figure 6-7. Circular dichroism spectra of ReO FKc-A (blue) and B (purple) diastereomers dissolved in methanol; Inset: CD spectra of ^{99}TcO FKC anti and syn diastereomers dissolved in methanol.

Circular dichroism spectra of ReO FKc diastereomers were taken in methanol at 25 ^{0}C. Diastereomer B converted easily to A and the sample of B that was isolated from prep HPLC converted to a mixture of about 75 % A, according to HPLC. The sample used for circular dichroism of B (**Figure 6-7**) contained about 75% A and 25 % B. The data shows similar features to those observed for the MO tripeptide models containing all L-amino acids (**Figure 6-7**).

Specifically, in the visible region, ReO FKc-A showed a peak at about 220 nm with positive ellipticity and a peak at 300-350 nm with negative ellipticity; this profile matches that of the TcO FKC syn, discussed in chapters 3,4,and 5. ReO FKc-B, on the other hand, showed two maximum absorbances at 220 and 260 nm with both negative

elipticities, which is consistent with the CD spectrum of TcO FKC anti. At about 280 nm, we observed a positive ellipticity for ReO FKc-B which is not seen in the CD spectrum of TcO FKC anti. This is expected very likely due to the fact that the sample is a mixture of the two diastereomers.

The electronic transitions depicted by the CD profiles of ReO FKc-A and -B are consistent with the electronic transitions described for the TcO FKC syn and anti diastereomers. For example, the UV region ranging from 200 – 270 nm shows the peptide backbone of the diastereomers. Around 300 nm, the positive and negative ellipticities are indicative of oxygen to rhenium charge-transfer transitions. And the weak bands in the visible region demonstrate the presence of the ligand to metal charge transfer transitions. Comparing the CD spectra of the ReO FKc diastereomers with TcO FKC diastereomers, we note that the diastereomers A and B of ReO FKc match up with the syn and anti of TcO FKC, respectively. However, the colors of ReO FKc diastereomers are similar to ReO FKC diastereomers, but not to TcO FKC diastereomers. This is consistent with CD spectra showing similar maximum absorption bands at the Vis region for both compounds A and B of ReO FKc.

The HPLC peak stability profile for the ReO FKc diastereomers is reversed for ^{99m,99}Tc/ReO FKC diastereomers: for ReO FKc, the early eluting peak appears to be the more stable species. Therefore, we suggest that the early eluting peak (ReO FKc-A) on the HPLC chromatogram corresponds to the syn diastereomer, where the lysine is syn to the ReO group, in accordance with the structure shown in Figure 6-2. Based on our observations for ReO FKC, the more stable diastereomer is that with syn orientation. As we postulated earlier, it is possible that the syn orientation allows for interaction of the

lysine with the Re=O or C=O groups. We suggest that the late eluting peak (ReO FKc-B) is the anti diastereomer. However, these are relative conclusions which can only be supported by the X-ray crystallography.

The 1-D and 2-D proton NMR data of ReO FKc-A (from **Figure 6-8** to **Figure 6-11**) taken in acidic aqueous solvent, showed that the chemical shifts for the proton resonances for ReO FKc-A match those of ^{99}Tc/ReO FKC syn more closely than the ^{99}Tc/ReO FKC anti diastereomer. For example, in **Table 6-2**, a general trend of more upfield shift resonances for the phe and lys alpha protons can be observed for ReO FKc-A and ^{99}Tc/ReO FKC syn in comparison to the anti diastereomers of ^{99}Tc/ReO FKC complexes. Moreover, the most important comparison that validates our assumption about the stereoconfiguration of ReO FKc-A is to take into account the chemical shift of gamma (γ) proton on the lysine residue. In ^{99}Tc/ReO FKC anti, the chemical shifts of the gamma proton are 0.62 ppm, whereas in ^{99}Tc/ReO FKC syn, the chemical shifts are 1.30 ppm. The chemical shift of the gamma proton in ReO FKc-A is 1.40 ppm which is closer to 1.30 ppm compared to 0.62 ppm, thus, further suggesting that the structure of ReO FKc-A has a lysine syn to the ReO group, that is the syn diastereomer, according to the model in Figure 6-2. Finally, although we didn't have enough samples to carry out the NMR characterization of ReO FKc-B, we believe that this compound is an anti diastereomer.

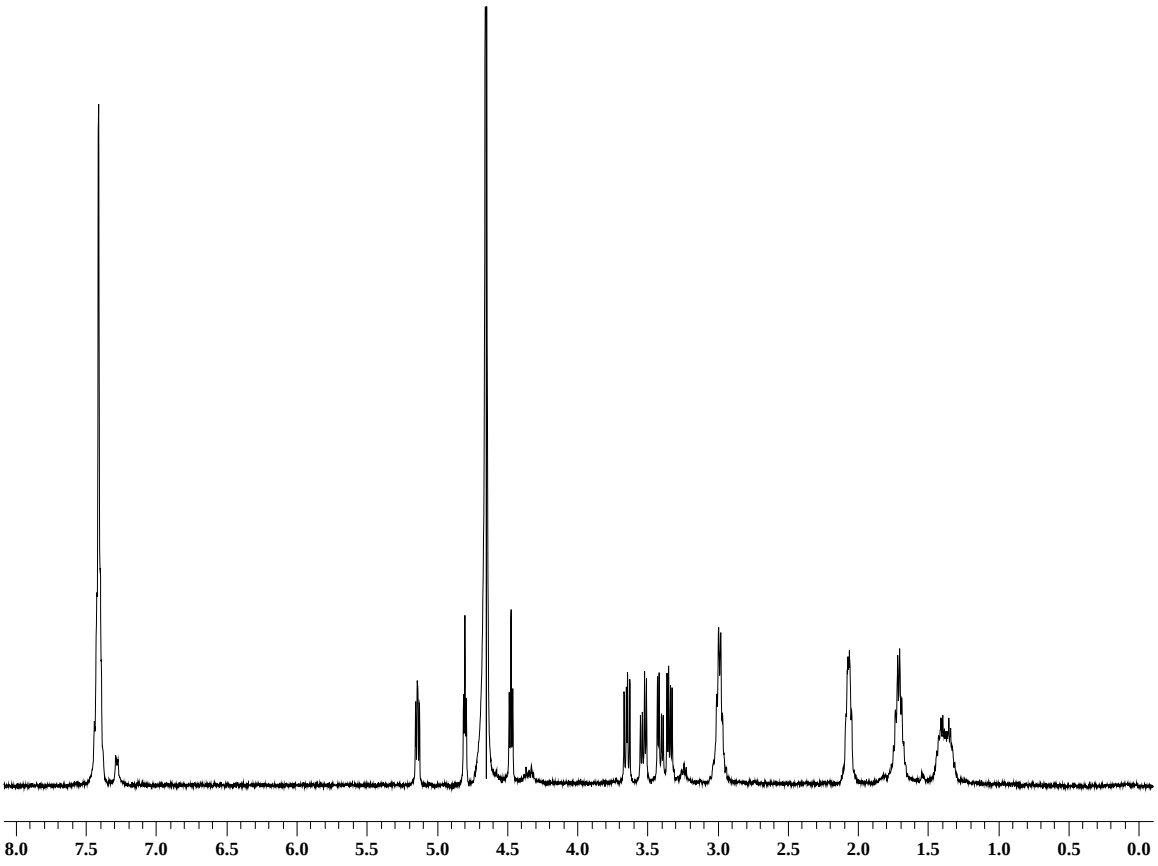

Figure 6-8. ^{1}H NMR spectrum of ReO FKc-A dissolved in 0.01 M DCl in D_2O.

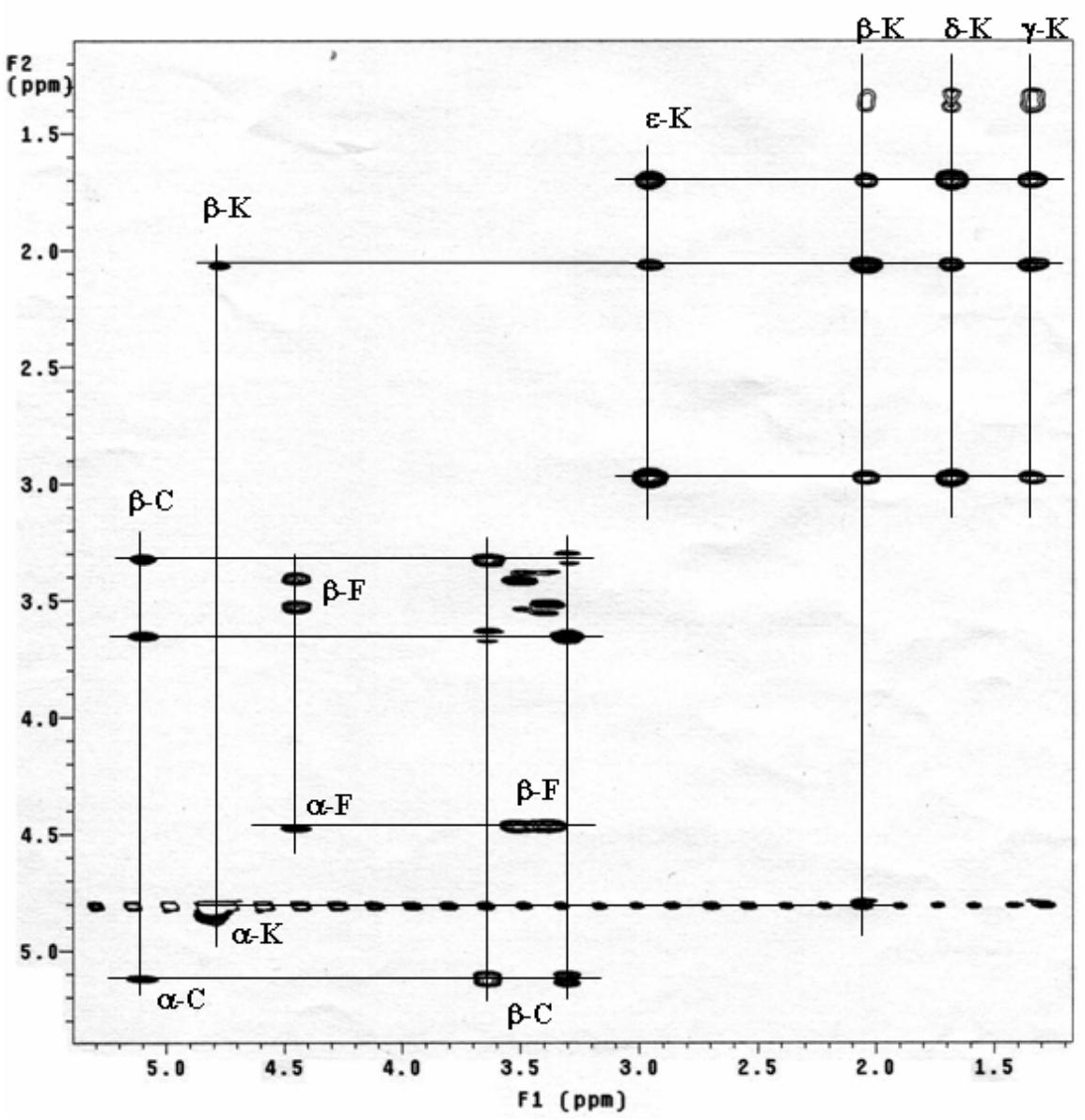

Figure 6-9. TOCSY spectrum of ReO FKc-A dissolved in 0.01 M DCl in D_2O.

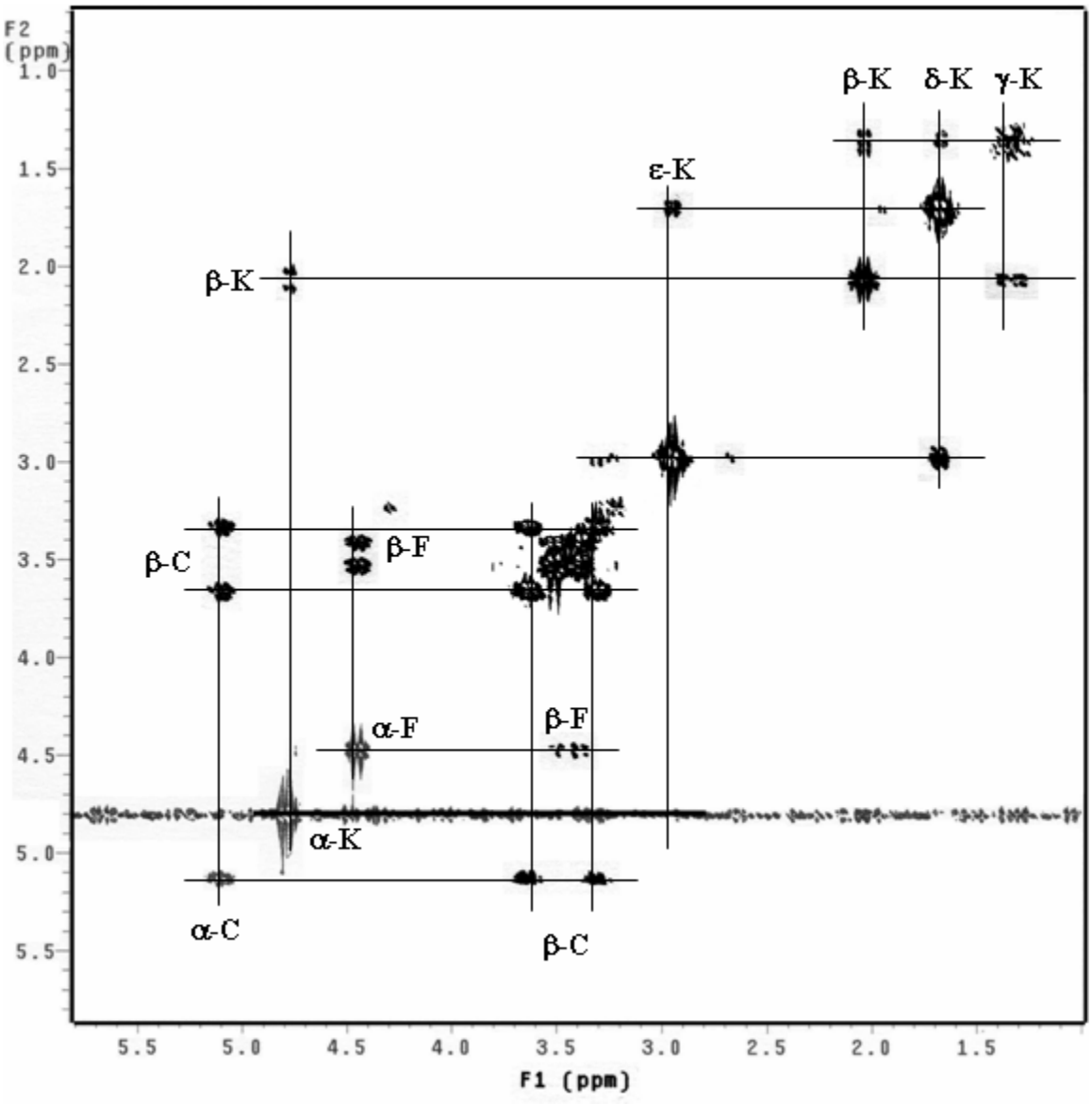

Figure 6-10. COSY spectrum of ReO FKc-A dissolved in 0.01 M DCl in D_2O.

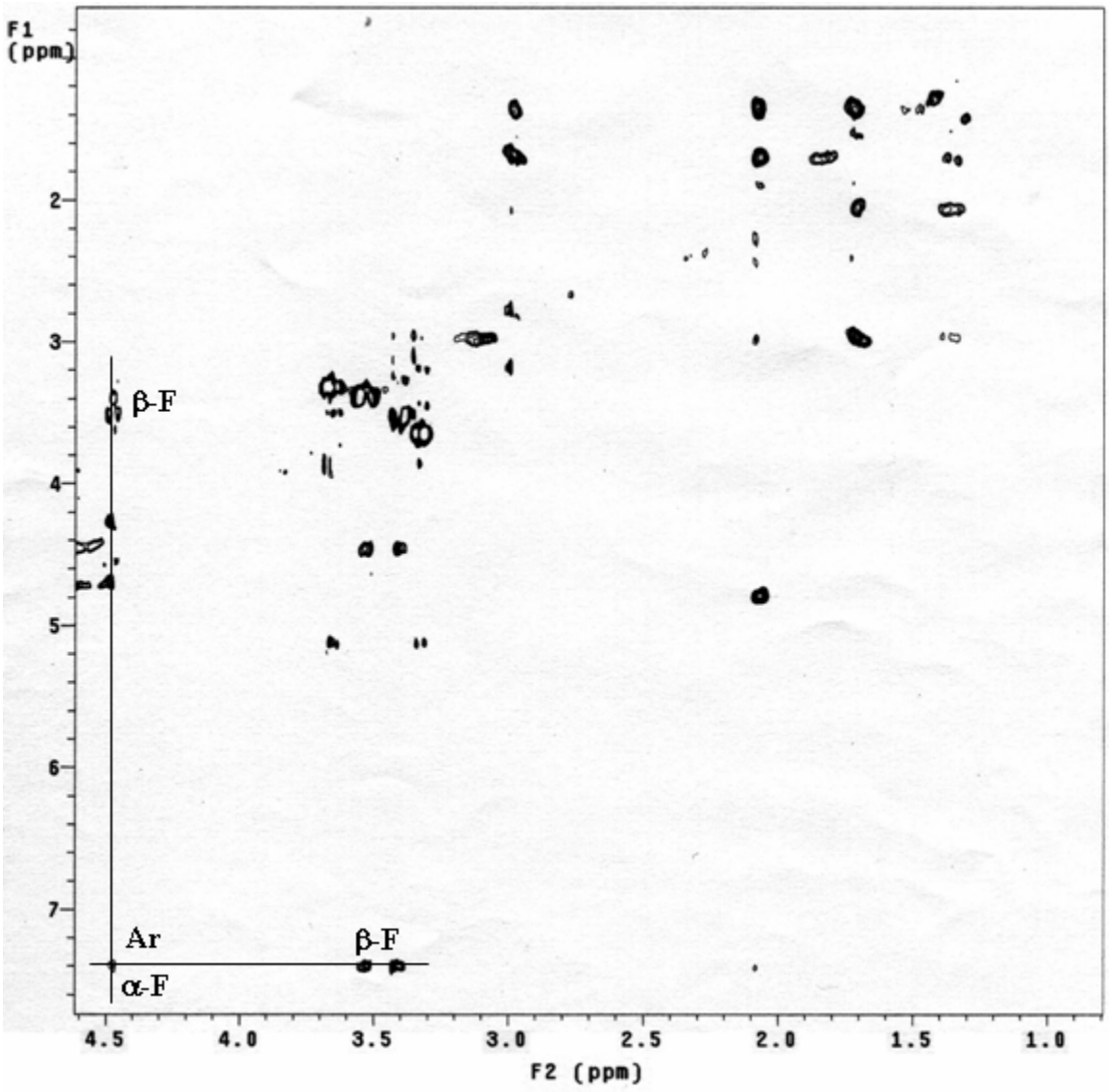

Figure 6-11. NOESY spectrum of ReO FKC-A dissolved in 0.01 M DCl in D_2O

Table 6-1. Chemical shifts (δ) for ReO FKc-A dissolved 0.01M DCl in D_2O vis-à-vis ^{99}Tc/ReO FKC syn and anti diastereomers dissolved in 0.01M HCl in H_2O.

Proton	ReO FKc-A δ, ppm	ReO FKC syn δ, ppm	TcO FKC syn δ, ppm	ReO FKC anti δ, ppm	TcO FKC anti δ, ppm
F-α	4.50	4.40	4.30	4.59	4.77
F-β	3.40, 3.51	3.35, 3.50	3.40, 3.51	2.99, 3.54	2.98, 3.54
K-α	4.80	4.83	4.76	5.11	5.04
K-β	2.10	2.00	2.01	1.86, 2.36	1.87, 2.38
K-γ	1.40	1.30	1.31	0.62	0.62
K-δ	1.70	1.61	1.66	1.50	1.51
K-ε	3.00	2.90	2.94	2.83	2.83
C-α	5.10	5.00	5.23	5.35	5.71
C-β	3.30, 3.65	3.53, 3.95	3.80	3.39, 3.61	3.57, 3.83

6.3.2. Radiolabeling of FKC, FKc, and FkC

Experimental results in Chapter 5 allow us to understand the interconversion process of the diastereomers. We realized that the amino acid residues dictate the dynamic interconversion behavior of the diastereomers and have the potential to stabilize one diastereomer over the other. In this study as well as in studies represented by the previous chapters, we have shown that the orientation of the amino acid residues, thus the stereoconfiguration (L and D) of amino acid, can influence the stability of ^{99m}TcO complex. For example, we have established the fact that on the Reverse-Phase HPLC, the early and late eluting peaks for the ^{99m,99}Tc/Re FKC diastereomers (where all amino acids are L configuration) are the anti and syn, respectively, wherein the syn is more

stable than the anti based on the synthetic observations, kinetic studies and preliminary DFT calculations.

Using the radiolabeling procedure described in this chapter, our HPLC data (**Figure 6-12**) showed the following:

(1) FKC – peak B is dominant after heating suggesting that B is more stable;

(2) FKc – peak A is dominant after heating suggesting that A is more stable;

(3) FkC – peak A is dominant after heating suggesting that A is more stable.

We know that FKC–B is the syn diastereomer and we postulate that this may be stabilized by a H-bonding interaction between the lysine and Re=O. This may be a dominant stabilizing interaction. Also, we know that the L-cysteine provides a stabilizing interaction in a potential H-bond between the amide N and the Re=O in the anti diastereomer of FGC. So in FKC you have two opposing interactions: the lysine –Re=O in the syn and the amide – Re=O in the anti. It appears that the lysine interaction may be the more dominant. Thus the FKC syn is more stable.

With the phe-lys-cys ligand where a D-cysteine or D-lysine is incorporated, the syn configuration is defined as the isomer having the lysine side-chain oriented on the same side of the M=O group. Conversely, the anti configuration is defined as the lysine residue oriented on the opposite side of the M=O group. If D-lysine is used in phe-lys-cys series (e.g. FkC), the syn configuration is thus expected to be more stable because it is in this conformation that allows H-bonding opportunity. If D-cysteine is used (e.g. FKc), the stability of the syn conformation is still maintained. Extending this premise to the HPLC co-elution experiments (**Figure 6-12**), the early eluting peaks which represent the more stable diastereomers are assigned as ^{99m}TcO FkC syn and ^{99m}TcO FKc syn.

Note that the position on the chromatograms of the syn diastereomers is reversed when switching from L- to D-amino acids, which we observed above for the ReO FKc. Again, these are relative conclusions which can only be supported by the X-ray crystallography. In summary, employment of D-amino acids can impact the selectivity of formation and the stability of Tc tripeptide complexes.

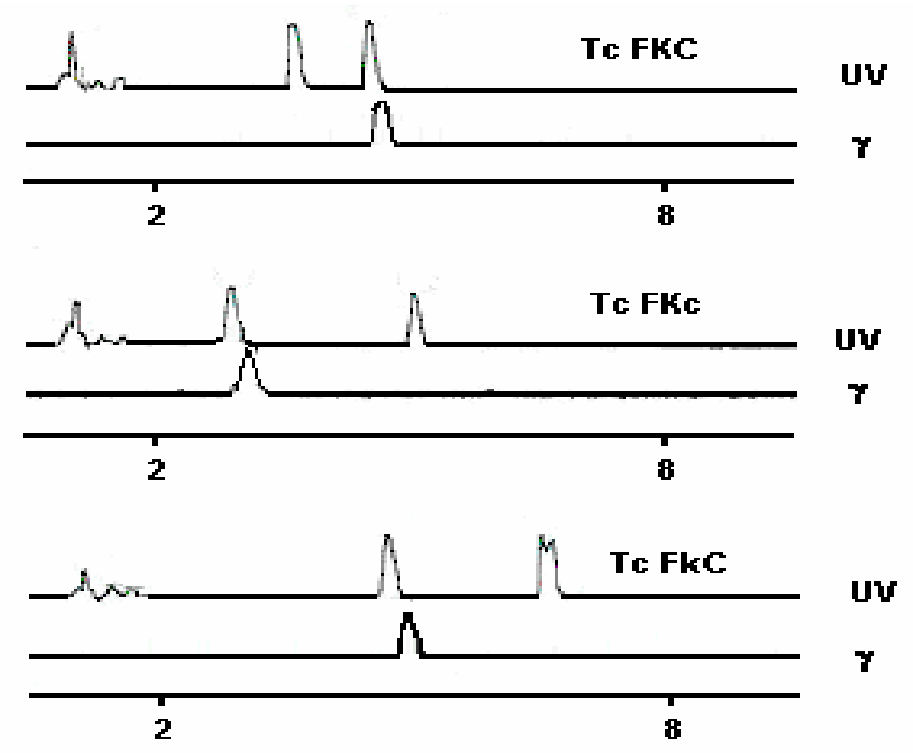

Figure 6-12. HPLC analyses of the tracer ^{99m}Tc tripeptide complexes (γ) co-eluting with the macroscopic ^{99}Tc complexes (UV) using Analytical Method 2. The ^{99}Tc complexes were used as a crude reaction mix.

6.4. Conclusion

As we have described in the previous work, the size, lipophilicity, and hydrogen-bonding opportunity of amino acid residues are essential components for selecting good tripeptide ligands in the development of targeted radiopharmaceuticals. When submitting a drug for FDA approval, it is more convenient for pharmaceutical industries to begin with only one active species during phase trials. Otherwise, complete characterization of the other contaminant species is required in most cases. In the extreme, the FDA may require the drug company to purify the substance. This absolutely requires greater budget and additional time to commercialize the finished product. In this work, we have studied the stereoconfiguration of individual amino acids in the tripeptide as another parameter for stabilizing one complex in a radiopharmaceutical kit. We have shown that replacing one L-amino acid with a D-configuration can shift the stability of one diastereomer to the other. To complete this work, spectroscopic characterizations should be carried out on ReO FKc-B and ReO FkC-A and B and the ^{99}Tc analogs. These will become important components in the early stage of syn and anti diastereomer assignment for this type of compounds.

6.5. References

1. Asano, Y., Lubbehusen, T. L., *Journal of Bioscience and Bioengineering*, **2000**. *89*(4): 295.
2. IUPAC, *Biochem. J.*, **1975**. *149*: 1.
3. Morrison, R. T., Boyd, R. N., *Organic Chemistry*. 4th ed. 1983, Newton, MA: Allyn & Bacon, Inc.
4. Lamzin, V. S., Dauter, Z. Wilson, K. S., *Current Opinion in Structural Biology*, **1995**. *5*(6): 830.
5. Prelog, V., *Science*, **1976**. *193*: 17.
6. Armstrong, D. W., Yang, X., Han, S. M., Menges, R. A., *Anal. Chem.*, **1987**. *59*: 2594.
7. Bruckner, H., Schieber, A., *J. High Resolut. Chromatogr.*, **2000**. *23*: 576.
8. Dunlop, D. S., Neidle, A., McHale, D., Dunlop, D. M., Lajtha, A., *Biochem. Biophys. Res. Commun.*, **1986**. *141*: 27.
9. Hashimoto, A., Nishikawa, T., Hayashi, T., Fujii, N., Harada, K., Oka, T., Takahashi, K., *FEBS Lett.*, **1992**. *296*: 33.
10. Hoopes, E. A., Peltzer, E. T., Bada, J. L., *J. Chromatogr. Sci.*, **1978**. *16*: 556.
11. Jones, W. M., Ringe, D., Soda, K., Manning, J. M., *Anal. Biochem.*, **1994**. *218*: 204.
12. Nagata, Y., Akino, T., Ohno, K., *Anal. Biochem.*, **1985**. *150*: 238.
13. Payan, I. L., Cadilla-Perezrios, R., Fisher, G. H., Man, E. H., *Anal. Biochem.*, **1985**. *149*: 484.

14. Pirkle, W. H., Finn, J. M., Schreiner, J. L. Hamper, B. C., *J. Am. Chem. Soc.*, **1981**. *103*: 3964.

15. Thorsen, G., Bergquist, J., *J. Chromatogr. B*, **2000**. *745*: 389.

16. Tsunoda, M., Kato, M., Fukushima, T., Santa, T., Homma, H., Yanai, H., Soga, T., Imai, K., *Biomed. Chromatogr.*, **1999**. *13*: 335.

17. Wakayama, M., Takashima, K., Tau, Y., Nakashima, S., Sakai, K.Moriguchi, M., *Anal. Biochem.*, **1997**. *250*: 252.

18. Zhao, S. L., Feng, Y. Z., LeBlanc, M. H., Liu, Y. M., *J. Chromatogr. B*, **2001**. *762*: 97.

19. Kumashiro, S., Hashimoto, A. Nishikawa, T., *Brain Res.*, **1995**. *681*: 231.

20. Fisher, G. H., D'Aniello, A., Vetere, A., Padula, L., Cusano, G. P., Man, E. H., *Brain Res. Bull.*, **1991**. *26*: 983.

21. Fuchs, S. A., Berger, R., Klomp, L. W. J., Koning, T. J. d., *Molecular Genetics and Metabolism*, **2005**. *85*: 168.

22. Hamase, K., Morikawa, A. Zaitsu, K., *Journal of Chromtography B*, **2002**. *781*: 73.

23. Yamada, H., Shimizu, S., *Angew. Chem. Int. Ed. Engl.*, **1988**. *27*: 622.

24. Hendrick, M. E., *Food Sci. Technol.* , **1991**. *48*(2): 29.

25. Yamada, R., Kera, Y., *EXS*, **1998**: 145.

26. Boyd, G. E., *Journal of Chemical Education*, **1959**. *36*: 3.

27. Davison, A., Trop, H. S., Depamphilis, B. V., Jones, A. G., *Inorganic Syntheses*, **1982**. *21*: 160.

28. Rose, D. J., Maresca, K. P., Kettler, P. B., Chang, Y. D., Soghomomian, V., Chen, Q., Abrams, M. J., Larsen, S. K., Zubieta, J., *Inorg. Chem.*, **1996**. *35*(12): 3548.

APPENDIX SECTION

Figure A1. Solid Phase Peptide Synthesis Apparatus.

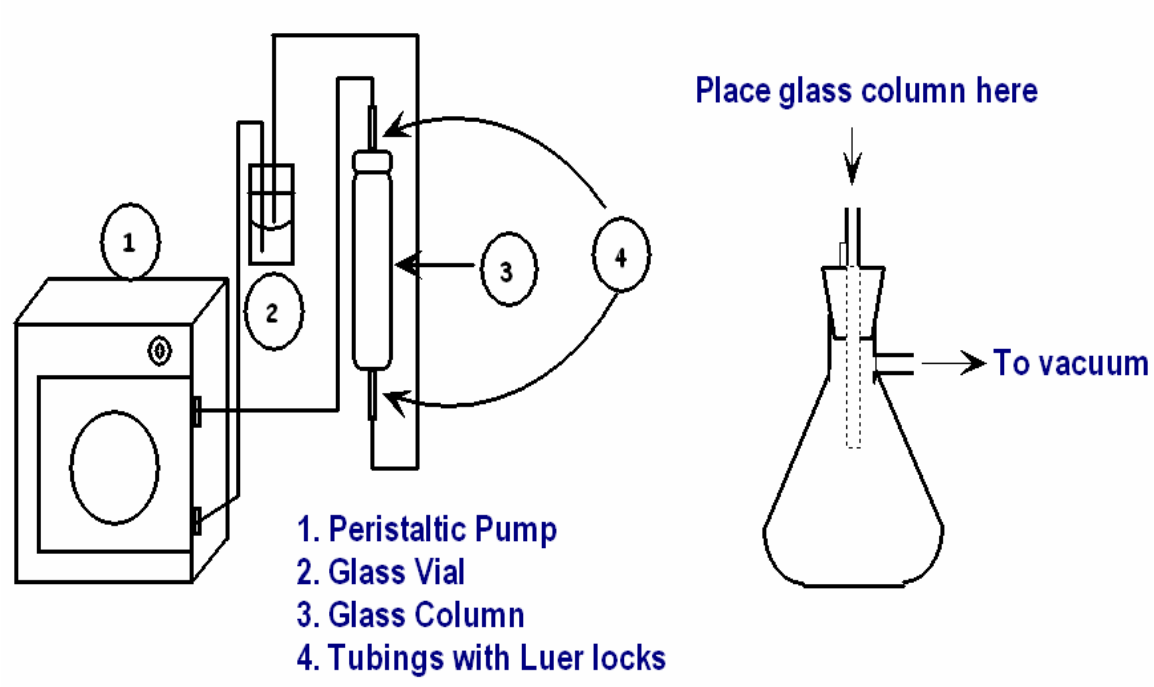

Figure A2. ORTEP Diagrams of all Crystal Structures.

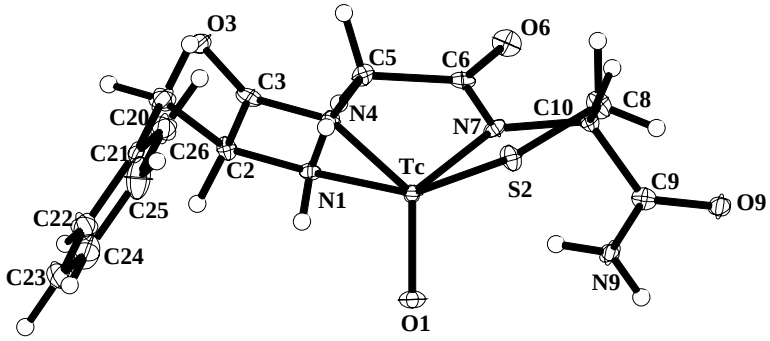

TcO FGC anti

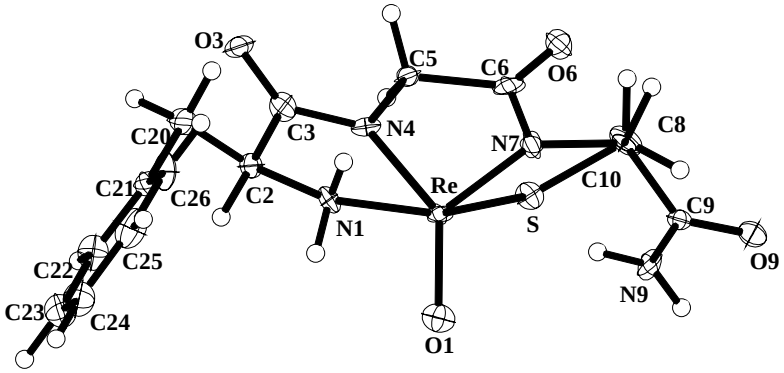

ReO FGC anti

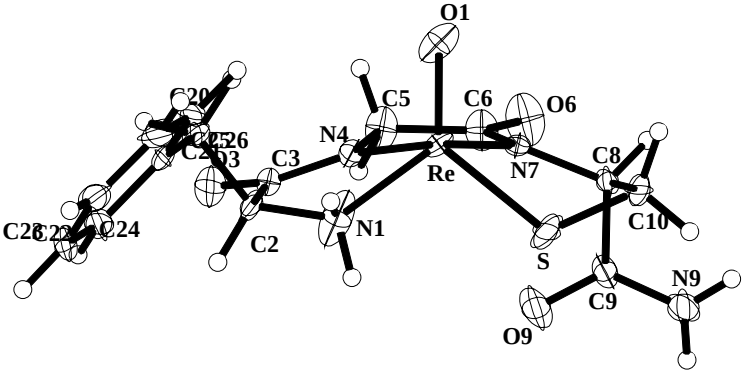

ReO FGC syn

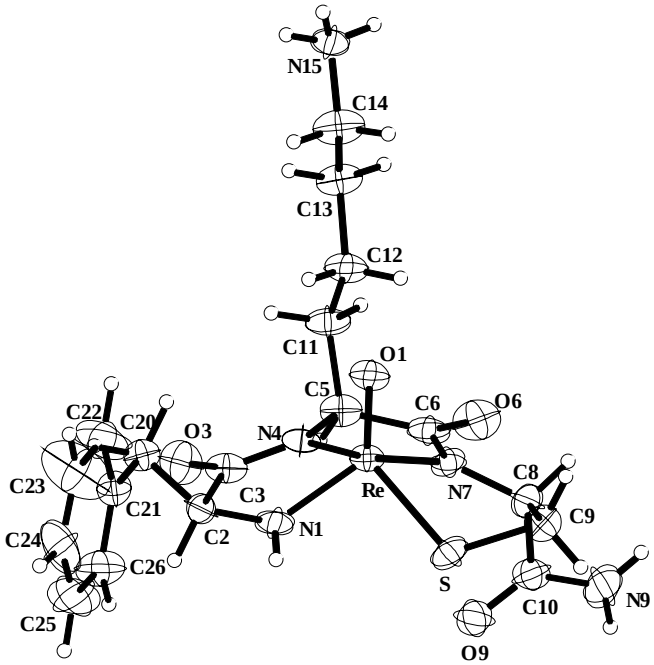

ReO FKC syn

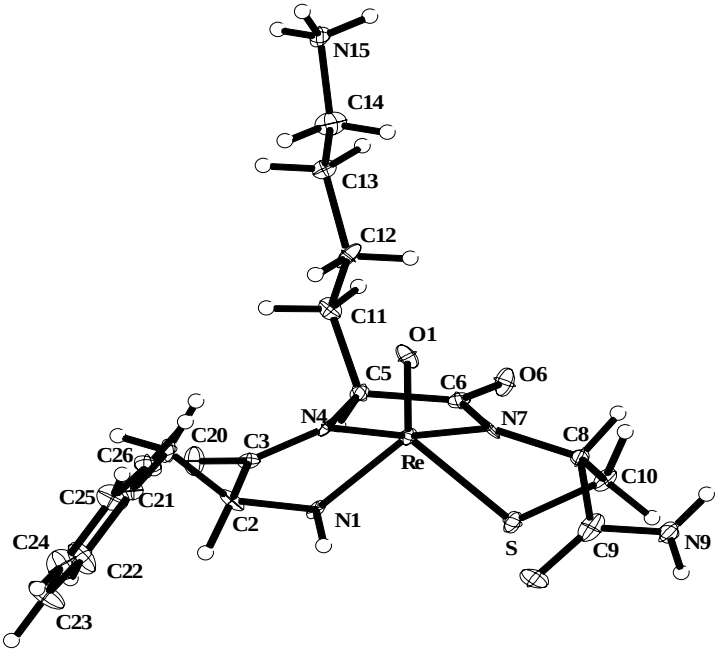

ReO FKC syn (prepared under aqueous conditions)

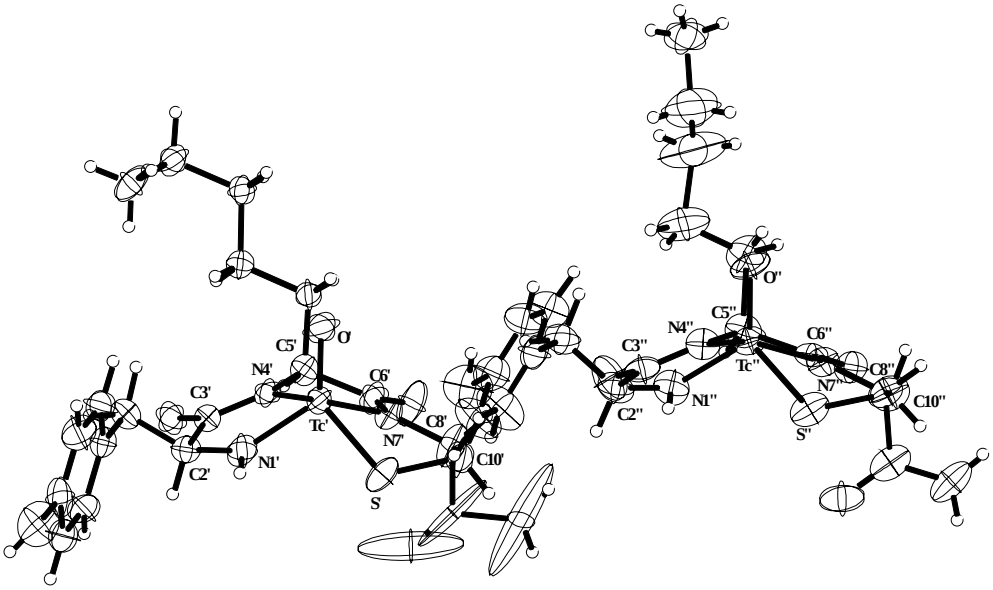

TcO YKC
(two of the three independent molecules; prepared under aqueous conditions)

Figure A3. Proton NMR spectra taken in DMSO showing amine protons for species ^{99}TcO FKC syn and anti complexes and ReO FKC syn and anti complexes.

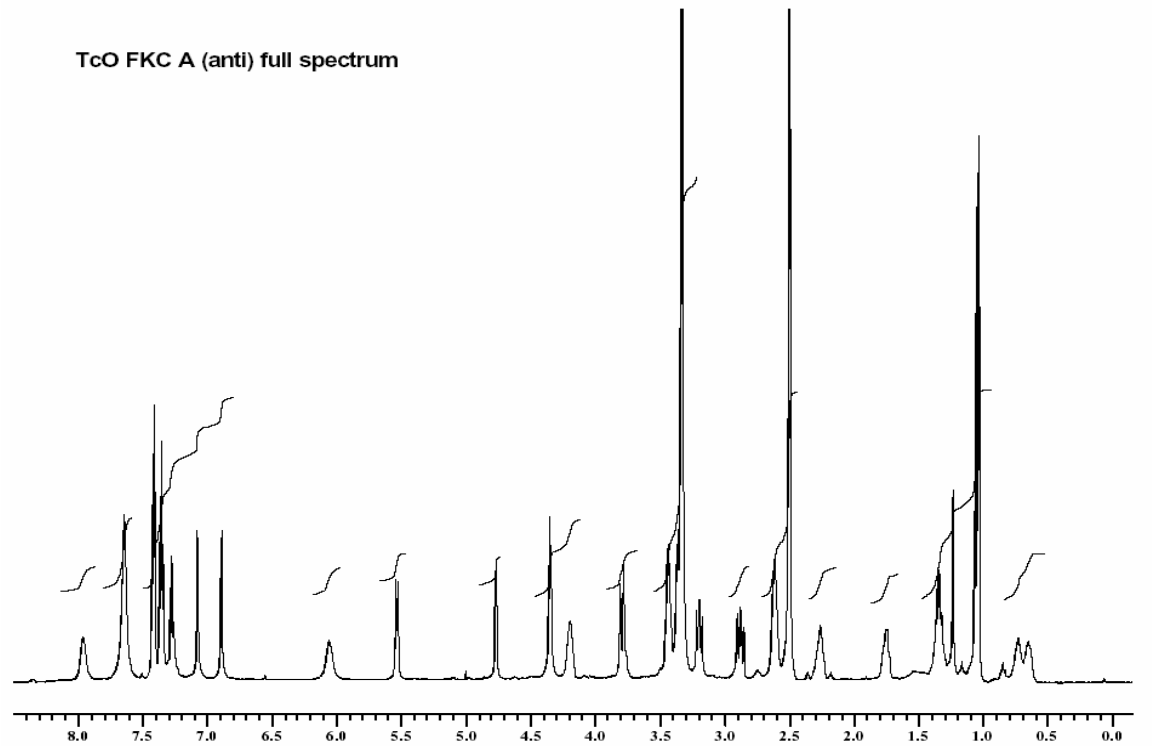

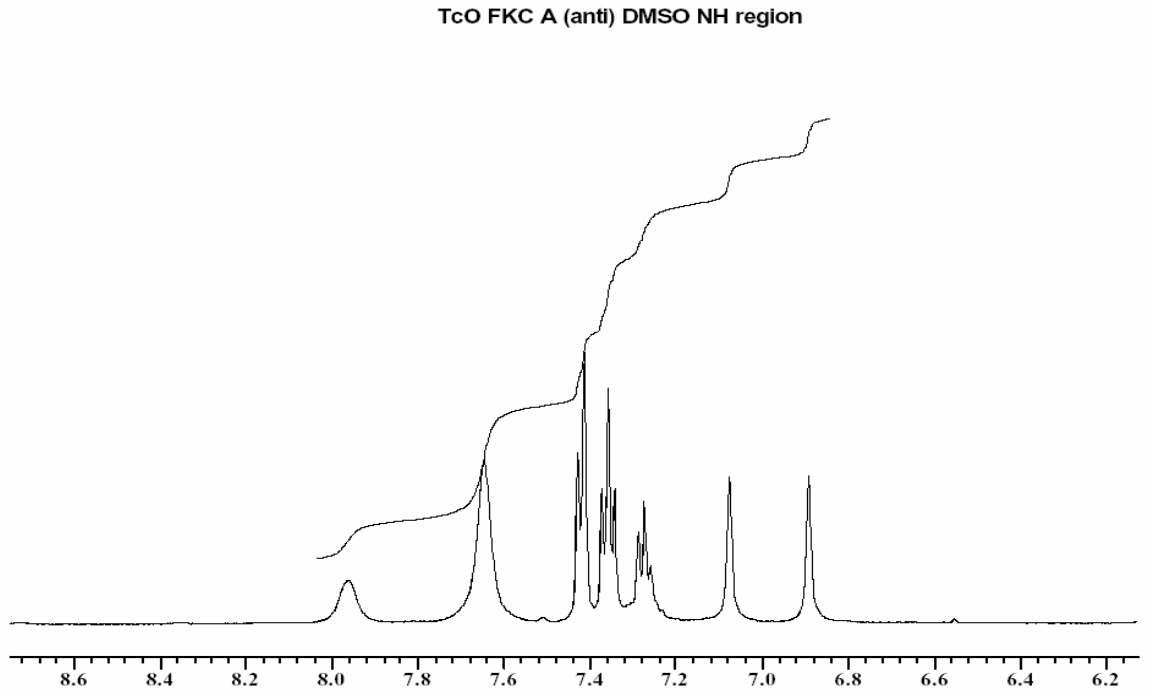

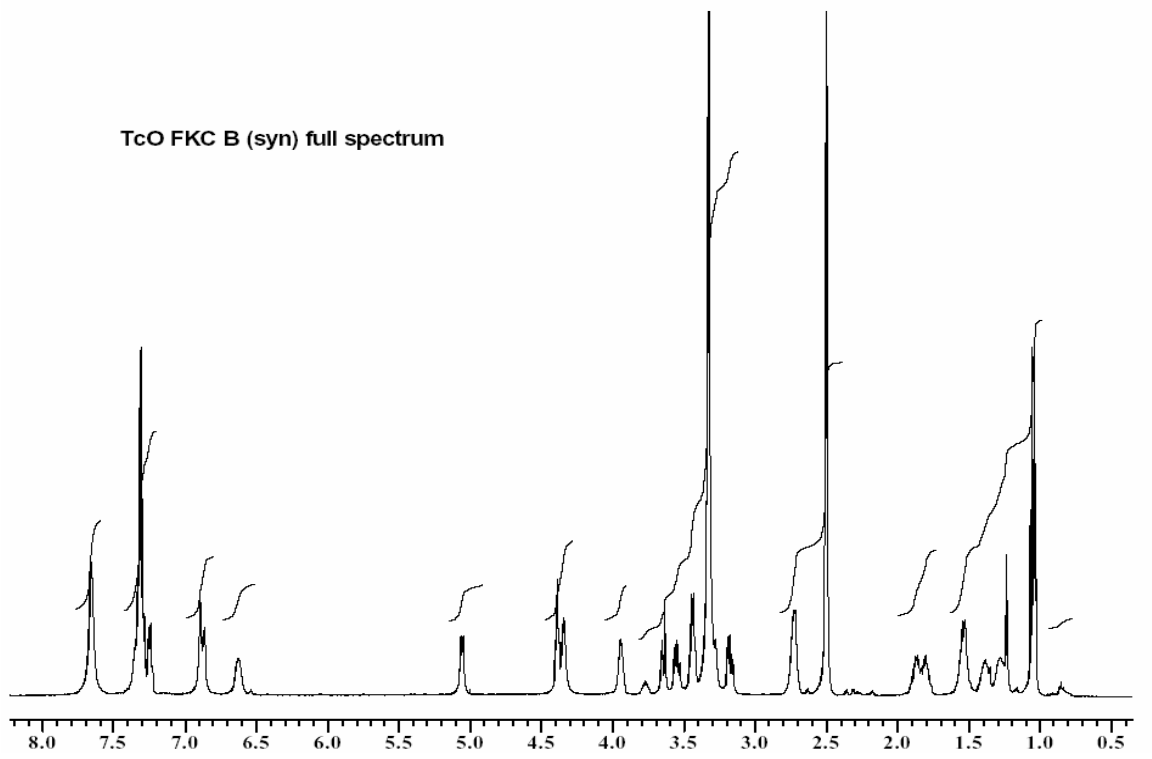
TcO FKC B (syn) full spectrum
8.0
7.5
7.0
6.5
6.0
5.5
5.0
4.5
4.0
3.5
3.0
2.5
2.0
1.5
1.0
0.5

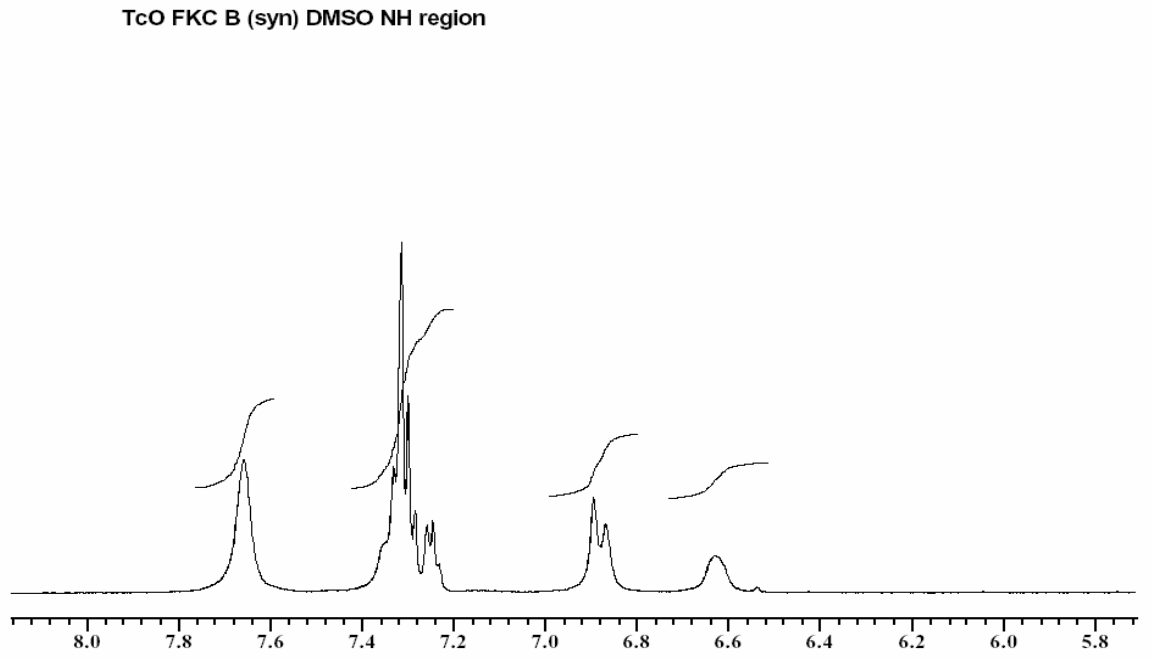
TcO FKC B (syn) DMSO NH region
8.0
7.8
7.6
7.4
7.2
7.0
6.8
6.6
6.4
6.2
6.0
5.8

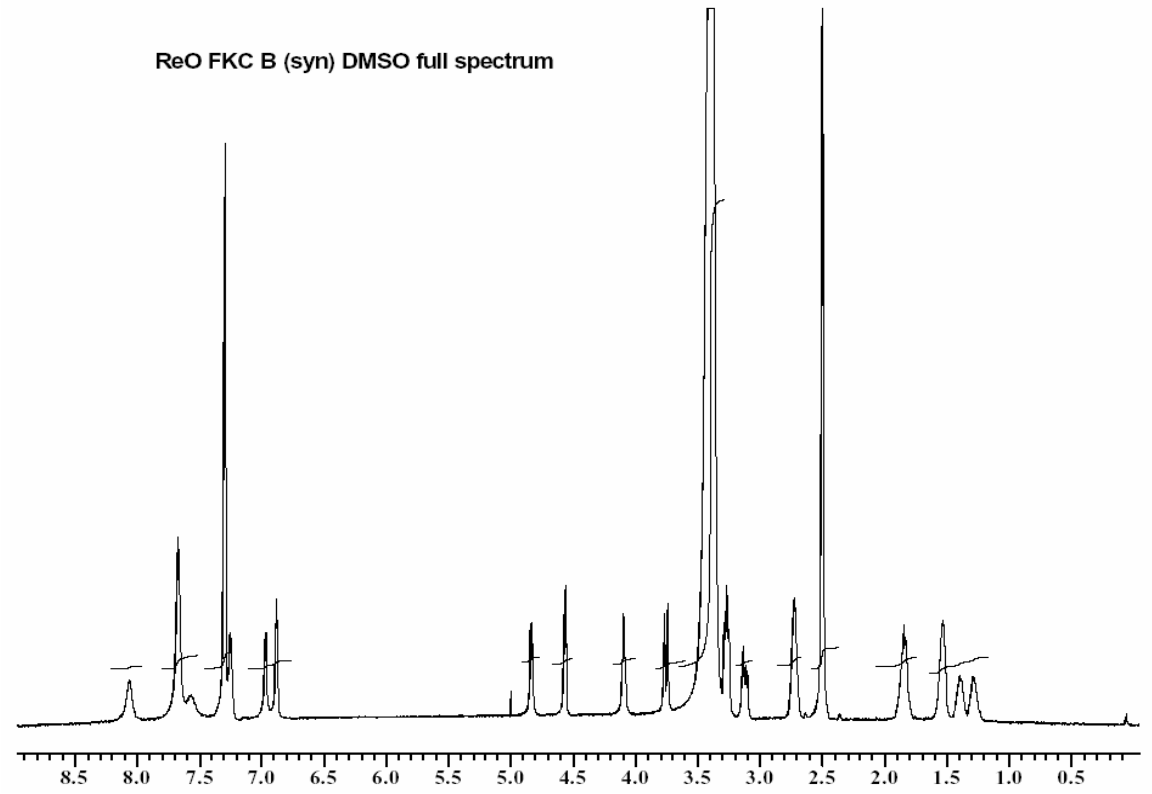

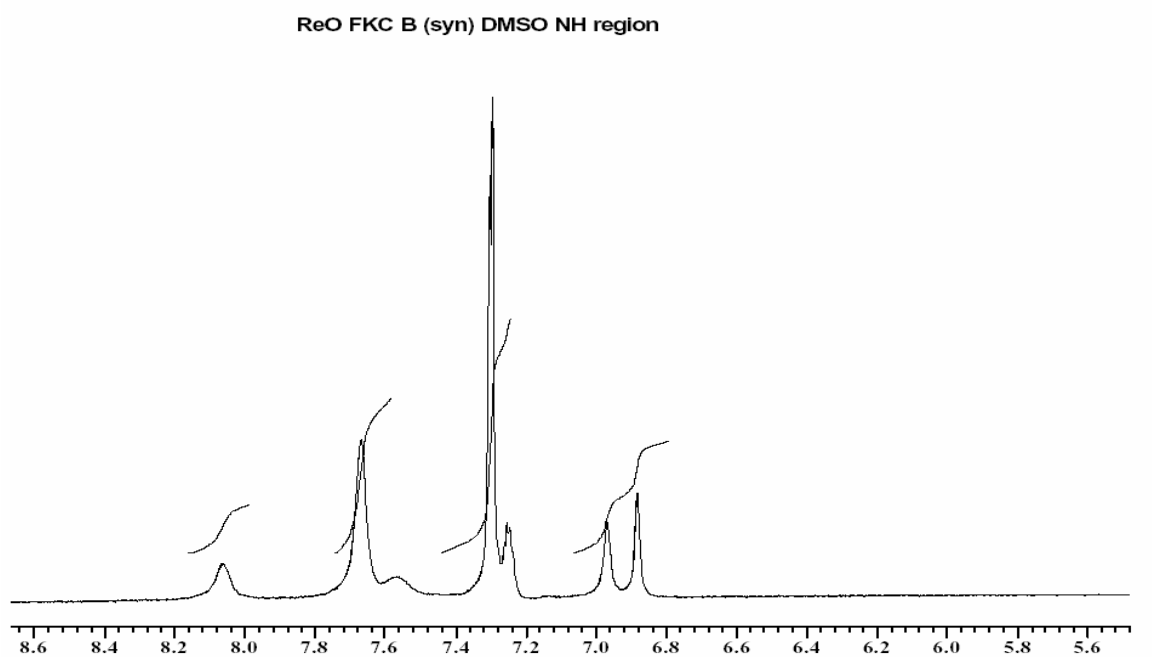

Proton NMR Spectra of TcO FKC A (anti) and TcO FKC B (syn) and ReO FKC B (syn) in DMSO showing the resonances assigned to the 2 protons of the amine of the first amino acid (phenylalanine or tyrosine).

Figure A4. Simulated and Experimental Mass Spectral Data of ReO FKC syn.

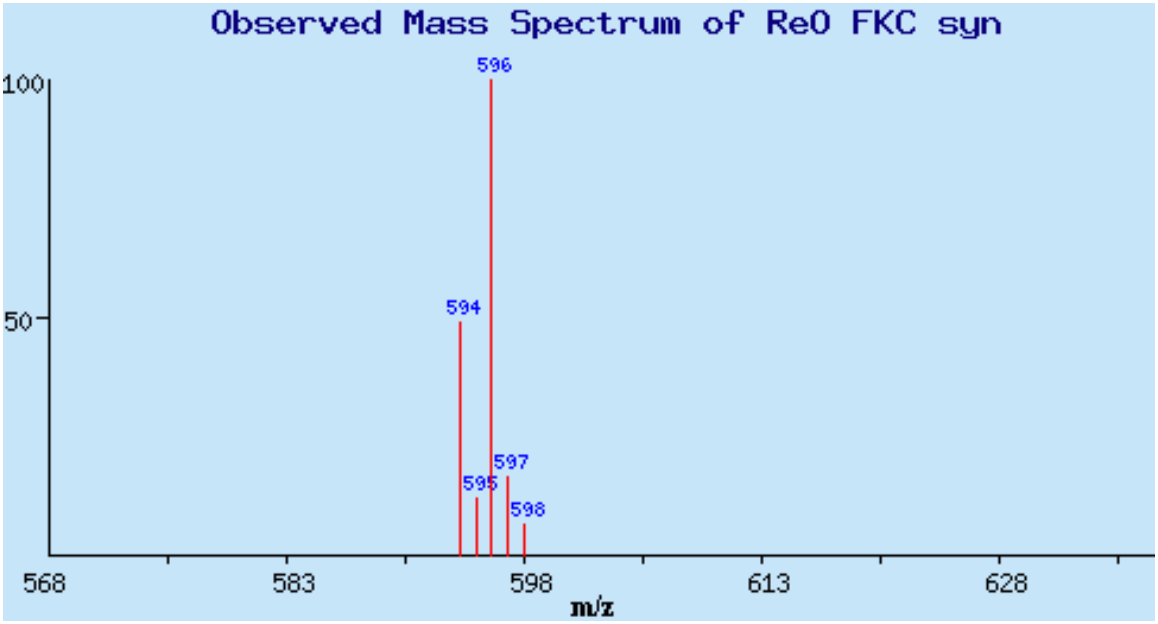

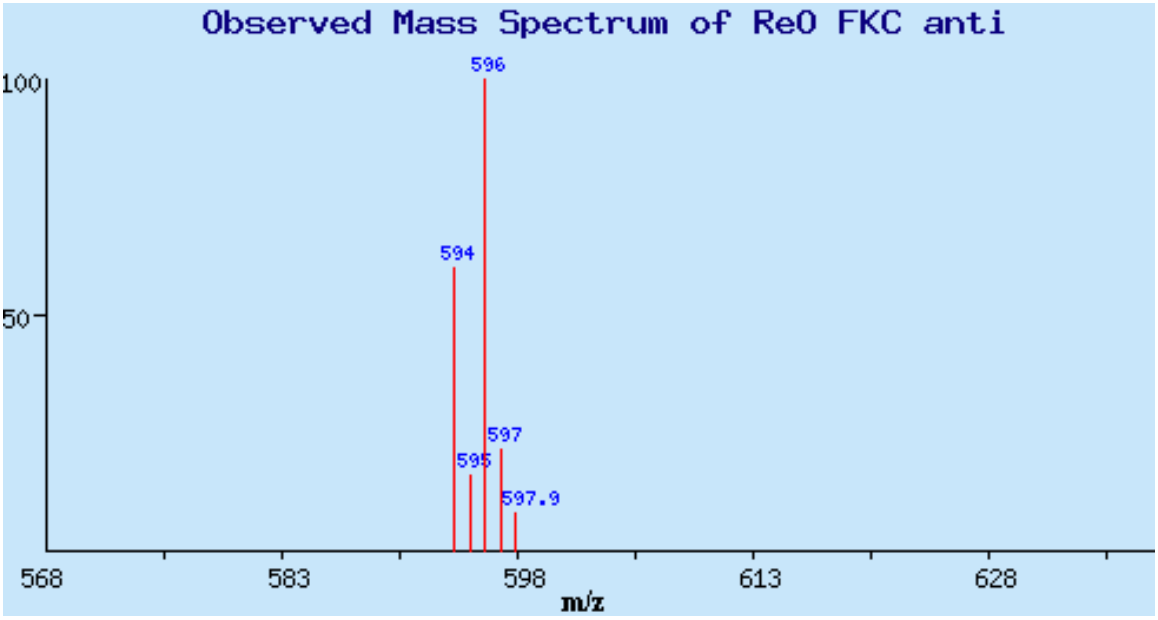

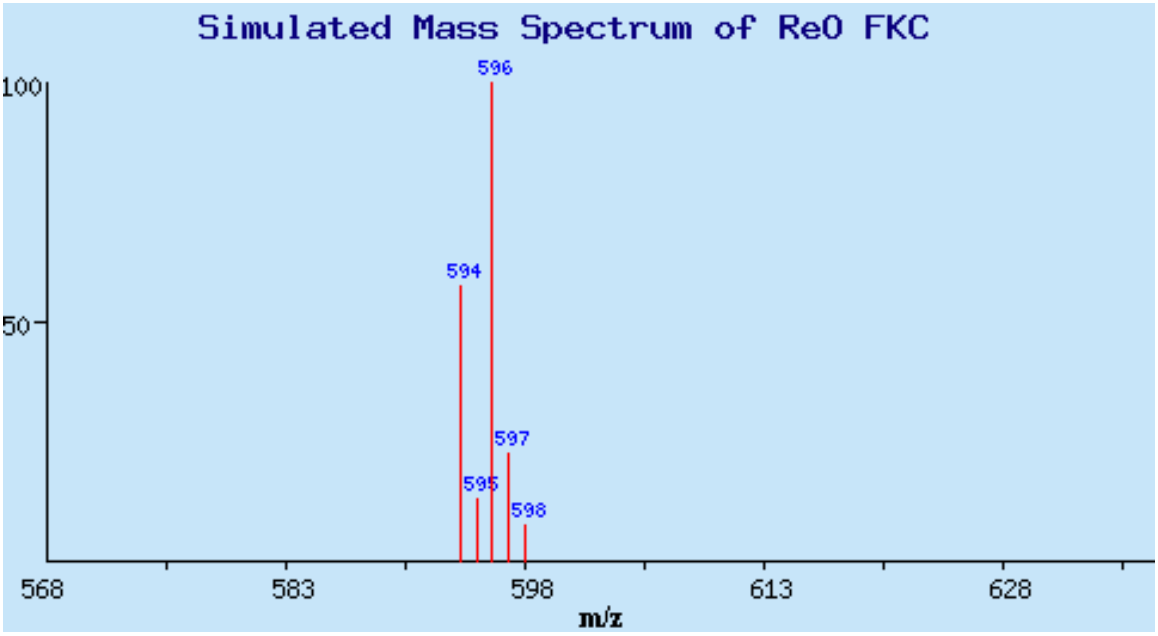
Simulated Mass Spectrum of ReO FKC
100
50
596
594
597
595
598
568
583
598
613
628
m/z

Figure A5. NMR Titration Curves for Determination of pK_a's for FKC, FGC, and ReO FGC anti using Popov procedure (see Chapter 4, Section 4.2.7.2).

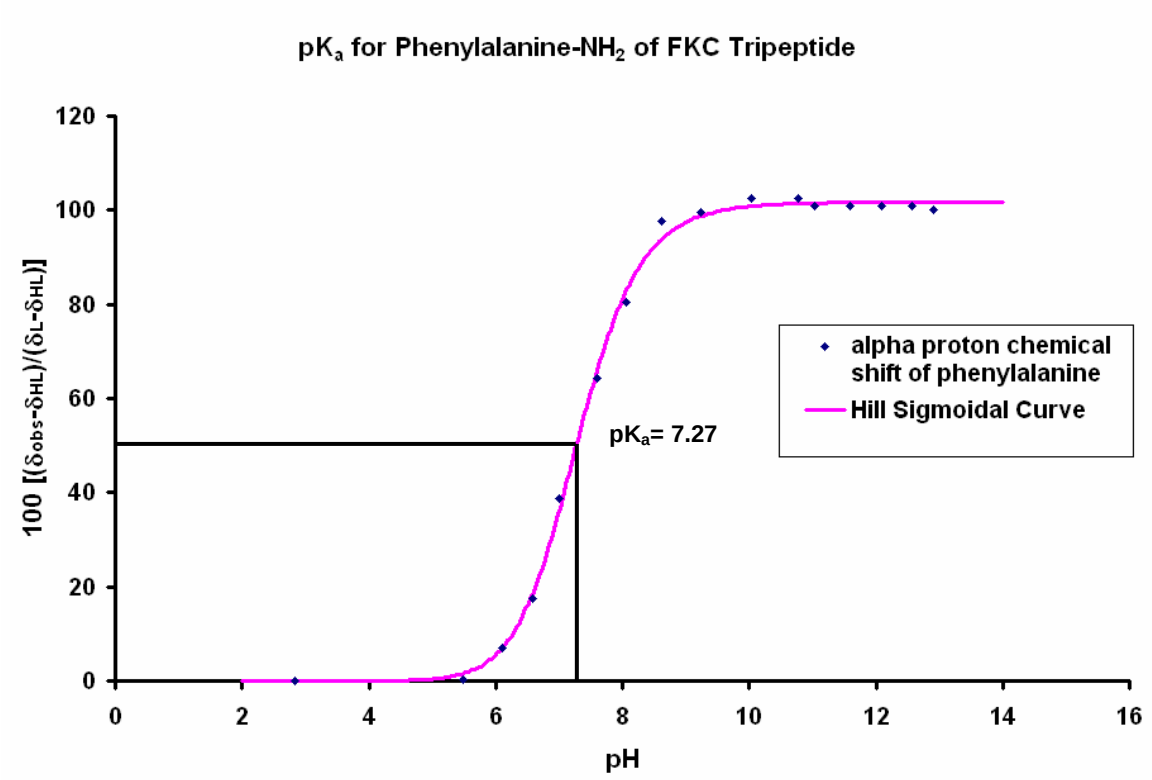

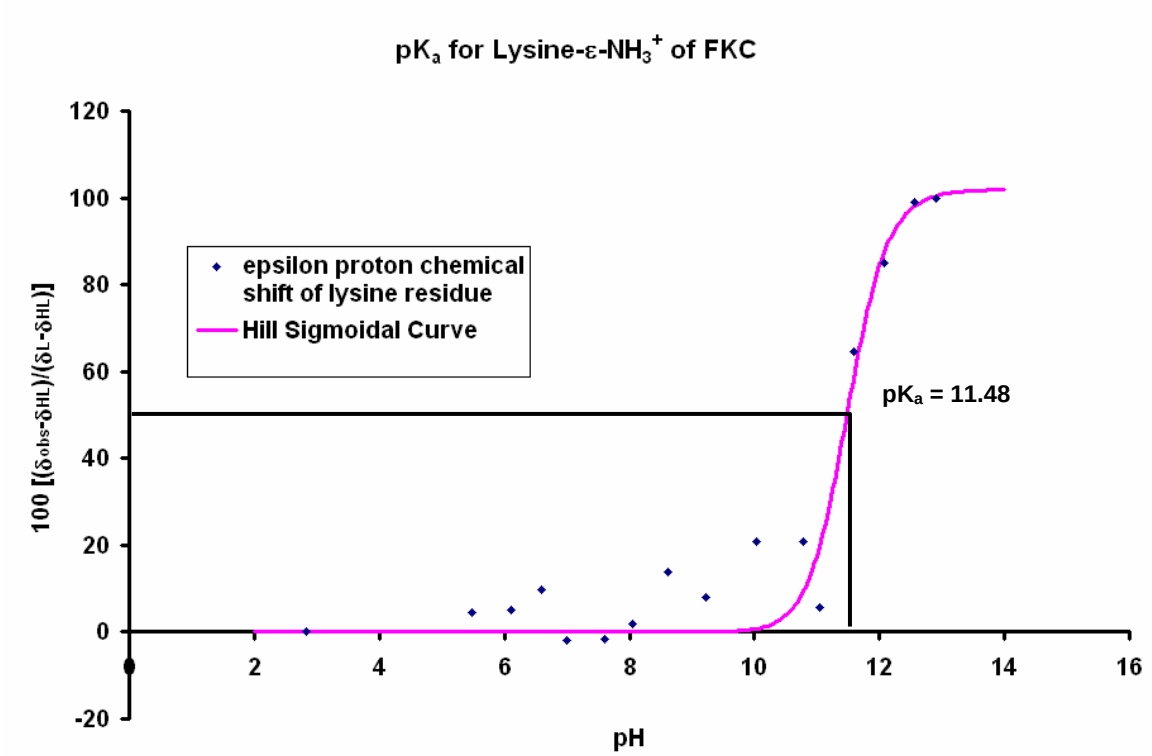
pK$_a$ for Lysine-ε-NH$_3^+$ of FKC
epsilon proton chemical shift of lysine residue
Hill Sigmoidal Curve
pK$_a$ = 11.48
100 [(δobs-δHL)/(δL-δHL)]
pH
120
100
80
60
40
20
0
-20
2
4
6
8
10
12
14
16

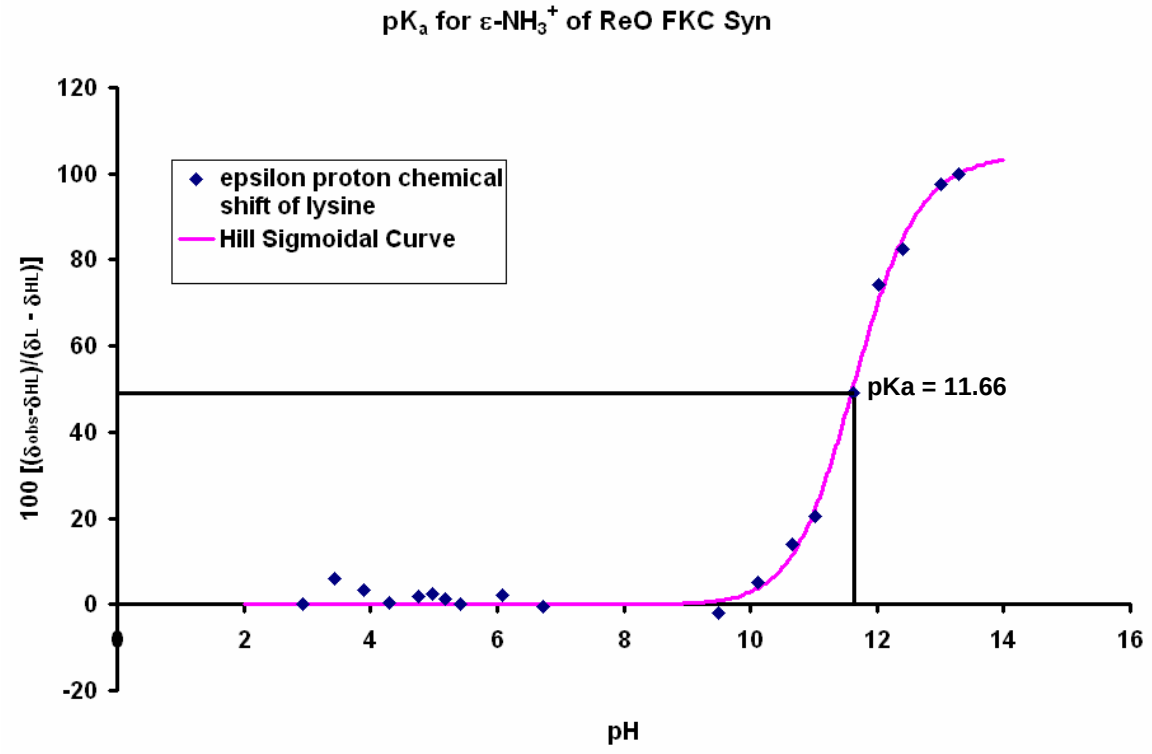
pK$_a$ for ε-NH$_3^+$ of ReO FKC Syn
epsilon proton chemical shift of lysine
Hill Sigmoidal Curve
pKa = 11.66
100 [(δobs-δHL)/(δL - δHL)]
pH
120
100
80
60
40
20
0
-20
2
4
6
8
10
12
14
16

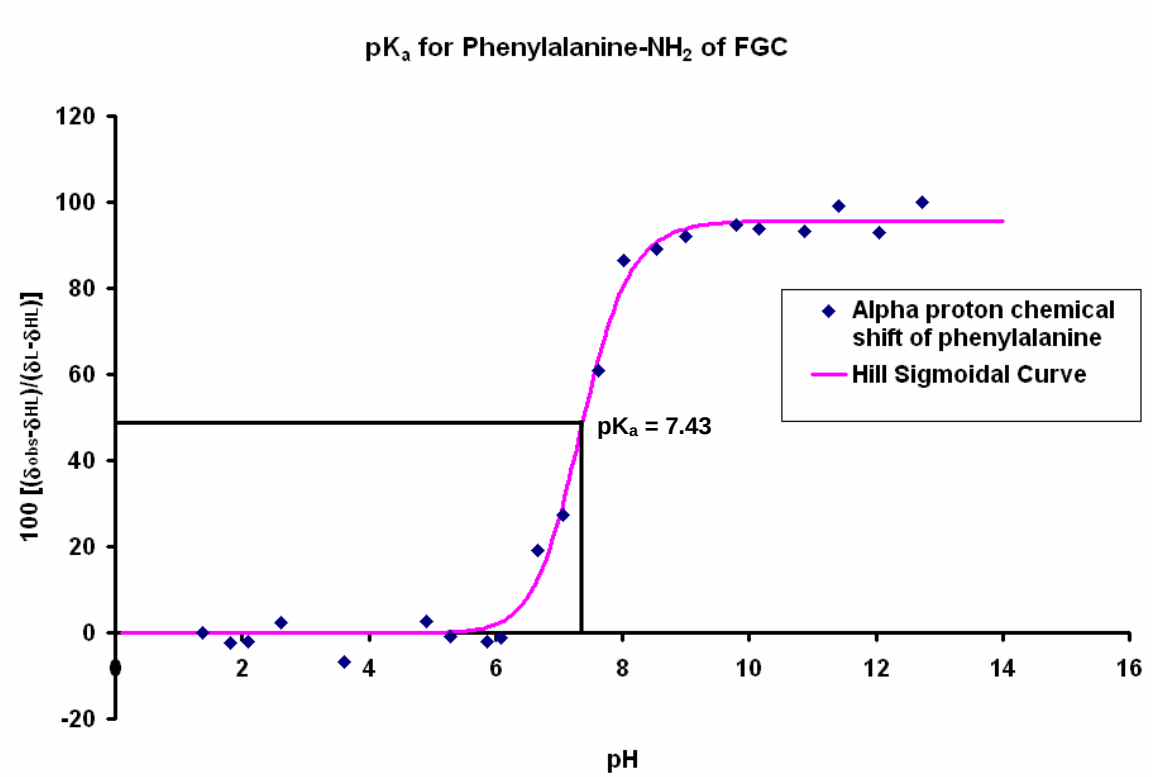
pK$_a$ for Phenylalanine-NH$_2$ of FGC
120
100
80
60
40
20
0
-20
2
4
6
8
10
12
14
16
100 [(δobs-δHL)/(δL-δHL)]
pH
pK$_a$ = 7.43
Alpha proton chemical shift of phenylalanine
Hill Sigmoidal Curve

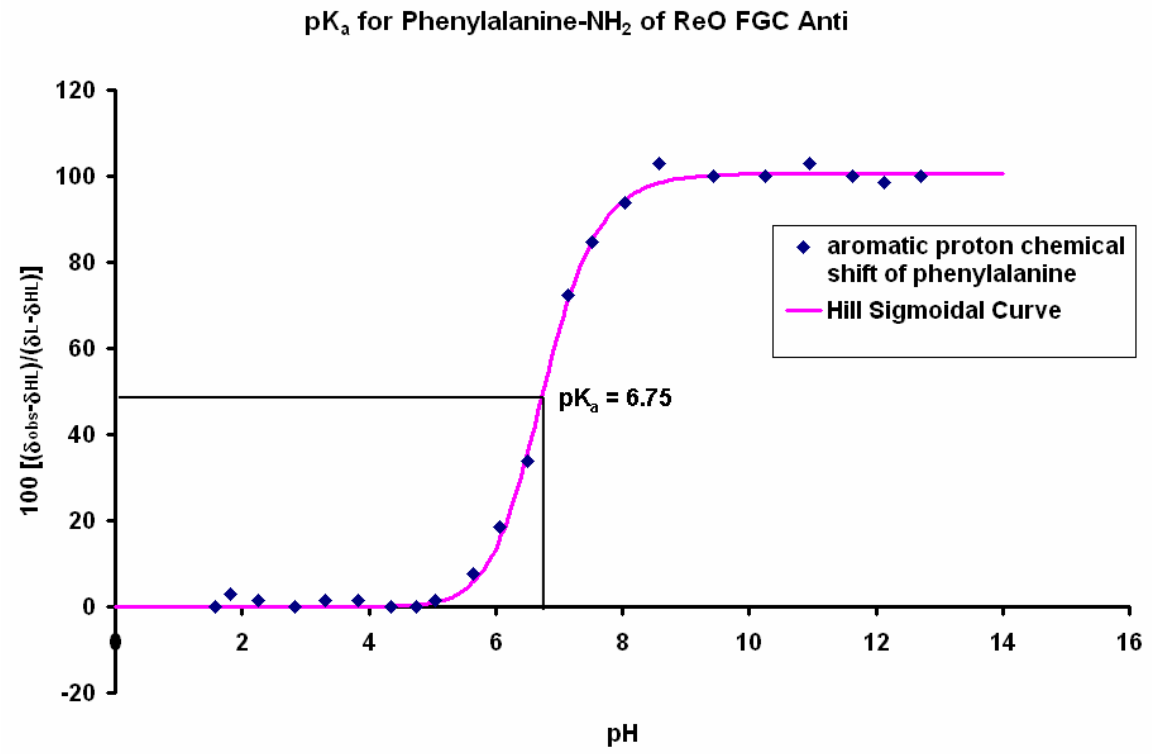
pK$_a$ for Phenylalanine-NH$_2$ of ReO FGC Anti
120
100
80
60
40
20
0
-20
2
4
6
8
10
12
14
16
100 [(δobs-δHL)/(δL-δHL)]
pH
pK$_a$ = 6.75
aromatic proton chemical shift of phenylalanine
Hill Sigmoidal Curve

Figure A6. Time Dependence of ^{99}TcO FGC Syn and Anti Diastereomer Concentrations at pH 8.02, and pH 9.01, and at 37 ^{0}C.

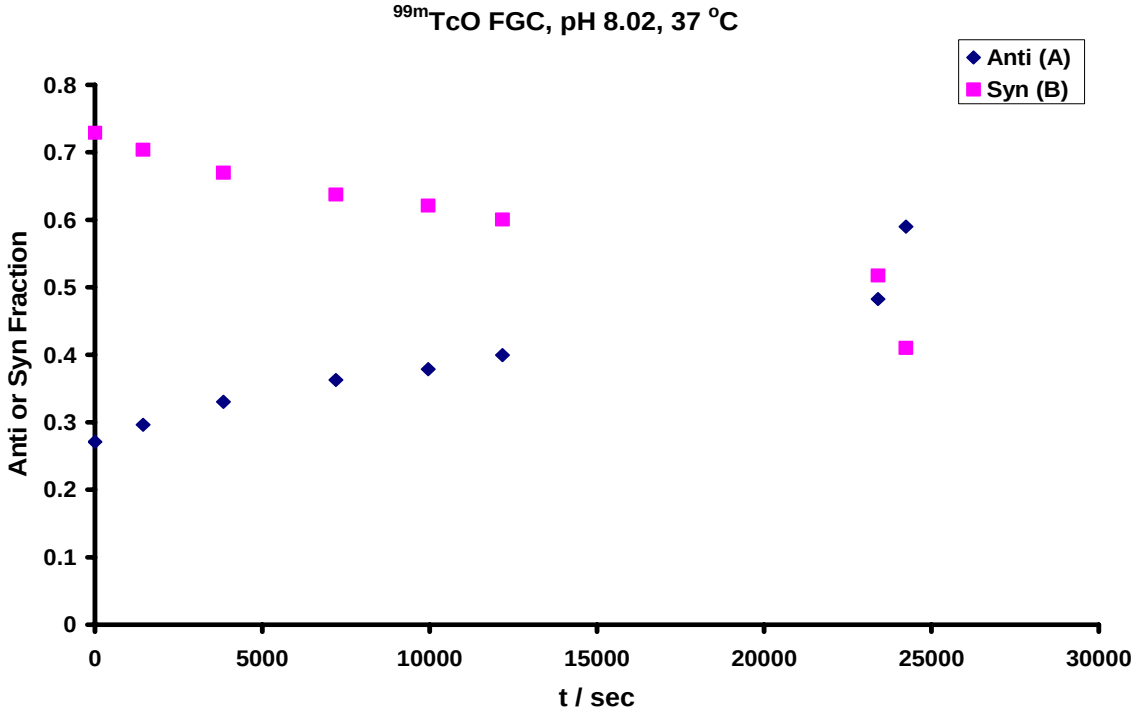

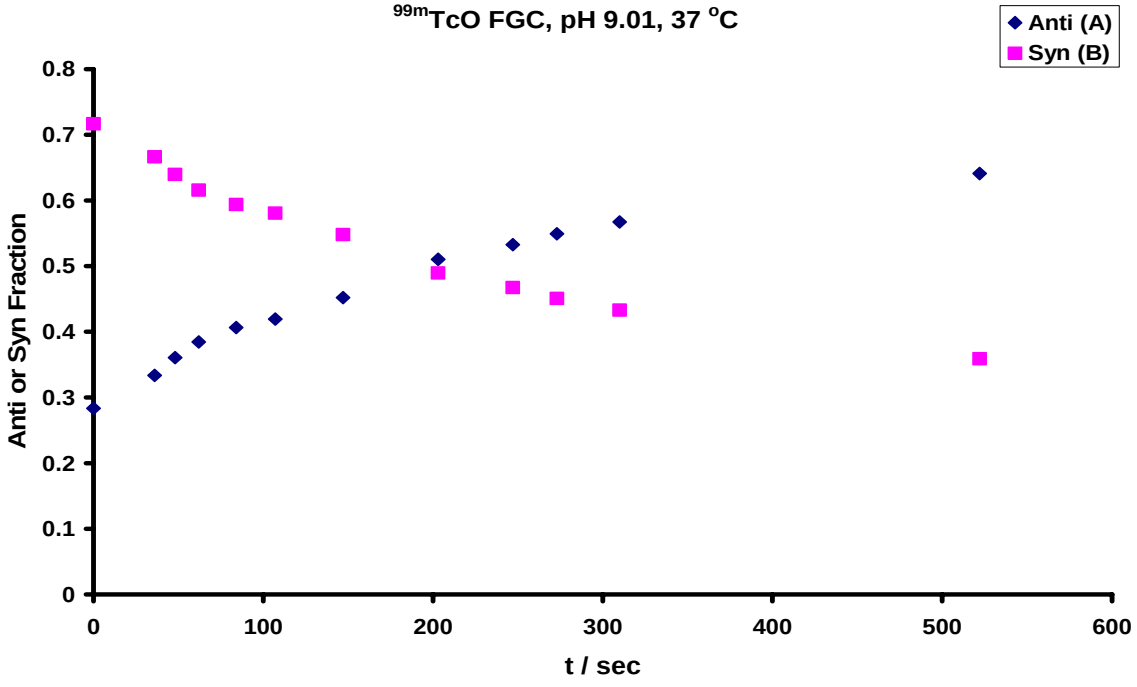

Figure A7. Time Dependence of ^{99}TcO FKC Syn and Anti Diastereomer Concentrations at pH 5.03, pH, 8.02, and pH 9.01, and at 37 ^{0}C.

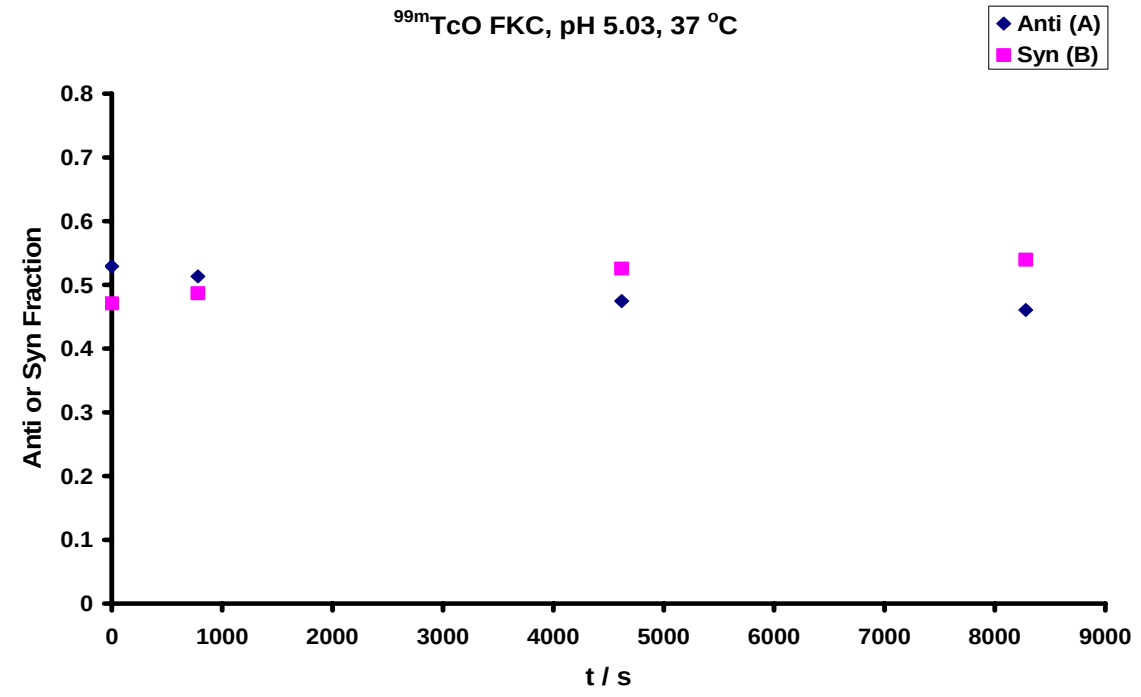

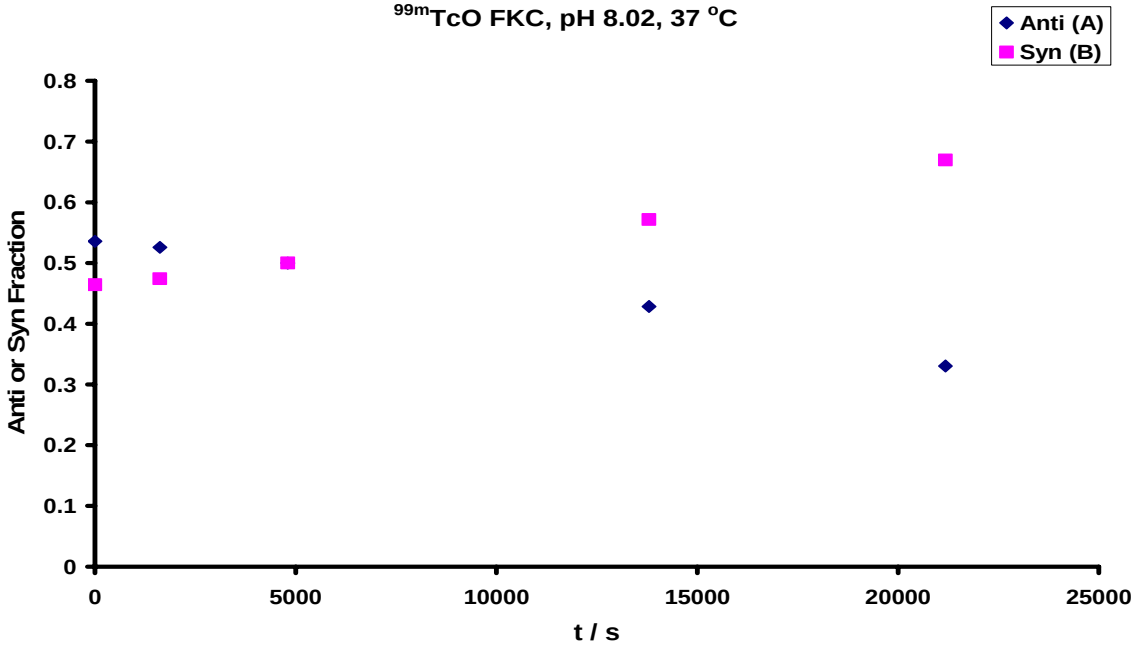

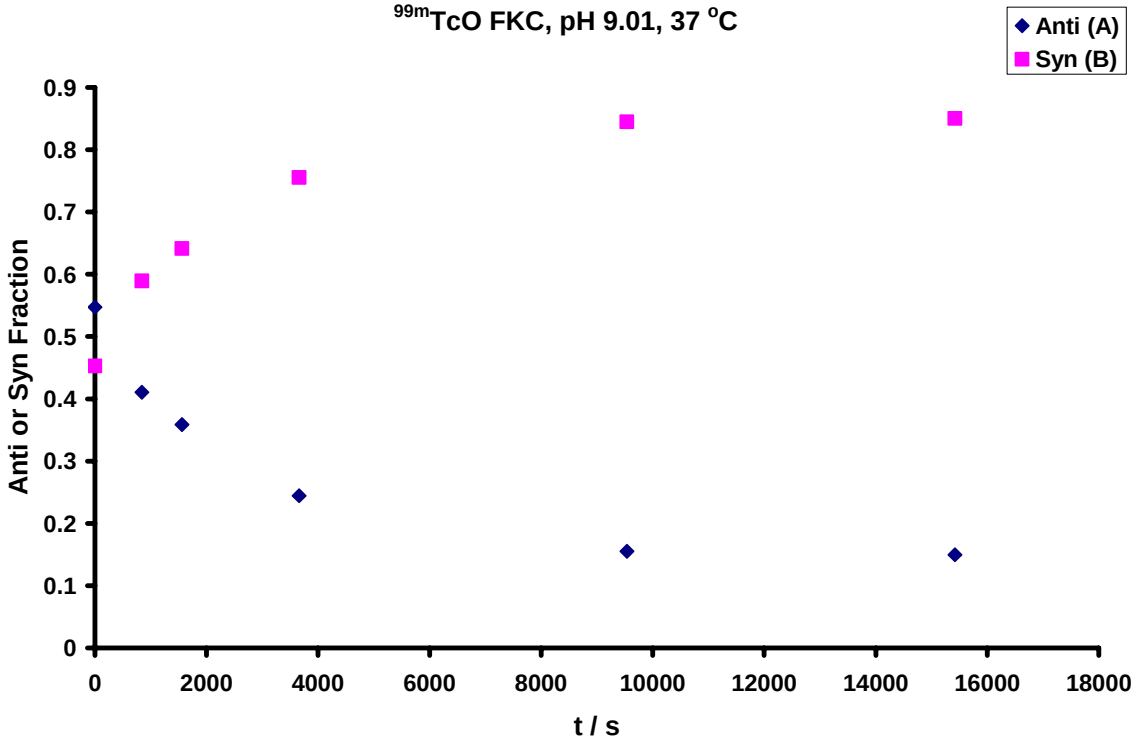
99mTcO FKC, pH 9.01, 37 °C
Anti (A)
Syn (B)
Anti or Syn Fraction
0.9
0.8
0.7
0.6
0.5
0.4
0.3
0.2
0.1
0
0
2000
4000
6000
8000
10000
12000
14000
16000
18000
t / s

Table A1. Retention times for all of the MO tripeptide complexes and Selected M=O Infrared stretching frequencies.

MO Tripeptides	Retention time, min[a]		M=O stretch, cm^{-1}	
	A	B	A	B
Re FGC	14.6	17.2	984	
Re FKC	12.9	14.2		991
Re FDC	18.7	22.6		
Re MKC	9.1	11.1		
Tc FGC	11.2	12.4		
Tc FKC	9.4	10.2		
Tc FSC	10.0	10.7		
Tc MKC	7.4	8.7		
Tc YKC	7.5	8.6		980
Tc YSC	8.5	9.3		
Tc YDC A&B	8.3	8.7		
Tc YDC C&D	10.1	10.7		
Tc YGC	7.9	8.2		

[a]HPLC conditions: Column: Waters XTerra 5µ C_{18} 100 Å, 3.9 x 150 mm; Mobile Phase Gradient: 0 % - 55 % B over 15 min; Flow Rate: 1.0 mL/min; Software: ProStar WorkStation.

Table A2. Crystal data and structure refinement data for ^{99}TcO YKC syn (showing 3 independent molecules) and ReO FKC syn diastereomers prepared under aqueous conditions.

	TcO YKC syn	ReO FKC syn
empirical formula	C54 H88 N15 O20 S3 Tc3	C18 H30 N5 O6 Re S
fw	1657.57	630.73
cryst syst	orthorhombic	monoclinic
space group	P2(1)2(1)2(1)	P2(1)
temp, K	295(2)	100(2)
wavelength, Å	0.71073	0.71073
a, Å	10.074(2)	9.6480(19)
b, Å	20.966(4)	10.186(2)
c, Å	30.939(6)	12.272(3)
α, deg	90	90
β, deg	90	106.36(3)
γ, deg	90	90
V, Å^3	6943(2)	1157.2(4)
Z	4	2
calcd density, g/cm^3	1.586	1.810
abs coeff, mm^{-1}	0.759	5.384
F (000)	3416	624
θ range, deg	2.99–27.52	3.11–27.44
limiting indices	-13 ≤ h ≤ 12 -27 ≤ k ≤ 23 -40 ≤ l ≤ 40	-12 ≤ h ≤ 11 -13 ≤ k ≤ 13 -14 ≤ l ≤ 15
reflns collected/unique	52560 / 15704 [R(int)=0.0604]	10247 / 4820 [R(int)=0.0914]
refinement meth	full-matrix least-squares on F^2	full-matrix least-squares on F^2
data / restraints / parameters	15704 / 0 / 857	4820 / 13 / 281
GOF on F^2	1.011	1.043
final R indices [I>2σ(I)]	R1=0.0445 wR2= 0.0971	R1=0.0416 wR2= 0.0930
R indices (all data)	R1=0.0713 wR2= 0.1050	R1=0.0492 wR2= 0.0965
largest diff.peak and hole (eÅ^{-3})	0.779 and –0.394	3.304 and –2.787

Table A3. Selected bond lengths and angles for ReO FKC syn diastereomers prepared under aqueous conditions.

Bond Length, Å	**ReO FKC syn**
M-O	1.686(5)
M-S	2.293(2)
M-N1	1.956(7)
M-N2	2.015(6)
M-N3	2.029(5)
N1-C4	1.469(10)
Bond Angle, deg	
N1-M-N2	78.1(3)
N1-M-S	91.41(19)
N2-M-N3	76.7(2)
N3-M-S	82.1(3)
O-M-N1	111.2(3)
O-M-N2	112.8(3)
O-M-N3	114..0(4)
O-M-S	109.5(2)
C5-N2-C6	121.5(6)
C7-N3-C8	116.0(6)
C5-N2-M	119.7(5)
C6-N2-M	118.3(5)
C7-N3-M	119.1(6)
C8-N3-M	124.6(5)
C4-N1-M	117.3(5)
C5-C4-N1	107.3(6)

Table A4. Proton NMR data for all isolated syn and anti diastereomers of ^{99}Tc and Re tripeptides

^{99}TcO Peptide	assignment	Anti Isomer (Product A)		Syn Isomer (Product B)	
		δ (ppm)	*J* (Hz)	δ (ppm)	*J* (Hz)
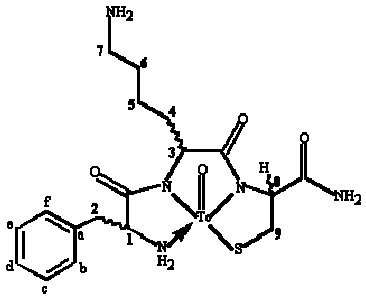 **^{99}TcO FKC** [1]	H1	4.77		4.30 (t, 1H)	
	H2a	2.98 (dd, 1H)	$J_{H1\text{-}H2a}$ = 10.3, $J_{H2a\text{-}H2b}$ = 14.2	3.40 (m, 1H)	$J_{H1\text{-}H2a}$ = 6.4, $J_{H2a\text{-}H2b}$ = 14.7
	H2b	3.54 (m, 1H)		3.51 (dd, 1H)	$J_{H1\text{-}H2b}$ = 5.9
	N-H(1)	5.91 (br s, 2H)		**not observed**	
	Ar-H	7.43 (m, 5H)		7.39 (m, 5H)	
	H3	5.04 (br s, 1H)		4.76	
	H4a	1.87 (m, 1H)		2.01 (m, 2H)	
	H4b	2.38 (m, 1H)		--	
	H5	0.62 (m, 2H)		1.31 (m, 2H)	
	H6	1.50 (m, 2H)		1.66 (m, 2H)	
	H7	2.83 (m, 2H)		2.94 (m, 2H)	
	N-H(7)	7.48 (m, 2H)		7.53 (br s, 2H)	
	H8	5.71 (dd, 1H)	$J_{H8\text{-}H9a}$ = 7.6, $J_{H8\text{-}H9b}$ = 2.2	5.23 (d, 1H)	$J_{H8\text{-}H9}$ = 6.4
	H9a	3.57 (m, 1H)	$J_{H9a\text{-}H9b}$ = 12.5	3.80 (m, 2H)	
	H9b	3.83 (dd, 1H)		--	
	CON-Ha	7.15 (m, 1H)		7.04 (m, 1H)	
	CON-Hb	7.39 (m, 1H)		7.63 (m, 1H	
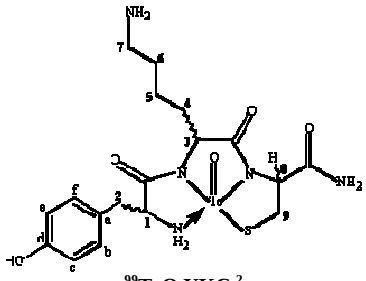 **^{99}TcO YKC** [2]	H1			4.26 (t, 1H)	
	H2a			3.35 (dd, 1H)	$J_{H1\text{-}H2a}$ = 5.9, $J_{H2a\text{-}H2b}$ = 14.8
	H2b			3.49 (dd, 1H)	$J_{H1\text{-}H2b}$ = 5.1
	N-H(1)			**not observed**	
	Ar-H(c,e)			6.87 (d, 2H)	$J_{Hb\text{-}Hc}$ = $J_{He\text{-}Hf}$ = 8.1
	Ar-H(b,f)			7.29 (d, 2H)	
	H3			4.70 (t, 1H)	$J_{H3\text{-}H4}$ = 4.8
	H4			2.02 (m, 2H)	
	H5			1.31 (m, 2H)	
	H6			1.67 (m, 2H)	
	H7			2.94 (m, 2H)	
	N-H(7)			**not observed**	
	H8			5.25 (d, 1H)	$J_{H8\text{-}H9}$ = 6.6
	H9			3.83 (m, 2H)	
	CON-H			**not observed**	

^{99}TcO Peptide	assignment	Anti Isomer (Product A)		Syn Isomer (Product B)	
		δ (ppm)	*J* (Hz)	δ (ppm)	*J* (Hz)
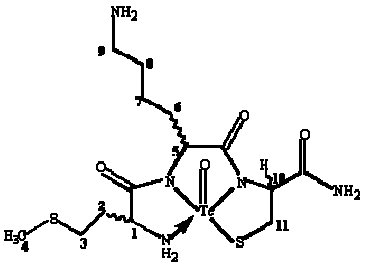 **^{99}TcO MKC** [1]	H1	4.43 (br t, 1H)		4.10 (t, 1H)	J_{H1-H2} = 6.4
	H2a	1.95 (m, 1H)		2.38 (dd, 2H)	
	H2b	2.32 (m, 1H)		--	
	H3a	2.72 (m, 1H)		2.81 (m, 2H)	
	H3b	2.74 (m, 1H)		--	
	H4	2.13 (s, 3H)		2.14 (s, 3H)	
	N-H(1)	6.21 (s, 2H)		**not observed**	
	H5	4.98 (br s, 1H)		4.98	
	H6a	1.82 (m, 1H)		2.02 (m, 2H)	
	H6b	2.38 (m, 1H)		--	
	H7	0.65 (m, 2H)		1.42 (m, 2H)	
	H8	1.44 (m, 2H)		1.67 (m, 2H)	
	H9	2.78 (m, 2H)		2.92 (m, 2H)	
	N-H(9)	7.39		7.49 (br s, 2H)	
	H10	5.68 (dd, 1H)	$J_{H10-H11a}$ = 7.9, J_{H1-H2b} = 2.0	5.26 (dd, 1H)	
	H11a	3.56 (dd, 1H)	$J_{H11a-H11b}$ = 12.7	3.87 (d, 2H)	$J_{H10-H11a}$ = 5.4, J_{H1-H2b} = 3.4
	H11b	3.82 (dd, 1H)		--	
	CON-Ha	7.13 (s, 1H)		7.04 (s, 1H)	
	CON-Hb	7.41		7.64 (s, 1H)	
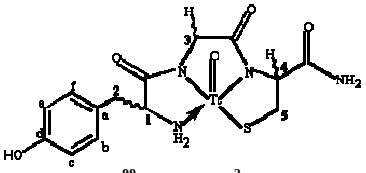 **^{99}TcO YGC** [2]	H1	4.51 (dd, 1H)			
	H2a	2.92 (dd, 1H)	J_{H1-H2a} = 8.8, $J_{H2a-H2b}$ = 14.7		
	H2b	3.33 (dd, 1H)	J_{H1-H2b} = 3.9		
	N-H(1)	**not observed**			
	Ar-H(c,e)	6.84 (d, 2H)	J_{Hb-Hc} = 8.3		
	Ar-H(b,f)	7.14 (d, 2H)	J_{He-Hf} = 8.8		
	H3a	4.42 (d, 1H)	$J_{H3a-H3b}$ = 18.6		
	H3b	4.63 (d, 1H)			
	H4	5.57 (dd, 1H)			
	H5a	3.48 (dd, 1H)	J_{H4-H5a} = 7.6, $J_{H5a-H5b}$ = 12.5		
	H5b	3.72 (dd, 1H)	J_{H4-H5b} = 3.7		
	CON-H	**not observed**			

^{99}Tc Peptide	assignment	Anti Isomer (Product A)		Syn Isomer (Product B)	
		δ (ppm)	*J* (Hz)	δ (ppm)	*J* (Hz)
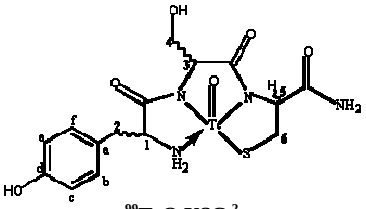 **^{99}TcO YSC** [2]	H1	4.53(dd, 1H)	$J_{H1\text{-}H2a}$ = 10.8, $J_{H1\text{-}H2b}$ = 3.9	4.21(t, 1H)	$J_{H1\text{-}H2}$ = 7.1
	H2a	2.88 (dd, 1H)	$J_{H2a\text{-}H2b}$ = 14.7	3.37 (m, 2H)	
	H2b	3.47 (dd, 1H)		--	
	N-H(1)	**not observed**	$J_{Hb\text{-}Hc}$ = $J_{He\text{-}Hf}$ = 8.3	**not observed**	
	Ar-H(c,e)	6.92 (d, 1H)		6.86 (d, 1H)	$J_{Hb\text{-}Hc}$ = $J_{He\text{-}Hf}$ = 8.3
	Ar-H(b,f)	7.28 (d, 1H)		7.25 (d, 1H)	
	H3	4.94 (br t, 1H)	$J_{H3\text{-}H4a}$ = 2.4, $J_{H3\text{-}H4b}$ = 1.7	4.63 (br t, 1H)	
	H4a	3.94 (dd, 1H)	$J_{H4a\text{-}H4b}$ = 11.9	4.02 (dd, 1H)	$J_{H3\text{-}H4a}$ = 2.9, $J_{H3\text{-}H4b}$ = 2.4
	H4b	4.38 (dd, 1H)		4.04 (dd, 1H)	$J_{H4a\text{-}H4b}$ = 11.7
	H5	5.75 (dd, 1H)	$J_{H5\text{-}H6a}$ = 7.8, $J_{H5\text{-}H6b}$ = 2.4	5.26 (dd, 1H)	$J_{H5\text{-}H6a}$ = 6.6, $J_{H5\text{-}H6b}$ = 2.2
	H6a	3.57 (dd, 1H)	$J_{H6a\text{-}H6b}$ = 12.2	3.84 (dd, 1H)	$J_{H6a\text{-}H6b}$ = 12.7
	H6b	3.79 (dd, 1H)		--	
	CON-H	**not observed**		**not observed**	
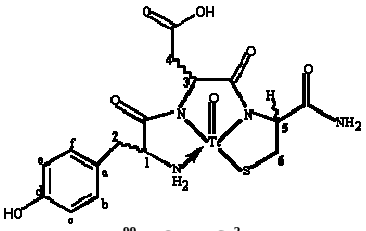 **^{99}TcO YDC** [2]	H1	4.49(dd, 1H)	$J_{H1\text{-}H2a}$ = 8.8, $J_{H1\text{-}H2b}$ = 3.9	4.21(t, 1H)	$J_{H1\text{-}H2a}$ = 6.4, $J_{H1\text{-}H2b}$ = 5.9
	H2a	2.92 (dd, 1H)	$J_{H2a\text{-}H2b}$ = 14.7	3.28 (d, 1H)	$J_{H2a\text{-}H2b}$ = 14.4
	H2b	3.29 (dd, 1H)		3.36 (d, 1H)	
	N-H(1)	**not observed**		**not observed**	
	Ar-H(c,e)	6.84 (d, 2H)	$J_{Hb\text{-}Hc}$ = $J_{He\text{-}Hf}$ = 8.3	6.84 (d, 2H)	$J_{Hb\text{-}Hc}$ = 8.3
	Ar-H(b,f)	7.20 (d, 2H)		7.22 (d, 2H)	$J_{He\text{-}Hf}$ = 8.8
	H3	5.09 (br t, 1H)		4.73 (br t, 1H)	
	H4a	2.98 (dd, 1H)		3.10 (m, 2H)	$J_{H3\text{-}H4a}$ = $J_{H3\text{-}H4b}$ = 4.6
	H4b	3.38 (dd, 1H)		--	$J_{H4a\text{-}H4b}$ = 10.3
	H5	5.62 (dd, 1H)	$J_{H5\text{-}H6a}$ = 7.8, $J_{H5\text{-}H6b}$ = 3.4	5.25 (dd, 1H)	
	H6a	3.57 (dd, 1H)	$J_{H6a\text{-}H6b}$ = 12.5	3.85 (m, 2H)	$J_{H5\text{-}H6a}$ = 5.9, $J_{H5\text{-}H6b}$ = 3.9
	H6b	3.79 (dd, 1H)		--	
	CON-H	**not observed**		**not observed**	
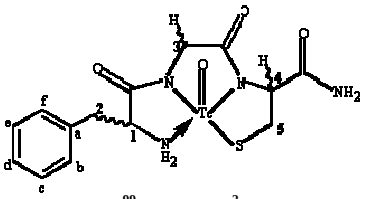 **^{99}TcO FGC** [2]	H1	4.53 (dd, 1H)	$J_{H1\text{-}H2a}$ = 9.8, $J_{H1\text{-}H2b}$ = 3.9		
	H2a	2.92 (dd, 1H)	$J_{H2a\text{-}H2b}$ = 14.7		
	H2b	3.45 (dd, 1H)			
	N-H(1)	**not observed**			
	Ar-H	7.35 (m, 5H)			
	H3a	4.41 (d, 1H)	$J_{H3a\text{-}H3b}$ = 18.3		
	H3b	4.62 (d, 1H)			
	H4	5.58 (dd, 1H)			
	H5a	3.53 (dd, 1H)	$J_{H4\text{-}H5a}$ = 7.8, $J_{H5a\text{-}H5b}$ = 12.3		
	H5b	3.71 (dd, 1H)	$J_{H4\text{-}H5b}$ = 3.7		
	CON-H	**not observed**			

^{99}Tc Peptide	assignment	Anti Isomer (Product A)		Syn Isomer (Product B)	
		δ (ppm)	*J* (Hz)	δ (ppm)	*J* (Hz)
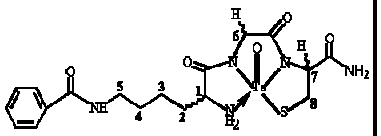 **^{99}TcO (ε-K)GC** [3]	H1	3.9		3.6	
	H2	1.6		2.0	
	H3	1.5		1.5	
	H4	1.7		1.5	
	H5a	3.3		3.2	
	H5b	3.4		-	
	N-H(5)	7.3		8.2	
	N-H(1a)	4.9		6.2	
	N-H(1b)	6.4		7.2	
	H6a	4.3		4.2	
	H6b	4.4		4.2	
	H7	5.7		5.0	
	H8a	3.3		3.6	
	H8b	3.85		3.6	
	CON-H	6.5		6.5	
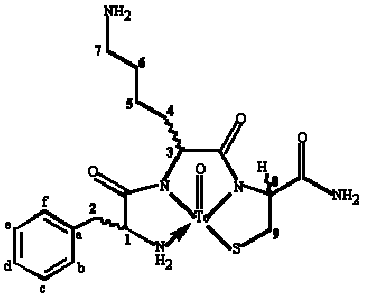 **^{99}TcO FKC** [4]	H1	4.20 (br s, 1H)		3.94 (br s, 1H)	
	H2a	2.89 (dd, 1H)	J_{H1-H2a} = 11.0, $J_{H1a-H2b}$ = 2.9	3.17 (dd, 1H)	J_{H1-H2a} = 7.3, J_{H1-H2b} = 6.6
	H2b	3.43 (m, 1H)	$J_{H2a-H2b}$ = 13.9	3.44 (dd, 1H)	$J_{H2a-H2b}$ = 13.4
	N-H(1a)	6.06 (br s, 1H)		6.63 (br s, 2H)	
	N-H(1b)	7.97 (br s, 1H)		--	
	Ar-H	7.40 (m, 5H)		7.31 (m, 5H)	
	H3	4.76 (br s, 1H)		4.39 (t, 1H)	J_{H3-H4a} = 10.3, J_{H3-H4b} = 5.1
	H4a	1.75 (m, 1H)		1.83 (m, 2H)	
	H4b	2.26 (m, 1H)		--	
	H5a	0.65 (m, 1H)		1.26 (m, 1H)	
	H5b	0.73 (m, 1H)		1.38 (m, 1H)	
	H6	1.34 (m, 2H)		1.54 (m, 2H)	
	H7	2.61 (br s, 2H)		2.73 (m, 2H	
	N-H(7)	7.65 (m, 2H)		7.65 (s, 2H)	
	H8	5.54 (d, 1H)	J_{H8-H9a} = 7.3, J_{H8-H9b} = 3.7	5.05 (d, 1H)	J_{H8-H9a} = 7.3, J_{H8-H9b} = 4.4
	H9a	3.19 (dd, 1H)	$J_{H9a-H9b}$ = 11.7	3.55 (dd, 1H)	$J_{H9a-H9b}$ = 12.4
	H9b	3.80 (d, 1H)		3.64 (d, 1H)	
	CON-Ha	6.89 (s, 1H)		6.88 (d, 2H)	$J_{CONHa-CONHb}$ = 13.2
	CON-Hb	7.08 (s, 1H)		--	

Re Peptide	assignment	Anti Isomer (Product A)		Syn Isomer (Product B)	
		δ (ppm)	*J* (Hz)	δ (ppm)	*J* (Hz)
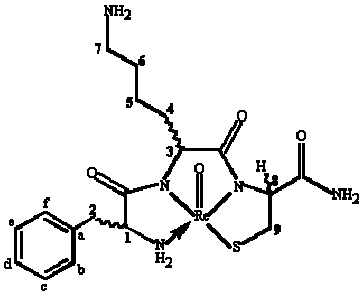 **ReO FKC** [1]	H1	4.59 (dd, 1H)		4.40 (t, 1H)	
	H2a	2.99 (dd, 1H)	$J_{H1\text{-}H2a}$ = 10.6, $J_{H2a\text{-}H2b}$ = 14.4	3.35 (m, 1H)	$J_{H1\text{-}H2a}$ = 6.4, $J_{H1\text{-}H2b}$ = 5.9
	H2b	3.54 (m, 1H)	$J_{H1\text{-}H2b}$ = 3.7	3.50 (dd, 1H)	$J_{H2a\text{-}H2b}$ = 14.7
	N-H(1)	**not observed**		**not observed**	
	Ar-H	7.47 (m, 5H)		7.39 (m, 5H)	
	H3	5.11 (dd, 1H)	$J_{H3\text{-}H4a}$ = 4.9, $J_{H3\text{-}H4b}$ = 2.5	4.83 (t, 1H)	
	H4a	1.86 (m, 1H)		2.00 (m, 2H)	
	H4b	2.36 (m, 1H)		--	
	H5	0.62 (m, 2H)		1.30 (m, 2H)	
	H6	1.50 (m, 2H)		1.61 (m, 2H)	
	H7	2.83 (t, 2H)		2.90 (m, 2H)	
	N-H(7)	**not observed**		7.42 (s, 2H)	$J_{H8\text{-}H9a}$ = 8.1, $J_{H8\text{-}H9b}$ = 4.4
	H8	5.35 (dd, 1H)		5.00 (d, 1H)	$J_{H9a\text{-}H9b}$ = 12.8
	H9a	3.39 (dd, 1H)	$J_{H8\text{-}H9a}$ = 8.3, $J_{H8\text{-}H9b}$ = 2.9	3.53 (d, 1H)	
	H9b	3.61 (dd, 1H)	$J_{H9a\text{-}H9b}$ = 12.7	3.95 (d, 1H)	
	CON-Ha	**not observed**		6.92 (s, 1H)	
	CON-Hb			7.55 (s, 1H)	
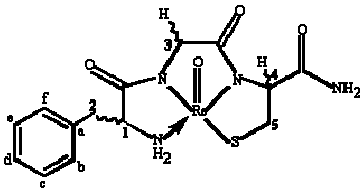 **ReO FGC** [1]	H1	4.60 (dd, 1H)	$J_{H1\text{-}H2a}$ = 9.5, $J_{H1\text{-}H2b}$ = 3.9	4.60 (m, 1H)	
	H2a	3.01 (dd, 1H)	$J_{H2a\text{-}H2b}$ = 14.9	3.39 (m, 2H)	
	H2b	3.52 (dd, 1H)		--	
	N-H(1)	**not observed**		**not observed**	
	Ar-H	7.44 (m, 5H)		7.40 (m, 5H)	
	H3	4.71 (br s, 2H)		4.79 (br s, 2H)	
	H4	5.26 (dd, 1H)		5.10 (d, 1H)	$J_{H4\text{-}H5a}$ = 8.6, $J_{H5a\text{-}H5b}$ = 12.5
	H5a	3.41 (dd, 1H)	$J_{H4\text{-}H5a}$ = 8.3, $J_{H5a\text{-}H5b}$ = 12.5	3.57 (dd, 1H)	
	H5b	3.59 (dd, 1H)	$J_{H4\text{-}H5b}$ = 3.9	3.99 (d, 1H)	
	CON-Ha	**not observed**		7.05 (s, 1H)	
	CON-Hb			7.70 (s, 1H)	

Re Peptide	assignment	Anti Isomer (Product A)		Syn Isomer (Product B)	
		δ (ppm)	*J* (Hz)	δ (ppm)	*J* (Hz)
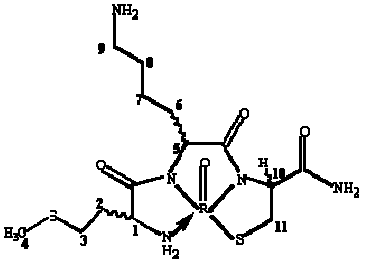 **ReO MKC** [1]	H1 H2a/H3a H2b/H3b H4 N-H(1) H5 H6 H7 H8 H9 N-H(9) H10 H11a H11b CON-Ha CON-Hb			4.22 (m, 1H) 2.34 (m, 2H) 2.81 (m, 2H) 2.13 (m, 3H) **not observed** 4.76 (m, 1H) 2.02 (m, 2H) 1.42 (m, 2H) 1.67 (m, 2H) 2.92 (m, 2H) 7.47 (br s, 2H) 5.03 (m, 1H) 3.56 (m, 1H) 3.99 (m, 1H) 7.04 (s, 1H) 7.71 (s, 1H)	

Re Peptide	assignment	Anti Isomer (Product A)		Syn Isomer (Product B)	
		δ (ppm)	*J* (Hz)	δ (ppm)	*J* (Hz)
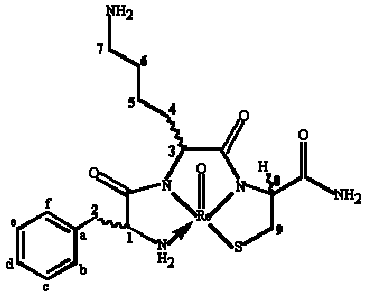 **ReO FKC** [4]	H1 H2a H2b N-H(1)a N-H(1)b Ar-H H3 H4 H5a H5b H6 H7 N-H(7) H8 H9a H9b CON-Ha CON-Hb			4.09 (t, 1H) 3.13 (dd, 1H) 3.25 (dd, 1H) 7.57 (broad s, 1H) 8.06 (broad s, 1H) 7.30 (m, 5H) 4.57 (t, 1H) 1.84 (dd, 2H) 1.28 (m, 1H) 1.39(m, 1H) 1.53 (m, 2H) 2.73 (m, 2H) 7.67 (s, 2H) 4.84 (d, 1H) 3.29 (dd, 1H) 3.77 (d, 1H) 6.88 (s, 1H) 6.97 (s, 1H)	 J_{H1-H2a} = 6.6, J_{H1-H2b} = 5.9 $J_{H2a-H2b}$ = 14.7 J_{H3-H4a} = 10.3, J_{H3-H4b} = 5.1 J_{H8-H9a} = 8.1, J_{H8-H9b} = 3.7 $J_{H9a-H9b}$ = 12.5
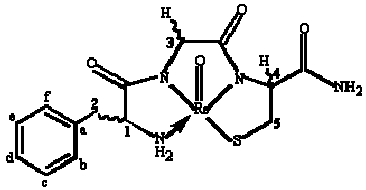 **ReO FGC** [4]	H1 H2a H2b N-H(1)a N-H(1)b Ar-H H3a H3b H4 H5a H5b CON-Ha CON-Hb	4.20 (s, 1H) 2.83 (t, 1H) 3.32 (m, 1H) 6.84(t, 1H) 8.60(s, 1H) 7.40 (m, 5H) 4.25 (d, 1H) 4.57(d, 1H) 5.18 (d, 1H) 3.11 (t, 1H) 3.57(d, 1H) 7.00(s, 1H) 7.18(s, 1H)	J_{H1-H2a} = 9.5, J_{H1-H2b} = 3.9 $J_{H2a-H2b}$ = 14.9 J_{H4-H5a} = 8.3, J_{H4-H5b} = 3.9 $J_{H5a-H5b}$ = 12.5 		

1 dissolved in 0.01M HCl in H_2O
2 dissolved in 0.01M HCl in D_2O
3 dissolved in Acetonitrile-d3
4 dissolved in DMSO-d6

Table A6. Mass Spectral Data for TcO and ReO tripeptides.

ReO Tripeptides	Isotope pattern			Mass	
	Calculated Mass (abundance)	A (anti), Observed Mass (abundance)	B (syn), observed Mass (abundance)	monoisotopic	average
ReO FGC	$(M+H)^+$	A $(M+H)^+$ obsd	$(M+H)^+$ obsd		
	523.06(57.4)	523.05(51.6)	523.10(65.5)	524.05	523.58
	524.06(10.5)	524.15(12.6)	524.20(9.76)		
	525.06(100)	525.10(100)	525.10(100)		
	526.06(18.1)	526.10(18.3)	526.15(19.4)		
	527.06(6.60)	527.15(7.38)	526.95(3.69)		
	$(M-H)^-$	A $(M-H)^-$ obsd	B $(M-H)^-$ obsd		
ReO FKC	(M+H)+	A $(M+H)^+$ obsd	B $(M+H)^+$ obsd		
	594.13(57.1)	594.00(59.9)	593.95(48.6)	595.13	594.70
	595.13(13.2)	594.96(15.6)	595.05(11.6)		
	596.13(100)	596.00(100)	596.00(100)		
	597.14(22.9)	596.95(21.4)	597.00(16.2)		
	598.13(7.55)	597.90(7.78)	598.05(6.33)		
	$(M-H)^-$	A $(M-H)^-$ obsd	B $(M-H)^-$ obsd		
	592.12(57.1)	592.00(56.8)	592.10(64.7)		
	593.12(13.2)	593.00(13.9)	593.05(17.3)		
	594.12(100)	594.00(100)	594.00(91.6)		
	595.12(22.9)	595.05(24.0)	595.00(34.5)		
	596.12(7.54)	596.00(6.80)	596.00(9.26)		
ReO MKC	(M+H)+	A $(M+H)^+$ obsd	B $(M+H)^+$ obsd		
	578.10(55.9)	578.00(59.7)	578.00(56.5)	580.11	579.73
	579.11(10.9)	579.10(12.8)	579.10(11.2)		
	580.11(100)	580.00(100)	580.10(100)		
	581.11(19.4)	581.00(18.1)	581.00(18.4)		
	582.10(11.0)	582.05(10.7)	582.05(10.8)		
	$(M-H)^-$	A $(M-H)^-$ obsd	B $(M-H)^-$ obsd		

Mass Spectral Data for Tc tripeptide complexes							
Complex	Anti $(M+H)^+$	Syn $(M+H)^+$	Anti $(M+Na)^+$	Syn $(M+Na)^+$	Mono Isotopic Mass	Average Mass	Nominal Mass
TcO FGC	436.9		458.9		436.00	436.28	436
TcO FKC	508.1	508.1			506.08	507.40	507
TcO FSC	466.8		488.7		466.01	466.28	466
TcO YSC		483.1		504.8	482.01	482.31	482
TcO YGC	453.1		474.6		452.00	452.28	452
TcO (ε-K)GC[1]			544.04 (566.08: $(M+ 2Na-H)^+$)	1065: $[M_2+ Na]^+$ 544 566	521.06	521.39	521
TcO YDC-complex D[2]		507.9		525.0			
TcO P2450	837.4$(M+H)^+$ 419.3$(M+2H)^{2+}$	837.4$(M+H)^+$ 419.3$(M+2H)^{2+}$			835.25	836.76	

1. The syn compound appears to be a tightly associated dimer with $[M_2 + Na]^+$ at m/z 1065, consistent with the molecular weight of 521. This persists as the base peak even upon tenfold dilution. The ions associated with the monomer at m/z 499, 544 and 566 are present at lower abundance.
2. Both ^{99}Tc and Re YDC show 2 HPLC peaks initially upon reaction, labeled A and B. These eventually convert to C and D. The mass spectrum of ^{99}Tc YDC- D shows a mass that is 2 lower than expected for the complex (m/z_{expected}: 510).

Biodistribution Studies of MO Tripeptide Diastereomers (M = ^{99m}Tc, ^{99}Tc, Re)

It was of interest to probe whether there are any inherent differences in biological behavior between the *syn* and the *anti* diastereomers of the metal tripeptide complexes. Therefore, three of the tripeptide ligands, FGC, FSC, and FKC, were radiolabeled with ^{99m}Tc and the individual diastereomers were isolated by reverse phase preparative HPLC. By utilizing an ethanol/water HPLC mobile phase system, pH adjustment or evaporation steps on the collected fractions were not necessary (as they are with TFA/acetonitrile mobile phase systems) to make the injection solutions amenable for injection into animals; the samples were simply diluted with saline and injected into female nude mice. Animals were sacrificed at 1, 4, and 24 hours, and biodistribution data collected. Results for selected tissues are given in **Table A7**.

In **Figure A8**, the biodistribution results show in general rapid clearance, and accumulation of radioactivity mainly in the liver (1.3 – 4.9 %ID/g at 1 hour p.i.) and intestines (6.4 – 16.7 %ID/g at 1 hour p.i.). The FGC compound exhibited higher liver accumulation than FSC or FKC. These results attest to the relative lipophilicity of the model compounds. Some uptake in the kidneys (0.7 - 5.8 %ID/g) was also noted. Uptake in the thyroid is often indicative of free pertechnetate, and therefore can give a measure of the relative stability of the ^{99m}Tc complex. Although the absolute amounts of the 3 tracers in the thyroid are relatively low (**Figure A9**), it is clear that the FGC products gave significantly more thyroid uptake than the FSC or FKC products, and therefore may be the least stable.

In comparing results between the diastereomers, it is apparent that the *syn* complexes had significantly higher uptake in several tissues, including kidney and lung (and liver at the early timepoint), as compared to the *anti* complexes. The *syn* complexes also exhibited substantially more radioactivity in the blood than the *anti* complexes (**Figure A10)**. Taken together, these results might indicate that that the *anti* diastereomers would be preferred as imaging agents (less residual uptake in organs and better clearance). However, it is difficult to predict the behavior of larger bioconjugate molecules where the biological distribution profile could be driven more by the pharmacophore than the chelator.

Table A7. Biodistribution of ^{99m}TcO[F-X-C] (X = G, S, K) *syn* and *anti* diastereomers in female nude mice. Data are expressed as mean ± SD (N=3) .

% ID/g		1 hour		4 hours		24 hours	
		Anti	*Syn*	*Anti*	*Syn*	*Anti*	*Syn*
Lung	FGC	0.23 ± 0.02	1.41 ± 0.25	0.18 ± 0.01	0.85 ± 0.10	0.06 ± 0.02	0.12 ± 0.03
	FSC	0.31 ± 0.31	0.60 ± 0.09	0.07 ± 0.03	0.23 ± 0.07	0.03 ± 0.02	0.05 ± 0.01
	FKC	0.23 ± 0.04	0.42 ± 0.04	0.13 ± 0.01	0.09 ± 0.04	-	-
Kidney	FGC	1.52 ± 0.07	5.76 ± 1.78	1.11 ± 0.13	4.84 ± 1.15	0.56 ± 0.09	0.88 ± 0.07
	FSC	0.65 ± 0.11	2.91 ± 1.06	0.34 ± 0.04	0.81 ± 0.24	0.16 ± 0.04	0.23 ± 0.07
	FKC	1.37 ± 0.19	2.21 ± 0.41	0.44 ± 0.07	0.24 ± 0.05	-	-
Liver	FGC	4.90 ± 0.54	3.75 ± 0.71	3.57 ± 0.13	2.00 ± 0.08	1.10 ± 0.18	0.54 ± 0.05
	FSC	1.26 ± 0.59	3.39 ± 0.62	0.95 ± 0.12	1.07 ± 0.61	0.35 ± 0.07	0.17 ± 0.03
	FKC	1.57 ± 0.62	4.30 ± 1.64	0.55 ± 0.09	0.96 ± 0.37	-	-
Intestine	FGC	9.60 ± 0.91	10.40 ± 2.42	7.70 ± 1.84	11.06 ± 2.19	0.35 ± 0.21	0.21 ± 0.09
	FSC	15.73 ± 8.47	15.01 ± 4.07	9.29 ± 5.27	12.22 ± 4.31	0.15 ± 0.04	0.12 ± 0.07
	FKC	6.37 ± 0.71	11.81 ± 2.19	3.21 ± 0.74	10.76 ± 5.72	-	-
Stomach	FGC	0.19 ± 0.07	1.42 ± 1.45	0.91 ± 0.42	1.44 ± 0.58	0.15 ± 0.07	0.17 ± 0.03
	FSC	0.25 ± 0.20	0.43 ± 0.27	0.37 ± 0.23	0.64 ± 0.78	0.06 ± 0.02	0.07 ± 0.03
	FKC	0.84 ± 0.28	0.73 ± 0.53	0.43 ± 0.04	0.34 ± 0.07	-	-
Thyroid	FGC	0.53 ± 0.33	0.51 ± 0.18	0.48 ± 0.08	0.86 ± 0.31	0.28 ± 0.02	0.33 ± 0.04
	FSC	0.09 ± 0.02	0.19 ± 0.03	0.14 ± 0.03	0.20 ± 0.14	0.16 ± 0.05	0.24 ± 0.09
	FKC	0.19 ± 0.03	0.26 ± 0.04	0.07 ± 0.03	0.13 ± 0.04	-	-
Pancreas	FGC	0.10 ± 0.02	0.24 ± 0.04	0.06 ± 0.02	0.17 ± 0.01	0.04 ± 0.01	0.07 ± 0.01
	FSC	0.19 ± 0.12	0.23 ± 0.15	0.03 ± 0.01	0.06 ± 0.02	0.02 ± 0.00	0.03 ± 0.01
	FKC	1.43 ± 0.45	0.53 ± 0.13	0.14 ± 0.02	0.12 ± 0.06	-	-
Blood	FGC	0.35 ± 0.07	2.52 ± 0.21	0.20 ± 0.01	1.50 ± 0.06	0.06 ± 0.01	0.12 ± 0.02
	FSC	0.20 ± 0.01	1.17 ± 0.16	0.06 ± 0.01	0.36 ± 0.07	0.02 ± 0.00	0.03 ± 0.01
	FKC	0.16 ± 0.09	0.45 ± 0.03	0.04 ± 0.01	0.12 ± 0.03	-	-
% ID							
Feces	FGC	ND	ND	9.17 ± 9.68	7.63 ± 6.28	30.61 ± 9.36	33.17 ± 5.48
	FSC	ND	ND	25.87±18.02	11.54 ± 8.69	39.87 ± 5.25	39.09 ± 3.29
	FKC	ND	ND	19.71±11.61	20.70±17.58	-	-
Urine	FGC	62.49 ± 4.76	55.47 ± 4.28	60.63 ± 0.89	49.48 ± 7.44	51.82±18.47	51.44 ± 5.29
	FSC	51.69 ± 2.56	46.38 ± 3.81	48.48 ± 9.38	44.68±21.45	56.39 ± 6.43	55.53 ± 3.29
	FKC	74.06 ± 0.86	44.34 ± 4.59	54.83±14.93	30.08 ± 8.69	-	-

Figure A8. 1- Hour Biodistribution Profile of Syn and Anti Diastereomers of ^{99m}TcO Tripeptide Complexes in Various Organs of Female Nude Mice.

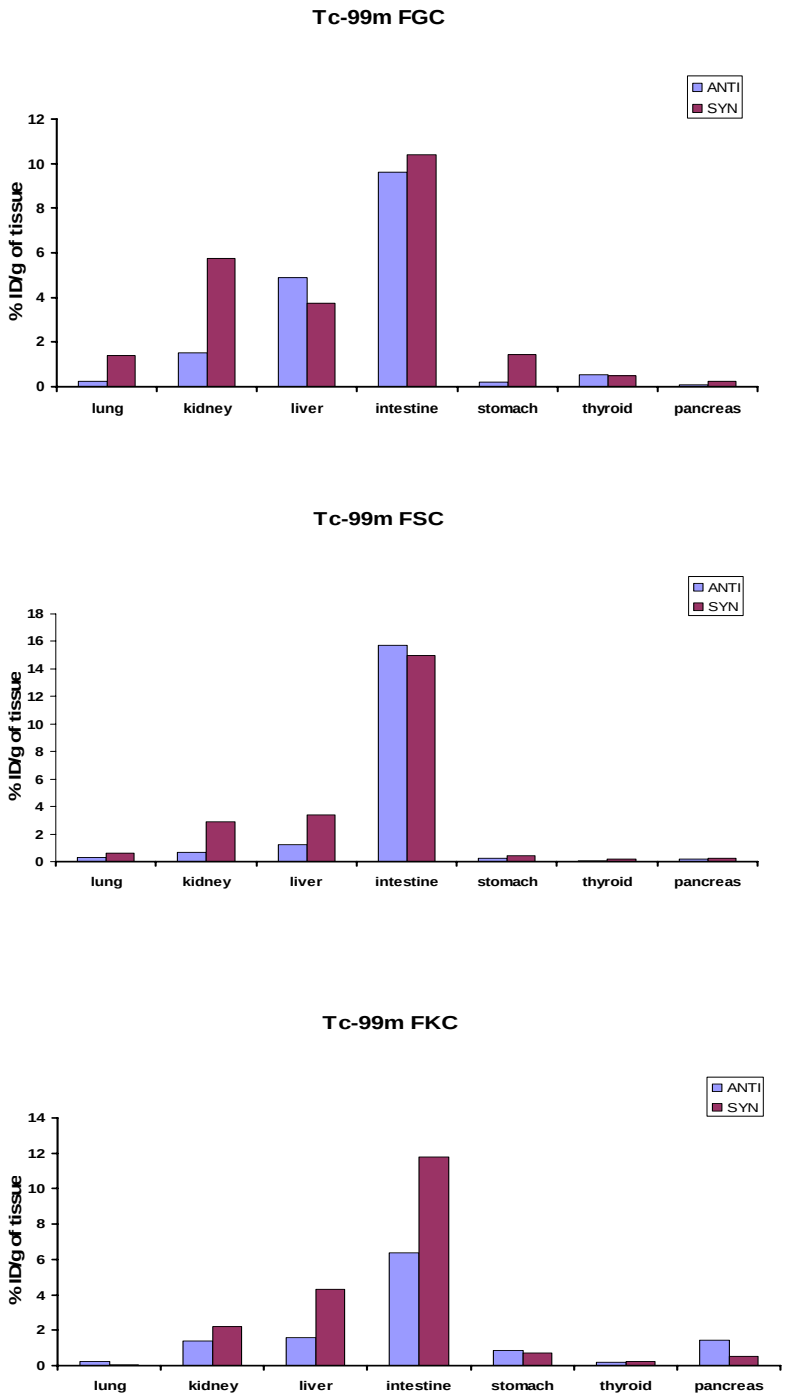

Figure A9. 1- Hour Biodistribution Profile of Syn and Anti Diastereomers of ^{99m}TcO Tripeptide Complexes in Liver, Kidney, and Thyroid of Female Nude Mice.

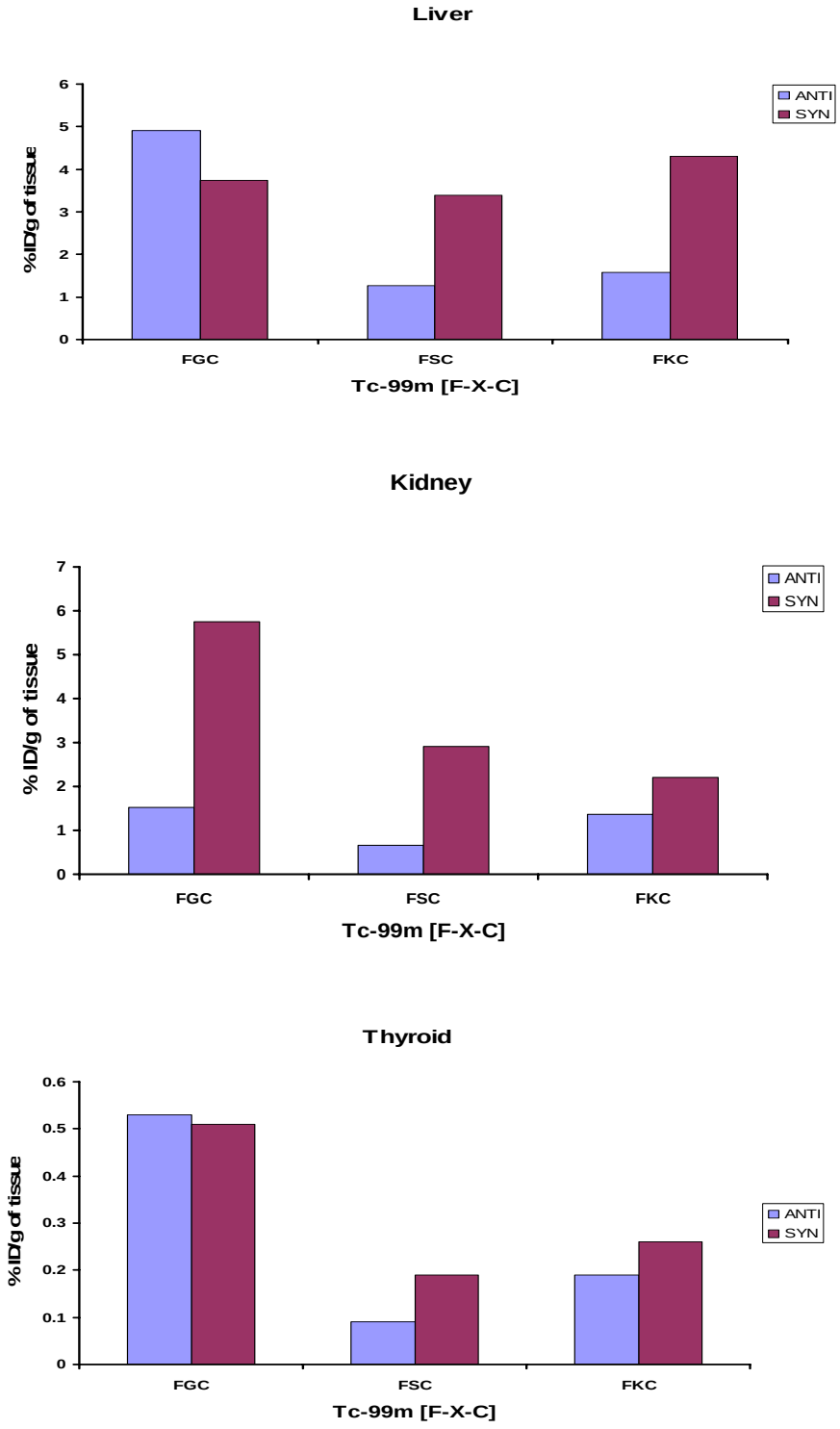

Figure A10. 24- Hour Biodistribution Profile of Syn and Anti Diastereomers of ^{99m}TcO Tripeptide Complexes in Blood of Female Nude Mice.

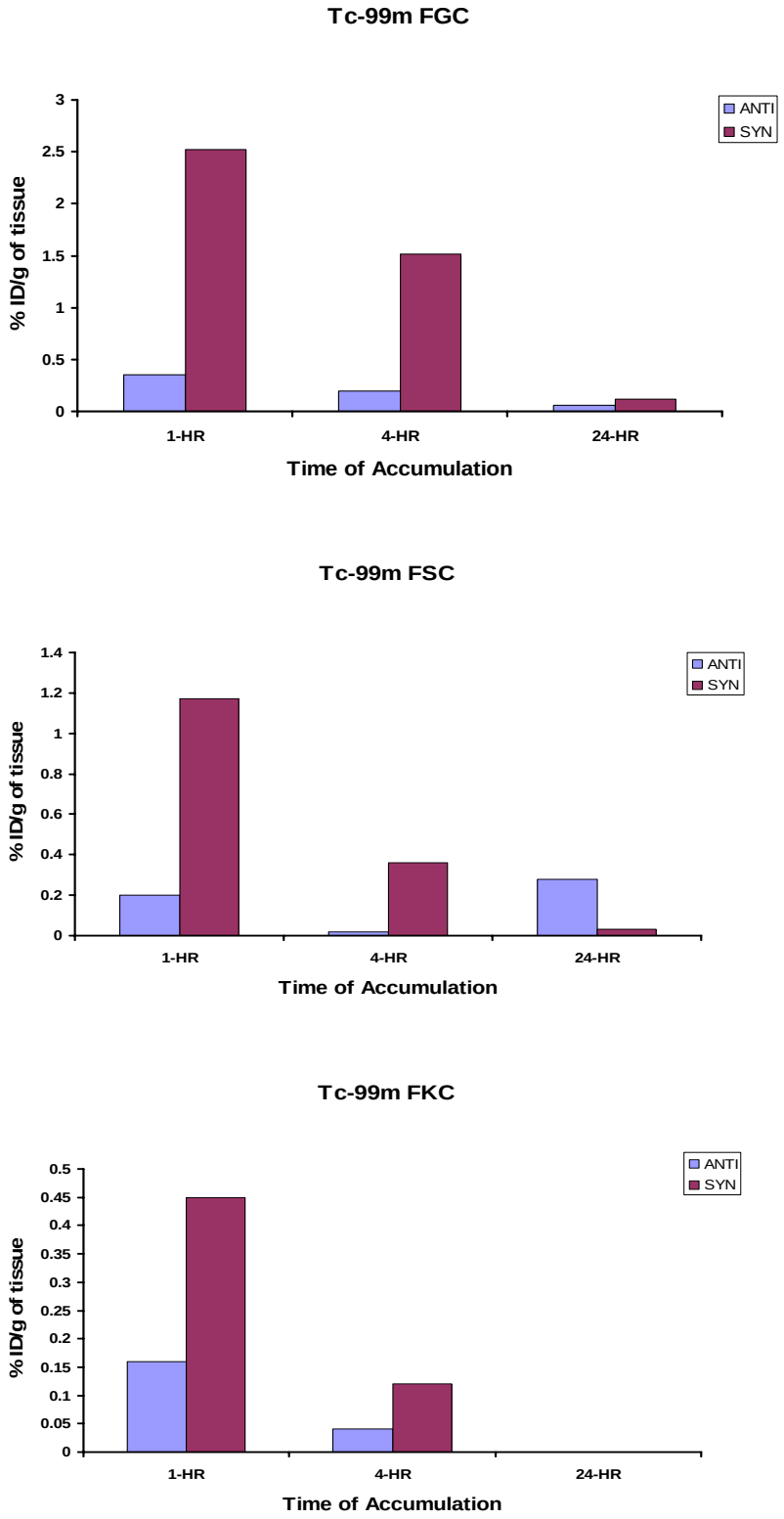

BIBLIOGRAPHY

Chapter 1

1. *Cancer Facts and Figures*. 2005, American Cancer Society.
2. Femia, F. J., *Coordination chemistry of rhenium: design of radiopharmaceuticals for diagnostics and therapeutics in nuclear medicine.* Ph.D. Dissertation, Syracuse University **2001**.
3. Fitzsimmons, J. M., *The synthesis and characterization of metal complexes for imaging and therapy*. Ph.D. Dissertation, University of Columbia **2005**.
4. Rusckowshi, M., Qu, T., Gupta, S., Ley, A. Hnatowich, D. J., *Journal of Nuclear Medicine*, **2001**. *42*(12): 1870
5. Blower, P., *Dalton Trans.*, **2006**: 1705.
6. Alberto, R., Pak, J. K., Staveren, D. v., Mundwiler, S. Benny, P., *Peptide Science*, **2004**. *76*(4): 324.
7. Heeg, M. J. Jurisson, S. S., *Acc. Chem. Res.*, **1999**. *32*(12): 1053.
8. Rusckowski, M., Qu, T., Gupta, S., Ley, A. Hnatowich, D. J., *J Nucl Med*, **2001**. *42*(12): 1870.
9. Schibli, R. Schubiger, A., *European Journal of Nuclear Medicine and Molecular Imaging*, **2002**. *29*(11): 1529.
10. Stalteri, M. A., Bansal, S., Hider, R. Mather, S. J., *Bioconjugate Chem.*, **1999**. *10*(1): 130.
11. Thakur, M. L., Kolan, H., Li, J., Wiaderkiewicz, R., Palella, V. R., Duggaraju, R.Schally, A. V., *Nuclear Medicine and Biology*, **1997**. *24*: 105.

12. Lazarova, N., *Technetium and rhenium radiopharmaceutical agents in nuclear medicine: design and synthesis*. Ph.D. Dissertation, Syracuse University **2005**.

13. Riddoch, R. W., *Solid-phase synthesis of radiotracers*. Ph.D. Dissertation, McMaster University **2004**.

14. Safi, B., Mertens, J., Proft, F. D., Alberto, R. Geerlings, P., *J. Phys. Chem. A*, **2005**. *109*: 1944.

15. Volkert, W. A. Hoffman, T. J., *Chem. Rev.*, **1999**. *99*: 2269.

16. Frost, S., *J. Nucl. Med.*, **1998**. *39*(3): 20N.

17. Volkert, W. A. Jurisson, S., *Top. Curr. Chem.*, **1996**. *176*: 123.

18. Deutsch, E., Libson, K., Jurisson, S. Lindoy, L. F., *Prog. Inorg. Chem.* , **1983**. *30*: 75.

19. Melnik, M. Van Lier, J. E., *Coord. Chem. Rev.*, **1987**. *77*: 275.

20. Mazzi, U., *Polyhedron*, **1989**. *8*: 1633.

21. Jurisson, S., Berning, D., Jia, W. Ma, D., *Chem. Rev.*, **1993**. *93*: 1137.

22. Tisato, F., Refosco, F. Bandoli, G., *Coord. Chem. Rev.*, **1994**. *135*: 325.

23. Johannsen, B. Spies, H., *Top. Curr. Chem.*, **1996**. *176*: 79.

24. Frost, S., *J. Nucl. Med.*, **1998**. *39*(2): 27N.

25. Dilworth, J. R. Parrott, S. J., *Chem. Soc. Rev.*, **1998**. *27*: 43.

26. Grewal, R. K., Dadparvar, S., Yu, J. Q., Babaria, C. J., Cavanaugh, T., Sherman, M.Jacobstein, J., *Cancer J.*, **2002**. *8*(5): 400.

27. Morehead, R. S. Shih, W. J., *Clin. Nucl. Med.*, **2001**. *26*(11): 910.

28. Danielsson, R., Baath, M., Svensson, L., Forlov, U. Kolbeck, K. G., *Eur. J. Nucl. Med. Mol. Imaging*, **2005**. *32*(8): 925.

29. Martins, T., Lino, J. S., Ramos, S. Oliveira, L., *Cancer Biother. Radiopharm.*, **2004**. *19*(2): 253.

30. Cholewinski, W., Kowalczyk, J. R., Stefaniak, B., Stefaniak, J., Poniatowicz-Frasunek, E.Tarkowska, A., *Eur. J. Nucl. Med. Mol. Imaging*, **2004**. *31*(6): 820.

31. Cyr, J. E., Pearson, D. A., Nelson, C. A., Lyon, B. A., Zheng, Y., Bartis, J., He, J., Cantorias, M. V.Francesconi, L. C., *manuscript in preparation*.

32. *Ultra-TechneKow DTE (Technetium Tc 99m Generator), Mallinckrodt Medical, Inc., St. Louis, MO 63134*, **1996**.

33. *Technetium Tc 99m Generator, Medi-Physics, Inc., Amersham Healthcare, Arlington Heights,Illinois 60005*, **1997**.

34. Vinberg, N. Kristensen, K., *European Journal of Nuclear Medicine and Molecular Imaging*, **1980**. *5*(5): 435.

35. Patterson II, J. C. Mosley, M. L., *Mol. Imaging Biol.*, **2005**. *0*: 1.

36. Lee, C.-C., Sui, G., Elizarov, A., Shu, C. J., Shin, Y.-S., Dooley, A. N., Huang, J., Daridon, A., Wyatt, P., Stout, D., Kolb, H. C., Witte, O. N., Satyamurthy, N., Heath, J. R., Phelps, M. E., Quake, S. R.Tseng, H.-R., *Science*, **2005**. *310*: 1793.

37. Bandoli, G., Domella, A., Porchia, M., Refoso, F. Tisato, F., *Coord. Chem. Rev.*, **2001**. *214*: 43.

38. Deutsch, E., Libson, K., Vanderheyden, J., Ketring, A. R. Maxon, H. R., *Nucl. Med. Biol.*, **1986**. *13*: 465.

39. *Clinical SPECT Imaging*, ed. E.L. Kramer and J.J. Sanger. 1995, New York: Raven Press.

40. Clarke, M. Podbielski, L., *Coord. Chem. Rev.* , **1987**. *78*: 253.

41. Hom, R. K. Katzenellenbogen, J. A., *Nucl. Med. & Biol.*, **1997**. *24*: 485.

42. Dilworth, J. R. Parrott, S. J., *Radiopharmaceutically relevant chemistry of technetium and rhenium*, in *Current directions in radiopharmaceutical research and development*, 1996, Kluwer Academic Publishers. p. 29.

43. Tisato, F., Porchia, M., Bolzati, C., Refosco, F. Vittadini, A., *Coord. Chem. Rev.*, **2006**.

44. Banerjee, S., Raghavan, M., Pillai, A. Ramamoorthy, N., *Semin. Nucl. Med*, **2001**. *31*(4): 260.

45. Banerjee, S. R., Maresca, K. P., Francesconi, L., Valliant, J., Babich, J. W.Zubieta, J., *Nucl. Med. Biol.*, **2005**. *32*: 1.

46. Alberto, R., Schibli, R., Waibel, R., Abram, U. Schubiger, A. P., *Coord. Chem. Rev.*, **1999**. *190-192*: 901.

47. Bandoli, G., Tisato, F., Dolmella, A. Agostini, S., *Coord. Chem. Rev.*, **2006**. *250*: 561.

48. Perrier, C. Segré, E., *Nature* **1937**. *140*: 193.

49. Harper, P. V., Beck, R., Charleston, D. Lathrop, K. A., *Nucleonics*, **1964**. *22*(1): 50.

50. Harper, P. V., Lathrop, K. A. Richards, P. J., *Nucl. Med.*, **1964**. *16*: 533.

51. Liu, S. Edwards, D. S., *Chem. Rev.* , **1999**. *99*: 2235.

52. Francesconi, L. C., Cantorias, M. V. Howell, R. C., *Metal-based imaging agents*, in *Encyclopedia of Inorganic Chemistry*, Wiley & Sons, in press.

53. Darab, J. G. Smith, P. A., *Chem. Mater.*, **1996**. *8*: 1004.

54. Roodt, A. Libson, K., *J. Nucl. Med.*, **1989**. *30*: 732.

55. Volkert, W. A. Deutsch, E. A., *Adv. Metals Med.*, **1994**. *1*: 115.

56. Johnson, D. L., Fritzberg, A. R., Hawkins, B. L., Kasina, S. Eshima, D., *Inorg. Chem.*, **1984**. *23*: 4204.

57. Vajo, J. J., Aikens, D. A., Ashley, D., Poeltl, D. E., Bailey, R. A., Clark, H. M.Bunce, S. C., *Inorg. Chem.*, **1981**. *20*: 3328.

58. Mahmood, A. Jones, A. G., *Technetium radiopharmaceuticals*, in *Handbook of Radiopharmaceuticals*, 2003, Wiley & Sons.

59. Ehrlich, P., *The collected papers of Paul Ehrlich*, ed. F. Himmelweite;M. Marquard, and H. Dale. Vol. 1. 1956, Elmsford, New York: Pergamon

60. Weiner, R. E. Thakur, M. L., *BioDrugs*, **2005**. *19*(3): 145.

61. Hunter, D. H. Luyt, L. G., *J. Labelled Cpd. Radiopharm.*, **2000**. *43*: 403.

62. Giblin, M. F., Jurisson, S. S. Quinn, T. P., *Bioconjugate Chem.*, **1997**. *8*: 347.

63. Valliant, J. F., Riddoch, R. W., Hughes, D. W., Roe, D. G., Fauconnier, T. K.Thornback, J. R., *Inorganica Chimica Acta*, **2001**. *325*(1-2): 155.

64. Langer, M. Beck-Sickinger, A. G., *Curr. Med. Chem.-Anti-Cancer Agents*, **2001**. *1*: 71.

65. Okarvi, S. M., *Med. Res. Rev.*, **2004**. *24*(3): 357.

66. Francesconi, L. C., Zheng, Y., Bartis, J., Blumenstein, M., Costello, C.DeRosch, M. A., *Inorg. Chem.*, **2004**. *43*(9): 2867.

67. Leonard, J. P., Nowotnik, D. P. Neirinckx, R. D., *J Nucl Med*, **1986**. *27*(12): 1819.

68. Neirinckx, R. D., Canning, L. R., Piper, I. M., Nowotnik, D. P., Pickett, R. D., Holmes, R. A., Volkert, W. A., Forster, A. M., Weisner, P. S.Marriott, J. A., *J Nucl Med*, **1987**. *28*(2): 191.

69. Efange, S. M. N., Kung, H. F., Billings, J., Guo, Y. Z. Blau, M., *J. Nucl. Med.*, **1987**. *28*: 1012.

70. Kung, H. F., *Semin. Nucl. Med*, **1990**. *20*: 150.

71. Kung, H. F., Guo, Y. Z., Yu, C. C., Billings, J., Subraman, V.Calabrese, J. C., *J. Nucl. Med.*, **1989**. *32*: 433.

72. Wong, E., Fauconnier, T., Bennett, S., Valliant, J., Nguyen, T., Lau, F., Lu, L. F. L., Pollak, A., Bell, R. A.Thornback, J. R., *Inorganic Chemistry*, **1997**. *36*(25): 5799.

73. Wong, E., Bennett, S., Lawrence, B., Fauconnier, T., Lu, L. F. L., Bell, R. A., Thornback, J. R.Eshima, D., *Inorg. Chem.*, **2001**. *40*: 5695.

74. Baidoo, K. E. Lever, S. Z., *Bioconjugate Chem.*, **1990**. *1*: 132.

75. Bormans, G., *J. Lab. Comp. Radiopharm.*, **1993**. *33*: 1065.

76. Cyr, J. E., Nowotnik, D. P., Pan, Y., Gougoutas, J. Z., Malley, M. F., Di Marco, J., Nunn, A. D.Linder, K. E., *Inorg. Chem.*, **2001**. *40*(14): 3555.

77. Epps, L. A., *Appl. Radiat. Isot.*, **1987**. *38*: 661.

78. Luyt, L. G., Jenkins, H. A. Hunter, D. H., *Bioconjugate Chem.*, **1999**. *10*: 470.

79. Rao, T. N. J. Amer. Chem. Soc. 1990, 5798., *J. Am. Chem. Soc.*, **1990**. *112*: 5798.

80. Cantorias, M. V., Howell, R., Todaro, L., Cyr, J., Rogers, R. D.Francesconi, L. C., *manuscript in preparation*.

Chapter 2

1. Langer, M. Beck-Sickinger, A. G., *Curr. Med. Chem.-Anti-Cancer Agents*, **2001**. *1*: 71.

2. Costopoulos, B., Benaki, D., Pelecanou, M., Mikros, E., Stassinopoulou, C. I., Varvarigou, A. D.Archimandritis, S. C., *Inorg. Chem.*, **2004**. *43*: 5598.

3. Okarvi, S. M., *Med. Res. Rev.*, **2004**. *24*(3): 357.

4. Merrifield, R. B., *J. Am. Chem. Soc. 85*: 2149.

5. Jayalekshmy, P. Mazur, S., *J. Am. Chem. Soc.*, **1976**. *98*: 6710.

6. Chan, C. White, P. D., *Fmoc solid phase peptide synthesis*. 2000, New York: Oxfor University Press, Inc.

7. Floyd, C. D., Lewis, C. N. Whittaker, M., *Chem. Brit.*, **1996**. *32*: 31.

8. Bormans, G., Peeters, O. M., Vanbilloen, H., Blaton, N. Verbruggen, A., *Inorg. Chem.*, **1996**. *33*: 6240.

9. Francesconi, L. C., Zheng, Y., Bartis, J., Blumenstein, M., Costello, C.DeRosch, M. A., *Inorg. Chem.*, **2004**. *43*(9): 2867.

10. Bandoli, G., Domella, A., Porchia, M., Refoso, F. Tisato, F., *Coord. Chem. Rev.*, **2001**. *214*: 43.

11. Dilworth, J. R. Parrott, S. J., *Radiopharmaceutically relevant chemistry of technetium and rhenium*, in *Current directions in radiopharmaceutical research and development*, 1996, Kluwer Academic Publishers. p. 29.

12. *IUPAC-IUB Commission of Biochemical Nomenclature in J. Biol. Chem.*, **1972**. *247*: 977.

13. Kaiser, E., Colescott, R., Bossinger, C. D. Cook, P. I. A. B., 34, 595., *Anal. Biochem.*, **1970**. *34*(595).

14. Brown, A. R., Herinkens, P. H. H., Ottenheijin, H. C. J. Rees, D. C., *New Tools in Synthesis*, **1998**. *5*: 817.

15. Field, G. B. Noble, R. L., *Int. J. Peptide Protein Res.*, **1990**. *35*: 161.

16. *Novabiochem Catalog 2006/2007*: EMD Biosciences.

Chapter 3

1. Francesconi, L. C., Zheng, Y., Bartis, J., Blumenstein, M., Costello, C.DeRosch, M. A., *Inorg. Chem.*, **2004**. *43*(9): 2867.

2. Cyr, J. E., Pearson, D. A., Nelson, C. A., Lyon, B. A., Zheng, Y., Bartis, J., He, J., Cantorias, M. V.Francesconi, L. C., *manuscript in preparation*.

3. Boyd, G. E., *Journal of Chemical Education*, **1959**. *36*: 3.

4. Davison, A., Trop, H. S., Depamphilis, B. V. Jones, A. G., *Inorganic Syntheses*, **1982**. *21*: 160.

5. Wong, E., Fauconnier, T., Bennett, S., Valliant, J., Nguyen, T., Lau, F., Lu, L. F. L., Pollak, A., Bell, R. A.Thornback, J. R., *Inorganic Chemistry*, **1997**. *36*(25): 5799.

6. Liu, S. Edwards, D. S., *Chem. Rev.* , **1999**. *99*: 2235.

7. Cheng, Y., Yan, Y.-B. Liu, J., *Inorg. Biochem.*, **2005**. *99*: 952.

8. Jones, W. B., *et al. Inorg. Chem.*, **1994**. *33*: 5571.

9. Depamphilis, B. V., Jones, A. G. Davison, A., *Inorg. Chem.*, **1983**. *22*: 2292.

10. Bryson, N., *et al. Inorg. Chem.*, **1988**. *27*: 2154.

11. Franklin, K., Howard-Lock, H. Lock, C., *Inorg. Chem.*, **1982**. *21*: 1941.

Chapter 4

1. Ehrhardt, G., *et al. J. Nucl. Med.*, **1987**. *28*: 656.
2. Knapp, F. F., *et al. Anticancer Research*, **1997**. *17*: 1783.
3. Guhlke, S., *et al. J. Labelled Compounds and Radiopharm.*, **1997**. *39*: 294.
4. Ehrhardt, G., *et al. Radioactivity Radiochem.*, **1992**. *3*: 38.
5. Rose, D. J., Maresca, K. P., Kettler, P. B., Chang, Y. D., Soghomomian, V., Chen, Q., Abrams, M. J., Larsen, S. K.Zubieta, J., *Inorg. Chem.*, **1996**. *35*(12): 3548.
6. Popov, K., Ronkkomaki, H. Lajunen, L. H. J., *Pure Appl. Chem.*, **2006**. *78*: 663.
7. Canney, D. J., *et al. J. Med. Chem.*, **1993**. *36*: 1032.
8. Francesconi, L. C., *et al. J. Med. Chem.*, **1994**. *37*: 3282.
9. Francesconi, L. C., Graczyk, G., Wehrli, S., Shaikh, S. N., McClinton, D., Liu, S., Zubieta, J.Kung, H. F., *Inorg. Chem.*, **1993**. *32*(14): 3114.
10. Jurisson, S. S., Schlemper, E. O., Troutner, D. E., Canning, L. R., Nowotnik, D. P.Neirinckx, R. D., *Inorg. Chem.*, **1986**. *25*: 543.
11. Wong, E., Fauconnier, T., Bennett, S., Valliant, J., Nguyen, T., Lau, F., Lu, L. F. L., Pollak, A., Bell, R. A.Thornback, J. R., *Inorganic Chemistry*, **1997**. *36*(25): 5799.
12. Liu, S. Edwards, D. S., *Chem. Rev.* , **1999**. *99*: 2235.
13. Grummon, G., Rajagopalan, R., Palenik, G., Koziol, A. Nosco, D., *Inorganic Chemistry*, **1995**. *34*: 1764.
14. Kung, H. F., Guo, Y. Z., Yu, C. C., Billings, J., Subraman, V.Calabrese, J. C., *J. Nucl. Med.*, **1989**. *32*: 433.

15. Mahmood, A., Baidoo, K. E. Lever, S. Z., *Technetium and Rhenium in Chemistry and Nuclear Medicine 3*, 1989, Cortina International Raven Press. p. 119.

16. Melnik, M. Van Lier, J. E., *Coord. Chem. Rev.*, **1987**. *77*: 275.

17. Ohmomo, Y., Franceconi, L. C., Kung, M. Kung, H., *J.Med.Chem.*, **1992**. *35*: 157.

18. Takayama, T., Suzuki, K., Sekine, T. Kudo, H., *Radiochimica Acta*, **2000**. *88*(3-4): 247.

19. Hansen, L., Lipowska, M., Melendez, E., Xu, X., Hirota, S., Taylor, A. T.Marzilli, L. G., *Inorg. Chem.*, **1999**. *38*: 5351.

20. Bereau, V. M., Khan, S. I. Abu-Omar, M. M., *Inorg. Chem.*, **2001**. *40*: 6767.

21. Cheng, Y., Yan, Y.-B. Liu, J., *Inorg. Biochem.*, **2005**. *99*: 952.

Chapter 5

1. Takayama, T., Suzuki, K., Sekine, T. Kudo, H., *Radiochimica Acta*, **2000**. *88*(3-4): 247.

2. Valliant, J. F., Riddoch, R. W., Hughes, D. W., Roe, D. G., Fauconnier, T. K.Thornback, J. R., *Inorganica Chimica Acta*, **2001**. *325*(1-2): 155.

3. Wong, E., Fauconnier, T., Bennett, S., Valliant, J., Nguyen, T., Lau, F., Lu, L. F. L., Pollak, A., Bell, R. A.Thornback, J. R., *Inorganic Chemistry*, **1997**. *36*(25): 5799.

4. Boyd, G. E., *Journal of Chemical Education*, **1959**. *36*: 3.

5. Davison, A., Trop, H. S., Depamphilis, B. V. Jones, A. G., *Inorganic Syntheses*, **1982**. *21*: 160.

6. Rose, D. J., Maresca, K. P., Kettler, P. B., Chang, Y. D., Soghomomian, V., Chen, Q., Abrams, M. J., Larsen, S. K.Zubieta, J., *Inorg. Chem.*, **1996**. *35*(12): 3548.

7. Bormans, G., Peeters, O. M., Vanbilloen, H., Blaton, N. Verbruggen, A., *Inorg. Chem.*, **1996**. *33*: 6240.

8. Jurisson, S., Halihan, M. M., Lydon, J. D., Barnes, C. L., Nowotnik, D. P.Nunn, A. D., *Inorg. Chem.*, **1998**. *37*: 1922.

9. Francesconi, L. C., Graczyk, G., Wehrli, S., Shaikh, S. N., McClinton, D., Liu, S., Zubieta, J.Kung, H. F., *Inorg. Chem.*, **1993**. *32*(14): 3114.

10. Bereau, V. M., Khan, S. I. Abu-Omar, M. M., *Inorg. Chem.*, **2001**. *40*: 6767.

11. Liu, C.-b., Liu, G.-z., Liu, N., Zhang, Y. u.-m., He, J., Rusckowski, M.Hnatowich, D. J., *Nuclear Medicine and Biology*, **2003**. *30*(2): 207.

12. *PeakFit™ v.4.12 Users Guide*. 2003, SeaSolve Software Inc.: Framingham, MA.

13. McQuarrie, D. A. Simon, J. D., *Physical Chemistry: A Molecular Approach*. 1997, Sausalito, California: University Science Books.

14. Ismael, A. A., Sauriol, F. Butler, I. S., *Inorg. Chem.*, **1989**. *28*: 1007

15. Jurisson, S. S., Hirth, W., Linder, K. E., Rocco, R. J. D., Narra, R. K., Nowotnik, D. P.Nunn, A. D., *Nuclear Medicine and Biology*, **1991**. *18*(7): 735.

16. Benard, M., Rohmer, M.-M., Cantorias, M. V. Francesconi, L. C., *manuscript in preparation*.

17. Marie-Madeleine, Marc, Cantorias, M. V. Francesconi, L. C., *manuscript in preparation*.

Chapter 6

1. Fersht, A., *Enzyme structure and mechanism*. 2nd ed. 1984, New York: Freeman WH and Co. 221.
2. IUPAC, *Biochem. J.*, **1975**. *149*: 1.
3. Morrison, R. T. Boyd, R. N., *Organic Chemistry*. 4th ed. 1983, Newton, MA: Allyn & Bacon, Inc.
4. Lamzin, V. S., Dauter, Z. Wilson, K. S., *Current Opinion in Structural Biology*, **1995**. *5*(6): 830.
5. Prelog, V., *Science*, **1976**. *193*: 17.
6. Armstrong, D. W., Yang, X., Han, S. M. Menges, R. A., *Anal. Chem.*, **1987**. *59*: 2594.
7. Bruckner, H. Schieber, A., *J. High Resolut. Chromatogr.*, **2000**. *23*: 576.
8. Dunlop, D. S., Neidle, A., McHale, D., Dunlop, D. M. Lajtha, A., *Biochem. Biophys. Res. Commun.*, **1986**. *141*: 27.
9. Hashimoto, A., Nishikawa, T., Hayashi, T., Fujii, N., Harada, K., Oka, T.Takahashi, K., *FEBS Lett.*, **1992**. *296*: 33.
10. Hoopes, E. A., Peltzer, E. T. Bada, J. L., *J. Chromatogr. Sci.*, **1978**. *16*: 556.
11. Jones, W. M., Ringe, D., Soda, K. Manning, J. M., *Anal. Biochem.*, **1994**. *218*: 204.
12. Nagata, Y., Akino, T. Ohno, K., *Anal. Biochem.*, **1985**. *150*: 238.
13. Payan, I. L., Cadilla-Perezrios, R., Fisher, G. H. Man, E. H., *Anal. Biochem.*, **1985**. *149*: 484.

14. Pirkle, W. H., Finn, J. M., Schreiner, J. L. Hamper, B. C., *J. Am. Chem. Soc.*, **1981**. *103*: 3964.

15. Thorsen, G. Bergquist, J., *J. Chromatogr. B,* **2000**. *745*: 389.

16. Tsunoda, M., Kato, M., Fukushima, T., Santa, T., Homma, H., Yanai, H., Soga, T.Imai, K., *Biomed. Chromatogr.,* **1999**. *13*: 335.

17. Wakayama, M., Takashima, K., Tau, Y., Nakashima, S., Sakai, K.Moriguchi, M., *Anal. Biochem.,* **1997**. *250*: 252.

18. Zhao, S. L., Feng, Y. Z., LeBlanc, M. H. Liu, Y. M., *J. Chromatogr. B,* **2001**. *762*: 97.

19. Asano, Y. Lubbehusen, T. L., *Journal of Bioscience and Bioengineering,* **2000**. *89*(4): 295.

20. Kumashiro, S., Hashimoto, A. Nishikawa, T., *Brain Res.*, **1995**. *681*: 231.

21. Fisher, G. H., D'Aniello, A., Vetere, A., Padula, L., Cusano, G. P.Man, E. H., *Brain Res. Bull.*, **1991**. *26*: 983.

22. Fuchs, S. A., Berger, R., Klomp, L. W. J. Koning, T. J. d., *Molecular Genetics and Metabolism,* **2005**. *85*: 168.

23. Hamase, K., Morikawa, A. Zaitsu, K., *Journal of Chromtography B,* **2002**. *781*: 73.

24. Yamada, H. Shimizu, S., *Angew. Chem. Int. Ed. Engl.*, **1988**. *27*: 622.

25. Hendrick, M. E., *Food Sci. Technol. ,* **1991**. *48*(2): 29.

26. Yamada, R. Kera, Y., *EXS,* **1998**: 145.

27. Boyd, G. E., *Journal of Chemical Education,* **1959**. *36*: 3.

28. Davison, A., Trop, H. S., Depamphilis, B. V. Jones, A. G., *Inorganic Syntheses*, **1982**. *21*: 160.

29. Rose, D. J., Maresca, K. P., Kettler, P. B., Chang, Y. D., Soghomomian, V., Chen, Q., Abrams, M. J., Larsen, S. K.Zubieta, J., *Inorg. Chem.*, **1996**. *35*(12): 3548.